Analysis of individual wave overtopping volumes during time-varying water levels. Practical application to the Research Dike Raversijde at the Belgian coast

Manuel Medina Valverde
Student number: 02201919

Supervisor: Prof. dr. ir. Peter Troch
Counsellors: Prof. dr. Maximilian Streicher, Dr. Yuri Pepi (VLIZ)

Master's dissertation submitted in order to obtain the academic degree of
Master of Science in Civil Engineering

Academic year 2022-2023

Analysis of individual wave overtopping volumes during time-varying water levels. Practical application to the Research Dike Raversijde at the Belgian coast

Manuel Medina Valverde[1]

Supervisors: prof. dr. ir. Peter Troch, prof. dr. ir. Maximilian Streicher
Counsellor: dr. ir. Yuri Pepi [VLIZ]

Abstract – **The still water level (SWL) during a storm is always dynamic (storm surge). The variability of the water level can be schematized as a time-varying hydrograph of a certain duration. Typically, the individual overtopping volume distribution and probability of individual volume overtopping is a function of the ratio between the freeboard R_c (the structure crest elevation above SWL) and the significant wave height H_{m0}.**

Since the variation during a storm of the SWL changes the freeboard, the individual overtopping volume is variable. Typically, in the laboratory the wave overtopping on coastal defence structures is investigated for a constant water level (CWL) and a pre-determined structural exposure time frame, not considering any variable water level (VWL). For example, the individual volumes in the rise of the storm surge will pre-load (saturate) the dike and potentially weaken it before the largest overtopping volumes occur during the peak of the storm.

No research exists yet on the study of individual overtopping volumes for a VWL situation, so its realization is required. Then, a comparison of the available literature for the CWL situation is carried out to analyze the validity of the prediction formulae for this case within the UGent 17 dataset measured in the wave flume facility located at the Coastal Engineering Laboratory of Ghent University, in which constant and variable water levels were studied, hereafter referred to as UG17. Following a sensitivity analysis, the best results are found for a certain percentage of the highest overtopping volumes, around the 30%, while the equivalent non-dimensional freeboard predicts equally well both CWL and VWL situations.

Hence, a practical application of these considerations is applied to a real storm of a return period between 40 and 45 years to redesign the Research Dike Raversijde, located in the Belgian coast, in order to limit the overtopping of the structure to 1 *l/s/m*, following Belgian standards.

Keywords – **experimental modelling, individual overtopping volumes, variable water level, storm surge, coastal structure**

I. INTRODUCTION

The construction of coastal defence structures is becoming increasingly notorious as the concern about climate change and its impact in the sea level is growing. The most important parameter to design these structures according to a safety and economic framework is wave overtopping. Then, wave overtopping, from an energy balance perspective, is the amount of water which is transmitted over the crest instead of being reflected or dampened (breaking). It is also possible to distinguish between the average wave overtopping discharge, which refers to the volume of water passing over the structure per unit of time per meter, and the individual wave overtopping volume, which refers to the specific amount of water as a consequence of a certain overtopping event.

Historically, the estimation and calculation of wave overtopping is a difficult task in terms of accuracy because of the complexity of its parameters, despite the publications of several manuals and articles in recent years.

Meanwhile the mean overtopping discharge q has been considered as the key variable to define this phenomenon, several studies show the necessity to also focus the analysis on the overtopping volumes of individual waves and its maximum value V_{max}, following a wave-by-wave analysis and taking into account the irregularity of the phenomenon.

The fact that storms are more frequent and their intensity tends to be greater is a clear statement, supported by plenty of investigations about climate change. Thus, the probability of extreme values of waves and storm surges is increasing as well as the risk for coastal structures and population.

For that reason, despite the SWL is majorly treated as constant in literature, it needs to be considered as a variable value. The comparison between the individual overtopping values among CWL and VWL scenarios is definitely necessary to understand the real impact of the phenomenon.

II. THEORETICAL FRAMEWORK

A. Probability distribution of individual overtopping volumes

As individual wave overtopping events are random and irregular, a probability distribution is used to describe them, considering the exceedance probability of the event (P_v). Then, a two-parameter Weibull distribution [3][15] is usually used to describe the distribution of individual wave overtopping volumes:

$$P_v = P[V_i \geq V] = exp\left(-\left(\frac{V}{a}\right)^b\right) \qquad (1)$$

This equation has a shape parameter b and a scale parameter a. For the prediction of b, several authors have published

different formulae according to the structural conditions. On the other hand, the scale factor a can be calculated as a function of q using the ratio of the total overtopped volume (V_0), as the sum of individual volumes (V_i) and the sum (T_0) of the wave periods of each wave in the wave train (T_i), where T_m stands for the mean wave period and N_w in the number of incident waves, as Equation (2); which is then divided in Equation (3) by the number of overtopping waves (N_{ow}) to obtained the measured mean overtopping volume V_{meas} [17]:

$$q = \frac{V_0}{T_0} = \frac{\sum V_i}{\sum T_i} = \frac{\sum V_i}{N_w T_m} \qquad (2)$$

$$\bar{V}_{meas} = \frac{q N_w T_m}{N_{ow}} = \frac{\sum V_i}{N_{ow}} = \frac{V_0}{N_{ow}} \qquad (3)$$

Then, based on a two-parameter Weibull distribution, the theoretical mean overtopping volume follows the next expression [6], where Γ is the mathematical gamma function:

$$\bar{V}_{theor} = E[V]_{Weibull} = a\Gamma\left(1 + \frac{1}{b}\right) \qquad (4)$$

So, if both measured and theoretical values are equal, Equation (5) is reached, which can be simplified using factor a' as shows Equation (6) [17]:

$$a = \frac{1}{\Gamma\left(1 + \frac{1}{b}\right)} \bar{V}_{meas} \qquad (5)$$

$$a' = \frac{1}{\Gamma\left(1 + \frac{1}{b}\right)} \qquad (6)$$

B. Estimation of shape factor b in literature

Shape factor b has been studied by various authors in the past, according to a specific type of structure. The authors that are considered because of the applicability of the formulae are:

Victor et al., 2012 — Based on steep, low crested structures with smooth and impermeable slopes ($0.11 \leq R_c/H_{m0} \leq 1.69$ and $0.36 \leq \cot\alpha \leq 2.75$). The formula considers the effect of the slope angle and the relative crest freeboard R_c/H_{m0} on the individual wave overtopping volumes, which is intended for the highest 50% of the overtopping volumes [17]:

$$b = exp\left(-2.0\frac{R_c}{H_{m0}}\right) + 0.56 + 0.15 \cot\alpha \qquad (7)$$

Hughes et al., 2012 — Different tests were reanalyzed with the objective of improving the estimation of b. A range of applicability of $-2 < R_c/H_{m0} < 4$ and $0 \leq P_{ow} \leq 1$ is considered. The analysis resulted in a formulation which does not consider the slope angle of the structure and is defined for the highest 10% of the overtopping volumes [6]:

$$b = \left[exp\left(-0.6\frac{R_c}{H_{m0}}\right)\right]^{1.8} + 0.64 \qquad (8)$$

Zanuttigh et al., 2013 — Following the analysis of low crested rubble-mound breakwaters, it was concluded that rubble mound structures showed more scatter in the factor b than smooth impermeable structures, but the same trend was found. Hence, the authors of the formula suggested relating the shape factor to the dimensionless mean wave overtopping discharges instead of the relative crest freeboard (R_c/H_{m0}), as the mean overtopping discharge q implicitly includes

information about wave steepness or slope angle. The proposed formula for smooth structures is showed in Equation (9) and applicable for $-2 \leq R_c/H_{m0} \leq 3.2$ [18]. This formula is implemented in EurOtop Manual 2018, which also defines the formulation to calculate the value of q [2].

$$b = 0.73 + 55\left(\frac{q}{g H_{m0} T_{m-1,0}}\right)^{0.8} \qquad (9)$$

Gallach Sánchez, 2018 — Intended for the top 10% of the overtopping volumes and steep-low crested structures, an exponential formula depending on the relative crest freeboard ($0 < R_c/H_{m0} \leq 3.25$) as well as on the slope angle ($0 \leq \cot\alpha \leq 2$) was fitted according to 1223 tests [4]:

$$b = (0.59 + 0.23 \cot\alpha) exp\left(-2.2\frac{R_c}{H_{m0}}\right) + 0.83 \qquad (10)$$

Beyond the estimation of shape factor b, some theoretical distributions are also considered in the analysis to compare the CWL and VWL results:

Rayleigh — Represents the value of $b = 2$.
Exponential — Represents the value of $b = 1$.
EurOtop (2007) — According to a limited number of analyzed datasets, it was established an average value of $b = 0.75$ from [15], although it is now noticeable that the shape factor b may increase with increasing overtopping discharges, as mentioned in its most recent version [2].

C. Maximum volume V_{max}

Once both factors a and b are calculated, the maximum individual volume for a two-parameter Weibull distribution [9] can be obtained as:

$$V_{max} = a[\ln(N_{ow} + 1)]^{1/b} \qquad (11)$$

The argument of the logarithm adds one overtopping event to avoid the inconsistency of a null value of the logarithm if there was only one overtopping wave, showing a slightly difference with the formula from [2] proposed by [15].

D. Experimental campaigns with VWL

The role of water level variation in combination with the wave-structure interaction has been little studied and even not yet focused on individual wave overtopping.

Van Gent et al. (2018) [16] developed armour stability tests with small-scale physical models for different increasing and decreasing values of the water depth at the toe of the structure (h_t). The results of the tests showed that the changing water level conditions produces an increase in damage, in comparison with the CWL configuration. Kerpen et al. (2020) [7] studied the wave overtopping for this case with hydraulic model tests in a wave flume over a 1:6 smooth slope, in which three different approaches were considered regarding h_t. The results of the study showed that there were already some uncertainties on the role of dynamic wave steepness on wave overtopping. Pepi et al. (2022) [13] conducted a study to investigate the impact of the VWL on the average overtopping discharge q over a smooth dike. The study covered a wider range of hydraulic and geometric parameters than previous cases: $0.5 \leq R_c/H_{m0} \leq 2.0$. The slope of the tested dike was similar to [16] but steeper than [7], with $\cot\alpha = 2$. The results showed that the measured value of q for CWL appears to be well predicted by the existing formulation but an overprediction is occurred for

VWL situation, especially for smaller relative crest freeboards (R_c/H_{m0} < 1.5). Hence, a new equivalent non-dimensional freeboard $(R_c/H_{m0})_{eq}$ is proposed which predicts equally well both CWL and VWL situations.

Finally, there is a notable gap in the existing literature when coming up with the case of individual wave overtopping with variable VWL.

III. DATA ANALYSIS

A. Obtained dataset

The UG17 dataset was measured in the wave flume facility located at the Coastal Engineering Laboratory of the Ghent University. It is equipped with an advanced wave generator system that enables wave trains for both regular and irregular waves and a wave data analysis software. Furthermore, it is also possible to use the pump to perform tests with tidal level changes and variable SWL, as for this case.

Hence, a smooth (cotα = 2) and impermeable breakwater was tested, for which a tank with a chute is installed behind the freeboard of the model to measure the overtopped water with a weigh cell. In that sense, 127 VWL tests and 23 CWL tests were performed (see Table 1).

Table 1. Ranges of the geometrical and hydraulic parameters of the dataset, in model scale.

Parameter	Symbol	CWL	VWL	Unit
Duration	t	15 - 60	15 -120	min
Water level variation	dh	-	0.025-0.160	m
Crest freeboard	R_c	0.09 – 0.29	0.04 – 0.24	m
Water depth at the toe	h_t	0.35 – 0.55	0.40 – 0.60	m
Significant spectral wave height	H_{m0}	0.101 – 0.109	0.053 – 0.119	m
Dimensionless freeboard	R_c/H_{m0}	0.87 – 2.76	0.40 – 1.97	-
Relative water depth	h_t/H_{m0}	3.36 – 5.45	3.81 – 6.54	-
Spectral wave period	$T_{m-1,0}$	1.66 – 1.98	1.21 – 2.98	s
Peak period	T_p	1.65 – 1.73	1.19 – 2.56	s
Wave steepness	$S_{m-1,0}$	0.017 – 0.24	0.016 – 0.040	-
Breaker parameter	$\xi_{m-1,0}$	3.22 – 3.83	2.50 – 5.68	-

For both CWL and VWL it is possible to obtain the value of the parameters of the distribution from the measured data and then compare them with the predicted ones, according to the different mentioned methods in literature. By representing the measured data in a Weibull plot, the slope and the intercept of the fitted line allow to estimate the shape and scale factors of the Weibull distribution [11] b and a'. For this, the x-axis variable is the logarithm of the relative volume according to the mean value $\ln(V/V_{mean})$, meanwhile y-axis is represented by $\ln(-\ln(1 - F(V)))$; where the exceedance probability $1 - F(V)$, is obtained theoretically using Equation (12), suggested by [10], in which i represents the position of the sorted volumes:

$$1 - F(V) = \frac{i}{N_{ow} - 1} \qquad (12)$$

B. Constant water level analysis of shape factor and V_{max}

First, the 100% of the overtopping values are considered for the analysis but a sensitivity analysis needs to be carried out to reach to the final considerations. The results for this case can be observed in Figure 1, in which an underprediction is noticed when considering all overtopping events. Moreover, the relative mean-square-error (rMSE) in Equation (14) is defined to quantify the error of the prediction for both values of b and

$$MSE = \frac{\sum(Y_{measured} - Y_{predicted})^2}{N} \qquad (13)$$

$$rMSE = \frac{MSE}{var(Y)} \qquad (14)$$
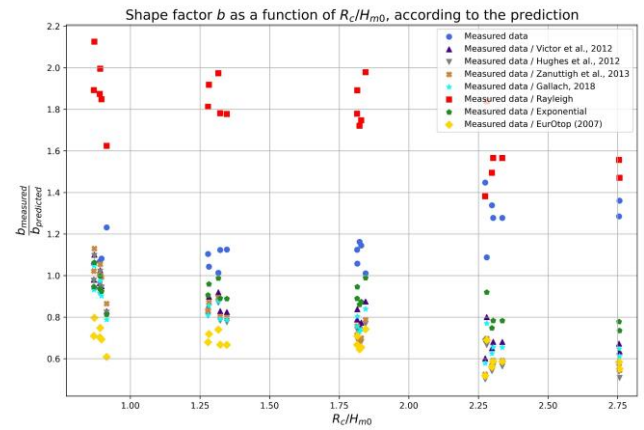
V_{max}, identified in the equations as Y:

Figure 1. Shape factor b as a function of R_c/H_{m0}, according to the predicted values of b for the CWL tests.

Hence, a sensitivity analysis is carried out to find the best fitting, as some of the prediction formulae in literature are intended for a specific portion of the upper volumes (Figure 2).
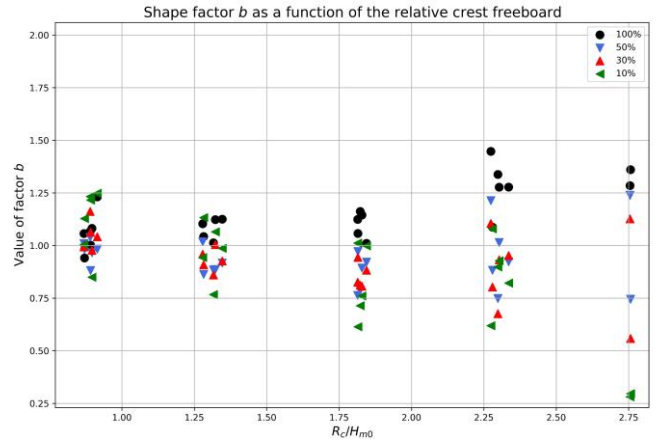

Figure 2. Shape factor b as a function of R_c/H_{m0}, for the upper 100 %, 50%, 30% and 10% volumes, for CWL.

Finally, as expected, the CWL formulation in literature is highly accurate for the prediction of the dataset.

C. Variable water level analysis

For the VWL analysis, 127 tests are considered. However for this case, tests with a considerably low value of P_{ow}, denoted as *non-reliable*, are going to be neglected. Then, the measured values of b can be compared with the predicted ones, firstly for the 100% of the overtopping volumes. As it can be seen from Figure 3, the positive regression displayed by the measured

values of b contrasts with the negative tendency of the prediction formulae when the value of R_c/H_{m0} increases.
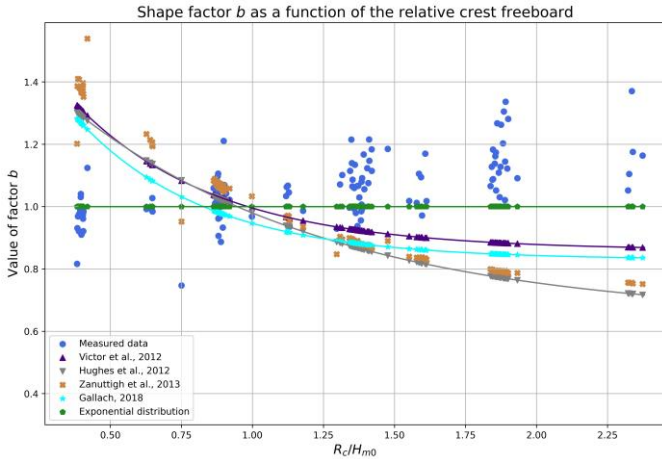

Figure 3. Comparison of the predicted values of b as a function of R_c/H_{m0}, for the considered VWL dataset.

Then, a different portion of the highest overtopping volumes is defined for the sensitivity analysis to see which threshold is the one that most accurately fits the data. Figures 4 and 5 show the measured values of b for the upper 100%, 50, 30% and 10%, as a function of R_c/H_{m0} and P_{ow}, respectively. Both figures show a different tendency of the values from the 100% to the other cases.
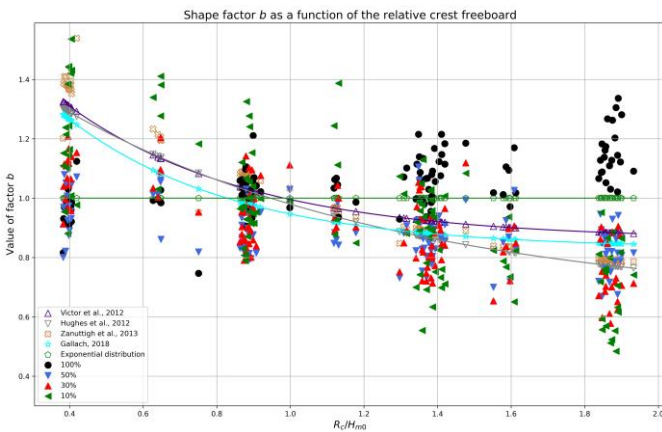
Figure 4. Shape factor b as a function of R_c/H_{m0}, for the upper 100 %, 50%, 30% and 10% volumes, for VWL. Compared between the predicted and measured values.
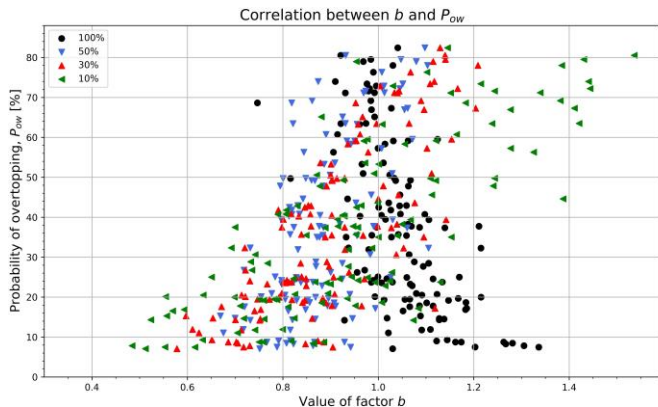
Figure 5. Shape factor b as a function of P_{ow}, for the upper 100 %, 50%, 30% and 10% volumes, for VWL.

Now it is possible to compare these results with the predicted values. Thus, an under and overestimation is observed, while

the overestimation is a bit more noticeable. Moreover, the top 10% case shows a much bigger dispersion, with high under and overestimations of the b-values. This can be seen in Figure 4, which also shows these predicted values.

Regarding the VWL, it is possible to observe that the error of the prediction of b decreases for all prediction methods when the percentage of volumes decreases as well, with very similar results between the formulae. On the other hand, the rMSE of V_{max} shows how the accuracy of the fitting for this variable improves when the portion of the data in the analysis decreases but after a certain threshold, around 25%, the error increases; probably because of the scatter of the results when the number of volumes becomes smaller (see Figure 6).
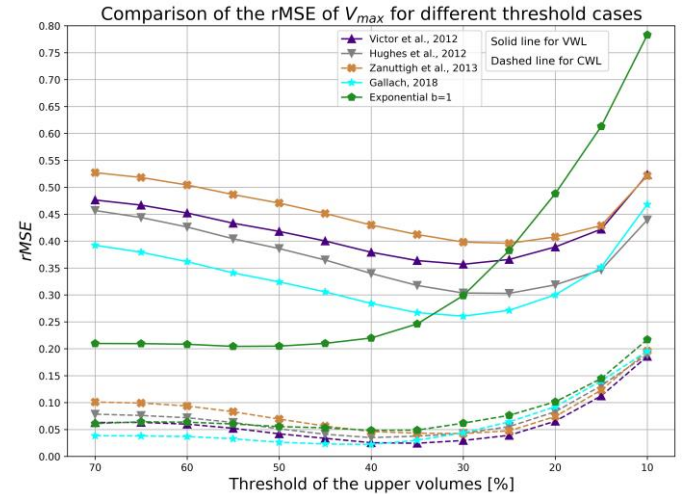
Figure 6. rMSE of Vmax for different thresholds, for the VWL case.

However, in comparison with the CWL situation, the results seem to be less accurate for the VWL case. Thus, the prediction formulae are useful but not as good as for the CWL case. According to these results, it could be said that for the VWL situation the most suitable threshold to predict these parameters is around the 30% of the highest overtopping volumes, for which the best results are found for both Gallach Sánchez, David (2018) and Hughes et al. (2012) formulae.

Finally, before summarizing the study, it can be said that no big differences between the duration of the tests or the seed number that generated the waves modify the results in a noticeable way.

IV. INDIVIDUAL OVERTOPPING ANALYSIS CONCLUSION

The main conclusion of the study claims to focus on the validity of the literature prediction formulae for the VWL situation to predict the individual overtopping volumes. Then, as it could be seen, although the accuracy of the results is not the same than for the CWL case, for which they are intended, the results are quite useful for some certain thresholds considering the upper overtopping volumes, and especially for some of the formulae.

In that sense, as this variable analysis only considers the crest freeboard at the beginning of the test, some considerations can be remarked. Thus, if the 30% threshold is considered for the VWL situation, the results can be compared according to a different value of the crest freeboard. Then, this analysis can be carried out for:

- R_c/H_{m0}. Crest freeboard at the beginning of the test.
- $R_{c,max}/H_{m0}$. Crest freeboard at the end of the test, so the maximum value of R_c is found.

- $R_{c,avg}/H_{m0}$. Average value between the relative crest freeboard considered at the start of the test (R_c) and at the end of it ($R_{c,max}$).
- $(R_c/H_{m0})_{eq}$. It refers to the equivalent non-dimensional freeboard which predicts equally well both CWL and VWL situations, defined by [13] as a function of the non-dimensional freeboard at the peak water level. Hence, its formulation refers to a $R_{c,peak}$ value which stands for the freeboard at the peak of the storm, i.e. the lowest one. The total variation of the water level dh is also considered. Then:

$$(R_c/H_{m0})_{eq} = \frac{R_{c,peak}}{H_{m0}} + exp\left(-1.14\,\frac{R_{c,peak}}{dh}\right)^{0.55} \quad (15)$$

Later, these four cases are compared according to the probability of overtopping P_{ow} in Figure 7, with the theoretical distributions of Gallach (2018), Victor et al. (2012) and the distribution for $b = 0.75$ proposed by Van der Meer and Janssen (1994). Thus, a big difference between both minimum and maximum values of R_c can be seen, as well as the average between them, with a better fitting. For the case considering the value of $(R_c/H_{m0})_{eq}$ defined by [13] a great fitting is found, with the measured values of b between the theoretical predictions and following their tendency even better that the average value.
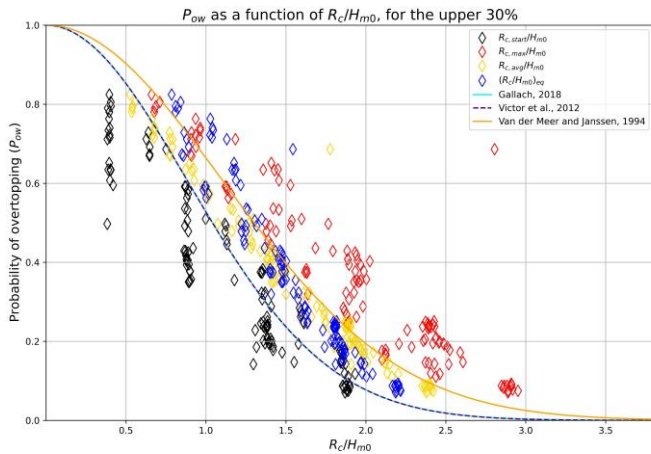
Figure 7. Comparison of P_{ow} with the different relative crest freeboards studied according to the theoretical prediction formulae.

As a conclusion of the analysis, the prediction formulae available in literature can predict the individual overtopping volumes for the VWL situation, if a corrective equivalent non-dimensional freeboard [13] is used, obtaining a huge reduction of the measured rMSE. Moreover, a specific portion of the data needs to be considered to achieve the best results, so only a determined percentage of the highest overtopping volumes is chosen following a sensitivity analysis to define it.

V. PRACTICAL APPLICATION TO THE BELGIAN COAST: RESEARCH DIKE RAVERSIJDE

The Research Dike Raversijde (RDR) falls under the Living Lab Raversijde project launched by the departments of Maritime and Coastal Service (MDK) and Mobility and Public Works (MOW) from the Flemish government, in collaboration with Flanders Marine Institute (VLIZ) [1]. The main objective of the project is to investigate the effects of storm surges as a consequence of an increase of the frequency of extreme sea level events [12]. The RDR is at the beach of Raversijde, in the municipality of Ostend, intentionally located in the backshore of the beach. It is a reinforced concrete structure of 19.5 x 16.5

meters with four different configurations according to its geometry: "A", without promenade; "B", with promenade; "1", without storm wall; and "2", with storm wall. The dike crest is 2.70 *m* high with respect to the dike toe and a 1:2 slope is chosen.

The main objective of the study is to analyze a 1 in 50 yearly return period storm ("Storm 6" measured by [12]) to determine the water level variations that may produce an overtopping event at the dike. For that reason, an estimation of the average overtopping discharge is done, whether for the measured data from the storm in deep conditions as well as for the equivalent non-dimensional freeboard. This comparison with the equivalent non-dimensional freeboard is conducted to redesign the dike for safety conditions following Belgian standards ($q = 1$ *l/s/m*) accurately [14]. The defined section for this purpose is A1, without both promenade and storm wall.

A. Theoretical framework

The available methods and formulae in literature to estimate the overtopping for shallow conditions can be divided in two branches: (*i*) those methods that aim to calculate q from parameters at the toe of the structures, for which a transformation process is required, as long as the known parameters are measured in offshore conditions. And (*ii*) those methods that aim to calculate q directly from deepwater input parameters. Then, the provided parameters from *Storm 6* are measured in deep conditions, and not at the toe of the structure. For that reason, the methods corresponding to case (*ii*) are considered.

Based on Goda et al., (1975), the formulation to estimate q developed by [8] for sloping structures when $h_t/H_{m0,deep} \leq 1$ is defined by Equation (16):

$$\frac{q}{\sqrt{g \cdot H_{m0,deep}^3}} = d \cdot exp\left(-e\,\frac{R_c}{H_{m0,deep}} + f\,\frac{h_t}{H_{m0,deep}}\right) \quad (16)$$

Which depends on 3 parameters d, e and f based on the foreshore slope ($\tan m$), the structure slope ($\tan \alpha$), and the wave steepness ($s_{om-1,0}$). Nevertheless, $s_{om-1,0}$ is obtained using parameters at the toe of the structure, so it is also necessary to use the formulation provided by [8] and [5] to transform the wave height and the wave period, respectively.

B. Overtopping analysis and redesign

The analysis is carried out for the moment in which the storm starts: 31st January of 2022. Hence, the average overtopping discharge is obtained using Equation (16) through the measured data. Moreover, it is noticed that the overtopping tank is fulfilled in the first storm surge cycle, at the peak of the storm. A stepways representation of this is displayed in Figure 8.

Then, the objective is to compare that estimation of Q obtained from Equation (16) with the one that can be obtained using the equivalent non-dimensional freeboard, as a valid method needs to be defined to redesign the dike for a certain value of q. Thus, different values of Q are calculated using both formulae from [2] in normal and shallow conditions using different values of the significant wave height for this purpose. The selected method for the redesign is the one in Figure 9, in which $H_{1/3}$ is used with $(R_c/H_{m0})_{eq}$ to estimate Q. Finally, solving the equation of Q for $R_{c,peak}$ it is possible to determine the freeboard for the most unfavourable situation, which has to be fulfilled at any time for this specific storm to limit the overtopping.
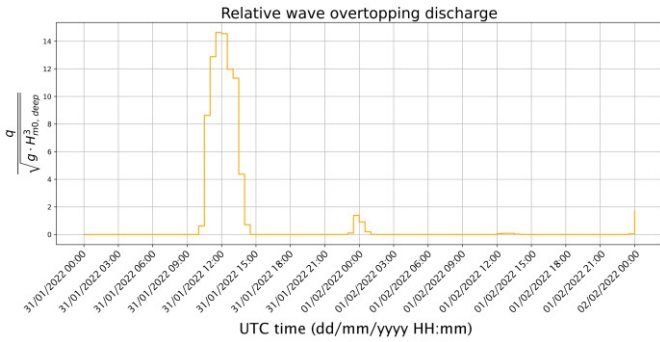
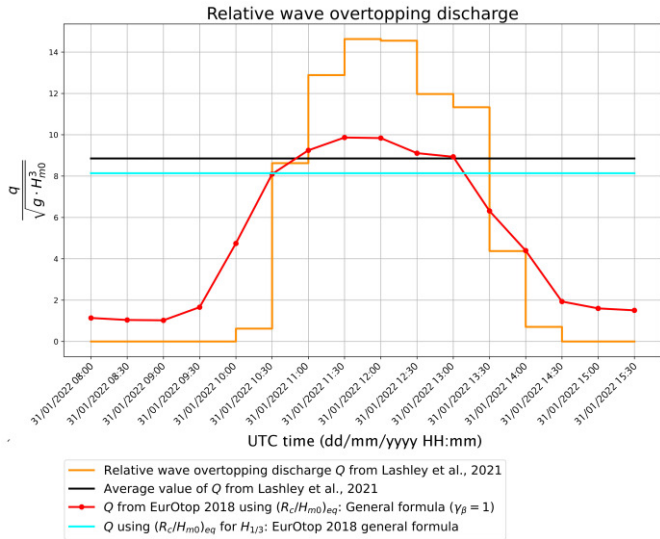Figure 8. Stepways representation for the wave overtopping discharge during the storm.

Figure 9. Comparison between the estimation of the average overtopping discharge from the data analysis and the chosen case using the equivalent non-dimensional freeboard.

With this, the new crest freeboard has to be increased in 2.7 m, up to a total height of 5.4 m. A conceptual sketch of the new geometry is displayed in Figure 10. Finally, it is also possible to do a cost estimation of the required works for the new geometry.
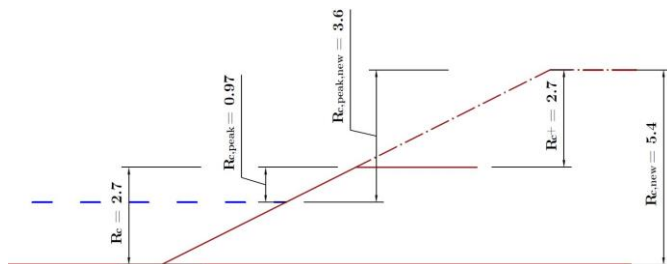

Figure 10. Conceptual sketch of the RDR considering the new crest freeboard.

VI. CONCLUSION

Prediction formulae available in literature are able to predict the individual overtopping volumes for the VWL situation, even though they are intended for a CWL situation. Nevertheless, these results are found when considering the average and the equivalent non-dimensional freeboard defined by [13]. In other words, the prediction formulae available in literature can predict the individual overtopping volumes for the VWL situation if a corrective equivalent non-dimensional freeboard is used.

Special interest is given to the fact of using $(R_c/H_{m0})_{eq}$ as it allows to unify both average and individual approaches with one single set of formulae while structures can be designed according to changes in the SWL as a consequence of storm surges and tidal effects. Moreover, a portion of the data needs to be defined to achieve the best results. Following a sensitivity analysis, it is set to be around the 30% of the upper volumes.

Finally, it is quite important to extend the range of application of the equivalent non-dimensional freeboard, if possible, to achieve an ambitious framework to unify all possible structures and conditions. Hence, more laboratory tests are needed to keep working on this topic and progressing in further understanding of wave overtopping.

REFERENCES

[1] Bellafkih, K. (2021). WL hoogtepunten 2020-2021. Vlaamse Overheid, Departement Mobiliteit en Openbare Werken, Waterbouwkundig Laboratorium: Antwerpen.

[2] EurOtop (2018). Manual on wave overtopping of sea defences and related sturctures: an overtopping manual largely based on European research, but for worlwide application. van der Meer, J. W. and Allsop, NWH and Bruce, T. and De Rouck, Julien and Kortenhaus, Andreas and Pullen, T. and Schüttrumpf, H. and Troch, Peter and Zanuttigh, B.

[3] Franco, L., De Gerloni, M., and Van der Meer, J. (1995). Wave overtopping on vertical and composite breakwaters. In Coastal Engineering 1994, pages 1030–1045.

[4] Gallach Sánchez, David (2018). Experimental study of wave overtopping performance of steep low-crested structures. PhD thesis, Ghent University.

[5] Gruwez, V. (2021). Hydrodynamic modelling of wave interactions with sea dikes on shallow foreshores: A systematic approach by physical and numerical modelling. PhD thesis, Ghent University.

[6] Hughes, S. A., Thornton, C. I., Van der Meer, J. W., and Scholl, B. (2012). Improvements in describing wave overtopping processes. Coastal engineering proceedings, 1(33):35.

[7] Kerpen, N. B., Daemrich, K.-F., Lojek, O., and Schlurmann, T. (2020). Effect of variations in water level and wave steepness on the robustness of wave overtopping estimation. Journal of Marine Science and Engineering, 8(2):63.

[8] Lashley, C. H., Van Der Meer, J., Bricker, J. D., Altomare, C., Suzuki, T., and Hirayama, K. (2021). Formulating wave overtopping at vertical and sloping structures with shallow foreshores using deep-water wave characteristics. Journal of Waterway, Port, Coastal, and Ocean Engineering, 147(6):04021036.

[9] Lykke Andersen, T., Burcharth, H. F., and Gironella, F. (2009). Single wave overtopping volumes and their travel distance for rubble mound breakwaters. In Coastal Structures 2007: (In 2 Volumes), pages 1241–1252. World Scientific.

[10] Makkonen, L. (2006). Plotting positions in extreme value analysis. Journal of Applied Meteorology and Climatology, 45(2):334–340.

[11] Molines, J., Herrera, M. P., Gómez-Martín, M. E., and Medina, J. R. (2019). Distribution of individual wave overtopping volumes on mound breakwaters. Coastal Engineering, 149:15–27.

[12] Peelman, M. (2022). Analysis of sea-swell wave field measurements from offshore until Living Lab Raversijde.

[13] Pepi, Y., Streicher, M., Ricci, C., Franco, L., Bellotti, G., Hughes, S., and Troch, P. (2022). The effect of variations in water level on wave overtopping discharge over a dike: An experimental model study. Coastal Engineering, 178:104199.

[14] Suzuki, T., De Roo, S., Altomare, C., Zhao, G., Kolokythas, G., Willems, M., Verwaest, T., and Mostaert, F. (2016). Toetsing kustveiligheid 2015-methodologie: toetsingsmethodologie voor dijken en duinen. WL Rapporten.

[15] Van der Meer, J.W. and Janssen, J. P. (1994). Wave run-up and wave overtopping at dikes and revetments. Delft Hydraulics.

[16] Van Gent, M. R., Zwanenburg, S. A., and Kramer, J. (2018). Effects of water level variations on the stability of rock armoured slopes. Coastal Engineering Proceedings, (36):44–44.

[17] Victor, L., Van der Meer, J., and Troch, P. (2012). Probability distribution of individual wave overtopping volumes for smooth impermeable steep slopes with low crest freeboards. Coastal Engineering, 64:87–101.

[18] Zanuttigh, B., van der Meer, J., Bruce, T., and Hughes, S. (2013). Statistical characterization of extreme overtopping wave volumes. In From Sea to Shore–Meeting the Challenges of the Sea: (Coasts, Marine Structures and Breakwaters 2013), pages 442–451. ICE Publishing.

Contents

List of Figures

List of Tables

1. Introduction

The still water level (SWL) during a storm is always dynamic (storm surge). The variability of the water level can be schematized as a time-varying hydrograph of a certain duration. Typically, the individual overtopping volume distribution and probability of individual volume overtopping is a function of the ratio between the freeboard R_c (the structure crest elevation above SWL) and the significant wave height H_{m0}.

Since the variation during a storm of the SWL changes the freeboard R_c, the individual overtopping volume is variable. Typically, in the laboratory the wave overtopping on coastal defence structures is investigated for a constant water level (CWL) and a predetermined structural exposure time frame. This exposure time frame is often representative for the storm surge peak or for a statistically representative number of individual waves (e.g., 1000 waves), not considering any variable water level (VWL). For example, the individual volumes in the rise of the storm surge will pre-load (saturate) the dike and potentially weaken it before the largest overtopping volumes occur during the peak of the storm.

An accurate realization of time-dependent individual overtopping volumes for variable water levels is therefore required and identified as lacking from literature. No research exists yet on the study of individual overtopping volumes for a variable water level situation.

2. Motivation of study

The construction of coastal defence structures is becoming increasingly notorious as the concern about climate change and its impact in the sea level is growing. The most important parameter to design these structures according to a safety and economic framework is wave overtopping.

Historically, the estimation and calculation of wave overtopping is a difficult task in terms of accuracy because of the complexity of its parameters. Moreover, different ways to express this overtopping are found in literature. Meanwhile the mean overtopping discharge q has been considered as the key variable to define this phenomenon, recent studies show the necessity to focus the analysis not only in this variable but in the overtopping volumes of individual waves and its maximum value, V_{max}, following a wave-by-wave analysis. Thus, the irregularity of the phenomenon is interpreted appropriately.

But not only recent investigations about climate change may be considered as the unique reasons to deepen in this topic. The fact that storms are more frequent and their intensity tends to be greater is a clear statement. Because of this, the probability of extreme values of waves and storm surges is increasing as well as the risk for coastal structures and population.

For that reason, the SWL needs to be considered as a variable value in time because it is never constant in nature, although it is majorly treated in literature. The comparison between the individual wave overtopping values among both scenarios, CWL and VWL, is definitely necessary to understand the real impact of the phenomenon.

In order to accomplish this project, hydraulic model tests in the wave flume of the Department of Civil Engineering at Ghent University have been carried out during May and June 2021 and a valuable data-set of wave and overtopping measurement for a situation with variable water level was obtained.

Following the motivation of study, the final purpose of this work claims to answer

the questions about how the individual overtopping changes if the water level and wave conditions change during a storm and how this affects to the current prediction guidelines derived for constant water level and wave conditions.

To answer these main questions, several objectives are established:

i) To conduct a thorough literature review with the focus on current prediction guidelines to calculate the individual overtopping volumes, the available experimental studies for a situation with variable water level and to present the natural variability of the water level during a storm surge.

ii) To study the experimental data-set in terms of individual overtopping measurements over a reference dike structure for a variable water level and related test conditions.

iii) To analyze the data-set regarding wave conditions offshore and at the toe of the structure. Most importantly the analysis should include the study of individual overtopping volumes comparing a situation with and without the variation in water level.

iv) To analyze whether the current prediction guidelines for individual overtopping volumes, derived for a constant water level, are also valid for the changing water level situation.

v) To apply the obtained results from the thesis to a practical situation on a real Belgian defence structure and to do preliminary analysis of a realistic and time-dependent representation of individual volumes for the duration of a storm, with and without variable water level.

vi) Finally, to comment and evaluate critically the obtained results and used methods in this Master Thesis.

3. Theoretical framework

The study of wave overtopping is focused on a determined type of structure, similar between each other. These structures are mainly dikes and seawalls, rubble mounds and vertical walls. To be able to understand this phenomenon is essential to enumerate the key parameters and variables which intervene on it.

3.1 Wave and structural parameters for coastal structure studies

3.1.1 Hydraulic conditions

i) **Wave height**. The value used for the wave height is the significant wave height H_s at the toe of the structure. This value can be defined from a statistical point of view as the average of the highest third of waves in a sea state, noted as $H_{1/3}$. On the other hand, the significant wave height can be also defined from the wave spectrum for the zeroth order moment m_0, as the spectral wave height H_{m0}, using the following formula: $H_{m0} = 4\sqrt{m_o}$.

ii) **Wave period**. Various wave periods can be defined for a wave spectrum or wave record. Conventionally, the wave period can be understood as the mean time between two consecutive wave crests at the same point. These wave periods are the peak period T_p (the period that gives the peak of the spectrum), the average period T_m (calculated from the spectrum but preferably from the wave record) and the significant period $T_{1/3}$ (the average of the highest 1/3 of the waves). For overtopping formulae, the spectral period $T_{m-1,0}$ is considered, as this period gives more weight to longer periods in the spectrum, defined as: $T_{m-1,0} = m_{-1}/m_0$; with $m_n = \int_0^\infty Sf^n df$. Where f is frequency and S the spectral density of the water sur-

Symbol	Unit	Definition
SWL	-	Still Water Level
CWL	-	Constant Water Level
VWL	-	Variable Water Level
H_s	m	Significant wave height
H_{m0}	m	Significant spectral wave height
$H_{m0,t}$	m	Significant wave height at the structure toe
$H_{m0,\text{deep}}$	m	Off-shore significant wave height
T_p	s	Peak wave period
$T_{p,\text{deep}}$	s	Off-shore peak wave period
$T_{m,\text{deep}}$	s	Off-shore mean wave period
$T_{p,t}$	s	Peak wave period at the structure toe
$T_{m,t}$	s	Mean wave period at the structure toe
$T_{m-1,0}$	s	Spectral wave period
$T_{m-1,0,\text{deep}}$	s	Off-shore spectral wave period
$T_{m-1,0,t}$	s	Spectral wave period at the structure toe
L	m	Wavelenght
h	m	Water depth at structure toe
h_t	m	Water depth at top of structure toe
h_{deep}	m	Off-shore water depth
h_o	m	Water depth at the paddle
$\cot \alpha$	-	Seaward slope of the structure
$\cot \alpha_u$	-	Seaward slope of the structure above the berm with a horizontal
$\cot \alpha_d$	-	Seaward slope of the structure below the berm with a horizontal
m	-	Foreshore slope, $1 : m$
t	s	Test duration
dh	m	Total variation of water level
R_c	m	Crest freeboard with respect to SWL
R_{cpeak}	m	Crest freeboard at the beginning of the test
R_{cend}	m	Crest freeboard at the end of the test
A_c	m	Armour freeboard
$s_{m-1,0}$	-	Wave steepness based on $T_{m-1,0}$
ξ	-	Breaker parameter
$\xi_{m-1,0}$	-	Breaker parameter based on $T_{m-1,0}$
B_t	m	Toe width
B	m	Berm width
h_b	m	Berm submergence
G_c	m	Crest width
β	$^\circ$	Angle of wave attack

Table 3.1: List of wave parameters symbols.

face elevation (Hofland et al. (2017b)).

iii) **Wavelenght**. It is the horizontal distance between two identical points of two consecutives waves. It is used to define the wave steepness ($s = H/L$) and the relative water depth (d/L). According to this relative water depth, it can be calculated as:

   - Shallow water: $L = T\sqrt{gd}$, where $\sqrt{gd}$ stands for the wave celerity, which is the speed at which a wave form propagates.

   - Deep water: $L = L_0 = \dfrac{gT^2}{2\pi}$

   - Transitional water: $L = \dfrac{gT^2}{2\pi}\tanh\left(\dfrac{2\pi d}{L}\right)$, in which an iterative calculation is usually needed.

iv) **Wave steepness**. Wave steepness is defined as the ratio between wave height and wavelength: $s = H/L$. This parameter is an indicator to know if the waves are breaking or not. Low values of steepness ($s_0 = 0.01$) are associated with swell sea states, meanwhile greater values ($s_0 = 0.04$ to 0.06) are associated with wind sea. A bigger value from $s_0 = 0.07$ indicates that the wave is getting too steep, and it will break. According to the value of the wave period that defines the wavelenght, in deep or shallow water, the value of the wave steepness parameter will vary.

v) **Breaker parameter**. The breaker parameter, also known as the Iribarren number, is used to describe the effects of wave breaking and wave run-up in different structures. It is denoted as ξ and defined with the following expression:

$$\xi = \frac{\tan\alpha}{\sqrt{H/L_0}} \quad \text{with} \quad L_0 = \frac{g}{2\pi}T^2 \tag{3.1}$$

With this, the breaker parameter relates the slope steepness $\tan\alpha$ to the wave steepnes in deep water conditions $s = H/L_0$. This formulation is also applicable to spectral parameters H_{m0} and $T_{m-1,0}$.

vi) **Depth**. The water depth is considered as the vertical distance between the water level and the seabed. Different definitions of water level can be found depending on water conditions. Moreover, as mentioned in the definition of the wavelenght, it is possible to make a classification according to water depth, in relative terms. Depending on the ratio d/L, the classification is shown in Figure 3.1.
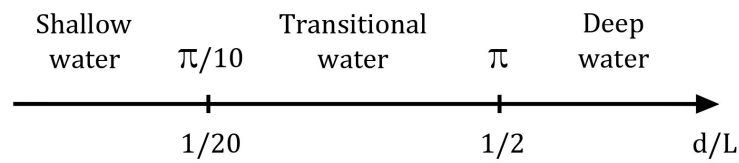
Figure 3.1: Classification according to water depth (CEM Part II. Chapter 1).
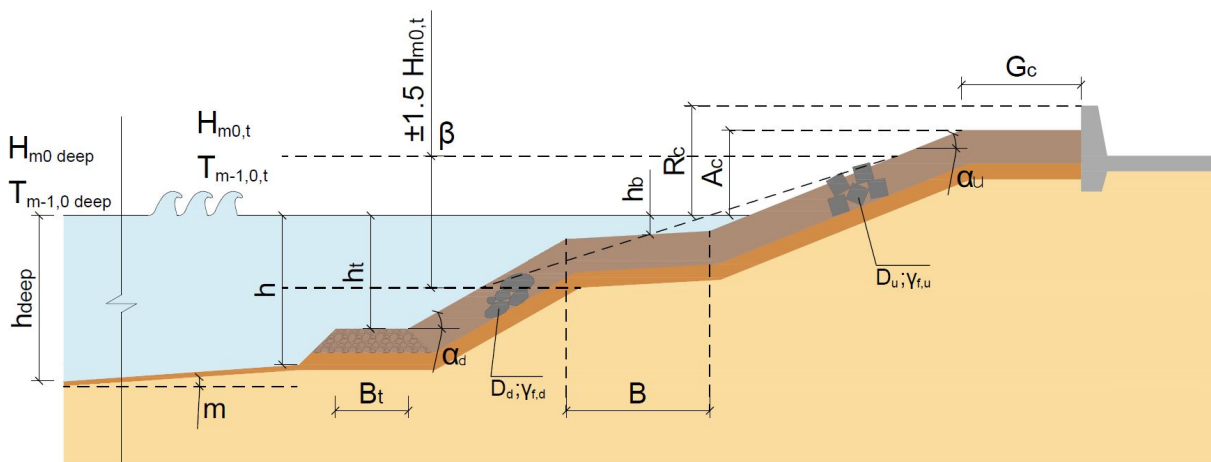
Figure 3.2: Conceptual sketch of wave parameters, adapted from EurOtop (2018).

3.1.2 Structure geometry

i) **Crest freeboard**. The crest freeboard R_c is defined as the vertical distance from the water level to the highest point of the structure where overtopping water can no longer return to the seaside. For rubber mound breakwaters, this crest freeboard is different to the value of the armour freeboard A_c, which is the height of the horizontal part of the rubble mound crest.

ii) **Crest width**. It is the horizontal distance from the end of the sloping side at seaside to the leeside edge. It is denoted with letters G_c.

3.2   Wave overtopping concept

To understand further topics, it is quite necessary to define the main concept of this work. Wave overtopping as a phenomenon, from an energy balance perspective, is the amount of water which is transmitted over the crest instead of being reflected or dampened (breaking).

Hence, different ways to measure this wave overtopping can be found. For instance, it is also possible to distinguish between the average wave overtopping discharge and the individual wave overtopping volume. While the first one refers to the volume of water passing over the structure per unit of time and per meter, the second one refers to the specific amount of water as the consequence of a certain overtopping event. Both concepts will be developed in further sections.

Both variables are related to tolerable amounts of wave overtopping in order to satisfy security and safety factors.

The concept of wave overtopping is also related to the wave run-up and run-down. Thus, wave run-up is just the elevation of the sea level produced by waves at the shoreline, in other words, it is the variation in time of the vertical position of the water's edge on the foreshore of the beach. It determines the design crest level in case where no overtopping is accepted. Besides, it has a high importance in coastal processes, especially during extreme conditions and combined with high tidal levels and large storm surges.

3.3   Wave overtopping predictions

Wave overtopping is fundamental to define the degree of safety of coastal structures, as well as people's safety in maritime areas. For that reason, the accuracy of the wave overtopping predictions is quite important in every design project. Due to the nature of the overtopping phenomenon, analytical formulae are not possible to be applied in this case. For that reason, the empirical data collected from wave flumes and basins is used to establish the framework of empirical formulae used to predict the overtopping discharges.

In this line, several physical models have been developed from the 1950s to measure the wave run-up and overtopping on different slopes Saville and Caldwell (1953) and Saville (1955). This data was used by Weggel (1977) to define an overtopping formula for regular waves. After that, various authors, Tsuruta and Goda (1968), Goda (1971),

Battjes (1974) and Ahrens (1977), used those results to predict the wave overtopping for irregular waves.

After that, different investigations were focused on the type and geometry of the structure although Douglass (1985) and Douglass (1986) concluded that more data about wave overtopping for irregular waves was needed to satisfy the admissible threshold of accuracy. By then, investigations tried to expand the knowledge for different wave and structural conditions.

De Waal and Van der Meer (1992) introduced the 2% run-up on a non-overtopped slope $R_{u2\%}$ for non-breaking waves. Then, Van der Meer and Janssen (1994) presented two different formulae for breaking and non-breaking wave conditions, depending on the crest freeboard and the incident spectral wave height. Franco et al. (1994) presented a new formula to predict the average overtopping of vertical walls in deep water conditions. This line of investigation was extended for different kind of wave conditions during the last years of 1990s.

Between 2002 and 2004, the CLASH Project (De Rouck et al. (2009), Verhaeghe et al. (2004) and Medina et al. (2005)) developed and studied in a much deeper way the wave overtopping process for various types of structures and wave conditions. Its main goal was to define an extensive dataset to fill the existing data and generate and homogeneous background. This was accomplished with physical model tests and field measurements in different European locations. According to this CLASH data, several research were developed to predict in a better way the wave overtopping as a neural network: Formentin et al. (2017) and Van Gent et al. (2007).

The overtopping neural networks are widely used to predict the average overtopping discharges of coastal structures with various complex geometries, and even recent studies continue to keep improving the existing tools, such as the article previously mentioned Formentin et al. (2017) and other authors such as Zanuttigh et al. (2016) or Molines and Medina (2016).

3.4 Wave overtopping manuals

Historically, overtopping has been treated as a part of coastal engineering itself, not as a separated topic. The first manual that included the specific aspects and parameters about wave overtopping was the Shore Protection Manual in 1973 (SPM, US Army Corps
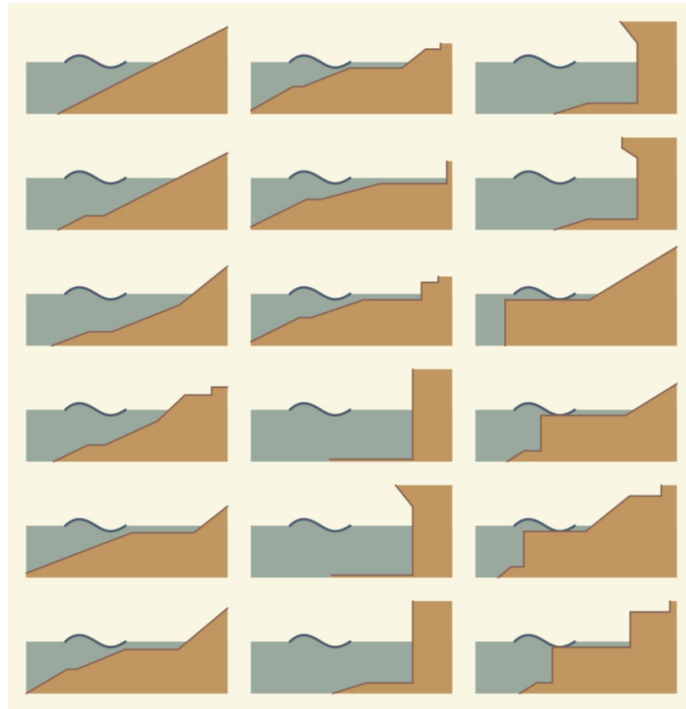
Figure 3.3: Overall view of different possible structure configurations for the neural network. Source: EurOtop (2018)

of Engineers). It also included all the available knowledge about coastal engineering by that time. After this first edition of the SPM, there were other four more editions until the year 1984.

After that, the Coastal Engineering Manual (CEM, US Army Corps of Engineers) was published in 2002 as an update and more complete version of the Shore Protection Manual. This manual is divided into six different chapters.

By that year, several specific manuals regarding wave overtopping were published in Europe: the (UK) Environment Agency Manual on Overtopping edited by Besley (EA, 1999); the (Netherlands) TAW Technical Report on Wave run-up and wave overtopping at dikes, edited by Van der Meer (TAW, 2002); and the German Die Küste (EAK, 2002) edited by Erchinger. According to this and in addition to the available data from the CLASH Project, the EurOtop (2007) manual was published to summarize all the available information as guideline of recommendations on the analysis and prediction of wave overtopping in different sea structures.

Almost ten years later, a second edition of the EurOtop manual (2016) was pub-

lished to improve the background knowledge about wave overtopping. This version was finally updated in 2018, reaching to the current version of the EurOtop manual.

EurOtop (2018) enumerates different methods to predict wave overtopping of coastal structures. It recommends approaches for calculating mean overtopping discharges, overtopping wave volumes and the proportion of waves overtopping a seawall. By this aim, the EurOtop is understood as a recommendation, not a strict guide. Limiting tolerable discharges or overtopping wave volumes for design wave conditions are set, so then the prediction methods are used to verify that these discharges are not exceeded.

3.5   Average overtopping discharge prediction formulae

The overtopping measured per unit of time and for meter $[l/s/m]$ is called average overtopping discharge (q). This is the volume of water passing over the structure per unit of time, indeed. Despite this work is focused on the individual overtopping volume, it is necessary to introduce the concept and prediction of the average overtopping.

The average overtopping discharge q can only be calculated for quasi-stationary wave and water level conditions (EurOtop (2018)). To determine the quantity of water that overtops a structure during a storm event, it is necessary to calculate the average overtopping discharge for each set of storm water levels and wave conditions.

As wave overtopping depends on the freeboard R_c and the wave height, Owen (1980) proposed an empirical formula with two fitted coefficients a and b, using the spectral significant wave height to determine the average overtopping discharge. With this, the average overtopping discharge (q) generally decreases exponentially as the crest freeboard (R_c) increases:

$$\frac{q}{\sqrt{gH_{m0}^3}} = a\exp\left(-b\frac{R_c}{H_{m0}}\right) \tag{3.2}$$

This proposed equation had the inconvenient of bad behaviours, with an overestimation of the overtopping discharge, at very small or inexistent freeboards, as it is an exponential-type formulation. For that reason, Van der Meer and Bruce (2014), who reanalysed the existing formulation with 15 different datasets from CLASH and three further datasets, two from the original dataset of Franco et al. (1994) and the basic dataset of vertical walls at the end of a 1:50 foreshore of Allsop (1995), reached to a formula to predict the overtopping at low and zero freeboard conditions using the Weibull distribution

with a fitted shape factor (c):

$$\frac{q}{\sqrt{gH_{m0}^3}} = a \exp\left[\left(-b\frac{R_c}{H_{m0}}\right)^c\right] \quad \text{for } R_c \geq 0 \tag{3.3}$$

After this contextualization, wave overtopping can be described according to the breaker parameter ($\xi_{m-1.0}$), for breaking waves (plunging) or non-breaking waves (surging). In addition to other parameters such as the influence factors, a general formulation is reached, for the specific case of the average overtopping discharge on a slope: dike, levee, embankment.

$$\frac{q}{\sqrt{gH_{m0}^3}} = \frac{0.023}{\sqrt{\tan\alpha}}\gamma_b \cdot \xi_{m-1,0} \cdot \exp\left[-\left(2.7\frac{R_c}{\xi_{m-1,0} \cdot H_{m0} \cdot \gamma_b \cdot \gamma_f \cdot \gamma_\beta \cdot \gamma_v}\right)^{1.3}\right] \tag{3.4}$$

with a maximum of

$$\frac{q}{\sqrt{gH_{m0}^3}} = 0.09 \cdot \exp\left[-\left(1.5\frac{R_c}{H_{m0} \cdot \gamma_f \cdot \gamma_\beta \cdot \gamma*}\right)^{1.3}\right] \tag{3.5}$$

Where the γ coefficients, which will be explained in detail in Section 3.5.4, are the influence factors for:

- γ_b: The berm.

- γ_f: The roughness of the elements on the slope.

- γ_β: The obliquity of the incident waves.

- γ_v: The effect of a wall at the end of a slope.

- And where $\gamma*$ is added for considering non-breaking waves on a slope.

This formulation is appropriate for the prediction of the average discharge or mean value approach. However, for the design and assessment approach it is strongly recommended to increase the average discharge by about one standard deviation. This statement leads to the following formulation:

$$\frac{q}{\sqrt{gH_{m0}^3}} = \frac{0.026}{\sqrt{\tan\alpha}}\gamma_b \cdot \xi_{m-1,0} \cdot \exp\left[-\left(2.5\frac{R_c}{\xi_{m-1,0} \cdot H_{m0} \cdot \gamma_b \cdot \gamma_f \cdot \gamma_\beta \cdot \gamma_v}\right)^{1.3}\right] \tag{3.6}$$

with a maximum of

$$\frac{q}{\sqrt{gH_{m0}^3}} = 0.1035 \cdot \exp\left[-\left(1.35\frac{R_c}{H_{m0} \cdot \gamma_f \cdot \gamma_\beta \cdot \gamma*}\right)^{1.3}\right] \qquad (3.7)$$

3.5.1   Influence of shallow foreshores on wave overtopping

The previous formulation could be transformed to evaluate the effect of a foreshore in front of the structure. The foreshore is defined according to its slope, so the effect of the incident waves will be different. Nevertheless, Goda (2009), the Rock Manual CIRIA, CUR and CETMEF (2007) and the Coastal Engineering Manual US Army Corps of Engineers (2002) use different definitions to approach it.

It is also defined according to the water depth at the toe of the dike Van Gent (1999), so thus it is possible to determine the effect of the foreshore on the incident waves.

The general formula for wave overtopping at shallow foreshores with $\xi_{m-1,0} > 7$ and $s_{m-1,0} > 0.01$ is given as mean value approach by:

$$\frac{q}{\sqrt{gH_{m0}^3}} = 10^c \cdot \exp\left(-\frac{R_c}{\gamma_f \cdot \gamma_\beta \cdot H_{m0} \cdot (0.33 + 0.022 \cdot \xi_{m-1,0})}\right) \qquad (3.8)$$

Where c is a stochastic variable that can be:

- $c = -0.79$ for mean value approach. With mean -0.79 and a standard deviation of $\sigma(-0.79) = 0.29$.

- $c = -0.50$ for design and assessment approach, adding one standard deviation of $(-0.79 + 0.29 = -0.5)$.

3.5.2   Vertical and steep slopes particularization

Steep slopes are in the range of general sloping structures and vertical walls. The formula for vertical walls is considered only for relatively deep water, without sloping foreshore. The mean value approach for this case is expressed by the following formula:

$$\frac{q}{\sqrt{gH_{m0}^3}} = 0.047 \cdot \exp\left[-\left(2.35\frac{R_c}{H_{m0} \cdot \gamma_f \cdot \gamma_\beta}\right)^{1.3}\right] \qquad (3.9)$$

Comparing both limiting cases, if slopes become very steep, up to vertical, the overtopping discharge is inversely proportional and will decrease.

To fill this gap, it is obvious that the link between both cases is the slope angle (cot alpha). In this line, an overall formula that combines these two general equations according to cot alpha is established:

$$\frac{q}{\sqrt{gH_{m0}^3}} = a \exp\left[-\left(b\frac{R_c}{H_{m0}}\right)^c\right] \tag{3.10}$$

(non-breaking waves)

$a = 0.09 - 0.01\,(2-\cot\alpha)^{2.1}$ for $\cot\alpha < 2$ and $a = 0.09$ for $\cot\alpha \geq 2$

$b = 1.5 + 0.42\,(2-\cot\alpha)^{1.5}$, with a maximum of $b = 2.35$ and $b = 1.5$ for $\cot\alpha \geq 2$

As expected, the formula gives the mean value approach. For a design or safety assessment approach it will be necessary to add one standard deviation, so both coefficient a and b are modified (EurOtop (2018)). However, this formula is appropriate for milder slopes rather than steep. For $\cot\alpha = 0$ it will be necessary to use the specific influence factor for vertical walls, available at Chapter 7 of EurOtop (2018).

3.5.3   Zero and negative freeboard

The zero freeboard case can be treated as the cases shown above for the value of $R_c = 0$, so the exponential component of the equation is not considered.

For the negative freeboard, it is quite clear that the overtopping discharge will be greater. In that sense, there will be an amount of water attributed to overflow and another component attributed to overtopping. The overflowing water can be calculated as:

$$q_{overflow} = 0.54 \cdot \sqrt{g \cdot |-R_c^2|} \tag{3.11}$$

The overtopping water is calculated in the same way as the zero freeboard case.

3.5.4   Effect of influence factors on wave overtopping

According to what mentioned in Section 3.5, the influence factors are different parameters that affect the wave run-up and overtopping. Those that are considered in the EurOtop (2018) formulation are:

- γ_f: Influence factor for roughness elements on the slope.

- γ_b: Influence factor for a berm.

- γ_β: Influence factor for oblique wave attack.

- γ_v: Influence factor for a wall on a slope (different from a vertical wall sea dike).

- γ_*: combined influence factor for a storm wall on a slope.

These parameters can be calculated using different methods or they can even be already tabulated. A value of 1 means no influence, meanwhile a smaller value than 1 means a certain influence of any of these factors, which may decrease the wave overtopping discharge. In laboratory conditions for model tests, these values are considered as 1.

The influence of roughness elements on the slope or the roughness of the slope by itself is an important factor to reduce wave overtopping. This fact can be reached through grass, asphalt, natural or artificial revetments, etc. The permeability of the structure is also taken into account with this factor. The objective of including these elements to reduce the wave run-up and wave overtopping is mainly the possibility to reduce the crest height too.

The influence of grass is noticeable for wave heights less than 0.75 m. For bigger values of H_{m0} the influence of grass can be neglectable. In that case, the influence factor γ_f follow equation 3.16:

$$\gamma_f = 1.15 H_{m0}^{0.5}, \quad \text{for } H_{m0} < 0.75\,m \tag{3.12}$$

For different revetment elements, the value of the influence factor is tabulated as in Table 3.2. Moreover, influence factors for roughness for rock and concrete armour layers are also deeply studied and tabulated, see Table 3.3.

The effect of oblique waves is also considered in the formulation, as these oblique waves with concave curves produce an increase of wave run-up and wave overtopping, due to the accumulation of wave run-up energy. This obliquity is measured according to the angle of wave attack β which is defined at the toe of the structure after any wave transformation transformation on the foreshore as the angle between the direction of the waves and the perpendicular to the long axis of the dike or revetment. Then, if waves

Embankment revetment material	γ_f
Concrete	1.0
Asphalth	1.0
Closed concrete blocks	1.0
Grass	1.0
Basalt, basalton	0.9
Placed revetment blocks (Haringman, Fixtone)	0.9

Table 3.2: Surface roughness factors for typical embankment revetments. Source: EurOtop (2018).

Type of armour layer	γ_f
Smooth impermeable surface	1.00
Rocks (1 layer, impermeable core)	0.60
Rocks (1 layer, permeable core)	0.45
Rocks (2 layers, impermeable core)	0.55
Rocks (2 layers, permeable core)	0.40
Cubes (1 layer, flat positioning)	0.49
Cubes (2 layers, random positioning)	0.47
Antifers	0.50
HARO	0.47
Tetrapods	0.38
Dolosse	0.43
Accropode I	0.46
Xbloc; Core Loc; Accropode II	0.44
Cubipods (1 layer)	0.49
Cubipods (2 layers)	0.47

Table 3.3: Surface roughness factors for permeable rubble mound and impermeable structures, and different type of armour layers, with a slope of 1:1.5. Source: EurOtop (2018).
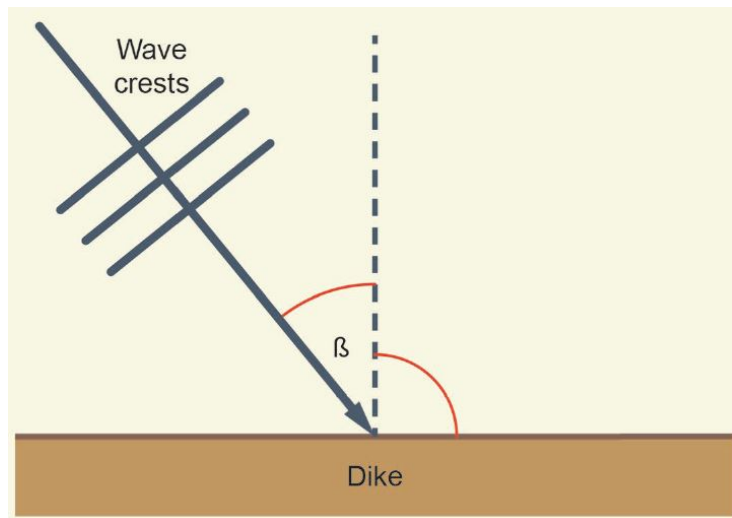
Figure 3.4: Definition af angle of wave attack β. Source: EurOtop (2018).

are perpendicular to the toe, this angle will be zero. The available formulation takes into account both short-crested and long-crested waves.

For short-crested waves:

- Wave run-up:

$$
\begin{aligned}
\gamma_\beta &= 1 - 0.0022|\beta| \quad \text{for: } 0° \leq \beta \leq 80° \\
\gamma_\beta &= 0.824 \quad \text{for: } |\beta| > 80°
\end{aligned}
\tag{3.13}
$$

- Wave overtopping:

$$
\begin{aligned}
\gamma_\beta &= 1 - 0.0033|\beta| \quad \text{for: } 0° \leq \beta \leq 80° \\
\gamma_\beta &= 0.736 \quad \text{for: } |\beta| > 80°
\end{aligned}
\tag{3.14}
$$

For long-crested waves:

$$
\begin{aligned}
\gamma_\beta &= \cos^2(|\beta| - 10°) \quad \text{with a minimum of: } \gamma_\beta = 0.6 \\
\gamma_\beta &= 1 \quad \text{for: } |\beta| = 0° - 10°
\end{aligned}
\tag{3.15}
$$

Currents are also another possible effect on overtopping however it is usually neglected. As this work is mainly focused on the effect of storm surges in the water level

Figure 3.5: Example of typical berm. Source: EurOtop (2018).

and currents are a consequence of storm surges, it is important to mention this effect. Although for small currents this is almost no notable, stronger currents may affect the wave height, wave period and the incident angle, so the overtopping. The following thresholds are considered to use currents in wave overtopping formulation, according to the velocity of current U:

- For wave heights $H_{m0} = 0.5 - 1\,m$: effects of current starts for $U > 0.75\,m/s$

- For wave heights $H_{m0} \sim 2\,m$: effects of current starts for $U > 1\,m/s$

Below these thresholds, equations 3.13 and 3.14 can be used.

Another key aspect to reduce wave run-up and wave overtopping is the presence of a berm. A berm is a part of a dike or coastal profile in which the slope varies between horizontal and 1:15. This parameter depends on the width of the berms and on the vertical distance from the SWL to the middle of the berm. The reduction of wave run-up is more effective is the berm is on the still water line and its influence reduces with the depth. Anyway, the presence of a berm makes smaller the equivalent slope angle, so it reduces overtopping and leads to a lower required crest level.

Then, influence factor for a berm depends on two parameters r_b and r_{db}:

$$\gamma_b = 1 - r_b(1 - r_{db}) \quad \text{for } 0.6 \leq \gamma_b \leq 1.0 \tag{3.16}$$

Where r_b represents the influence of the width of the berm L_{Berm}, with a value of zero is there is no berm; and r_{db} represents the vertical distance d_b between the still water level (SWL) and the middle of the berm, with a value of zero if the berm lies on the still water line. Thus:

$$r_b = \frac{B}{L_{berm}} \tag{3.17}$$

$$
\begin{aligned}
r_{db} &= 0.5 - 0.5\cos\left(\pi\frac{d_b}{R_{u2\%}}\right) && \text{for a berm above still water line} \\
r_{db} &= 0.5 - 0.5\cos\left(\pi\frac{d_b}{2\cdot H_{m0}}\right) && \text{for a berm below still water line} \\
r_{db} &= 1 && \text{for berms lying outside the area of influence}
\end{aligned}
\tag{3.18}
$$

3.6 Individual overtopping volumes

Until now, the main parameter to explain wave overtopping is the average overtopping discharge q, which as explained in Section 3.5, it is the amount of water that passes over the crest divided by the period of time in which that amount of water was measured. Although this value can be useful, the real behaviour of the structure is completely different as only the biggest waves produce overtopping and these volumes are completely irregular. Indeed, wave overtopping is not only irregular in time but also spatially along the whole dike.

In that sense, a wave-per-wave analysis is needed to understand the response of the structure to a single wave overtopping event that can affect its stability.

Moreover, the maximum wave overtopping discharge during an overtopping event may be extremely larger than the mean overtopping value. That's why recent manuals also include specifies values for a tolerable V_{max} in order to provide a security range for the structure stability, pedestrians and vehicles.

3.6.1 Probability distribution of individual overtopping volumes

Individual wave overtopping events are random and irregular, for this reason, it is also necessary to describe them by following a probability distribution about the ex-

ceedance probability of the event. This analysis takes into account the average overtopping discharge (q), the probability of overtopping (P_{ow}) and the storm duration.

A two-parameter Weibull distribution is usually used to describe the distribution of individual wave overtopping volumes (Franco et al. (1995) and Van der Meer and Janssen (1994)). Then, the exceedance probability of each overtopping volume (P_v):

$$P_v = P[V_i \geq V] = exp\left(-\left(\frac{V}{a}\right)^b\right) \tag{3.19}$$

This equation has a shape parameter b and a scale parameter a. Hence, coefficient b determines the shape of the distribution. A value of $b = 0.75$ was first established by Van der Meer and Janssen (1994) for sloped coastal structures. However, if the overtopping discharge is important (EurOtop (2018)), the shape factor b should increase. For small values of b, the average overtopping discharge is determined by a small number of overtopping volumes but with larger maximum volumes. When b increases, the overtopping volumes become more similar between each other and similarly distributed (Gallach Sánchez, David (2018)). For a shape factor of $b = 2$, the Weibull distribution describes a Rayleigh wave height distribution.

The scale factor a can be calculated using the ratio of the total overtopped volume (V_0), as the sum of individual volumes (V_i) and the sum (T_0) of the wave periods of each wave in the wave train (T_i) (Victor et al. (2012)). Then:

$$q = \frac{V_0}{T_0} = \frac{\sum V_i}{\sum T_i} = \frac{\sum V_i}{N_w T_m} \tag{3.20}$$

If this is divided by the number of overtopping waves N_{ow}, the measured mean overtopping volume V_{meas} is reached (Victor et al. (2012)).

$$\frac{q N_w T_m}{N_{ow}} = \frac{\sum V_i}{N_{ow}} \tag{3.21}$$

$$\bar{V}_{meas} = \frac{\sum V_i}{N_{ow}} = \frac{V_0}{N_{ow}} \tag{3.22}$$

Based on the definition of a two-parameter Weibull distribution, the theoretical mean overtopping volume follows the next expression (Victor et al. (2012)), where Γ is the mathematical gamma function:

$$\bar{V}_{theor} = E[V]_{Weibull} = a\Gamma\left(1 + \frac{1}{b}\right) \tag{3.23}$$

Then, if both measured and theoretical values are equal, the relationship between factors a and b is:

$$a = \frac{1}{\Gamma\left(1 + \dfrac{1}{b}\right)}\bar{V}_{meas} \tag{3.24}$$

Which can be simplified following Victor et al. (2012) using the parameter a' as:

$$a' = \frac{1}{\Gamma\left(1 + \dfrac{1}{b}\right)} \tag{3.25}$$

According to Victor et al. (2012), who performed 364 2D tests in the wave flume at Ghent University on smooth impermeable structures and obtaining the dataset UG10, for a range of slope angles between $0.36 \geq \cot\alpha \geq 2.75$, a range of relative crest freeboards R_c/H_{m0} between $0.11 \geq R_c/H_{m0} \geq 1.69$ and a range of wave steepness between $0.02 \geq s_{m1,0} \geq 0.05$; this relationship between a' and shape factor b can be expressed accurately by using a hyperbolic tangent fit for b, with a determination coefficient r^2 of 0.96.

$$a' = 1.13\tanh(1.132b) \tag{3.26}$$

The value of a' for a shape factor of $b = 0.75$ is 0.84. This shape factor is commonly applied for smooth structures, where wave steepness and the type of smooth structures are neglected.

3.6.2 Estimation of shape factor b

Shape factor b has been studied by various authors in the past, according to a specific type of structure.

For mild sloping structures, the previous value of $b = 0.75$ was adopted by Van der Meer and Janssen (1994) and Franco et al. (1994), considering no dependence on wave steepness or slope angle. Bruce et al. (2009), who performed a total of 179 tests over 13 different armour types/configurations, plus 18 tests with smooth slope ($\cot\alpha = 1.5$),
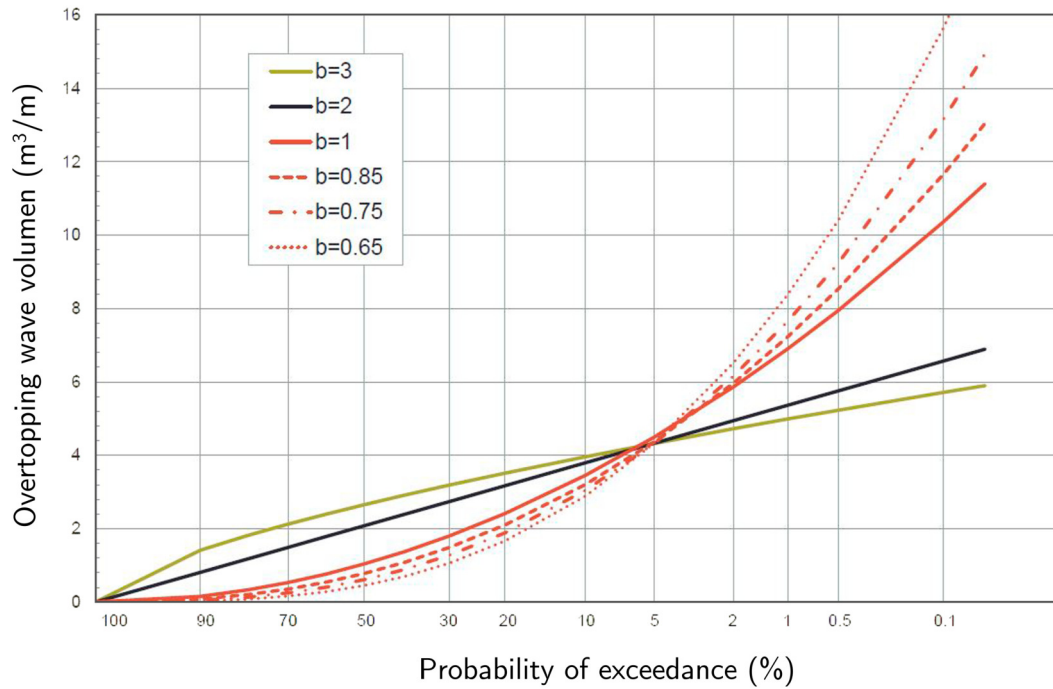
Figure 3.6: Theoretical probability distributions on a Rayleigh scale graph, for different values of *b*. Adapted from EurOtop (2018)

giving typically 14 tests per configuration, defined a value of $b = 0.74$ for both smooth sloping structures and rubble mound structures.

On the other hand, Besley (1999), who developed a manual to provide a set of consistent and reliable design techniques for wave overtopping as the result of re-analysing the existing researches for both normal and oblique wave attack as well as for both dyke and composite caisson structures, did find a relatively influence of steepness on the value of factor b. For a wave steepness of $s_{0p} = 0.02$, the proposed value of *b* is 0.76, but for $s_{0p} = 0.04$, the value of *b* increases to 0.92.

According to the further analysis in Chapter 6, the following authors and distributions will be considered as shown in the following enumeration.

i) Victor et al., 2012

For steep low-crested structures the previous considerations were not valid. For that reason, Victor et al. (2012) found an effect of the slope angle and the relative crest freeboard R_c/H_{m0} on the coefficient *b* and studied individual wave overtop-

ping volumes on steep, low crested structures with smooth and impermeable slopes ($0.11 \leq R_c/H_{m0} \leq 1.69$ and $0.36 \leq \cot\alpha \leq 2.75$). Using a composite Weibull distribution, they concluded that deviations were produces by depth induced breaking of the largest waves in the wave trains, which limited the maximum individual overtopping volume and produced a decrease in the value of the shape factor b. For the analysis, they considered the effect of the relative crest freeboard (R_c/H_{m0}), the slope angle ($\cot\alpha$) and the wave steepness ($s_{m-1,0}$), in which the derived potential effect of the wave steepness can be neglected. For this, the highest 50% of the overtopping volumes was considered. Hence, the following formula was proposed for the calculation of factor b:

$$b = \exp\left(-2.0\frac{R_c}{H_{m0}}\right) + 0.56 + 0.15\cot\alpha \qquad (3.27)$$

ii) Hughes et al., 2012

Hughes et al. (2012) did a second analysis based on the tests from Van der Meer and Janssen (1994), Hughes and Nadal (2009) and Victor et al. (2012) in order to achieve more accurate results to estimate the shape factor b of the Weibull distribution. The conclusion was a new formula that only considered the top 10% of the individual wave overtopping volumes and neglected the lower ones, using the relative crest freeboard as the only variable in the relationship. A range of $-2 < R_c/H_{m0} < 4$ and $0 \leq P_{ow} \leq 1$ is considered. Then, the best fit of the values is obtained following the next formula:

$$b = \left[\exp\left(-0.6\frac{R_c}{H_{m0}}\right)\right]^{1.8} + 0.64 \qquad (3.28)$$

iii) Zanuttigh et al., 2013

Zanuttigh et al. (2013) who analysed the dataset of Low Crested rubble-mound Breakwaters from 2D tests performed at the University of Firenze, and 3D tests carried out at Aalborg University and at the Polytechnic of Bari, as well as specific tests on overtopping from the CLASH (2004), studied the shape factor of both cases of smooth slope and rubble mound breakwater distributions. It was concluded that rubble mound structures showed more scatter in the factor b than smooth impermeable structures, but the same trend was found. Hence, the authors of the formula suggested relating the shape factor to the dimensionless mean wave overtopping

discharges instead of the relative crest freeboard (R_c/H_{m0}), as mean overtopping discharge implicitly includes information about wave steepness or slope angle. Finally, two formulae were proposed to calculate b, one for smooth structures and other for rubble mound structures. The one for smooth structures is the one considered in this analysis, which is shown in the next equation:

$$b = 0.73 + 55 \left(\frac{q}{g H_{m0} T_{m-1,0}} \right)^{0.8} \tag{3.29}$$

For this formula, as it is said in EurOtop (2018), the value of the average overtopping discharge q, although experimental tests are carried out and q can be easily obtained through this data, as in this study case, the input parameter of this value in the formula has to be calculated using Equation 3.7, also given in EurOtop (2018) for non-breaking conditions. Then, this is the procedure to follow in the further analysis. Its main parameters are the spectral wave height (H_{m0}) and the crest freeboard (R_c). Moreover, as mentioned in Section 3.5.4, the influence factors are all 1, as laboratory conditions are considered.

iv) Gallach Sánchez, 2018

Gallach Sánchez, David (2018) studied the wave overtopping of steep low-crested structures and aimed to reached to a more accurate formula than the ones available in literature. Thus, an exponential formula dependant on the relative crest freeboard (R_c/H_{m0}) as well as on the slope angle (α) was fitted according to 1223 tests. Hence, a more complete formula is obtained in comparison to Victor et al. (2012) and Hughes et al. (2012). The proposed formula is shown in equation 3.30, and especially intended for the top 10% of the overtopping volumes.

$$b = (0.59 + 0.23 \cot \alpha) \exp \left(-2.2 \frac{R_c}{H_{m0}} \right) + 0.83 \tag{3.30}$$

v) Rayleigh

The Rayleigh distribution corresponds with the value of $b = 2$. An example of this was shown in Figure 3.6, which is represented by a straight line on a Rayleigh scale.

vi) Exponential

The exponential case for the probability distribution is considered when $b = 1$.

vii) EurOtop (2007)

EurOtop (2007) established that the distribution of overtopping volumes for all kind
of structures had average values even smaller than $b = 1$, even steeper than an expo-
nential distribution. According to limited datasets analysed, the values of b were in
the range of $0.6 < b < 0.9$, so after comparing their distributions, an average value
of $b = 0.75$ was defined for smooth slopes, as well as for rubble mound structures.
However, it is now noticeable that the shape factor b may increase with increasing
overtopping discharge and that it should not be kept at 0.75 if overtopping really
becomes significant (EurOtop (2018)).

Other considered cases which have not been applied because of their ranges of ap-
plication and boundary conditions of the model are the formulae given by Molines et al.
(2019) and Mares-Nasarre et al. (2020). These formulae have been developed for porous
and permeable structures rather than impermeable slopes that, when applying them, the
deviation with the measured data is considerably big. Finally, the values of b given by
Besley (1999) are defined for a specific and constant value of the wave steepness which
is not fittable in this case, as the range of wave steepness on the tests is between 0.017
and 0.024 (see Section 5.3), and not fixed for the values proposed by Besley.

For vertical structures, Franco et al. (1994) maintains the validity of the constant
value of $b = 0.75$. However, Franco and Franco (1999), who according to the approxi-
mately 250 test carried out by Franco et al. (1994) reproducing a JONSWAP spectra with
a duration of more than 1000 waves per test, plus extensive tests on a 3D model carried
out in a multidirectional basin at Delft Hydraulics consisting on 13 caissons, found a re-
lation with wave steepness and reported a range of valid values of $[0.66 - 0.86]$. Besley
(1999), already mentioned, also found an effect of wave steepness and considered impul-
sive and non-impulsive waves. For the first case the author suggested a constant value of
$b = 0.85$ for any steepness, and for the second case it was defined a value of $b = 0.66$ for
$s_{0p} = 0.02$ and $b = 0.82$ for $s_{0p} = 0.04$.

The formula provided by Victor et al. (2012) to describe the factor b for steep low-
crested structures, as it depends on the slope angle alpha, it is possible to particularize for
the vertical structure case.

3.6.3   Probability of overtopping P_{ow}

The probability of overtopping is defined as the ratio between the number of overtopping waves (N_{ow}) and the number of incident waves (N_w).

$$P_{ow} = \frac{N_{ow}}{N_w} \tag{3.31}$$

Furthermore, Van der Meer and Janssen (1994) and Franco et al. (1994) defined a distribution for the theoretical probability of P_{ow} as follows:

$$P_{ow} = \exp\left(-\left(\frac{1}{\chi} \cdot \frac{R_c}{H_{m0}}\right)^2\right) \tag{3.32}$$

$$\chi = \frac{R_{u2\%}}{H_{m0}} \frac{1}{\sqrt{-\ln(0.02)}} \approx 0.51\frac{R_{u2\%}}{H_{m0}} \tag{3.33}$$

$$P_{ow} = \exp\left[-\left(\sqrt{-\ln 0.02}\frac{R_c}{R_{u2\%}}\right)^2\right] \tag{3.34}$$

Where coefficient χ is related to the relative 2% run-up height $R_{u2\%}/H_{m0}$.

The definition of the probability of overtopping is also dependent on the type of the structure, as well as different influence factors that affect the 2% run-up height $R_{u2\%}/H_{m0}$.

3.6.4   Measurement techniques for individual overtopping

Individual wave overtopping volume is measured according to the temporal evolution of the overtopped water, using a container at the other side of the structure. After this, the overtopped water can be classified into green water, runs up the face of the structure and over the crest in coherent water mass; and white water, which represents the spray of water that is overtopped when the waves break seaward the structure. Nevertheless, this white water has not a very significant contribution to overtopping volumes (Koosheh et al. (2021)).

To measure the water in the container, it is possible to use whereas a surface piercing wave gauge or a subsurface pressure transducer. Furthermore, to reduce the effect of
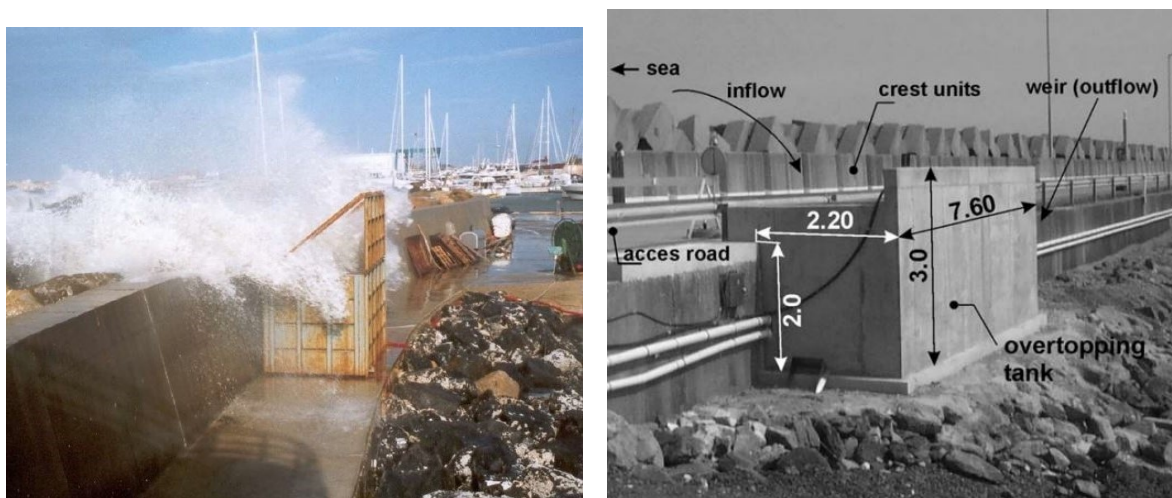
(a) Overtopping tank in Ostia, Italy. Source: Brig-   (b) Overtopping tank at the Zeebrugge breakwater.
anti et al. (2005).   Dimensions in meter. Source: Troch et al. (2004).

Figure 3.7: On field measurement techniques of wave overtopping with a water tank.

water level fluctuations inside the container, possible solutions are: averaging the signal from multiple gauges spread throughout the container, and installing a "stilling wall" in the centre of the container which allows water to pass underneath thus reducing the oscillations behind the wall (Koosheh et al. (2021)).

Another measurement technique to determine the volume of water is by measuring the mass of the overtopped water which is inside the container, using a weigh cell (Gallach Sánchez, David (2018)).

When a significant discharge is occurred, the water level of the seaward side may vary due to the loss of water. In that sense, it also may occur that the available volume of the container is too limited. This aspect can be controlled by installing a pump in the bottom of the container, although this turns the experimental set up much complex.

As not always these measurements are going to be field measurements, also scale effects my be considered when measuring wave overtopping to take into account the differences between model and prototype. Another important aspect to predict, evidently, is the maximum overtopping volume in order to guarantee that the container in the physical model is able to ensure the analysis during the maximum storm.

The detection of individual overtopping events following a wave-by-wave analysis is made by different techniques. One of these methods consists of calculating the cumu-

lative volume curve within individual wave volumes. This method, proposed by Franco et al. (1994), assumes that each sudden increase of the measured volume is an overtopping event. To identify which sudden increase is actually an overtopping event, the "up/down crossing analysis" is used, according to a constant threshold value. However, this methodology has disadvantages when measuring small events or consecutive events that should be considered independently.

Thus, several authors have developed different methodologies for the automatic detection of individual overtopping events (Koosheh et al. (2021)). Molines et al. (2019) defined the derivative of volume q_1 as:

$$q_1(t_i)\frac{V_0(t_i + T_m/2) - V_0(t_i)}{T_m/2} \tag{3.35}$$

Where T_m is the mean wave period and with a moving average function to eliminate frequencies higher than 3 Hz:

$$q_2(t_i) = 0.25q_1(t_{i-1}) + 0.5q_1(t_i) + 0.25q_1(t_{i+1}) \tag{3.36}$$

To reach to this, Molines et al. (2019) applied utility functions to 164 small-scale physical tests carried out in the Laboratory of Ports and Coasts at the Universitat Politècnica de València (LPC-UPV).

In this case, the threshold volume is V_t. If an event is below this value, it could mean that the detected value is part of a larger overtopping event or that that small value is actually a real small event by itself and the higher value is close to it.

Formentin and Zanuttigh (2019) proposed a similar up/down crossing procedure but they set a lower (l_{th}) and an upper (u_{th}) threshold. This interval has to be selected according to structural and wave characteristics, but it gets to eliminate the oscillations with a lower amplitude of ($u_{th} - l_{th}$). With this, at least two wage gauges have to be installed on the crest of the structure at a certain distance in the direction of overtopping flow (d_w). Thus, since each coupling pairs from two wave gauges belong to a unique overtopping event that travels between the gauges, it must be in the interval between dt_{tmin} and dt_{tmax}, otherwise it is discarded.

For this, Formentin and Zanuttigh (2019) used five different datasets to validate this procedure: the dataset *UB-num* with 94 2D numerical tests at smooth dikes for a

range or relative crest freeboards R_c/H_s of $[-1.5; 1.5]$, the dataset *HT* with 8 2D and 3D experiments at smooth dikes for a R_c/H_s range of $[0.319; 1.064]$, the dataset *HS* with 3 2D experiments on levees and R_c/H_s range of $[-0.430; -0.121]$, the dataset *UB-exp* with 54 2D experiments at smooth dikes for relative crest freeboard values of 0, 0.5 and 1, and the *AAU* dataset with 33 3D experiments tests at permeable breakwaters for cases of R_c/H_s in $[-1.59; 0.49]$.

3.7 Maximum Volume V_{max}

After the preceding sections, according to Lykke Andersen et al. (2009) the maximum individual overtopping volume V_{max} for a two-parameter Weibull distribution can be expressed as:

$$V_{max} = a[\ln(N_{ow} + 1)]^{1/b} \tag{3.37}$$

Where, a and b can be easily identified as the scale factor and the shape factor, respectively. The argument of the logarithm adds one overtopping event to avoid the inconsistency of a null value of the logarithm if there was only one overtopping wave, showing a slightly difference with the formula from EurOtop (2018) proposed by Van der Meer and Janssen (1994). N_{ow}, the number of overtopping waves, can be also redefined as the product between P_{ow} and N_w, so it will be only necessary to determine both shape factor b and the probability of overtopping P_{ow} to determine the maximum individual overtopping volume.

3.8 Water levels

The water level is the reference distance used to measure every dimension related to the sea. The prediction of this reference is such an important parameter to quantify the effect of wave run-up, therefore the crest freeboard. The design value of water level must consider the mean sea level, the astronomical tide, extreme storm surges and occasional river discharges. Moreover, the consideration of future climate change scenarios are also taken into account as an increasing of the water level.

3.8.1   Mean sea level

The mean sea level is a reference value according to one specific site which is used as the mean sea level of the oceans for a relative period of time. As mentioned, the design value of the water level for structures for more than 5 years of lifetime must consider a certain sea level rise due to climate change conditions (EurOtop (2018)).

3.8.2   Astronomical tide

The astronomical tide is produced by the gravitational attraction that Sun and Moon exert on seas and oceans of the Earth, according to Instituto Geográfico Nacional (2016). This effect creates horizontal currents that are translated into a rise and decrease of sea level. Other planets could also produce a similar effect, but its magnitude is so small that can be neglected.

Tidal force causes the Earth's water to move and protrude from the nearest side to the Moon and from the far side as well, although with less force. This is called high tide. While this happens, the terrestrial water that is not aligned with the Moon remains at low tide.

Taking into account the rotational movements of the Earth and the translation of the Moon, a tide cycle lasts approximately 12 hours between high tides. But between high tide and low tide, the cycle is about 6 hours.

The Sun produces a similar effect than the Moon but with less intensity. Tidal movements are therefore entirely predictable and easily to define in the design project (Instituto Geográfico Nacional (2016)).

3.8.3   Storm surges

Storm surges are the increase of the water level because of extreme meteorologic conditions in the atmosphere. This phenomenon is defined as the difference between the expected and the actual water level at a defined place and time (National Ocean Service (2000)).

Extreme meteorological conditions are understood as low values of atmospheric pressure and strong winds that push the water mass to the coast. Hence, extreme high wa-
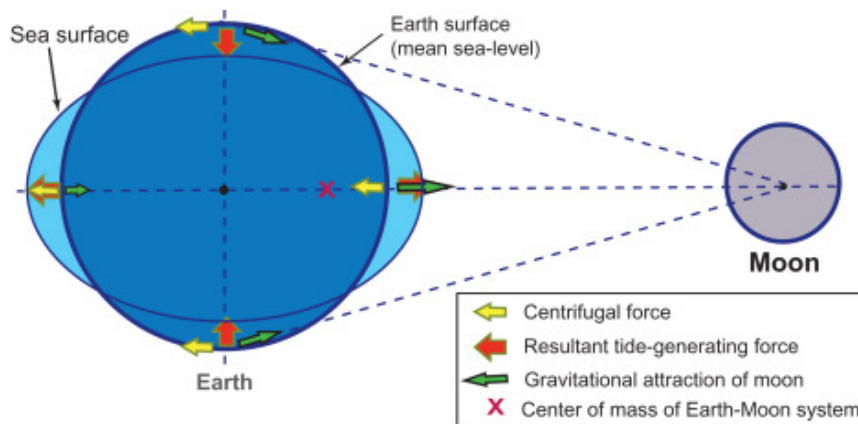
Figure 3.8: Origin of lunar tides as the sum of gravitational attraction and centrifugal forces. Source: Gani (2020).

ter levels are caused by a combination of high tidal elevations plus a positive surge, which usually comprise three main components: a variation of atmospheric pressure that leads into a barometric effect, a strong wind set-up, and a dynamic effect of surge amplification due to the shape of the Earth (World Meteorological Organization (2011)).

Then, storm surges are usually studied and predicted using historical time series. In cases where this data is not available, theoretical and empirical methods are used to obtain an estimation of extreme water levels.

Hence, storm surges, as waves and tidal oscillations, is one of the main components of extreme water levels. Its magnitude depends on several factors such as size, track, speed and intensity of the storm system, the local bathymetry and shape of the coastline.

3.8.4 Constant water level

As mentioned above, the SWL is not constant at all. However, for experimental purposes and, a fixed value of the SWL is determined in order to proceed with standard laboratory routines. As mentioned in one of the objectives of this work, its main goal is to provide a more realistic approach of individual overtopping volumes, as water levels and wave characteristics are rarely constant in nature.

Figure 3.9: Consequences of a storm surge at Daytona Beach (Florida) during Hurricane Matthew. Source: AP Photo/Eric Gay.

3.8.5   Variable water level

The water level is increasing as a consequence of climate change, so coastal hazards are even more important in terms of population and socio-economical activities. This also produces extreme events such as storm surges, which can produce severe damage to coastal defenses. If the current situation is extended to the year 2100 (Kopp et al. (2014), Wahl et al. (2017) and Vousdoukas et al. (2018)), there will be an increase of the intensity and frequency of this phenomena.

This VWL (variable water level) is discussed in Vousdoukas et al. (2016), which shows the changes of future storm surge levels in Europe. Hence, noticeable variations can be found in the North Sea and the Belgian coast. Similar studies have been also carried out for the US coast, specially considering hurricanes and tropical cyclones. It is quite obvious that storm surge processes have a strong relationship with wave overtopping phenomenon, as long as wave overtopping is heavily influenced by the crest freeboard, which is modified by the variable water level.

These considerations reflect that storm surge processes are completely needed to analyse wave overtopping and minimize their consequences in terms of damage.

3.9   Experimental campaigns with variable water level

If the aim of this work is focused on individual wave overtopping, it is important to declare that, as a consequence of climate change, an increase of storm surges in terms of intensity and frequency will occur. With this, storm surges are one of the most dangerous natural hazards along the coast that can destroy coastal defenses and damage properties, the environment and cause loss of human lives.

The role of water level variation in combination with the wave-structure interaction has been little studied and even not yet focused on individual wave overtopping. Van Gent et al. (2018) developed armour stability tests with small-scale physical models, in which the damage of a rock armoured dike with a 1:3 slope was measured. For this, tests with (1) constant water depth ($h_t = 0.75\,m$) were measured as well as (2), (3), (4) the effect of increasing and decreasing the water level in 3 steps ($0.65\,m \leq h_t \leq 0.85\,m$) and (5) a final methodology of resembling a peak of a storm decreasing or increasing. The results of the tests showed that the changing water level conditions produces an increase in damage, in comparison with the constant water level configuration.

On the other hand, Kerpen et al. (2020) studied the wave overtopping for this case with hydraulic model tests in a wave flume over a 1:6 smooth slope. Hence, three different approaches were considered: (1) a linear increase over the entire test duration, (2) a linear increase over the first half plus a linear decrease in the second half, and (3) the opposite case of the last one. The water depth was established for the range of $0.74\,m \leq h_t \leq 0.77\,m$ and a duration about 3 hours ($t = 999\,s$) divided in intervals of 333 s with 100 to 240 waves generated. H_{m0}/dh was in a range of 1.6-3.3, and R_c/H_{m0} between 1.0-2.0. The results of the study showed that the influence of a variation of the SWL is already covered with the existing design formulae, although there are already some uncertainties on the role of dynamic wave steepness on wave overtopping in hydraulic model tests, which effects are not fully covered.

Pepi et al. (2022) have studied the influence of this variable SWL on the average overtopping discharge q, over a smooth dike. In comparison with the last two studies mentioned, this one tries to cover a wider range of hydraulic and geometric parameters, with a range of relative freeboard even smaller than 1.0: $0.5 \leq R_c/H_{m0} \leq 2.0$. In this case, the slope of the tested dike (slope of $\cot \alpha = 2$) is similar to the one in Van Gent et al. (2018) (1:3), not as gentle as the one in Kerpen et al. (2020) (1:6). For a duration of approximately 1 h (15 min in prototype), 535 irregular waves were generated in the test.

With this, similar conditions to nature were recreated for storm surge variations ($dh = 0.75 - 4.8\,m$) and storm durations ($t = 2.7 - 22\,h$). The main objectives were to implement the variable water level into the wave flume facility of Ghent University, to measure the wave overtopping for these conditions, to create a data-set of these overtopping results for variable water level and to compare both constant and variable cases. Finally, the results showed that the measured q for the average overtopping discharge at constant water level appears to be well predicted by the existing formulation. Nevertheless, for the case of variable water level, an overprediction is occurred, especially for smaller relative crest freeboards ($R_c/H_{m0} < 1.5$). Hence, the existing formula for overtopping discharge q (Eq. 3.5) was adjusted, by replacing the relative freeboard with the new equivalent relative freeboard $(R_c/H_{m0})_{eq}$, together with the empirical coefficients $a = -1.14$ and $b = 0.55$, so accurate predictions for both CWL and VWL situations are obtained, for a certain range or application.

Finally, there is a notable gap in the existing literature when coming up with the case of individual wave overtopping with variable water level conditions, which is the main topic of this thesis and will be analysed in further sections.

4. Specific objectives

After setting the whole literature provided for this work, which derives in a fully better understanding of the main topic, specific objectives need to be defined in order to approach the individual wave overtopping volume for the variable VWL case:

i) To analyze deeply the obtained dataset to acquire an extensive understanding of the followed methodology that allows to get a further insight of the measurements and its preparation for the overtopping analysis.

ii) Starting from the CWL situation, to define the main overtopping parameters such as the probability of overtopping and the followed extreme value distribution by the data. An specific analysis of the definition of scale and shape parameters will be described to reason the statistical analysis.

iii) To compare the obtained results with the different applicable formulae in literature for the estimation of statistical parameters, providing quantitative error values. This analysis will take into account the cases considering (1) all of the dataset, (2) the highest 50% of individual wave overtopping volumes, (3) the highest 30% of individual wave overtopping volumes and (4) the highest 10% of individual wave overtopping volumes.

iv) Moving on to the VWL situation, to proceed as in the previous steps for the extreme value distribution of the data. A critical analysis needs to be done to compare the validity of the existing literature with the VWL case.

v) To carry out a sensitivity analysis to reach to further considerations about the validity of the provided prediction formulae, as well as for the CWL analysis.

vi) To conclude whether the current prediction guidelines for individual overtopping volumes, derived for a constant water level, are also valid for the changing water level situation and to explain the effects that are observed in the results.

5. Laboratory measurements

5.1 Geometry conditions

The wave flume used for the laboratory measurements is located at the Coastal Engineering Laboratory of the Ghent University. It measures 30 m long, 1 m wide and 1.2 m high. According to these values, the maximum design water depth is approximately 0.8 m, meanwhile the maximum wave height in the flume is about 0.35 m Ghent University (2017).

Its walls are made of reinforced concrete but it also has a fifteen meter long wall on one side made of glass, with a thickness of 30 mm, at the opposite end from the wave paddle. Openings in the side walls of the wave flume allow connection with pumps for tide and current simulations. Moreover, it is equipped with an advanced wave generator system that enables wave trains for both regular and irregular waves, active wave absorption, data acquisition system and wave data analysis software. The AWASYS active wave absorption system enables the wavemaker to generate the desired incoming waves and to absorb reflected waves simultaneously.

The wave paddle of the wave flume is a piston type paddle which is fixed to a moving open framework and moves on linear bearings. Its movement is accomplished by an electro servo motor in step mode. Thus, the maximum stroke length is limited to 1.5 m. To accomplish the necessities of overtopping measurements, the wave flume has also a pump circuit for steady flow generation. It allows a reversible current in the wave flume, and it is located just next to it. It is important that at any time the water level in the wave flume is bigger that the highest point of the pump house to guarantee a correct functioning. Furthermore, it is also possible to use the pump to perform tests with tidal level changes and variable SWL.

For this exact case, a smooth and impermeable breakwater is tested, for which a tank

Figure 5.1: Model section with glass wall of the Large Wave Flume and geometry of the tested model during a test. Source: Chiara Ricci.

with a chute is installed behind the freeboard of the model to measure the overtopping, as mentioned in Section 3.6.4 about the measurement techniques. This model can be seen in Figures 5.1 and 5.3.

5.2   Methodology

To measure the water level and the free surface oscillations, the wave flume is equipped with several wave gauges (WG), a pressure sensor (PS) and an ultra-distance sensor (UDS) (Ricci (2021)). Wave gauges measures the current flowing between the probes wires and then this current is transformed into an output voltage. Hence, they are based on the proportionality between the depth of immersion and this output voltage. The operational sample frequency of the data acquisition console of wave gauges is 40 Hz. Moreover, it is necessary to maintain a high level of cleaning of the wave gauges to guarantee correct measurements.

(a) The Large Wave Flume from inside

(b) Wave paddle of the Large Wave Flume

Figure 5.2: Detail pictures of the wave flume at Ghent University. Ghent University (2017)

A first wage gauge installed at the paddle is used to measure the reflected waves to actively absorb them. Then, two arrays of wave gauges are used to measure both incident and reflected waves. The first one consists of three wave gauges [WG1, WG2, WG3], located at the deepest section. The distance between WG1 and WG2 is named $x_{1,2}$ and between WG2 and WG3 it is $x_{2,3}$. The second array consists of six wave gauges [WG4, WG5, WG6, WG7, WG8, WG9], in which WG9 is located at a certain distance of the toe of the dike of $0.4L_P$, where L_P depends on the peak period T_P and is defined as $L_P = gT_P^2/2\pi$. Finally, two more wave gauges are installed: WG10 in front of the overtopping chute to detect the overtopping events and WG11 behind the overtopping tank to control the water level variations.

On the other hand, the pressure sensor [PS12] is located approximately at 0.1 m above the bottom, closer to the paddle. The ultra-distance sensor [UDS13] is located at the end of the wave flume behind the dike structure. Nevertheless, WG10 and USD13 obtained a too noisy signal and were neglected (Ricci (2021)).

Variable water levels are generated with the assistance of different pumps with a
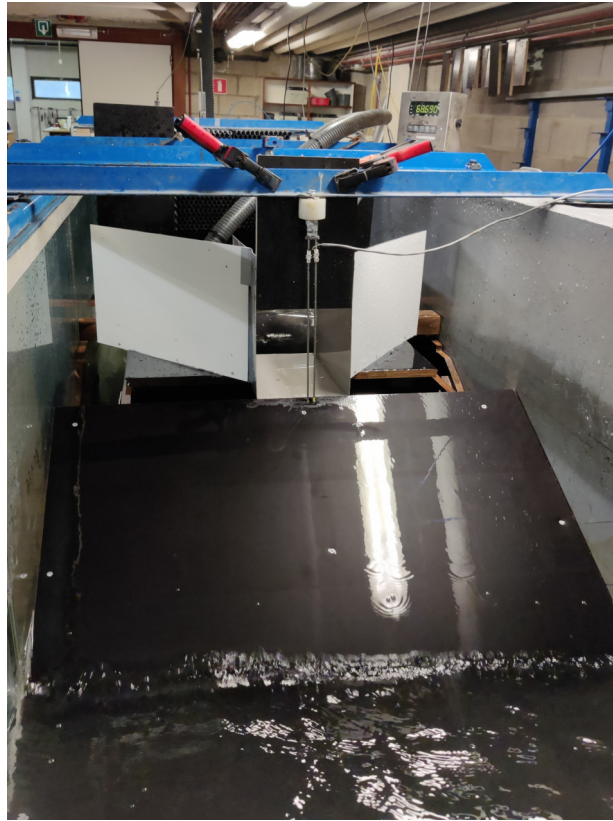
Figure 5.3: Tested model and chute to allow measurement of volumes. Source: Ricci (2021).

Figure 5.4: Wave gauges at the wave flume. Source: Ricci (2021).

Figure 5.5: A: Power supply valve actuators pump. B: Steering pump box. C: Flow Controller. D: Local control panels of the pumps. Source: Ricci (2021).

minimum discharge of 1200 rpm. A flow controller, manually operated with 9 full rotation positions, allows to open and close a valve inside the pipe so the amount of water that reaches the pump is also controlled. For the results, it is assumed that they are valid both for the situation with falling water levels and rising water levels, so only one flow control and pump needs to be calibrated, as results are focused on the falling part of the water level/storm surge.

The wave overtopping is later measured using a system behind the dike crest with a 20 cm wide chute, a water tank and a pump. Under it there is a weigh cell that allows to measure the weight of the overtopped water, with a sensibility of less than 0.005 liters (5 grams). The capacity of the overtopping tank is about 80 liters but reduced because of the space needed for the pump, which is in charge of emptying the water tank when its capacity is reached. Then, this effective volume is approximately 30 liters. Overtopping

events are measured continuously and converted to a cumulative curve according to the moments when the pump is activated and when the water is pumped out and eliminated from the signal.

5.3 Obtained dataset

The provided data correspond to the UGent 17 dataset, in which constant and variable water levels were studied at Ghent University and collected during the experimental campaign described in Ricci (2021) and Pepi et al. (2022), hereafter referred to as UG17. Moreover, average and individual overtopping were measured for both water level situations. In that sense, there are 127 variable water tested situations and 23 tests for constant water conditions. Different values in terms of geometrical and hydraulic conditions are established for each test. In the following paragraphs, a list of ranges will be showed to illustrate the dataset as well as detailed information of each situation of water level will be described. For each case, the number of overtopping waves (N_{ow}) is measured, as well as the number of incident waves (N_w). With this, the probability of overtopping P_{ow} is calculated following equation 3.31.

Besides, it is established a naming convention for the tests which is going to be maintained during this work. Hence, every test has a name like:

$$C* + VW/CW + D* + H* + T* + S* + h* + R + * + N*$$

Where the * represents the number that is changing from one test to another. For example, one arbitrary test name would be "*C4 VW D3600 H010 T170 S7 h065 R 212 N001*". The meaning of each component is represented in Table 5.1 for this specific case.

5.3.1 Constant water level

For the 23 tests carried out for the CWL situation, as shown in Table 5.2, the duration of the test is in a range of 15 minutes and 1 hour. However, only one of the tests has been performed for 1 hour and the remaining 22 tests have a duration of 15 minutes. The variation water level (d_h) is null as the constant case is considered.

For geometrical parameters, the crest freeboard is in the range of 0.09 and 0.29 meters. Only two tests have been carried out for 0.29 meters, while the cases for 0.24, 0.19 and 0.14 m have been carried out five times each and six times for the 0.09 m case.

C4:	case 4
VW:	variable water level
D3600:	duration 3600 seconds
H010:	significant spectral wave height $H_{m0} = 0.1$ m
T170:	peak period $T_p = 1.7$ s
S7:	seed number 7
h065:	water depth h = 0.65 m
R 212:	rotations of the valve to regulate the speed of water level variation
N001:	running number (e.g. repetition tests would be N002)

Table 5.1: Naming convention of tests.

Parameter	Symbol	Range	Units
Duration	t	15 - 60	*min*
Crest wall freeboard	R_c	0.09 - 0.29	*m*
Water depth at the toe	h_t	0.35 - 0.55	*m*
Significant spectral wave height	H_{m0}	0.101 - 0.109	*m*
Dimensionless freeboard	R_c/H_{m0}	0.87 - 2.76	-
Relative water depth	h_t/H_{m0}	3.36 - 5.45	-
Spectral wave period	$T_{m-1,0}$	1.66 - 1.98	*s*
Peak period	T_p	1.65 - 1.73	*s*
Wave steepness	$s_{m-1,0}$	0.017 - 0.024	-
Breaker parameter	$\xi_{m-1,0}$	3.22 - 3.83	-

Table 5.2: Ranges of the main parameters from the dataset for the CWL situation, in model scale. Water depths and wave parameters refer to structure toe.

Type of slope	Range of $\cot \alpha$
Mild slopes	$\cot \alpha \geq 2$
Steep slopes	$2 > \cot \alpha > 0.27$
Very steep slopes	$0.27 \geq \cot \alpha > 0$
Vertical structures	$\cot \alpha = 0$

Table 5.3: Definition of the structure according to the slope. Source: Gallach Sánchez, David (2018).

The water depth at the toe has a range of 0.20 meters, from 0.35 to 0.55 m in steps of 0.05 m, following a similar pattern than the crest freeboard.

Then, hydraulic parameters are firstly defined by the spectral wave height H_{m0}. The variations between tested situations are in the order of millimetres, from 0.101 to 0.109 m. For practical purposes they are considered as values of 0.1 m for the spectral wave height, although all decimals are considered in the calculations. With this, dimensionless freeboard (R_c/H_{m0}) and relative water depth (h_t/H_{m0}) can be calculated for each test. Thus, large relative freeboards are considered.

Both peak and mean spectral wave periods are considered in the analysis. Meanwhile the peak period refer to the maximum value of the frequency in the wave spectrum, the mean spectral wave period gives more weight to lower frequencies and longer periods in the spectrum (Hofland et al. (2017a)). Their ranges are shown in Table 5.2. In all cases, a value of $\cot \alpha = 2$ is considered, so the analysed structure stays at the edge of mild and steep structures, see Table 5.3. Besides, wave steepness $s_{m-1,0}$ is defined for the range from 0.017 to 0.024. The breaker parameter $\xi_{m-1,0}$ is always greater than 2, so surging waves are described in model tests (EurOtop (2018)).

5.3.2 Variable water level

For the 127 test for VWL conditions, the same description is followed than for the CWL situation. In this case, tests have been carried out with a wider range of duration, from 15 to 120 minutes; of which 97 tests have been performed with a 15 minutes duration, which represents almost the 75% of the total tests. Now, the variation water level is one of the most important parameters to understand the data. Then, *dh* is in the range from 0.025 to 0.16 meters.

Parameter	Symbol	Range	Units
Duration	t	15 - 120	*min*
Water level variation	dh	0.025 - 0.160	*m*
Crest wall freeboard	R_c	0.04 - 0.24	*m*
Water depth at the toe	h_t	0.40 - 060	*m*
Significant spectral wave height	H_{m0}	0.053 - 0.119	*m*
Dimensionless freeboard	R_c/H_{m0}	0.40 - 1.97	-
Relative water depth	h_t/H_{m0}	3.81 - 6.54	-
Spectral wave period	$T_{m-1,0}$	1.21 - 2.98	*s*
Peak period	T_p	1.19 - 2.56	*s*
Wave steepness	$s_{m-1,0}$	0.016 - 0.040	-
Breaker parameter	$\xi_{m-1,0}$	2.50 - 5.68	-

Table 5.4: Ranges of the main parameters from the dataset for the VWL situation, in model scale. Water depths and wave parameters refer to structure toe.

Values of crest freeboard are in the range of 0.04 - 0.24 m, with specific tests for the cases of 0.04, 0.06, 0.07, 0.09, 0.11, 0.12, 0.14, 0.15, 0.16, 0.17, 0.19, 0.20 and 0.24 m, so a wider range of situations is considered than in the constant case. The water depth at the toe goes from 0.40 to 0.60 m, with different intermediate situations also.

The spectral wave height H_{m0} is defined from 0.053 to 0.119 m, although most of the tests are concentrate for intermediate values or this interval. Hence, ranges of dimensionless freeboard (R_c/H_{m0}) and relative water depth (h_t/H_{m0}) are defined in Table 5.4. In this case, according to its classification, dimensionless freeboard includes both large ($R_c/H_{m0} \geq 0.8$) and small ($0.8 > R_c/H_{m0} \geq 0.11$) relative freeboards definitions.

Peak period and mean spectral wave period are also defined as in Table 5.4, with a wider range than for the CWL case. Same information can be defined for wave steepness and breaker parameter.

6. Data analysis

6.1 Constant water level

As mentioned in the description of the data, there are 23 tests for CWL situation. In this sense, the first step of the analysis must consider the reliability of the obtained results.

To do so, the probability of overtopping P_{ow} is the main parameter to define it. If $P_{ow} < 10\%$ or $P_{ow} < 5\%$, then the test can be defined as non reliable. See Table 6.1. However, at the beginning of this analysis, all tests will be included in the calculation and further considerations will be considered at the moment of interpretation.

Following this, each test is considered individually for the next steps and the same procedure will be followed for the rest of them.

Furthermore, in order to help to visualize the data, Figure 6.1 aims to represent an example of the overtopping events for three consecutive cases (see Table 6.1 below). With these graphs, it is possible to see the distribution of overtopping events according to the position that each wave represents without time dependency. Tests in Figure 6.1 show an increasing in overtopping events when the value of water depth at the toe of the structure (h) increases as well, considering 60, 65 and 70 cm for tests 16, 17 and 18, respectively (see Table 6.1). Further considerations will be analysed in the following sections.

6.1.1 Estimation of a and b Weibull distribution factors

As first step, the probability of observing an individual wave overtopping volume larger than or equal to V, this is the exceedance probability $1 - F(V)$, is obtained theoretically using the following formula suggested by Makkonen (2006):
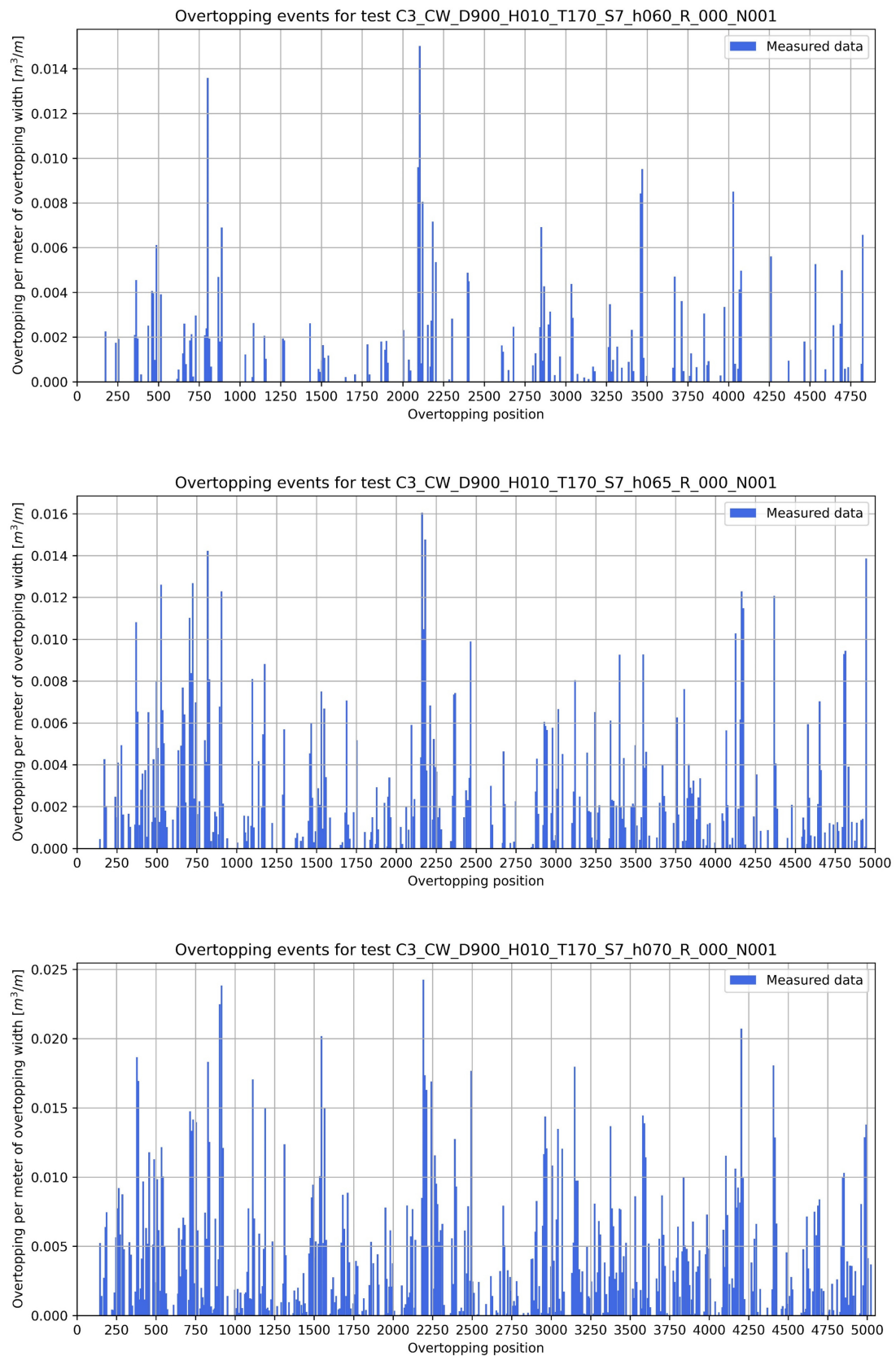
Figure 6.1: Overtopping events from the CWL dataset for tests 16, 17 and 18.

Name	Conventional test name	N_{ow}	N_w	$P_{ow}[\%]$	Rel.
0	C3 CW D3600 H010 T170 S1 h070 R 000 N001	1508	2536	59.46	YES
1	C3 CW D900 H010 T170 S1 h050 R000 N001	11	627	1.76	NO
2	C3 CW D900 H010 T170 S1 h050 R 000 N002	14	618	2.27	NO
3	C3 CW D900 H010 T170 S1 h055 R 000 N001	49	615	7.97	NO
4	C3 CW D900 H010 T170 S1 h060 R 000 N002	128	618	20.72	YES
5	C3 CW D900 H010 T170 S1 h065 R 000 N002	265	626	42.33	YES
6	C3 CW D900 H010 T170 S1 h070 R 000 N002	356	634	56.15	YES
7	C3 CW D900 H010 T170 S2 h055 R 000 N001	58	626	9.27	NO
8	C3 CW D900 H010 T170 S2 h060 R 000 N001	125	630	19.84	YES
9	C3 CW D900 H010 T170 S2 h065 R 000 N001	263	636	41.35	YES
10	C3 CW D900 H010 T170 S2 h070 R 000 N001	386	641	60.22	YES
11	C3 CW D900 H010 T170 S3 h055 R 000 N001	44	619	7.11	NO
12	C3 CW D900 H010 T170 S3 h060 R 000 N001	125	621	20.12	YES
13	C3 CW D900 H010 T170 S3 h065 R 000 N001	238	631	37.72	YES
14	C3 CW D900 H010 T170 S3 h070 R 000 N001	377	636	59.28	YES
15	C3 CW D900 H010 T170 S7 h055 R 000 N001	54	622	8.68	NO
16	C3 CW D900 H010 T170 S7 h060 R 000 N001	132	626	21.09	YES
17	C3 CW D900 H010 T170 S7 h065 R 000 N001	267	614	43.49	YES
18	C3 CW D900 H010 T170 S7 h070 R 000 N001	402	623	64.53	YES
19	C3 CW D900 H010 T170 S9 h055 R 000 N001	48	614	7.82	NO
20	C3 CW D900 H010 T170 S9 h060 R 000 N001	131	607	21.58	YES
21	C3 CW D900 H010 T170 S9 h065 R 000 N001	270	608	44.41	YES
22	C3 CW D900 H010 T170 S9 h070 R 000 N001	397	628	63.21	YES

Table 6.1: Calculation of P_{ow} in terms of defining the reliability of the CWL tests.

$$1 - F(V) = \frac{i}{N_{ow} - 1} \tag{6.1}$$

Where i represents the position of the sorted volumes and N_{ow} is the number of overtopping waves.

By representing the measured data in a Weibull plot, the slope and the intercept of the fitted line allow to estimate the shape and scale factors of the Weibull distribution, respectively (Molines et al. (2019)). For this, the x-axis variable is the logarithm of the relative volume according to the mean value $\ln(V/V_{mean})$, meanwhile y-axis is represented by $\ln(-\ln(1 - F(V)))$. All these calculations are done considering the 100% of the volumes for all tests. In further sections, different thresholds will be set to carry out the analysis (Section 6.1.3.1).

An example of this graph can be seen in Figure 6.2 for one of the CWL tests, specifically for test 5 (numbered by its Name as a numeric index), *C3 CW D900 H010 T170 S1 h065 R 000 N002*, where the value of factor b is also showed explicitly as the slope of the regression line in the legend. Once the value of b is obtained, a can be calculated using equation 3.24. Hence, Figure 6.3 shows the coefficient a' from equation 3.25 as a function of shape factor b.

After calculating the parameters of the probability distribution for each test, the probability distribution itself can be obtained using equation 3.19.

6.1.2   Estimation of V_{max}

Once that the coefficients of the Weibull probability distribution are known, the value of V_{max} is calculated using equation 3.37. With this, the maximum overtopping volume during a certain event is fairly uncertain, as it also depends on the duration of the event itself. Hence, the value given by equation 3.37 is actually the maximum value that can be expected. In this sense, it is possible that laboratory results could show greater values for the maximum volume which is measured, as this is comparing real test values with the expected value given by the probability distribution.

For the analysis of the data, the value of V_{max} is going to be considered to define an indicator of the error to determine the accuracy of the different equations and values available in literature, in comparison with the estimated probability parameters obtained by the measured data.
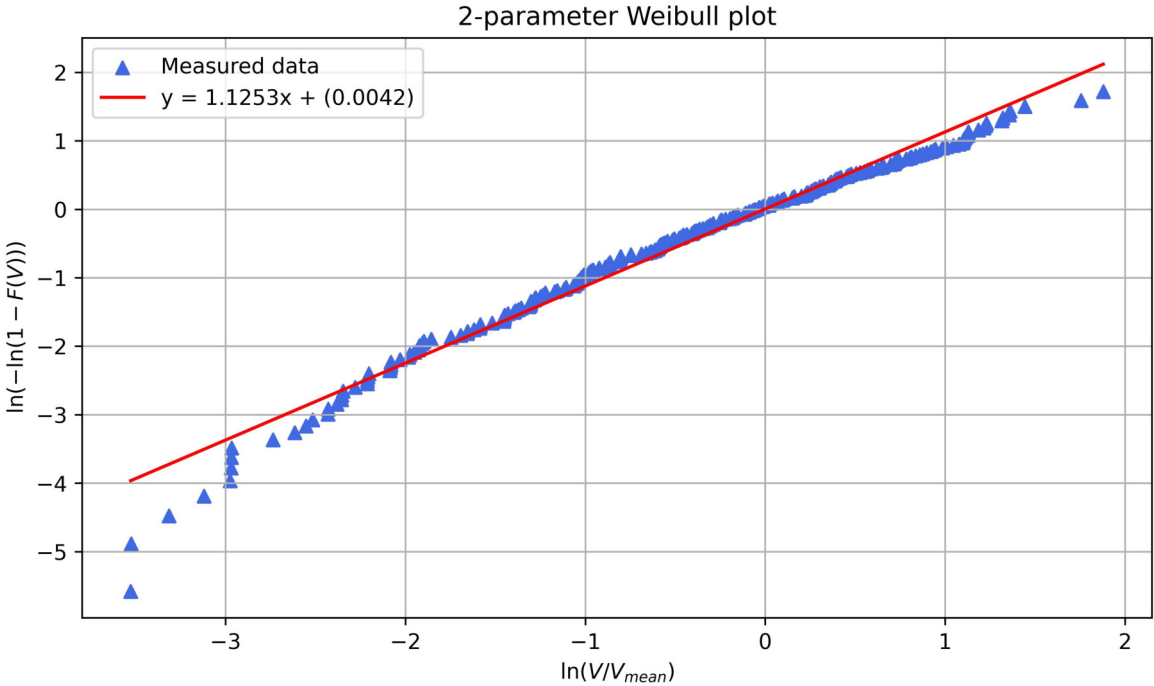
Figure 6.2: Two-parameter Weibull plot of the measured data, for test 5 at CWL.
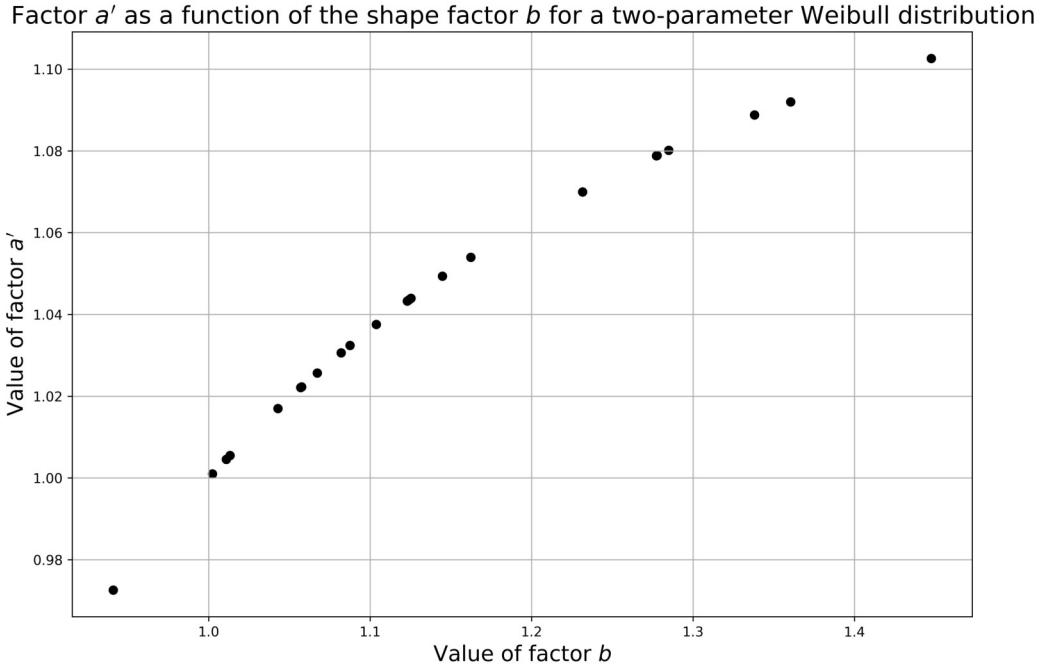

Figure 6.3: Factor a' as a function of shape factor b, for a two-parameter Weibull distribution, using Equation 3.25.

Case	Shape factor	R_c/H_{m0}	$\cot \alpha$
Victor et al. (2012)	Equation 3.27	[0.11, 1.69]	[0.36, 2.75]
Hughes et al. (2012)	Equation 3.28	(-2, 4)	-
Zanuttigh et al. (2013)	Equation 3.29	[0, 2]	[2, 4]
Gallach Sánchez, David (2018)	Equation 3.30	[0, 0.1]	[0, 2.75]
Rayleigh	$b = 2$	-	-
Exponential	$b = 1$	-	-
EurOtop (2007)	$b = 0.75$	> 2	≥ 2

Table 6.2: Summary of formulae and values in literature to estimate shape factor b.

6.1.3   Discussion of the results

The obtained results according to the measured data are compared with the different formulae and values given in literature for the estimation of the shape factor b, and then the rest of the parameters that are derived from this value. The cases that have been considered in this analysis for the comparison are those given in Section 3.6.2. A summary table of the used formulae in literature and ranges of application can be seen in Table 6.2.

After calculating all probability distributions and their parameters it is necessary to compare them in order to verify the accuracy of the fitting. Hence, the data from the tests, considering the 100% of the overtopping volumes at first instance, is displayed in Figures 6.4, for each test, and 6.5, according to the crest freeboard, as a key parameter.

As a first approach, if the values from Figure 6.5 are displayed with the predicted ones using these measured values as a third parameter to compare the results (Figure 6.6), it can be easily observed which values are over and underpredicted.

Then, the value of the shape factor b for all tests and its prediction can be observed in Figure 6.7. Some remarkable considerations can be observed from this graph:

- Rayleigh and EurOtop (2007) distributions remain constantly far from the values obtained from the measured data. The exponential distribution with $b = 1$ seems to be fairly accurate to the measured data, regarding to the prediction formulae used.

- While the value of b obtained from the measured data tends to be greater than 1, the available formulae in literature obtain a value of b below the threshold of 1 in
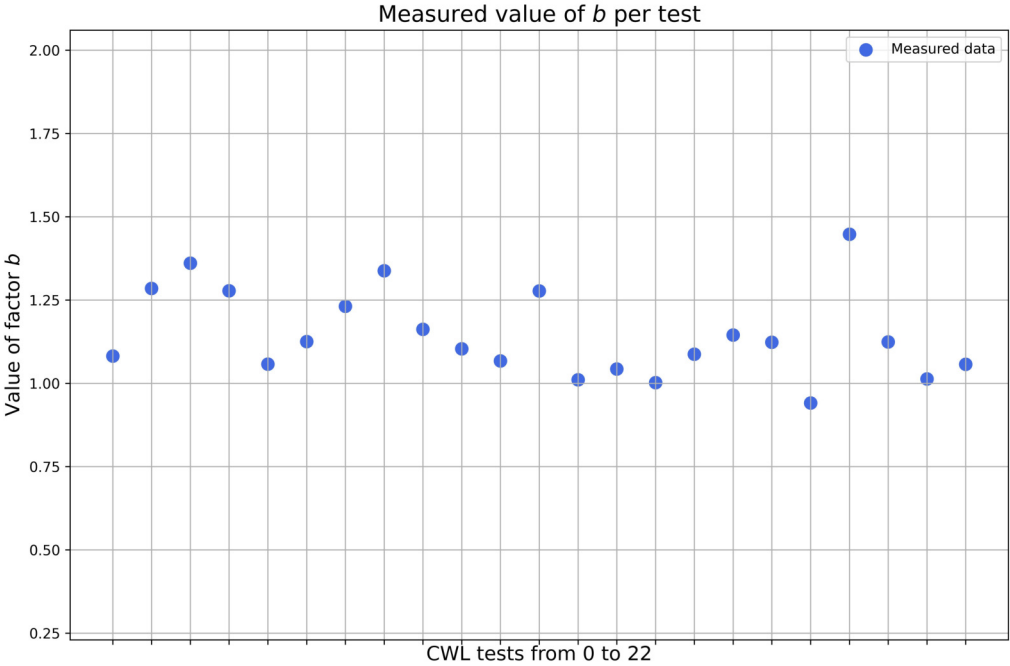
Figure 6.4: Measured values of b for the CWL tests, from test 0 to test 22.
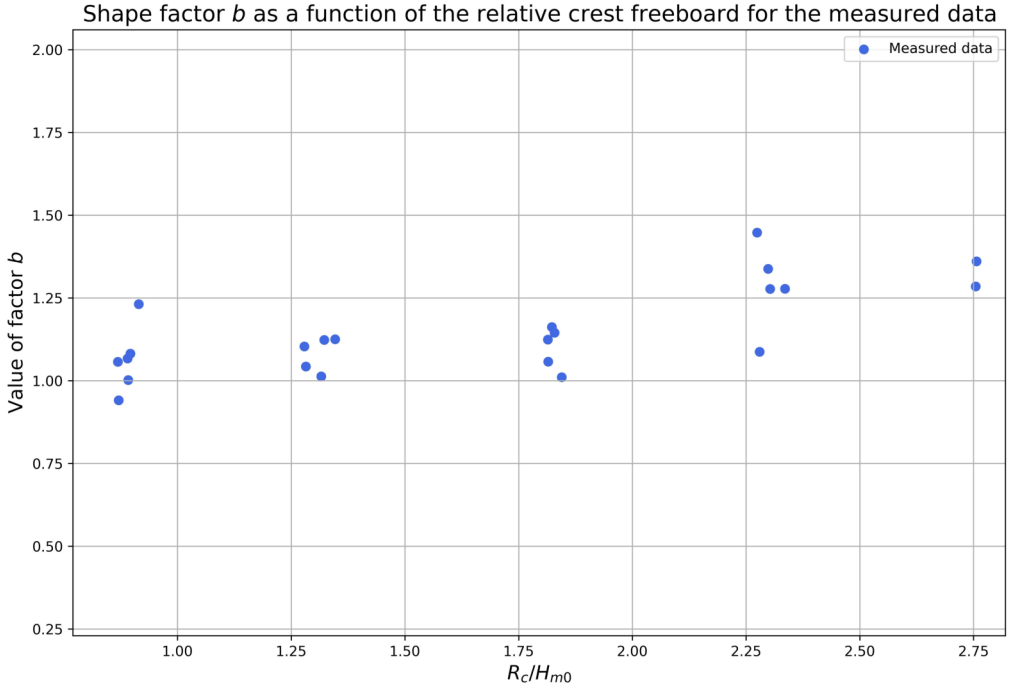
Figure 6.5: Measured values of b as a function of the relative crest freeboard, for the CWL tests.
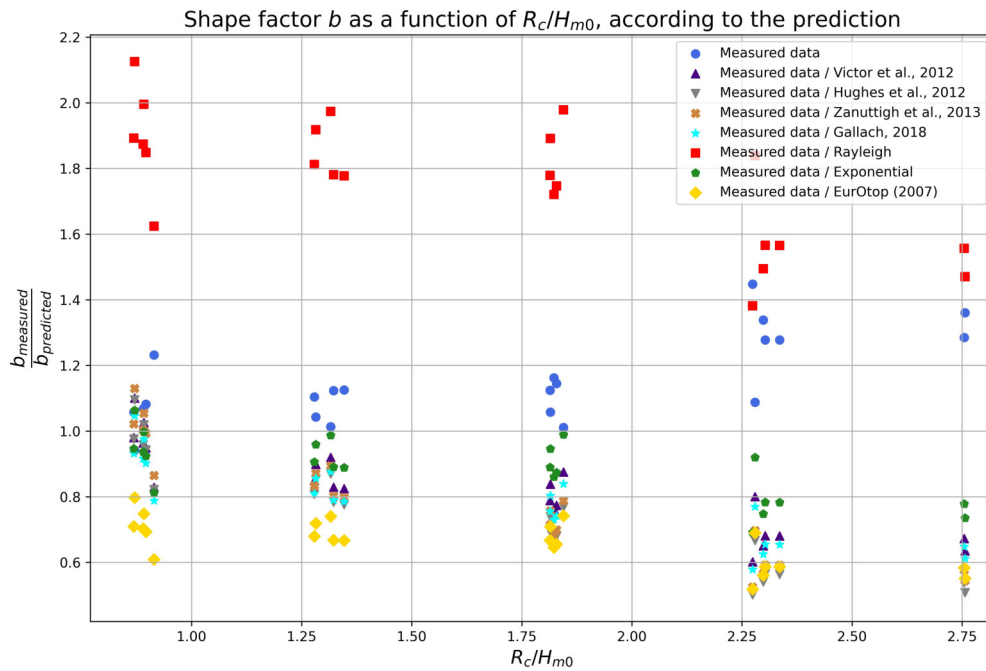
Figure 6.6: Measured values of *b* as a function of the relative crest freeboard, according to the predicted values of *b*, for the CWL tests.
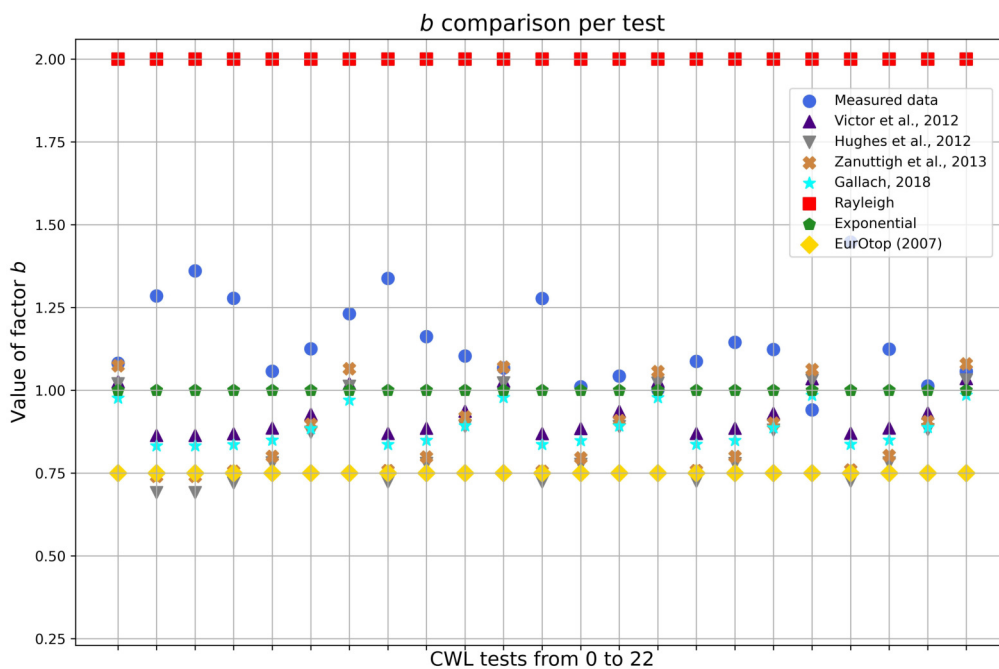
Figure 6.7: Comparison of all *b*-values for the CWL tests, from test 0 to test 22.
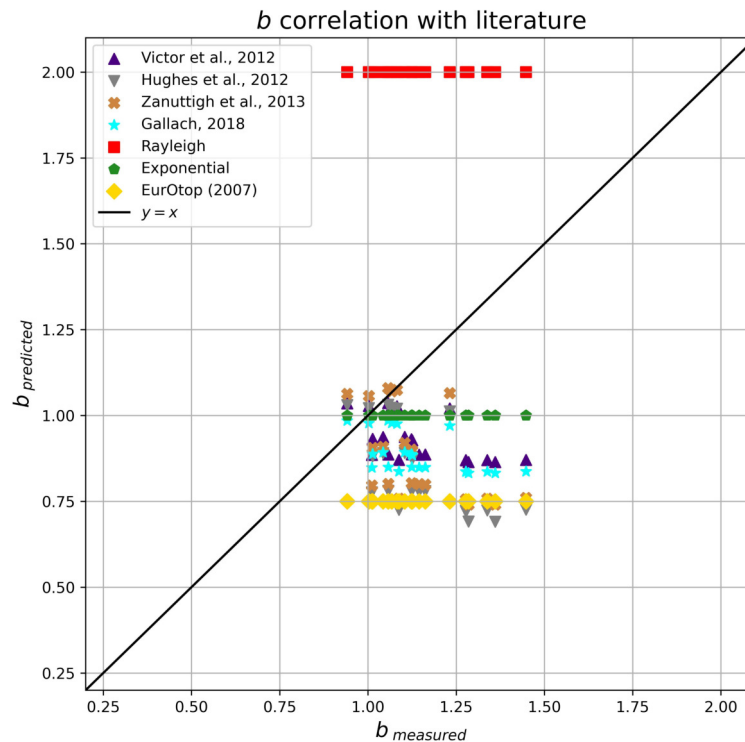
Figure 6.8: Comparison of the measured *b*-values according to the predicted ones.

most of the tests. See also Figure 6.8, in which most values are underpredicted with regard to the measured ones.

- The tests in which the value from the measured data and the prediction formulae are close enough to consider them as clearly alike, coincides with those tests with the lowest freeboard that lead to the highest values of P_{ow}. These tests, according to their Name in Table 6.1, are tests 0, 10, 14, 18 and 22. In all of these cases the probability of overtopping is around 60%. It could be also expected that for test 6, with a high P_{ow} and for which the formulae provide similar values of b, the given shape factor by the measured data was also in the same range but it tends to some scatter.

- In the same way than the previous item, those tests with a low probability of over-topping P_{ow} show a greater dispersion in the predicted values between them and between the measured data. It coincides with those tests which did not pass the reliability criterion shown in Table 6.1. These considerations can also be seen in
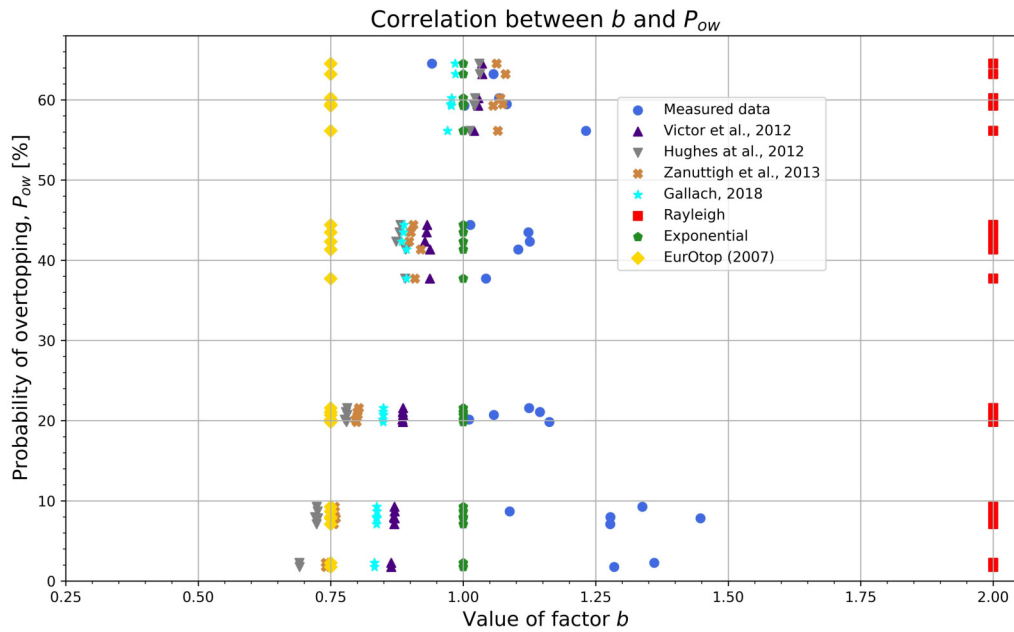
Figure 6.9: Correlation between factor b and the probability of overtopping P_{ow}.

Figure 6.9, which shows how the b-values which correspond to higher probabilities are concentrated in the same location (approximately where $b = 1$ and $P_{ow} = 60$).

- These tests with the highest values of the water depth at the toe of the structure (h), where the b-values tend to equalize, are also those tests with the the lowest values of the crest freeboard (R_c). As a consequence of this, they also coincide with the higher values of P_{ow}. For the tests mentioned before (0, 10, 14, 18 and 22), the value of h is the maximum possible in the tested model. It is clear that for low values of the crest freeboard the number of overtopping waves will increase, and so the P_{ow}. This observation shows the relationship between the overtopping phenomenon and these parameters. Its relation with the shape factor b can be seen in both graphs of Figure 6.10. For high values of h/H_{m0} and low values of R_c/H_{m0}, b-values are kind of concentrated in a certain value.

Another plot related to this last item to understand the data has to do with the relationship between the probability of overtopping P_{ow} and the relative crest freeboard R_c/H_{m0}, rather than with the shape factor b. As expected, this relationship shows a decreasing tendency, according to Figure 6.11.

These interpretations about the similarity of the value of b can be also measured
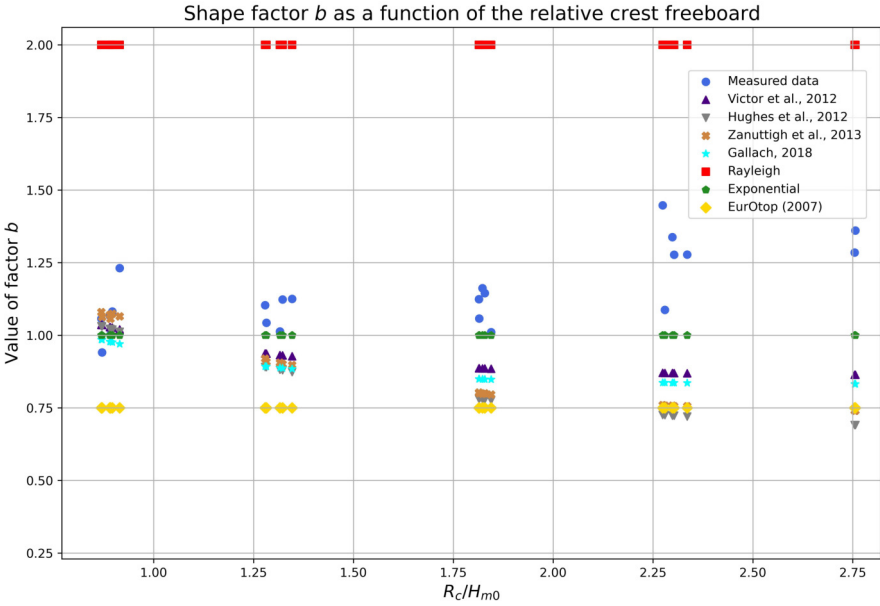
(a) Shape factor as a function of the relative crest freeboard
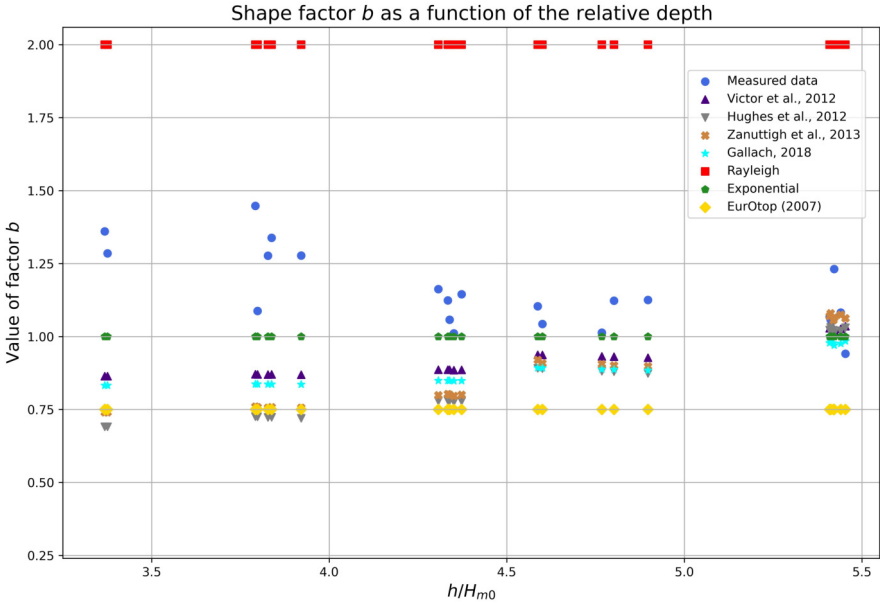
(b) Shape factor as a function of the relative depth

Figure 6.10: Correlation of the values of shape factor b regarding to geometric and hydraulic parameters.

according to the probability distribution of the tests. Hence, for those tests with similar values of b, the probability distributions obtained through the prediction formulae have almost the same line than the measured data.
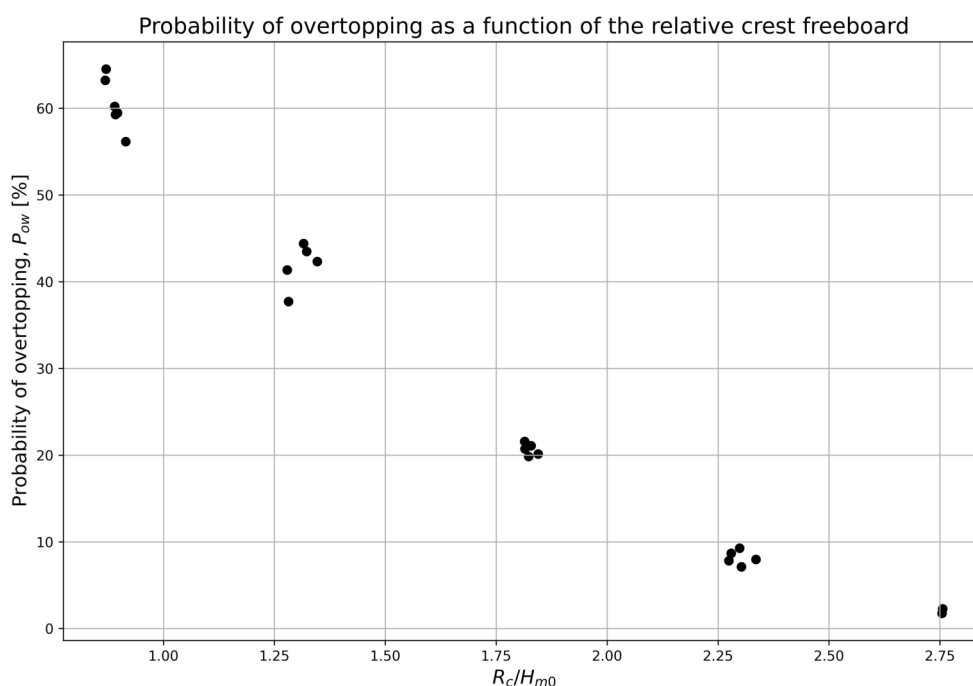
Figure 6.11: Probability of overtopping as a function of the crest freeboard.

An example of this can be seen in Figure 6.12. In this case, 6.12(a) represents the case of a test with a high value of P_{ow}, then similar b-values between the measured and the predicted data. 6.12(b) represents the case of a test with low P_{ow} in which the scatter of the values is clearly remarkable. The tests shown in Figure 6.12 are tests 18 and 16, respectively for 6.12(a) and 6.12(b).

Finally, as mentioned in Paragraph 6.1.2, the value of V_{max} can also be used as an indicator of the accuracy of the prediction formulae. In that sense, it is possible to measure the error of each formula or value in literature with regard to the measured data. Then, the quadratic error of each value of V_{max} is obtained for each prediction method, i.e., $(V_{max,measured} - V_{max,predicted})^2$. As happened in the previous considerations, some tests show that they are very well fitted by these formulae and some of them show more scatter. According to previous Figure 6.12, the same tests 18 and 16 are going to be considered to visualize this case. An example of this calculation is shown in Figure 6.13.

This same procedure can be also applied to the error of the predicted value of b through the quadratic error as well: $(b_{measured} - b_{predicted})^2$. An example is displayed in Figure 6.14, for the same cases than the previous figure.
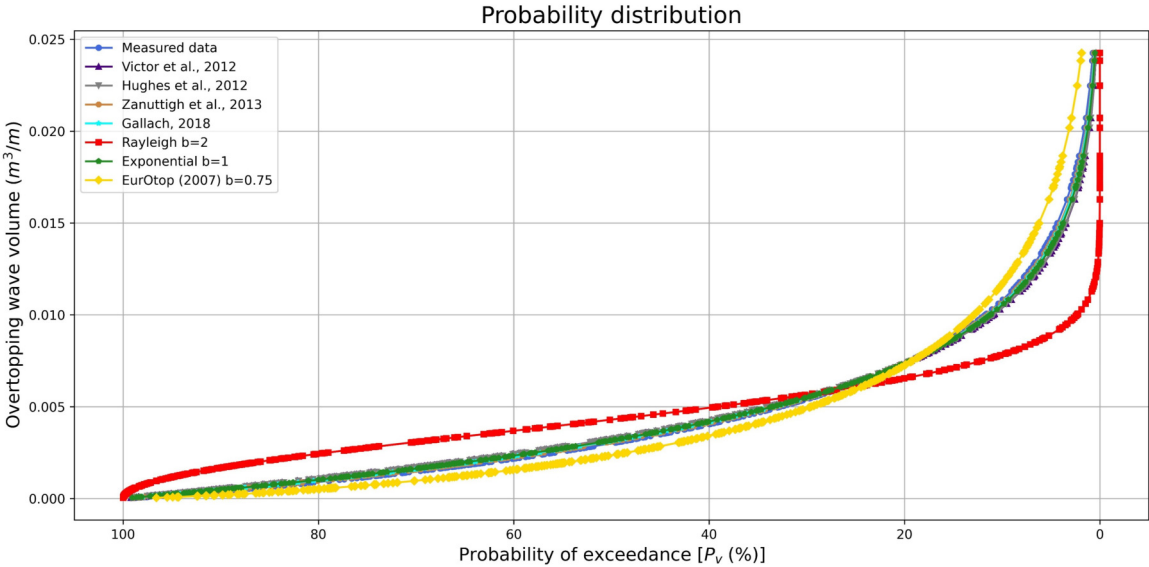
(a) Probability distribution according to available formulae in literature for test 18 at CWL.
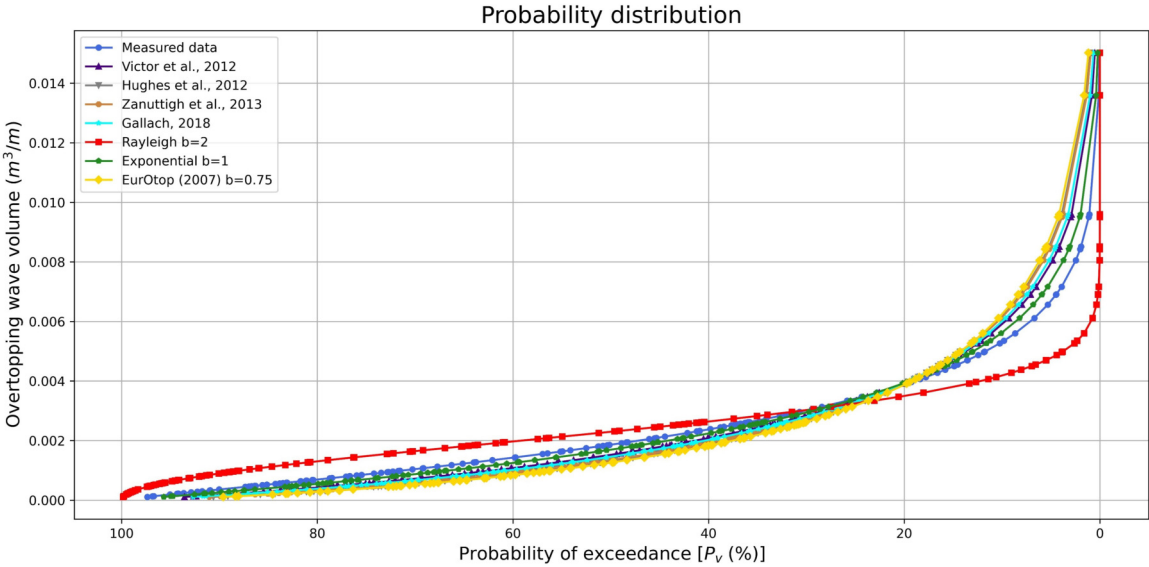
(b) Probability distribution according to available formulae in literature for test 16 at CWL.

Figure 6.12: Comparison of probability distributions between different tests.

Finally, this approach regarding the error to the measured value of V_{max} and b leads to the calculation of the mean squared error (MSE), and then, the relative mean square
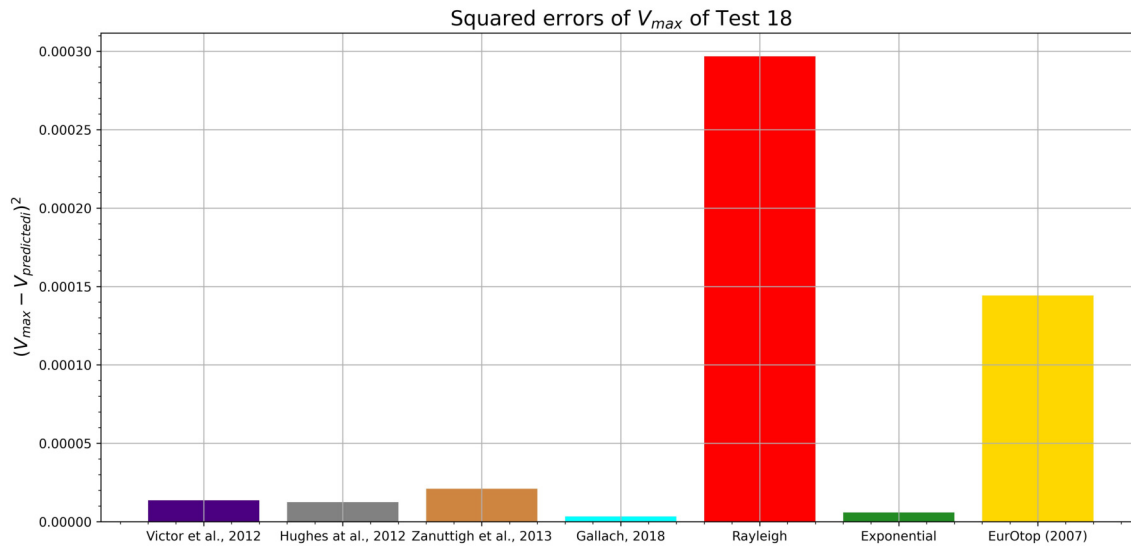
(a) Squared error of the considered prediction methods with regard to the measured data, for test 18 at CWL.
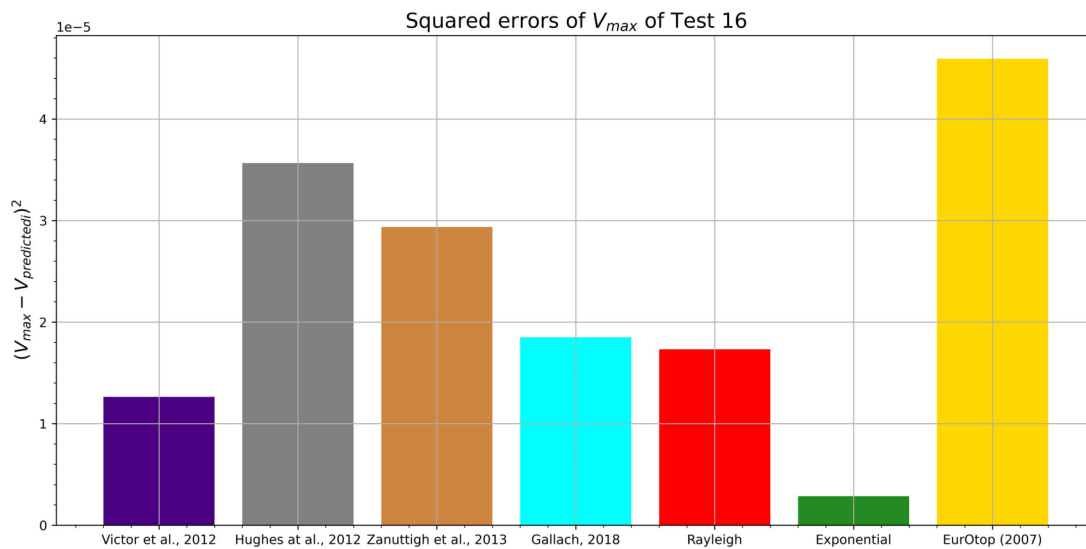
(b) Squared error of the considered prediction methods with regard to the measured data, for test 16 at CWL.

Figure 6.13: Comparison of the quadratic error of V_{max} between different tests.

error ($rMSE$) for each method using the value of the variance as follows in Equations 6.3 and 6.2, where N represents the number of total tests. The relative mean squared error is a dimension-less MSE, similar to that used in Van Gent et al. (2007) for the CLASH Neural Network estimator (Molines and Medina (2016)). $rMSE$ measures the proportion of variance in the observations, which are not explained by the estimator. Hence, it is
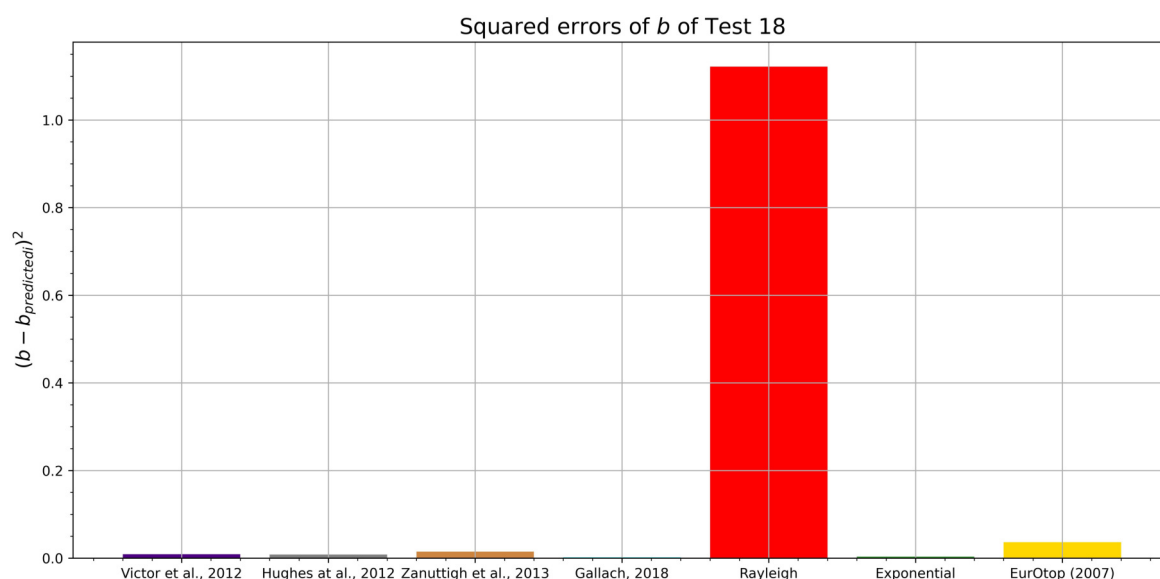
(a) Squared error of the considered prediction methods with regard to the measured data, for test 18 at CWL.
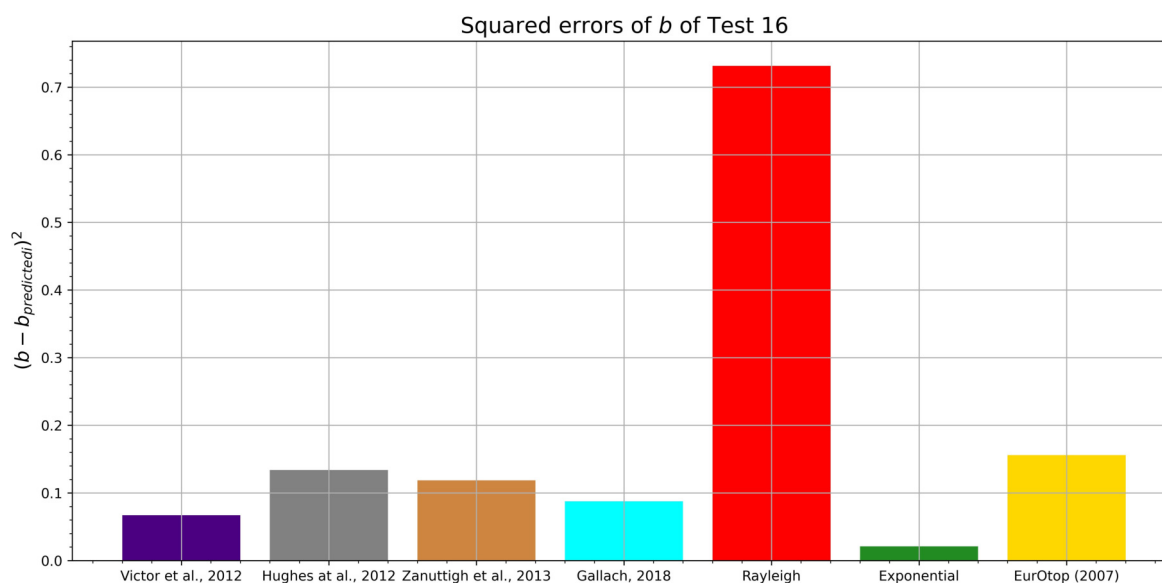
(b) Squared error of the considered prediction methods with regard to the measured data, for test 16 at CWL.

Figure 6.14: Comparison of the quadratic error of b between different tests.

possible to observe how accurate these prediction methods are by comparing them using the value of the *rMSE*. The lower this value, the lower the error. Following several articles and investigations carried out by Jorge Molines and Josep R. Medina, *rMSE* values lower than 0.2 are defined as good estimations, based on the experience of these
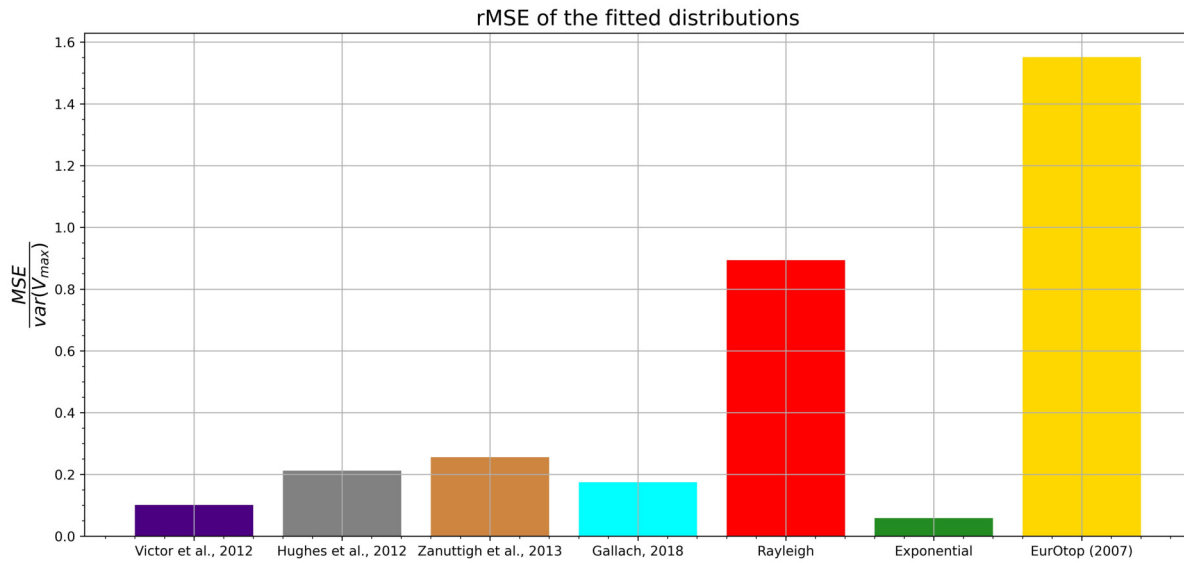
Figure 6.15: Relative mean squared error of the prediction methods for V_{max}.

authors (Molines and Medina (2015), Molines and Medina (2016), Molines et al. (2018) or Molines et al. (2019)). The obtained results are displayed in Figures 6.15 and 6.16 for V_{max} and b, respectively. However, this results are not comparable between each other. Besides, the obtained values for b have no physical sense. The reason for this is that these variables have different errors and different deviations, as well as a big difference in the order of magnitude.

$$MSE = \frac{\sum (V_{max,measured} - V_{max,predicted})^2}{N} \tag{6.2}$$

$$rMSE = \frac{MSE}{var(V_{max})} \tag{6.3}$$

Then, all prediction formulae are relatively accurate for the CWL case, as it was expected although all overtopping volumes are considered in this case, especially the formula from Victor et al. (2012). It is also noticeable that the exponential distribution is the one which best fits the measured data.

Another possibility to visualize the effect of the prediction method used from literature is represented in Figure 6.17, similar to Figure 6.8. In this case, it is quite noticeable that EurOtop (2007) overpredicts the value of V_{max}, while Rayleigh distribution produces
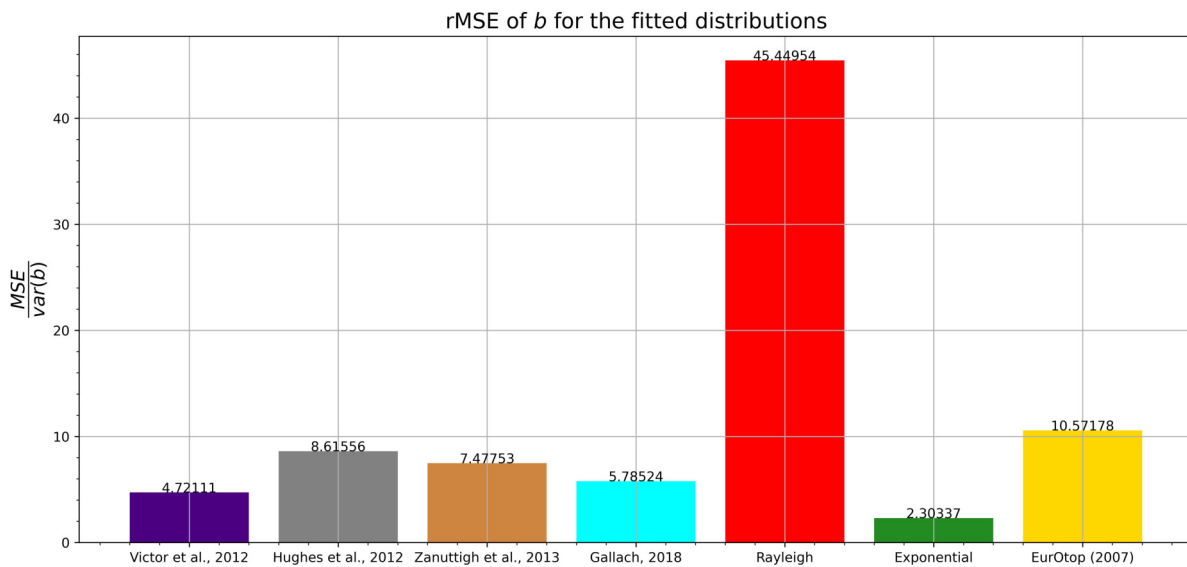
Figure 6.16: Relative mean squared error of the prediction methods for *b*.

the opposite effect. The rest of the formulae, as analysed in this Section, are quite close to each other regarding this value.

6.1.3.1 Sensitivity analysis

Furthermore, the same procedure for the analysis is going to be made for the highest 10% of individual wave overtopping volumes, the 30% and the 50%. With this approach, the aim of the analysis is then focused on the highest volumes in order to compare the fitting of these cases. Moreover, the formula from Hughes et al. (2012) is particulary designed for the top 10% of the individual wave overtopping volumes, so a more accurate prediction could be expected, as well as the formula suggested by Gallach Sánchez, David (2018), also for the upper 10% of individual volumes. The prediction formula by Victor et al. (2012) uses the 50% of the upper data (see Section 3.6.2).

With this, a more accurate estimation of the shape factor *b* is expected, in comparison with Figure 6.7, where a slight scatter is observed. However, it is also remarkable that if the percentage of the values considered is reduced and the amount of these values is too low, the accuracy of the fitting could be affected. The number of considered events can be seen in Table 6.3. To apply a certain percentage as a threshold, as the number of events need to be an integer number, the result of the percentage is truncated, so the
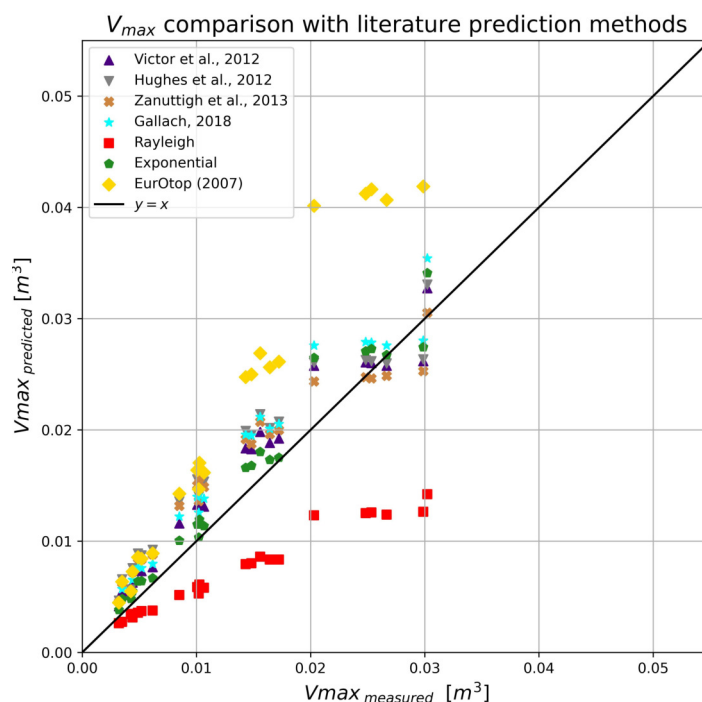
Figure 6.17: Comparison of the measured and predicted values of V_{max}.

threshold is always fulfilled and never exceeded. Moreover, at the end of this section, a comparison between the different threshold situations will be displayed.

At a very first approach, to compare these three situations with different thresholds, some plots are displayed to understand this analysis (see Paragraph 6.1.3.2). In Figure 6.18, the values of the shape parameter b are showed as a function of R_c/H_{m0}, in which the highest values of b are found for the 100% case. The same conclusion can be reached in Figure 6.19, in which all b-values are displayed for each test, with great variability between the thresholds. Finally, the shape factor can be also plotted as a function of a' (see Equation 3.25 from Paragraph 6.12) to clearly see the range of b for each case, as in Figure 6.20. In Figure 6.21, b-values are showed with respect the the probability of overtopping P_{ow} of the test.

i) **Top 50% of the individual wave overtopping volumes analysis.**

First, the highest 50% of the overtopping volumes are considered. Only the formula by Victor et al. (2012) from the prediction formulae used in this analysis is actually in-
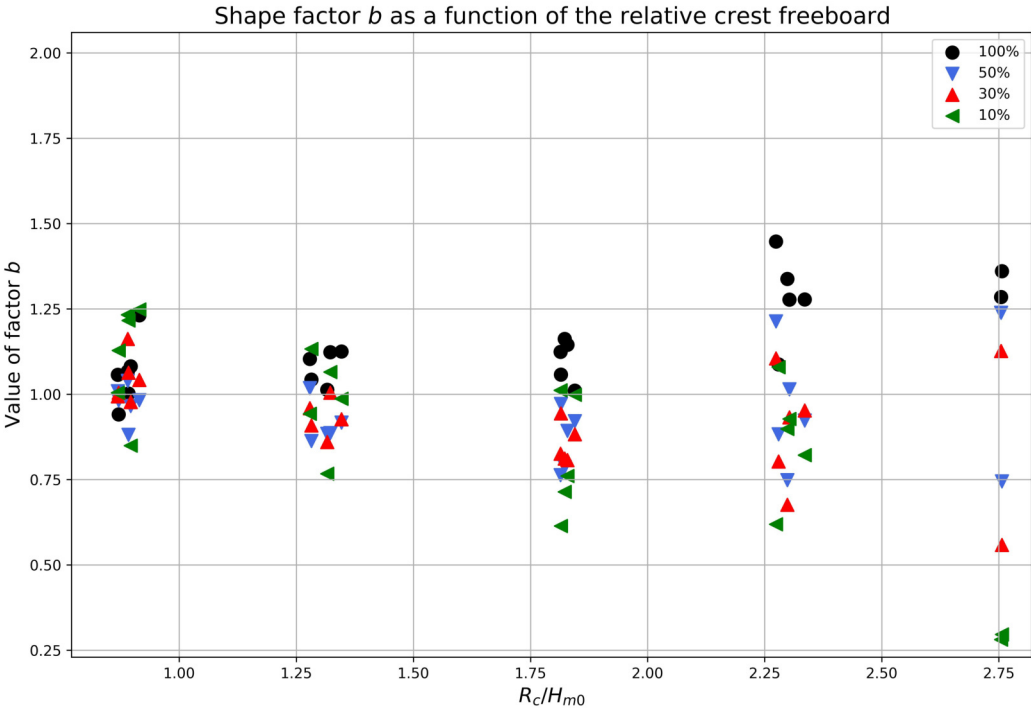
Figure 6.18: Shape factor b as a function of the relative crest freeboard, for the upper 50%, 30% and 10% volumes, including the 100% case.
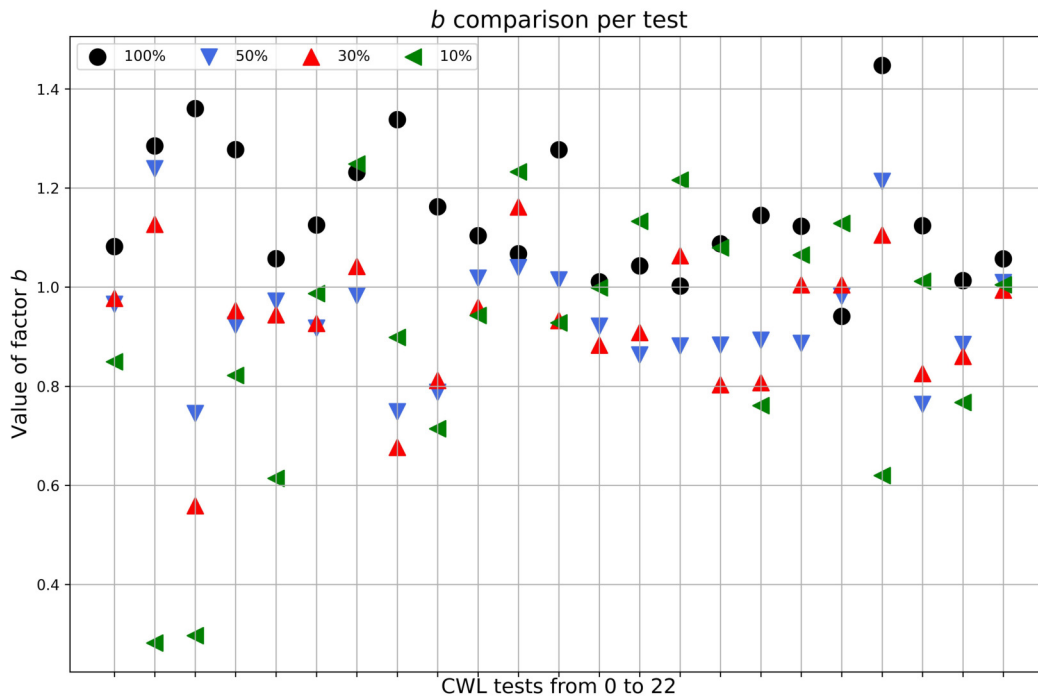
Figure 6.19: Comparison of the value of shape factor b per test, for the upper 50%, 30% and 10% volumes, including the 100% case.
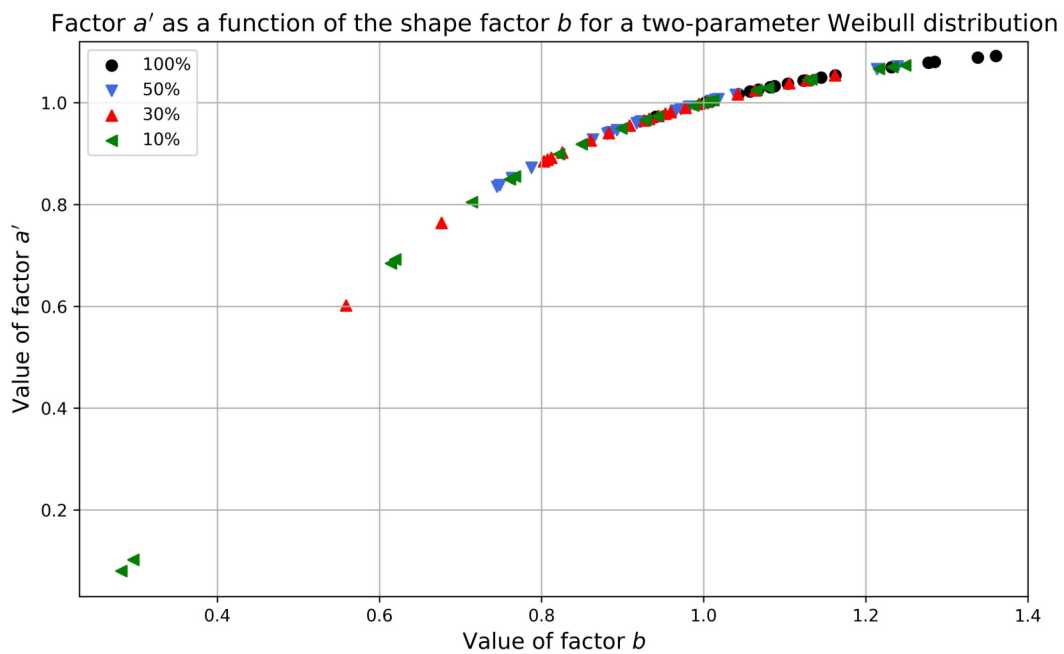
Figure 6.20: Factor a' as a function of shape factor b, for the upper 50%, 30% and 10% volumes, including the 100% case.

Case	N_{ow}	$P_{ow}[\%]$	50%	30%	10%
Test 0	1508	59.46	754	452	150
Test 1	11	1.76	5	3	1
Test 2	14	2.27	7	4	1
Test 3	49	7.97	24	14	4
Test 4	128	20.72	64	38	12
Test 5	265	42.33	132	79	26
Test 6	356	56.15	178	106	35
Test 7	58	9.27	29	17	5
Test 8	125	19.84	62	37	12
Test 9	263	41.35	131	78	26
Test 10	386	60.22	193	115	38
Test 11	44	7.11	22	13	4
Test 12	125	20.12	62	37	12
Test 13	238	37.72	119	71	23
Test 14	377	59.28	188	113	37
Test 15	54	8.68	27	16	5
Test 16	132	21.09	66	39	13
Test 17	267	43.49	133	80	26
Test 18	402	64.53	201	120	40
Test 19	48	7.82	24	14	4
Test 20	131	21.58	65	39	13
Test 21	270	44.41	135	81	27
Test 22	397	63.21	198	119	39

Table 6.3: Number of events considered in the sensitivity analysis for CWL tests.
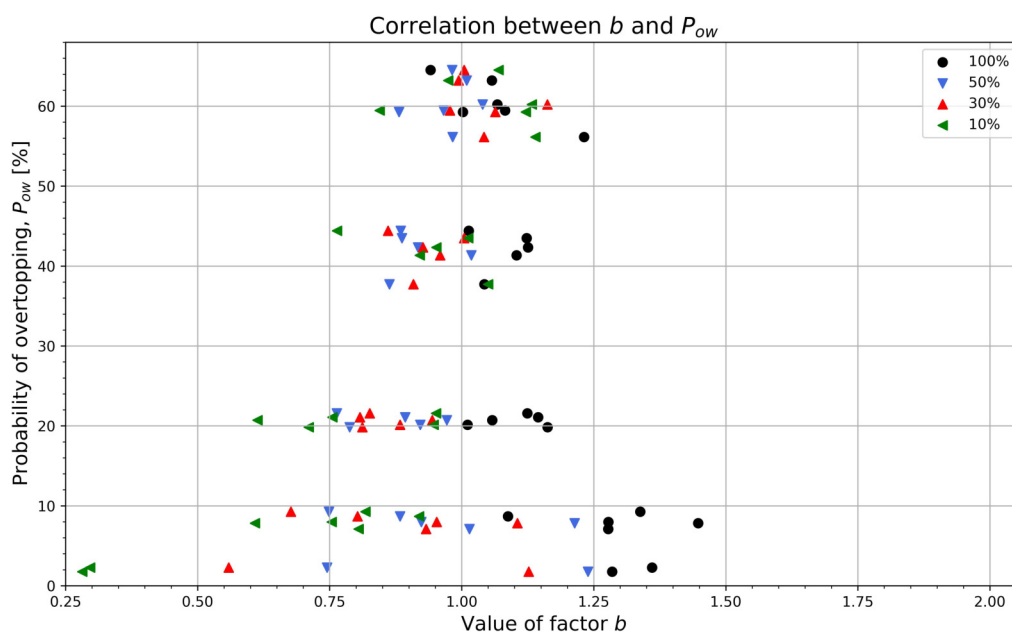
Figure 6.21: Comparison of the value of shape factor b according to P_{ow}, for the upper 50%, 30% and 10% volumes, including the 100% case.

tended for that exact portion of the data, but a significant reduction of the scatter in the results is observed for the majority of them.

If the results from Figure 6.7, in which the 100% of the volumes are considered, are compared with that same plot for this case, see Figure 6.22, a much less dispersion of the b-values is observed. Moreover, while in Figure 6.7, the value of shape factor b tends to be greater than 1, slightly far from the prediction formulae, in this case b is closer to what is supposed to be expected, showing a quite similar tendency with these formulae in literature. This effect is also verified even for those tests in which the number of overtopping events is limited and the probability of overtopping was quite low (see Figure 6.23). The same interpretation can be reached from Figure 6.24.

The fact that now most of the values of b are below the unit, can be also seen in Figure 6.25. In comparison with Figure 6.3, most of the values are now below 1 in x-axis.

For example, the fitting threshold can be clearly noticed if we compare the fitted distribution of the measured data for different and arbitrary tests as in Figure 6.26, where it is possible to see the difference between tests 4, 10, and 17 (see Table 6.1), considering all data (right) and the upper 50% of the volumes (left).
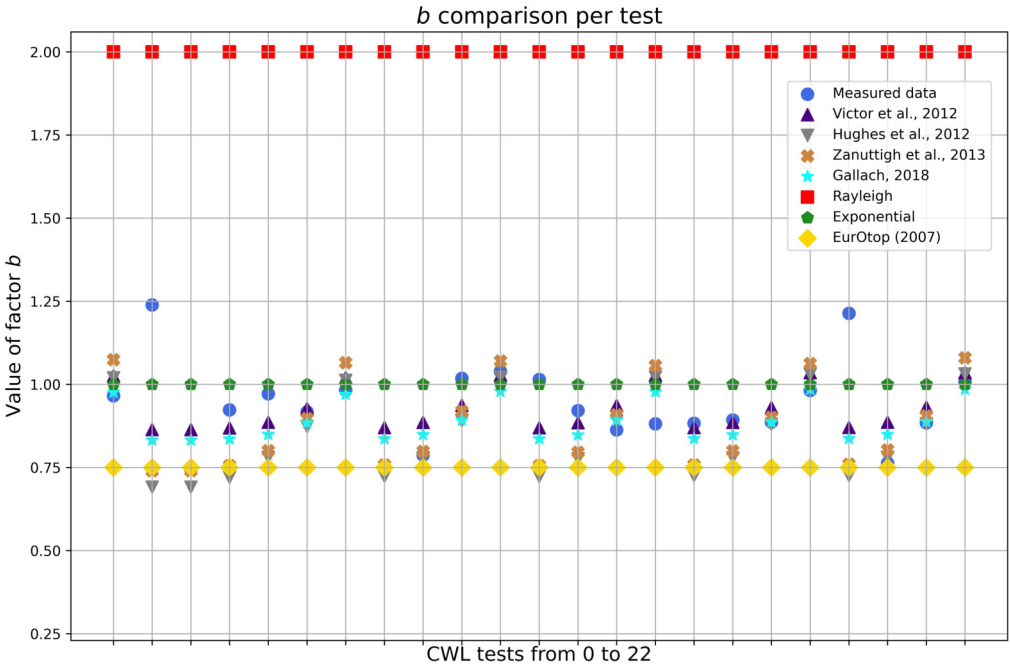
Figure 6.22: Comparison of all *b*-values for the CWL tests, from test 0 to test 22, for the upper 50% of the overtopping volumes.
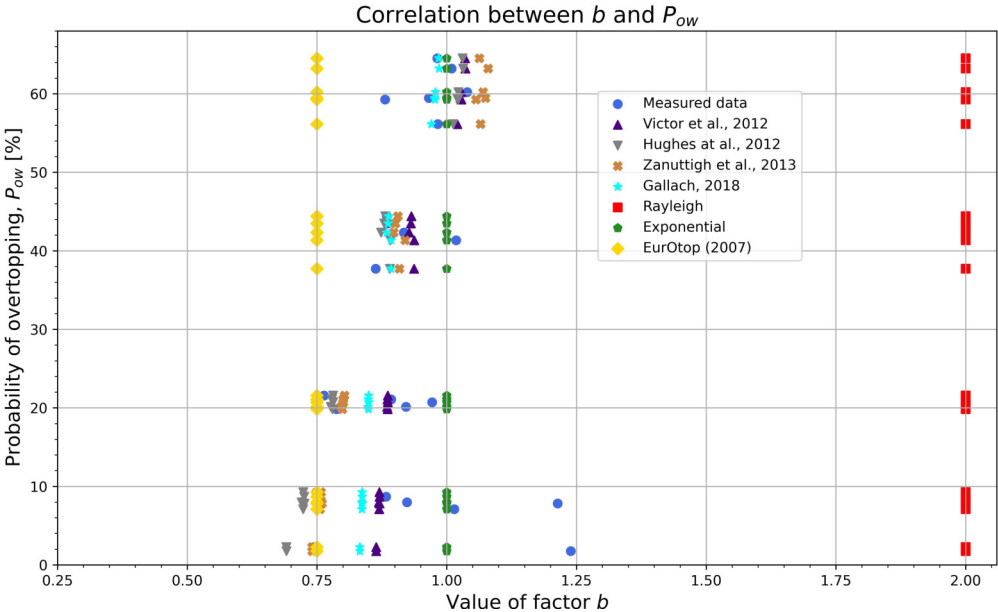
Figure 6.23: Correlation between factor *b* and the probability of overtopping P_{ow}, for the upper 50% of the overtopping volumes.
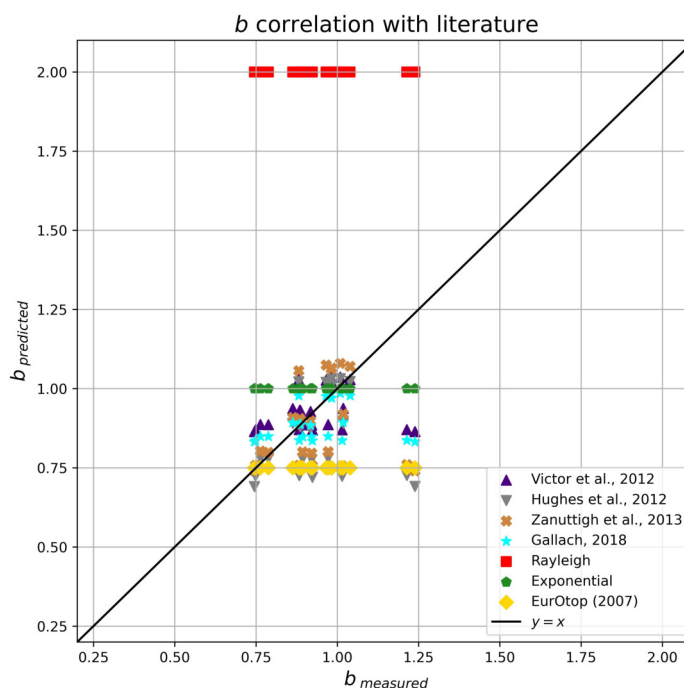
Figure 6.24: Comparison of the measured b-value according to the predicted ones, for the upper 50% of the overtopping volumes.

Following the same analysis than for the whole set of volumes, it is possible to compare the b-values with the water depth at the toe of the structure and with the relative crest freeboard, displayed in Figure 6.27. In this case, a lower scatter of the values of b is observed for the same values of both h/H_{m0} and R_c/H_{m0}.

Finally, using the value of V_{max} as well as for the whole set of overtopping volumes, as this is a variable that takes into account the value of b, it is possible to determine the accuracy of the fitting by the prediction formulae and distributions in literature. Then, Figure 6.28 shows that now the obtained error from the prediction formulae is lower than before, especially for Victor et al. (2012), Hughes et al. (2012) and Zanuttigh et al. (2013), around the value of 0.2, and Gallach Sánchez, David (2018) below it. See Figure 6.15 for the comparison. The $rMSE$ regarding the predicted values of b is displayed as well in Figure 6.29.

This same value of the predicted V_{max} can be compared as well with the measured one. In this case, the slight overprediction that can be noted in Figure 6.17 is now much more reduced between both values, as can be seen in Figure 6.30.

Factor *a′* as a function of the shape factor *b* for a two-parameter Weibull distribution
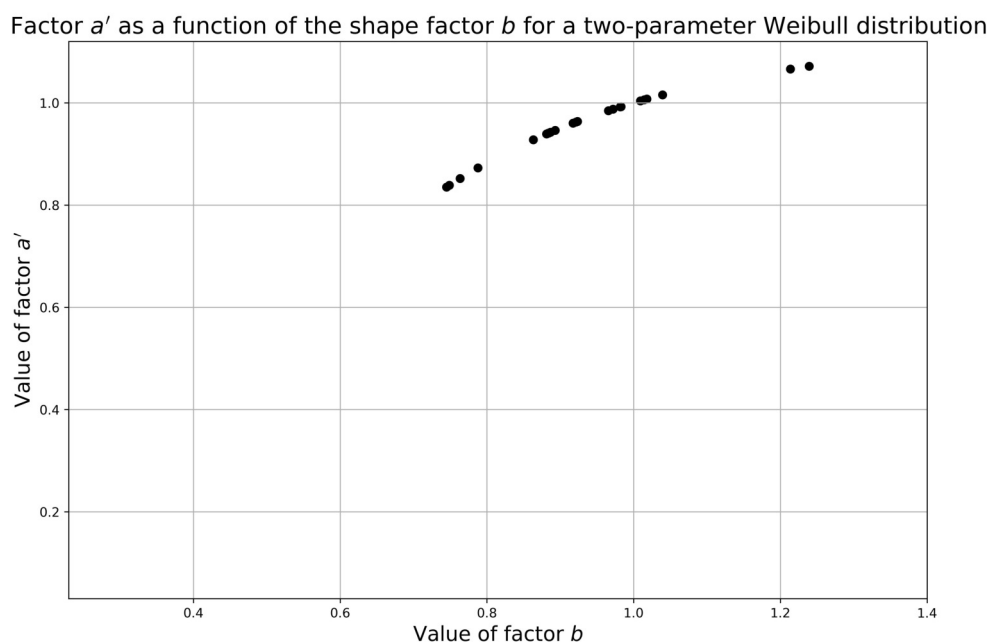
Figure 6.25: Factor a' as a function of shape factor b, for a two-parameter Weibull distribution, for the upper 50% of the overtopping volumes.

ii) **Top 30% of the individual wave overtopping volumes analysis.**

For the case in which the highest 30% of the overtopping volumes are considered, none of the applicable formulae in literature is especially defined for but the best and most accurate results are found. In this case, such an extensive analysis as for the upper 50% is not going to be followed but same plots and comparisons can be found in Section 6.1.3.2.

Nevertheless, a continuation of the data showed in Figure 6.26 can be seen in Figure 6.31 in order to understand the fitting threshold in this particular case, for the same tests.

iii) **Top 10% of the individual wave overtopping volumes analysis.**

Finally, for the highest 10% of the overtopping volumes, a detailed comparison of the results can be found in Section 6.1.3.2. Thus, as it will be explained in that section, results for this case show a bigger dispersion than for previous thresholds, despite the fact that some formulae are especially intended for this situation. The main reason for this result could be the reduction of the available values as a consequence of the threshold
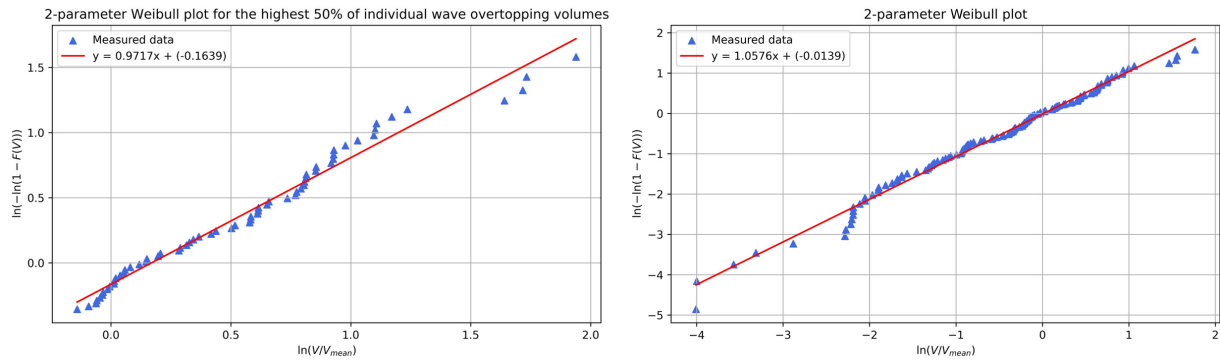
(a) Comparison of the fitted data for Test 4, for CWL.
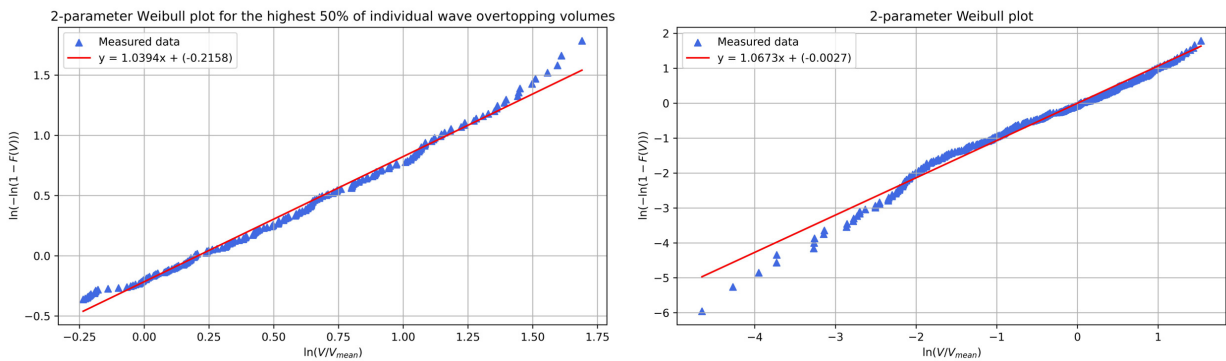
(b) Comparison of the fitted data for Test 10, for CWL.
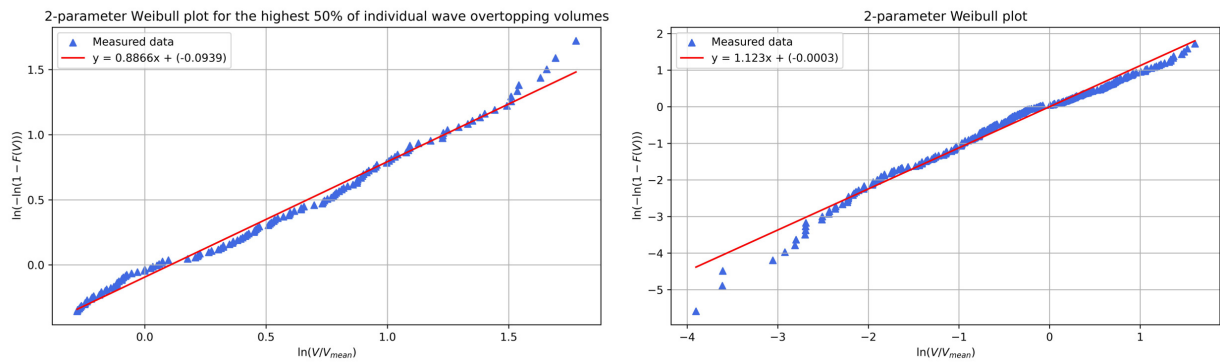
(c) Comparison of the fitted data for Test 17, for CWL.

Figure 6.26: Comparison of the fitted data for different test in a Weibull plot, considering the upper 50% of the volumes (left) and the whole data (right).

that leads in a less reliable analysis. It is also remarkable that a higher computational cost is required for this situation.

(a) Shape factor as a function of the relative crest freeboard
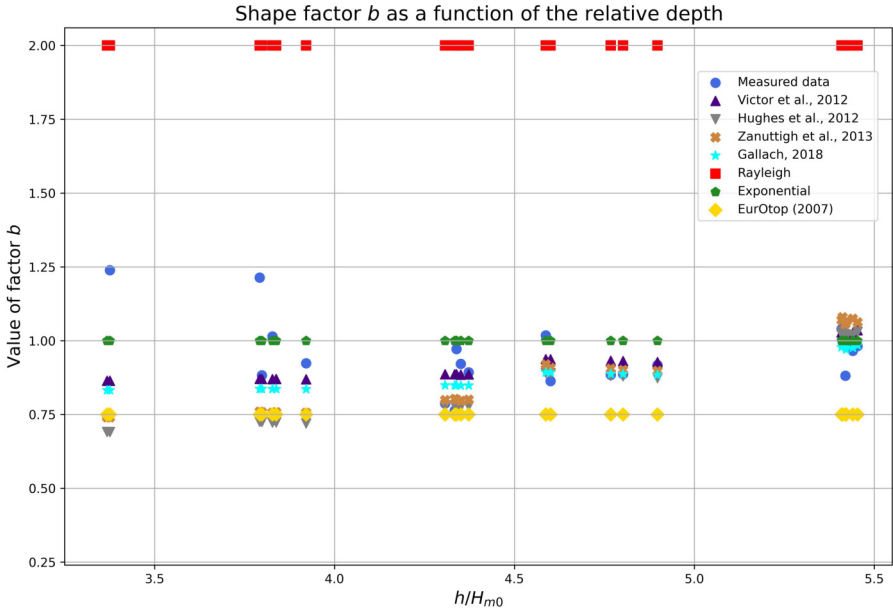
(b) Shape factor as a function of the relative depth

Figure 6.27: Correlation of the values of shape factor b regarding to geometric and hydraulic parameters, for the upper 50% of the overtopping volumes.

As for the previous case, in order to continue the comparison of the fitting thresholds, the fitted distribution of the measured data is displayed for tests 4, 10 and 17 in Figure 6.32.
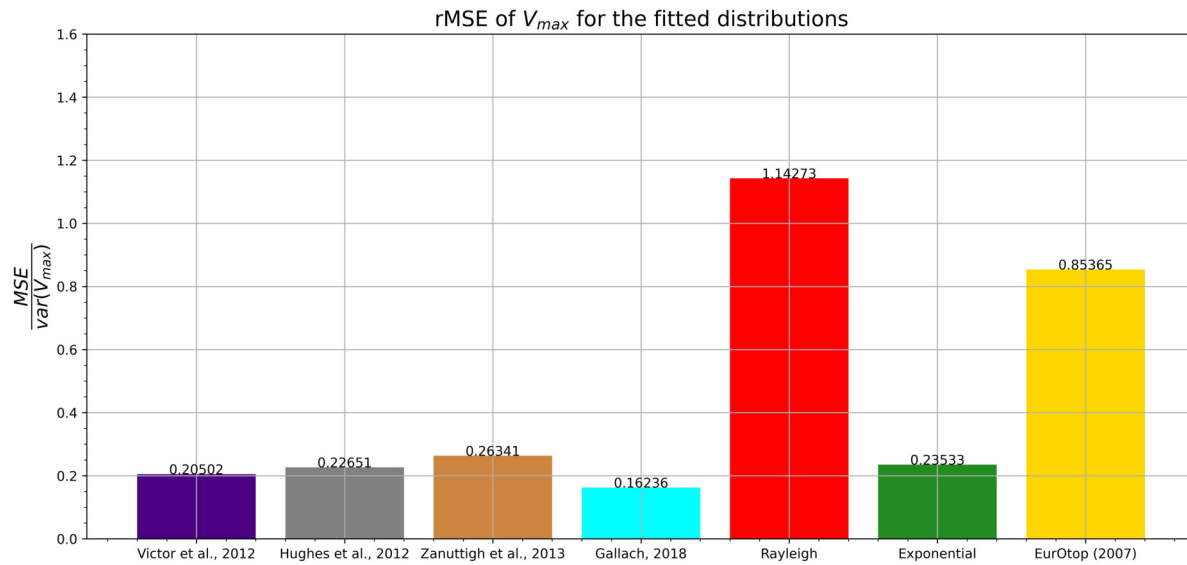
Figure 6.28: Relative mean squared error of the prediction methods for V_{max}, for the upper 50% of the overtopping volumes.
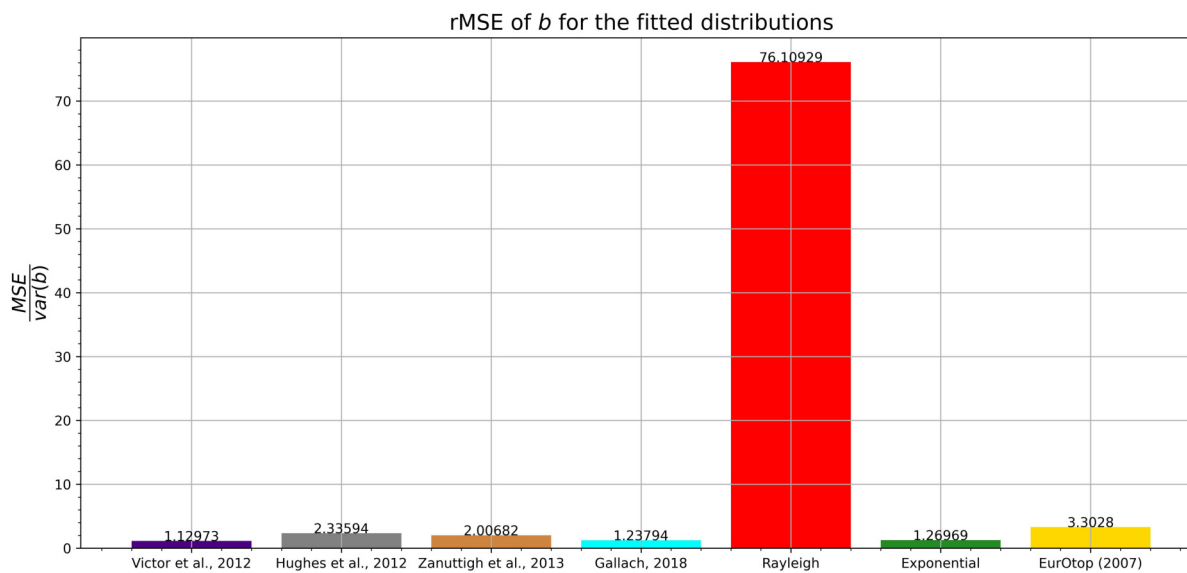
Figure 6.29: Relative mean squared error of the prediction methods for b, for the upper 50% of the overtopping volumes.
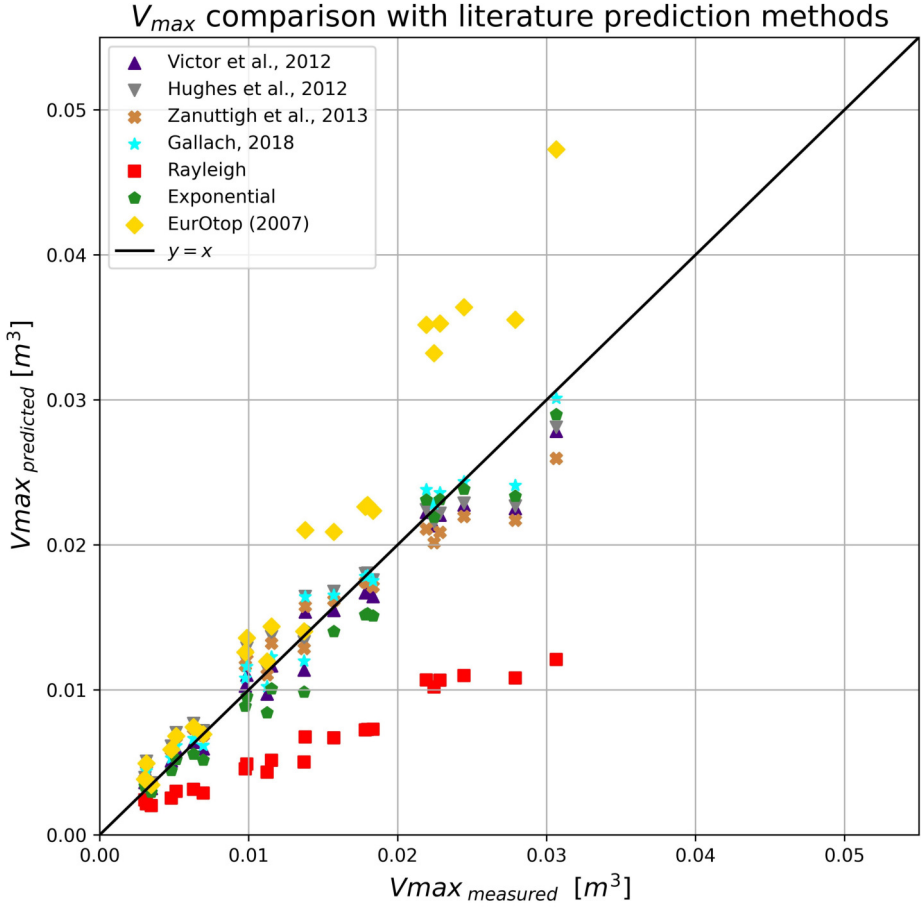
Figure 6.30: Comparison of the measured and predicted values of V_{max}, for the upper 50% of the overtopping volumes.
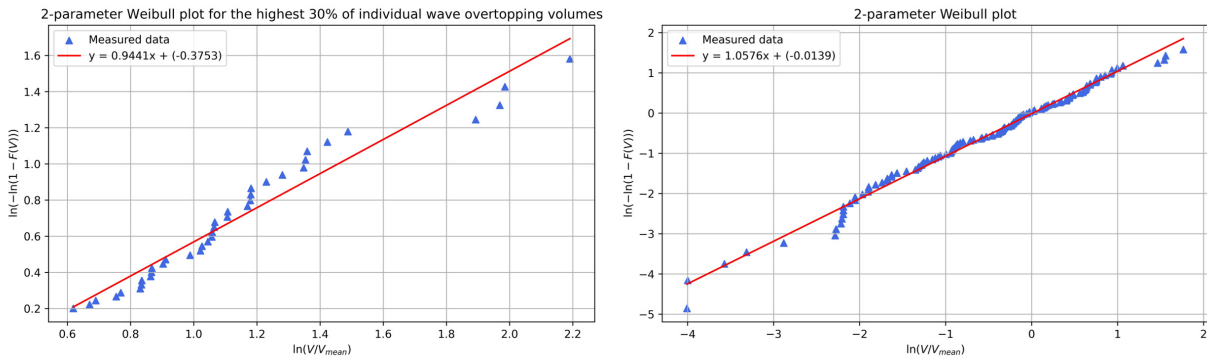
(a) Comparison of the fitted data for Test 4, for CWL.
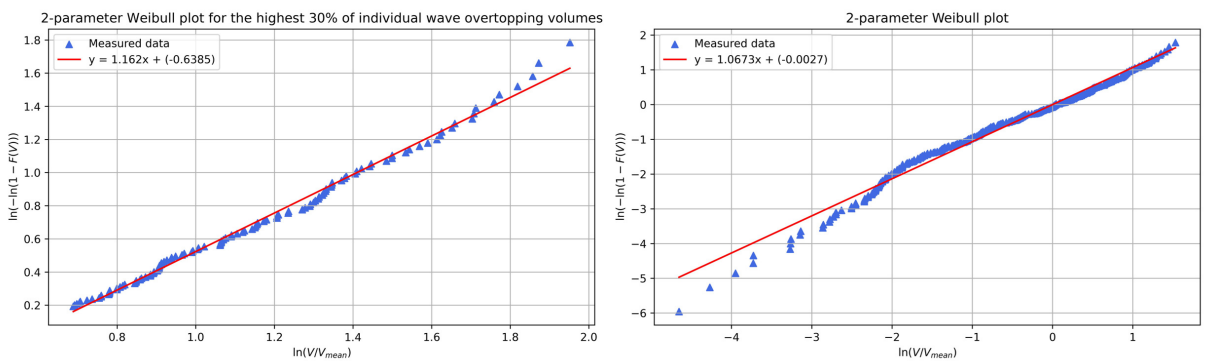
(b) Comparison of the fitted data for Test 10, for CWL.
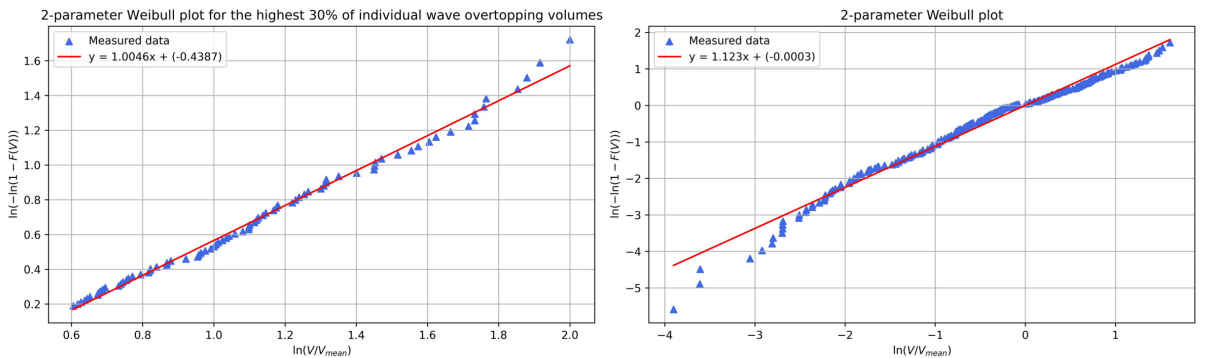
(c) Comparison of the fitted data for Test 17, for CWL.

Figure 6.31: Comparison of the fitted data for different test in a Weibull plot, considering the upper 30% of the volumes (left) and the whole data (right).
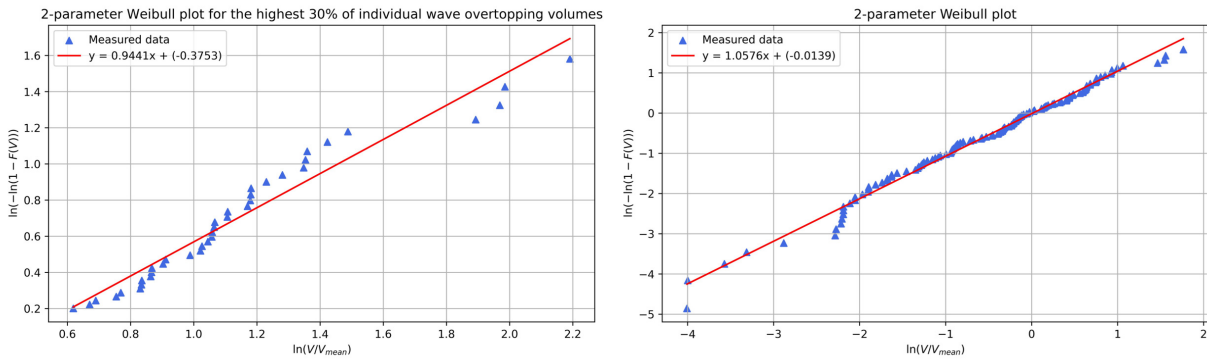
(a) Comparison of the fitted data for Test 4, for CWL.
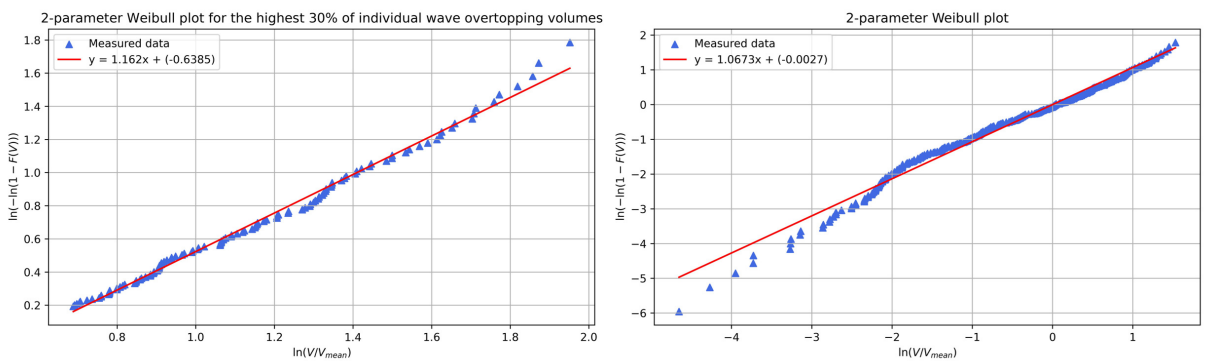
(b) Comparison of the fitted data for Test 10, for CWL.
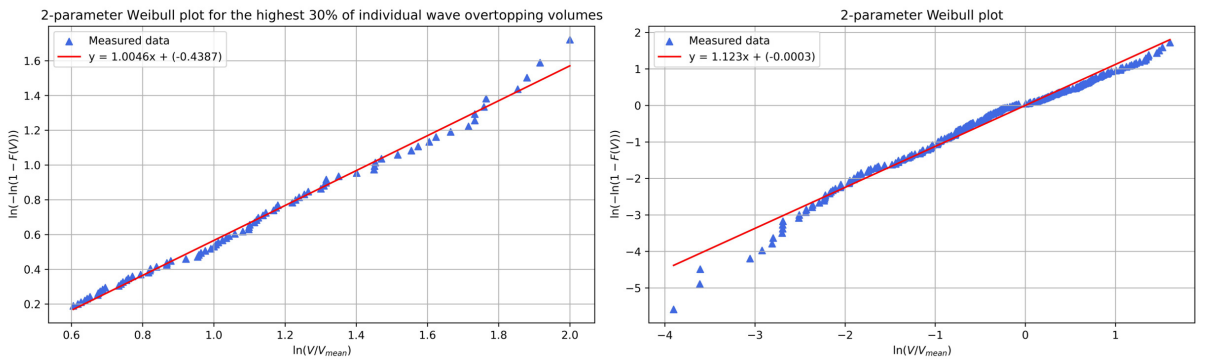
(c) Comparison of the fitted data for Test 17, for CWL.

Figure 6.32: Comparison of the fitted data for different test in a Weibull plot, considering the upper 10% of the volumes (left) and the whole data (right).

6.1.3.2   Comparison between thresholds

Once the analysis for different portions of the data is carried out, it is now possible to compare the results in a global way to reason the main conclusions. For this, plots

showed previously are now displayed next to each other to clearly visualize the main differences.

First, the plot comparing the different values of shape factor b with the predicted ones can be seen in Figure 6.33. It represents the extended version of Figure 6.19, in which only the measured values were displayed. Hence, compared with all of the volumes in (A), plots for the 50 and 30% in (B) and (C) show a lower dispersion of the results and a bigger concentration in a smaller range defined by the formulae. However, for the case of the upper 10%, the case for which the formulae by Hughes et al. (2012) and Gallach Sánchez, David (2018) are intended, a bigger dispersion is observed. This fact could be a consequence of the reduction of the available values due to the consideration of only a tenth of the overtopping volumes, which leads to a less reliable analysis for this particular experimental case.

Although from last Figure 6.33 it is also possible to visualize the range of the b-values, Figure 6.34 comparing a' and b shows this results easier. Then, in the case in which all the overtopping volumes are considered, most of the b-values are above 1. Considering just the 50% the result is practically the opposite, with most of the values below 1. For the 30 and 10% cases, a more balanced distribution of these values is observed around the unit.

Moving to Figure 6.35, the accuracy of the values in these plots is measured according to how the predicted values follow the line represented by the measured data. In this sense, as previously remarked, for the whole set of volumes both predicted and measured values are quite different, but for the cases of the upper 50 and 30% the reliability of the analysis increases, except for the most extreme values of the shape factor b measured. For the upper 10% case, a similar result is obtained but a bigger scatter is also observed for the extreme values of the range of the value of b.

As well as for previous results, for the comparison between b and the probability of overtopping in Figure 6.36, while for the whole data a big scattering is observed, a more accurate result is observed for the cases of the upper 30 and 50%. However, it can be seen again that for the specific case of the highest 10% of the overtopping volumes a bigger deviation is found, mainly because of the reduction of available values for the calculation of the results.

Finally, to clearly visualize the accuracy predicted in literature, the value of V_{max} is used as a representative value of the distribution parameters, displayed in Figure 6.37. Thus, from case (A) considering the whole set of volumes, a better correlation is found
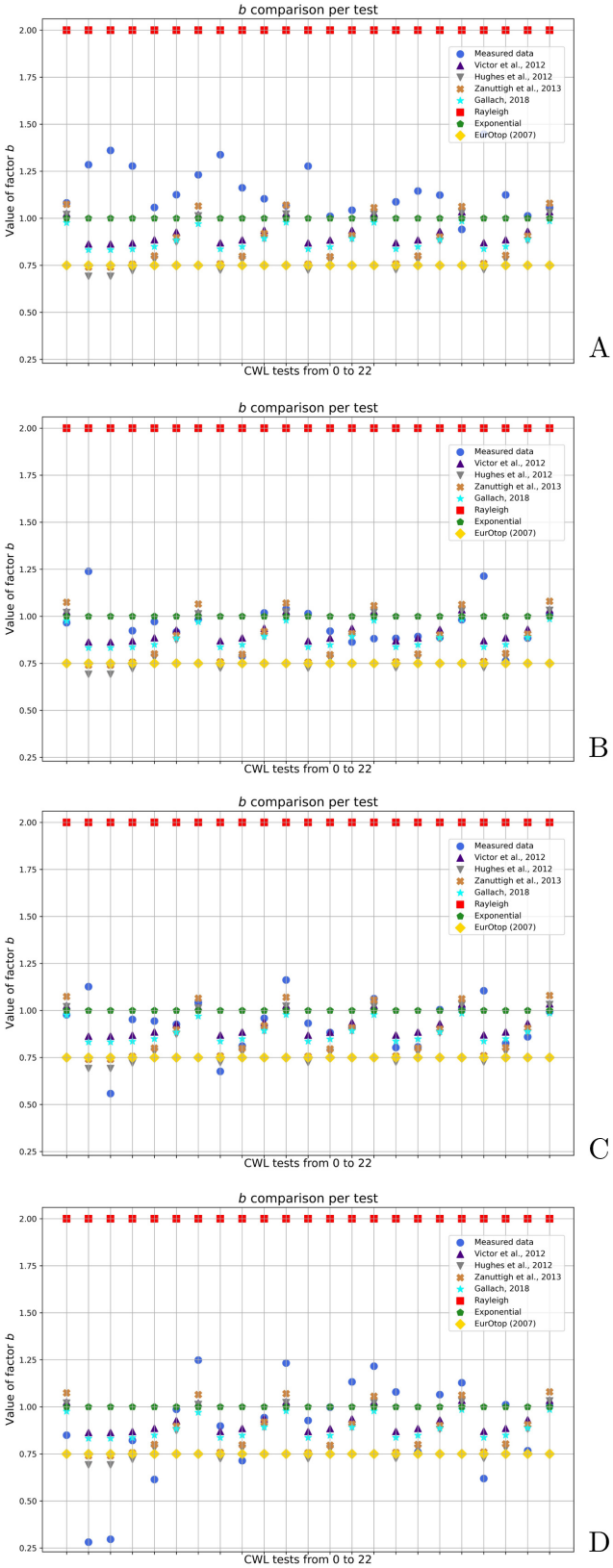
Figure 6.33: Comparison of the *b*-values for all tests according to the portion of the data considered. From above to below: A) All volumes. B) Upper 50%. C) Upper 30%. D) Upper 10%.

Factor *a'* as a function of the shape factor *b* for a two-parameter Weibull distribution

A

Factor *a'* as a function of the shape factor *b* for a two-parameter Weibull distribution

B

Factor *a'* as a function of the shape factor *b* for a two-parameter Weibull distribution

C

Factor *a'* as a function of the shape factor *b* for a two-parameter Weibull distribution

D

Figure 6.34: Comparison of the distribution parameters for all tests according to the portion of the data considered. From above to below: A) All volumes. B) Upper 50%. C) Upper 30%. D) Upper 10%.
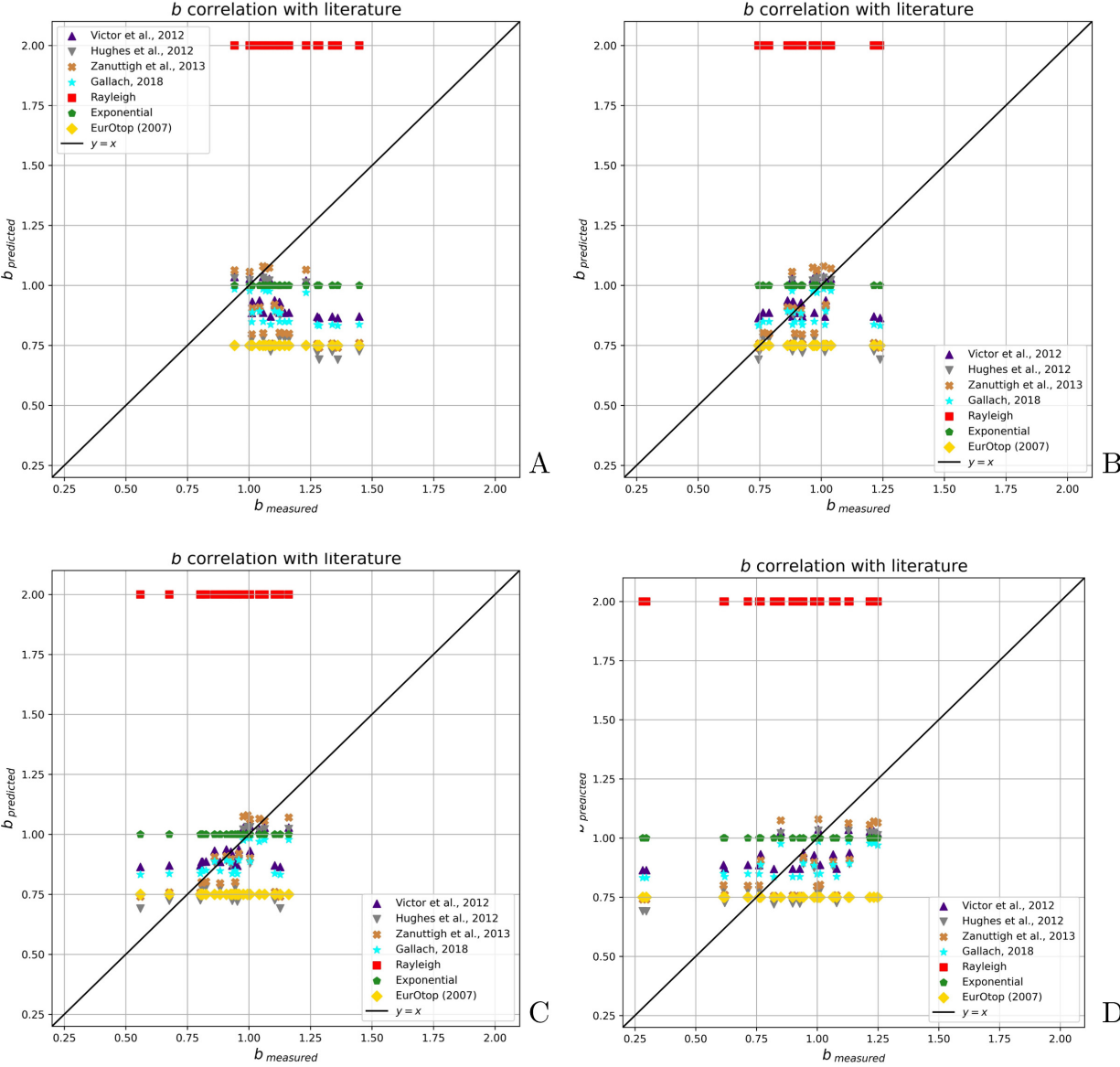
Figure 6.35: Comparison of the predicted and measured shape factor according to the portion of the data considered. From above to below, and left to right: A) All volumes. B) Upper 50%. C) Upper 30%. D) Upper 10%.
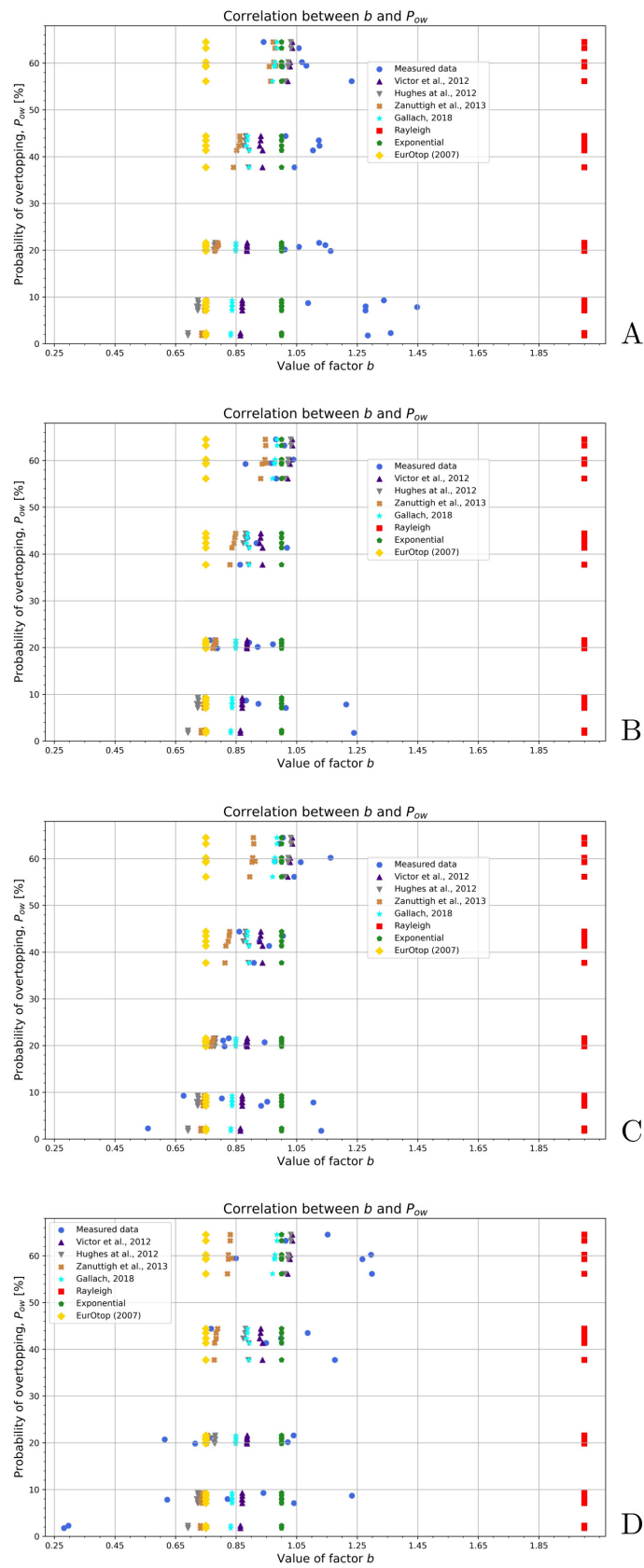
Figure 6.36: Comparison of *b* and *P_ow* according to the portion of the data considered. From above to below: A) All volumes. B) Upper 50%. C) Upper 30%. D) Upper 10%.

in terms of accuracy for the 50 and 30% cases in (B) and (C), respectively, and especially for the upper 30%, in which some of the formulae in literature are below to a *rMSE* value of 0.05. However, this same effect can be also seen for the *rMSE* of *b* in Figure 6.38, although the error is bigger according to this different variable.

For the upper 10%, as mentioned before, a bigger dispersion is found probably because of the small set of values for the analysis. With this, the formula of Victor et al. (2012) is defined for the highest 50% of the overtopping volumes and a very good performance is observed, although the formula of Gallach Sánchez, David (2018) is also quite accurate in this case. For the upper 30% of the values, none of these considered formulae are strictly defined but the best results are found for this case. Finally, for the upper 10% case in which the formulae defined by Hughes et al. (2012) and Gallach Sánchez, David (2018) are intended, a good performance in general terms is observed, mainly following the tendency of the previous analysis. The formula of Zanuttigh et al. (2013), the one considered in EurOtop (2018), despite it is intended for a wider range of values and this fact always leads to a bigger deviation, shows a good accuracy in most of the situations, although it is not the best one.

The Rayleigh distribution as well as the established value of $b = 0.75$ in EurOtop (2007) show a much bigger deviation, which can be also seen in Figure 6.39, comparing the predicted values of V_{max}.

As a conclusion of this section according to the results and plots displayed, the review of the available and applicable formulae in literature is majorly verified for this dataset, despite that it is an experimental approach and values will never be exactly the same. One of the most remarkable aspects of the analysis is the fact that those formulae specifically defined for the upper 10% of the overtopping volumes are not as accurate as expected. However, as it was mentioned, the reduction of the values available to the analysis as a consequence of the definition of the threshold can vastly affect the analysis.

Finally, to end this chapter, one last consideration has to be done regarding the percentage of the highest overtopping volumes. It is clear that both 50 and 30% cases are quite accurate to the data, but the main doubt is the exact percentage for what the best results are found. For that reason, the same analysis has been carried out for more different thresholds and without considering Rayleigh distribution and EurOtop (2007), in order to achieve a higher level of understanding of the dataset. Hence, percentages from 10 to 70 are considered. These results can be found in Figures 6.40 and 6.41.

Then, with a closer look to these results in Figure 6.42, it can be observed that:
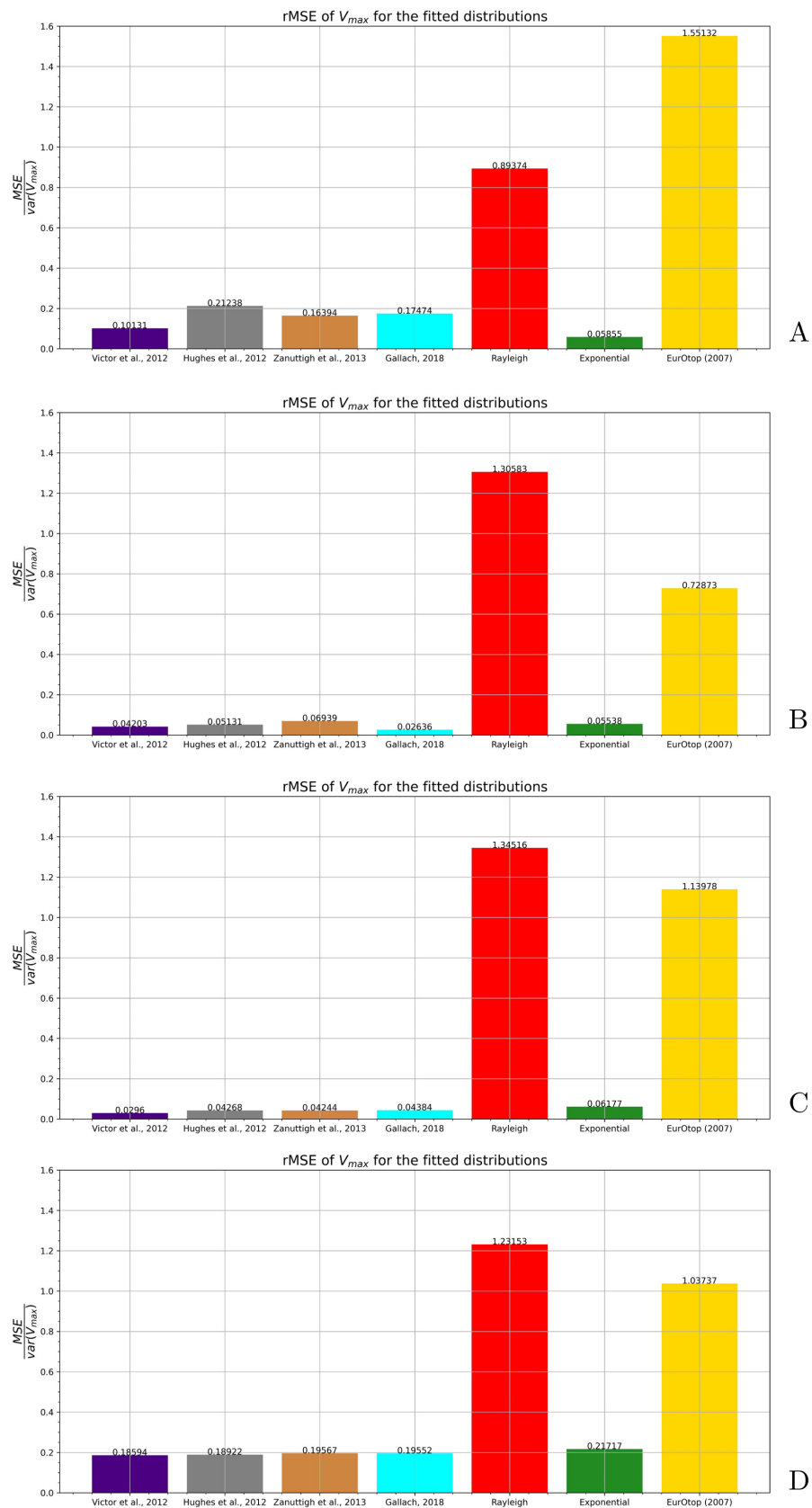
Figure 6.37: Comparison of the *rMSE* of V_{max} according to the portion of the data. From above to below: A) All volumes. B) Upper 50%. C) Upper 30%. D) Upper 10%.
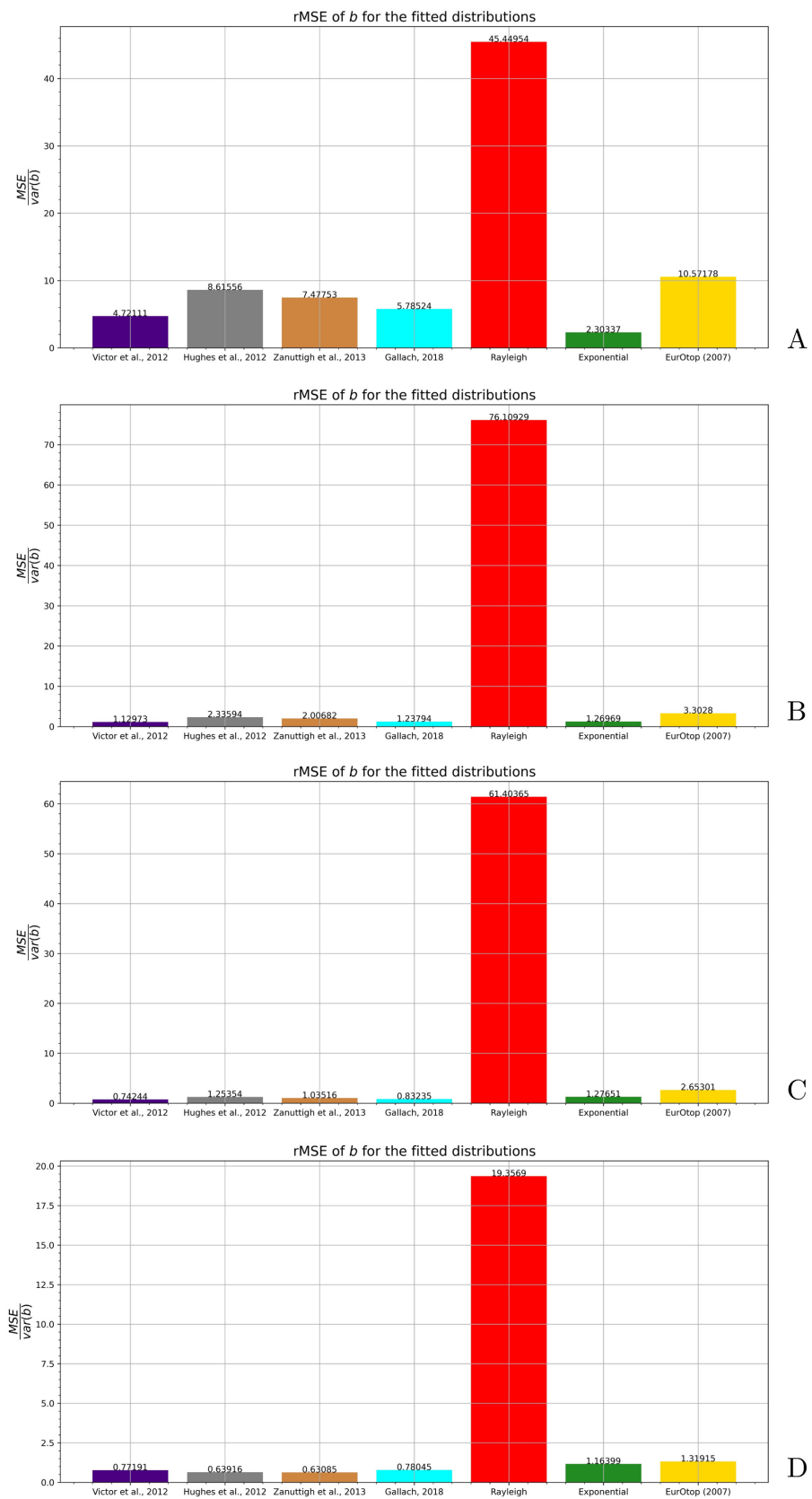
Figure 6.38: Comparison of the *rMSE* of *b* according to the portion of the data. From above to below: A) All volumes. B) Upper 50%. C) Upper 30%. D) Upper 10%.
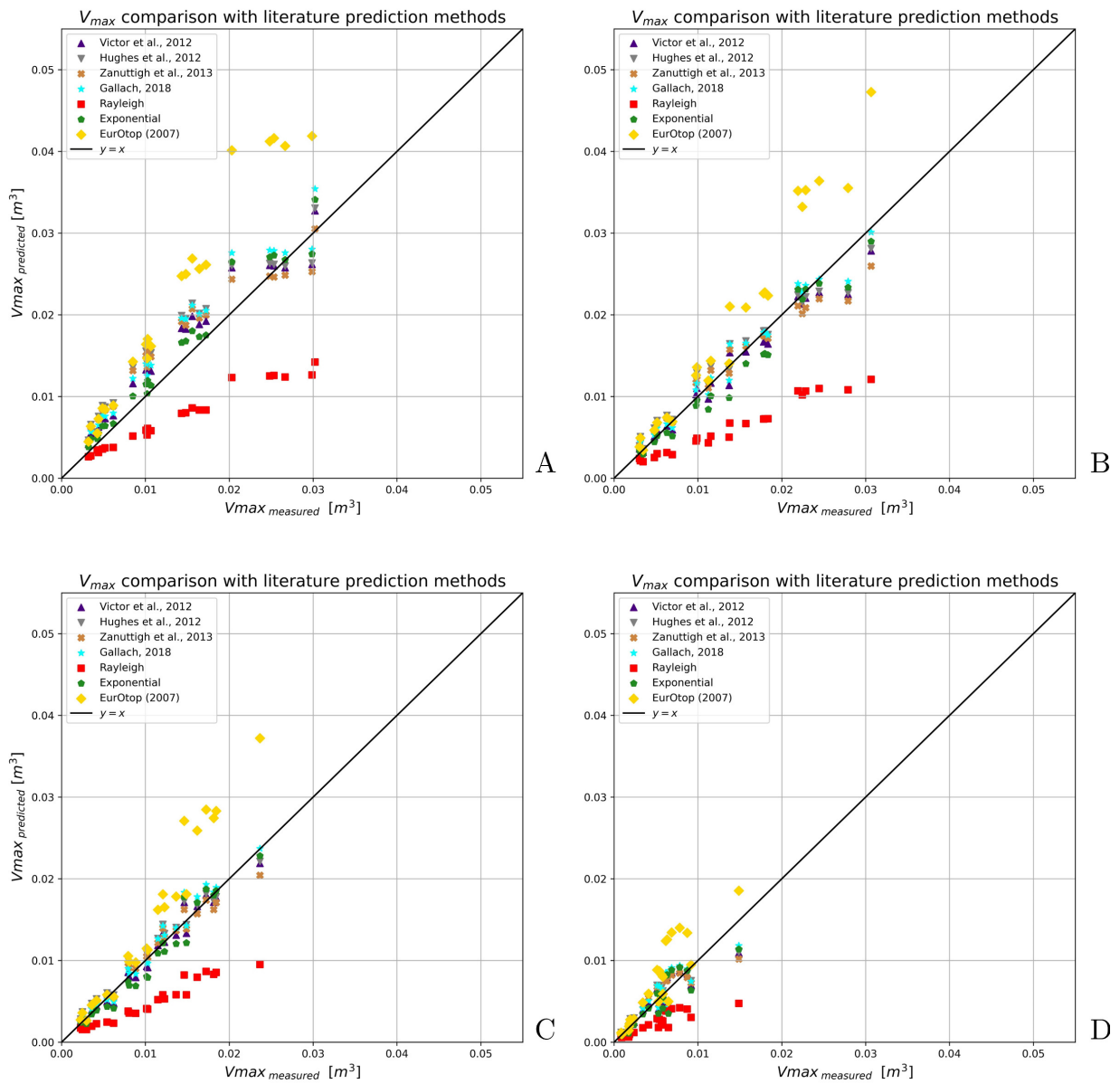
Figure 6.39: Comparison of the predicted and measured values of V_{max} according to the portion of the data considered. From above to below and left to right: A) All volumes. B) Upper 50%. C) Upper 30%. D) Upper 10%.
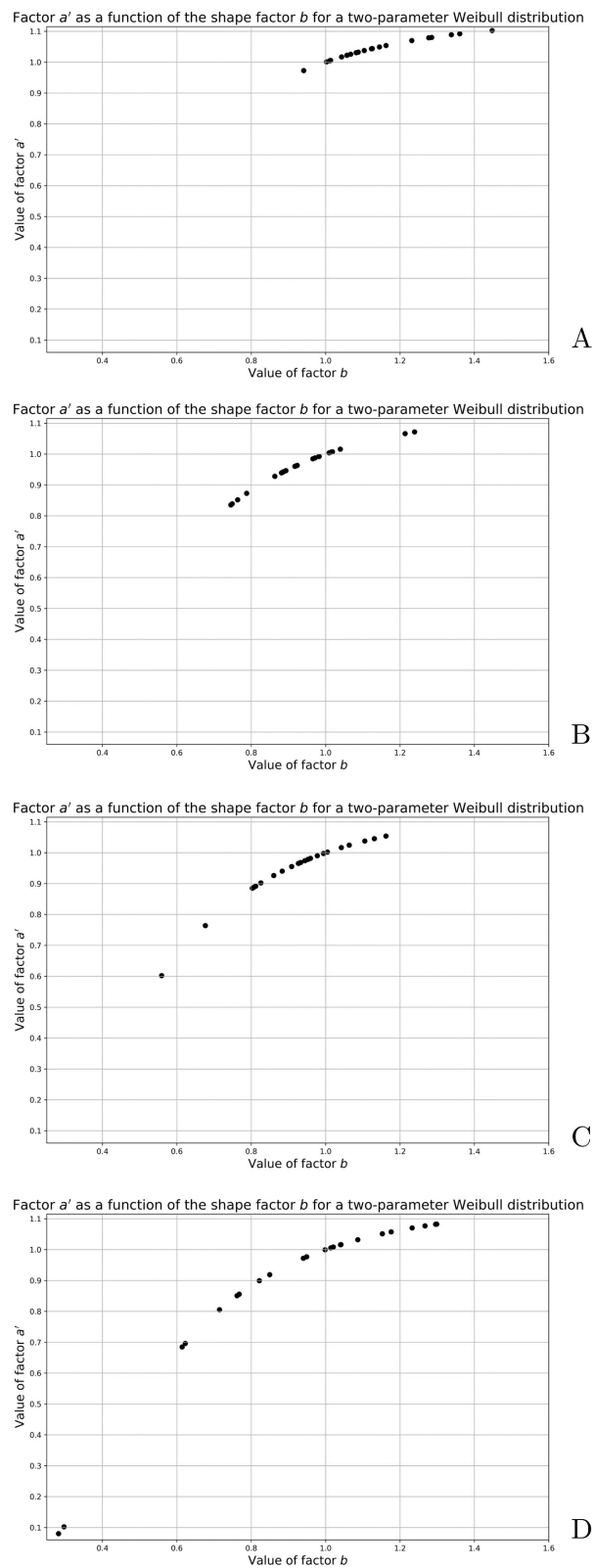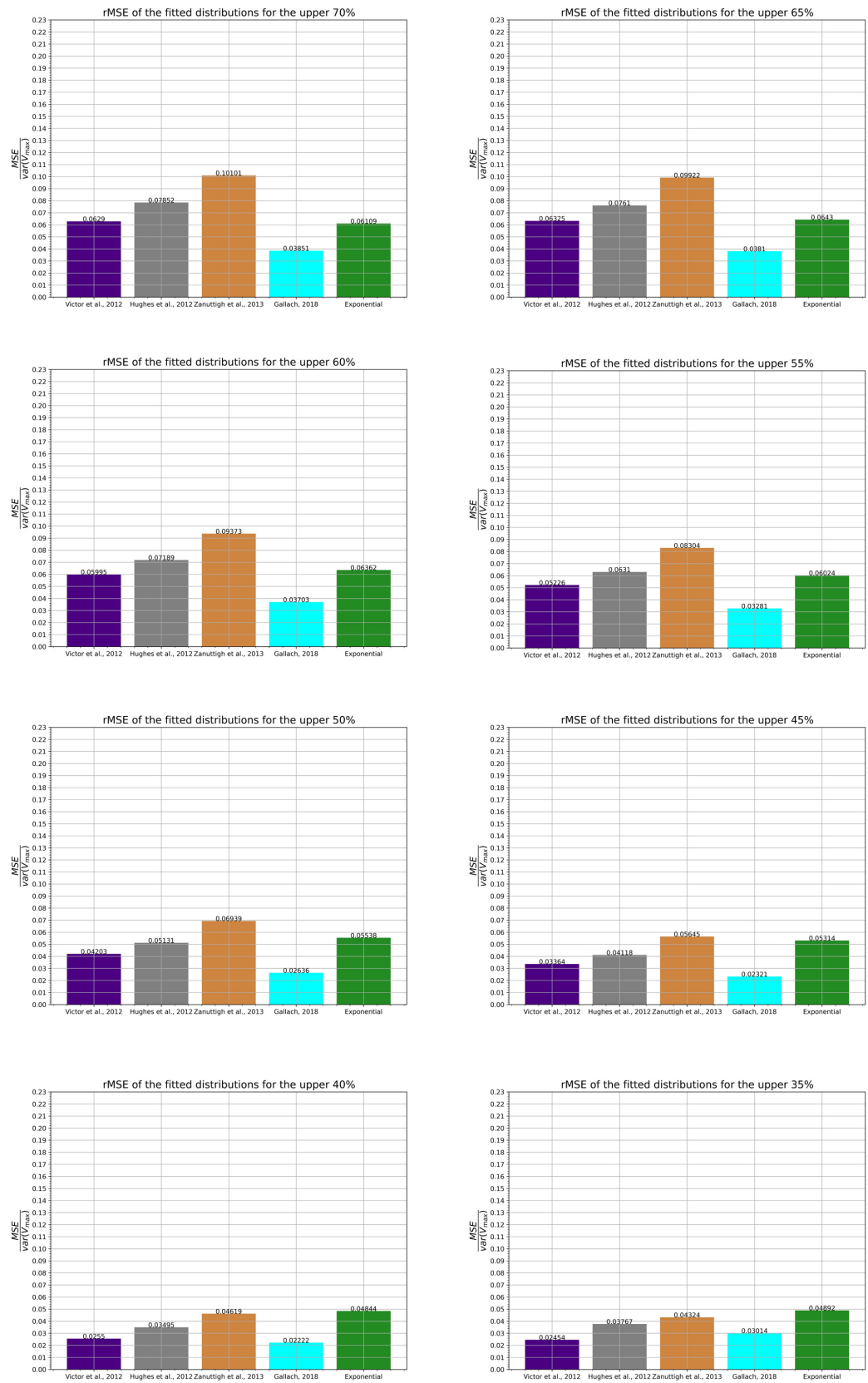
Figure 6.40: *rMSE* of the predicted values of V_{max} according to the threshold of volumes (1).
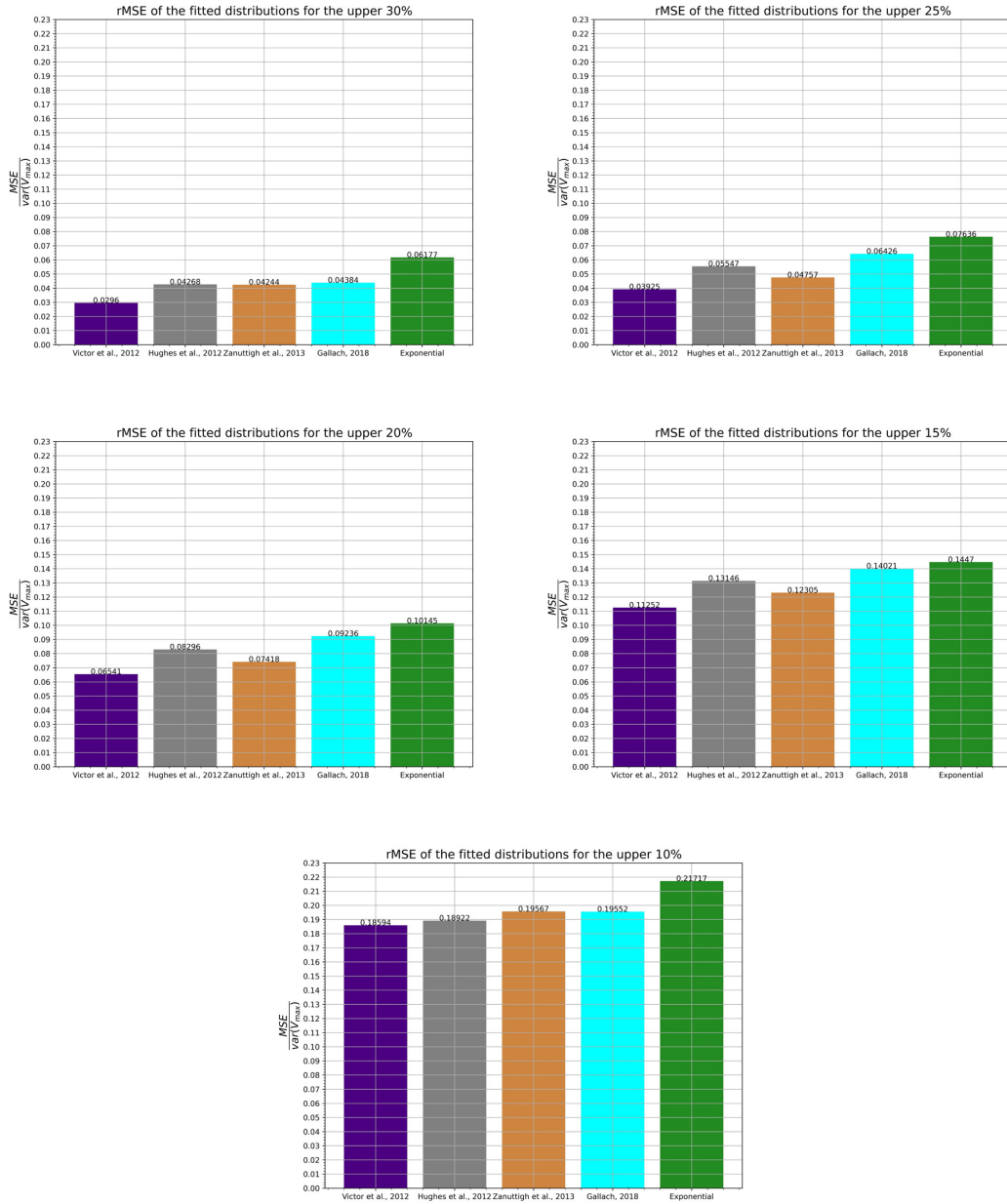
Figure 6.41: *rMSE* of the predicted values of V_{max} according to the threshold of volumes (2).

- The accuracy of the prediction by the formula of Zanuttigh et al. (2013) is lower when the number of overtopping volumes is reduced, but worse than the rest of the formulae when reaching the 50% in term of accuracy. It is important to remark that the value of q used in the formula is the one given by Equation 3.7 and not the value derived from the measurements.

- For the rest of the cases, the most accurate prediction is either the formula of Victor et al. (2012) or the formula of Gallach Sánchez, David (2018). The lower value of the *rMSE* in all cases is given for the upper 40% by the Gallach Sánchez, David (2018)'s formula.

- For 40% or more of the highest volumes, the most accurate formula is the one of Gallach Sánchez, David (2018), despite this is intended for the upper 10%. For 35% or less of the highest volumes, the formula of Victor et al. (2012) is the most accurate one.

- Between the 40% and the 35% there is a value around 38% for which these two last prediction methods are close to be similar in terms of the deviation.

- All 4 prediction methods and the exponential distribution show *rMSE* values below 0.2 in most of the cases. Then, as it was expected, the CWL formulation in literature is highly accurate for the prediction of the dataset.

This same approach can be followed for the error of shape factor b, although as expected due to it is a different variable, another tendency can be observed in Figure 6.43, although great results are also found for Victor et al. (2012) and Gallach Sánchez, David (2018).

To finish the sensitivity analysis, Figure 6.44 shows how the selection of the threshold can influence in the results of the analysis. Hence, b is displayed as a function of R_c/H_{m0} for the different cases but no Rayleight and EurOtop (2007) are considered.
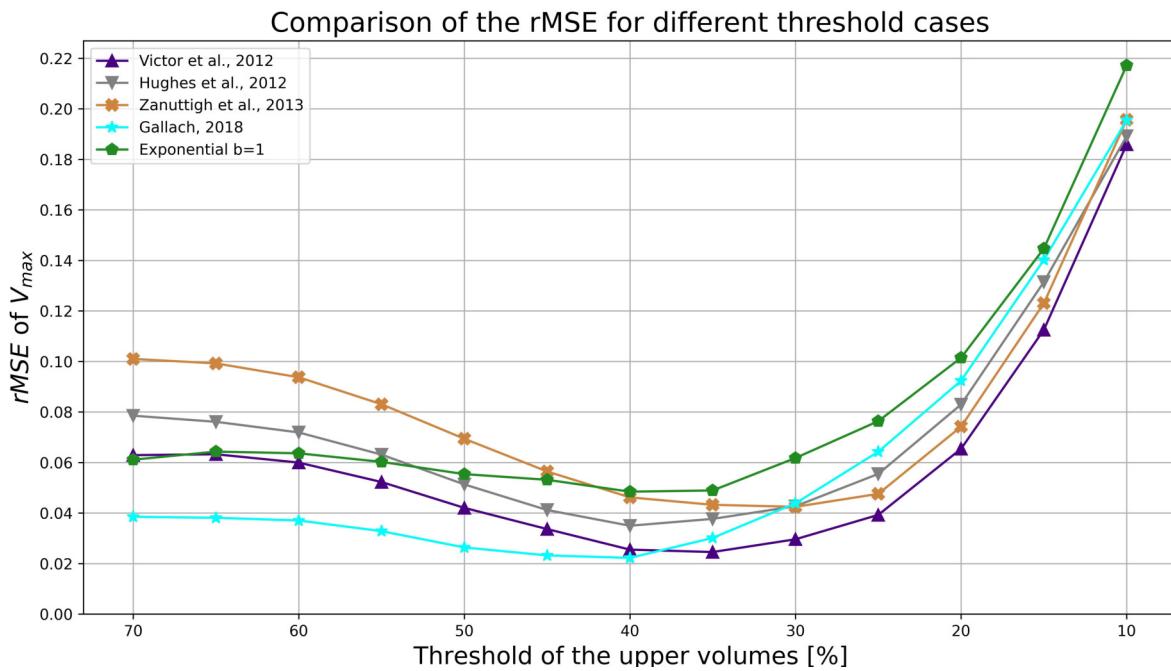
Figure 6.42: Comparison of the *rMSE* of the predicted values of V_{max} according to the threshold of volumes, for CWL.
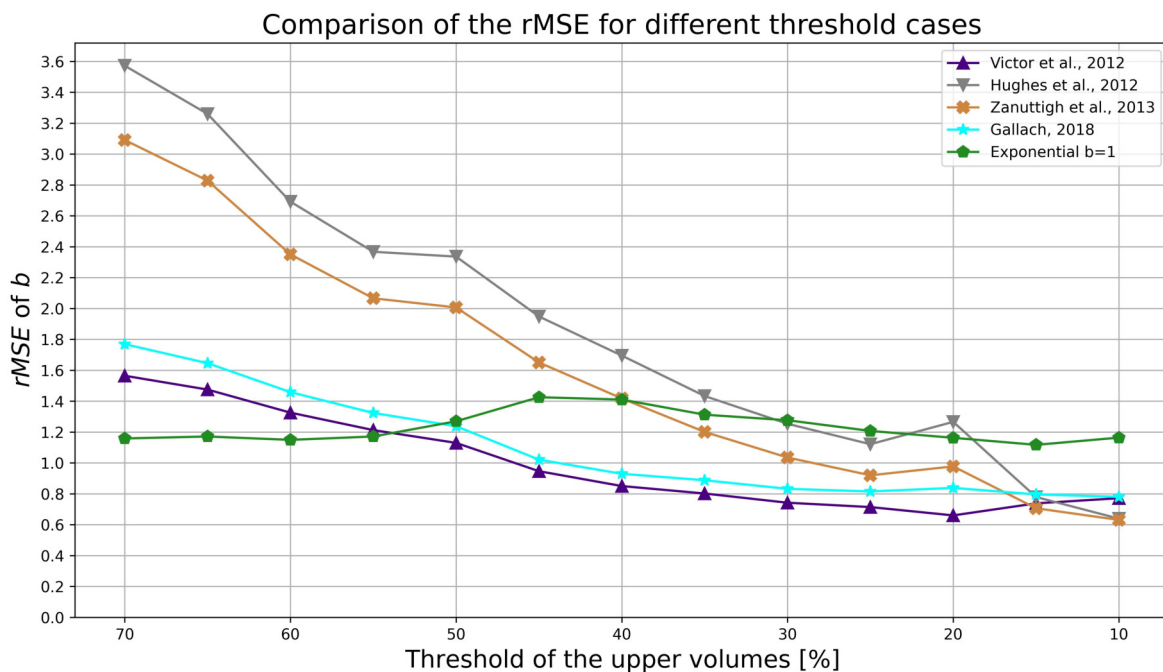
Figure 6.43: Comparison of the *rMSE* of the predicted values of b according to the threshold of volumes, for CWL.

Shape factor b as a function of the relative crest freeboard
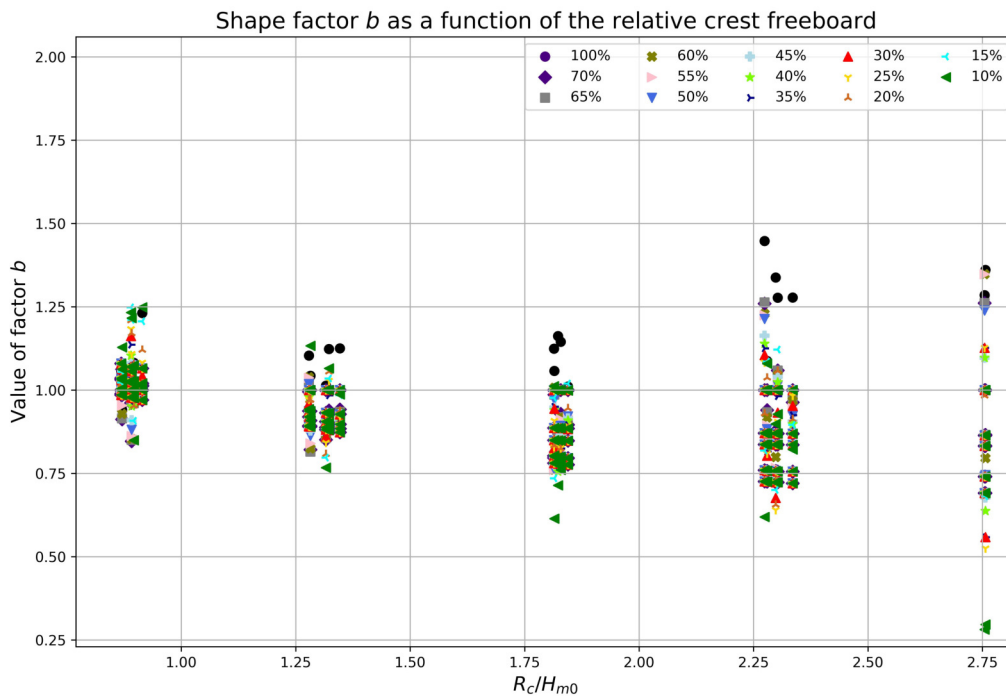
Figure 6.44: Shape factor b as a function of R_c/H_{m0} for all different thresholds, for CWL.

6.2 Variable water level

For the VWL analysis, 127 tests are considered, which are detailed in Tables 6.4, 6.5, 6.6 and 6.7. For this case, a first approach considering the whole dataset is going to be analyzed. Then, the same analysis will be defined for the same dataset but those tests with a considerably low value of P_{ow} are going to be neglected. Hence, as mentioned in Section 6.1, values of P_{ow} below 10 and 5% can be considered as *non reliable*.

Then, if a 5% threshold is applied to the value of P_{ow}, only three tests are neglected: 35, 92 and 108. These three tests correspond to tests with a water depth at the toe of the structure of 0.55 m. Thus, other two tests with this same value of h are found in the VWL dataset, which are tests 51 and 76, with a probability of overtopping of 5.03 and 5.37%. In that sense, it is reasonable to eliminate from the analysis all these five tests for $h = 0.55m$, for a P_{ow} threshold of 5.37%.

As a VWL situation, the value of R_c changes with time, so also a value at the beginning and at the end of the test are known. However, to apply the available formulation it is necessary to define a value for this parameter, so R_c is considered as a fix value of the

Factor a' as a function of the shape factor b for a two-parameter Weibull distribution
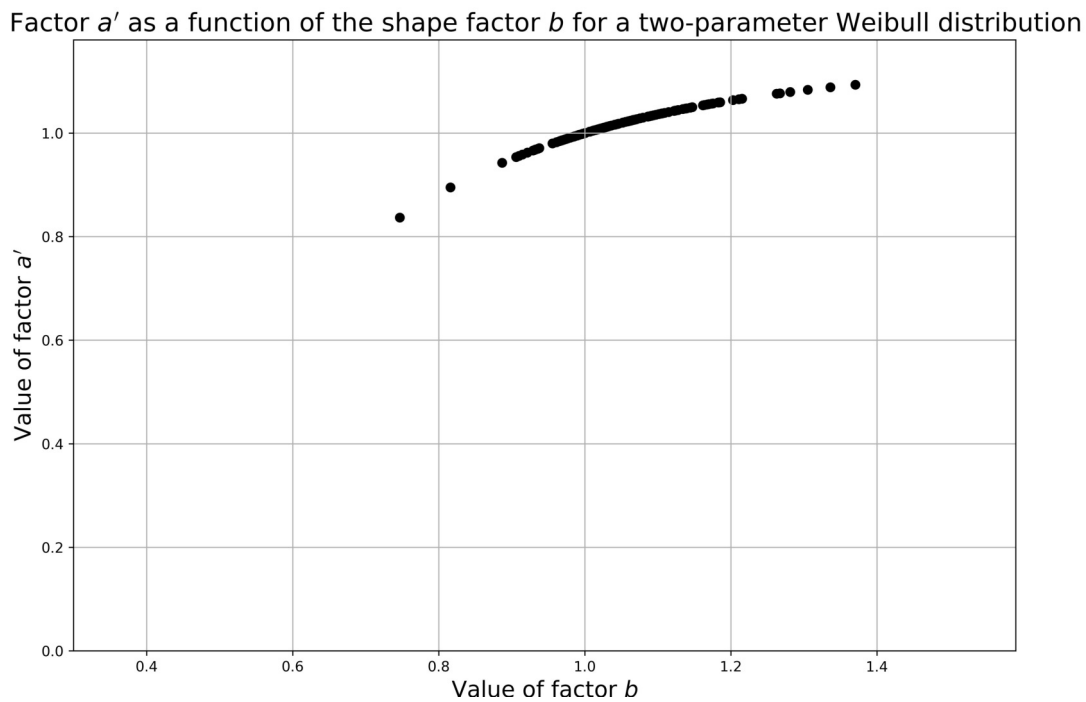
Figure 6.45: Correlation between factors a' and b for the VWL dataset.

crest height with respect to SWL for the moment at the beginning of the test.

The methodology to obtain both factors a and b, as well as the value of V_{max} is the same that the one followed for the CWL analysis in Paragraphs 6.1.1 and 6.1.2. Moreover, according to the results obtained from the CWL analysis from Section 6.1, both the Rayleigh distribution with $b = 2$ and the value of $b = 0.75$ from EurOtop (2007) are neglected from now on. In Figure 6.45, it is possible to observe the correspondence between a' and b for the measured data.

Then, for the 127 VWL tests, some plots can be displayed to visualize the behaviour of the dataset. Figure 6.46 shows the relation between the probability of overtopping and the crest freeboard. As expected, the P_{ow} decreases when the R_c is higher. Figure 6.47 represents the variability of the shape factor b according to the relative crest freeboard, with a visible positive regression.

Figure 6.48 shows the range of the different values of b for the 127 VWL tests. Finally, Figure 6.49 represents the relationship between the probability of overtopping and the shape factor b, with the higher values of b for the lowest probabilities.

Name	Conventional test name	N_{ow}	N_w	P_{ow} [%]
0	C4 VW D1200 H010 T170 S2 h059 R 209 N001	97	825	11.76
1	C4 VW D1350 H010 T250 S2 h065 R 400 N001	97	683	14.20
2	C4 VW D1350 H010 T250 S2 h075 R 412 N001	349	702	49.72
3	C4 VW D1800 H010 T170 S1 h060 R 312 N001	119	1320	9.02
4	C4 VW D1800 H010 T170 S1 h065 R 312 N001	268	1306	20.52
5	C4 VW D1800 H010 T170 S1 h070 R 312 N001	507	1245	40.72
6	C4 VW D1800 H010 T170 S2 h060 R 312 N001	97	1293	7.50
7	C4 VW D1800 H010 T170 S2 h065 R 312 N001	261	1306	19.98
8	C4 VW D1800 H010 T170 S2 h067 R 209 N001	439	1237	35.49
9	C4 VW D1800 H010 T170 S2 h070 R 312 N001	495	1312	37.73
10	C4 VW D1800 H010 T170 S2 h075 R 209 N001	880	1237	71.14
11	C4 VW D1800 H010 T170 S3 h060 R 312 N001	109	1289	8.46
12	C4 VW D1800 H010 T170 S3 h065 R 312 N001	253	1302	19.43
13	C4 VW D1800 H010 T170 S3 h070 R 312 N001	470	1317	35.69
14	C4 VW D1800 H010 T170 S7 h060 R 312 N001	99	1325	7.47
15	C4 VW D1800 H010 T170 S7 h065 R 312 N001	235	1321	17.79
16	C4 VW D1800 H010 T170 S7 h070 R 312 N001	462	1319	35.03
17	C4 VW D1800 H010 T170 S9 h060 R 312 N001	115	1314	8.75
18	C4 VW D1800 H010 T170 S9 h065 R 312 N001	251	1308	19.19
19	C4 VW D1800 H010 T170 S9 h070 R 312 N001	458	1293	35.42
20	C4 VW D3600 H010 T170 S1 h060 R 212 N001	218	2492	8.75
21	C4 VW D3600 H010 T170 S1 h065 R 212 N001	483	2478	19.49
22	C4 VW D3600 H010 T170 S1 h070 R 212 N001	1068	2493	42.84
23	C4 VW D3600 H010 T170 S2 h065 R 212 N001	489	2486	19.67
24	C4 VW D3600 H010 T170 S2 h070 R 212 N001	1059	2493	42.48
25	C4 VW D3600 H010 T170 S3 h065 R 212 N001	466	2497	18.66
26	C4 VW D3600 H010 T170 S3 h070 R 212 N001	987	2501	39.46
27	C4 VW D3600 H010 T170 S7 h065 R 212 N001	607	2472	24.56
28	C4 VW D3600 H010 T170 S7 h070 R 212 N001	1013	2502	40.49
29	C4 VW D3600 H010 T170 S9 h065 R 212 N001	520	2484	20.93
30	C4 VW D3600 H010 T170 S9 h070 R 212 N001	1035	2476	41.80
31	C4 VW D7200 H010 T170 S1 h070 R 109 N001	2464	5010	49.18
32	C4 VW D7200 H010 T170 S2 h070 R 109 N001	2013	4999	40.27
33	C4 VW D900 H010 T120 S2 h065 R 512 N001	140	815	17.18
34	C4 VW D900 H010 T120 S2 h075 R 512 N001	487	818	59.54
35	C4 VW D900 H010 T170 S1 h055 R 312 N001	27	623	4.33

Table 6.4: VWL tests with N_{ow}, N_w and P_{ow} (Table 1/4).

Name	Conventional test name	N_{ow}	N_w	P_{ow} [%]
36	C4 VW D900 H010 T170 S1 h060 R 212 N001	103	623	16.53
37	C4 VW D900 H010 T170 S1 h060 R 312 N001	90	614	14.66
38	C4 VW D900 H010 T170 S1 h060 R 512 N001	58	624	9.29
39	C4 VW D900 H010 T170 S1 h0625 R 212 N001	172	621	27.70
40	C4 VW D900 H010 T170 S1 h065 R 212 N001	233	622	37.46
41	C4 VW D900 H010 T170 S1 h065 R 312 N001	181	628	28.82
42	C4 VW D900 H010 T170 S1 h065 R 512 N001	147	619	23.75
43	C4 VW D900 H010 T170 S1 h0675 R 212 N001	308	625	49.28
44	C4 VW D900 H010 T170 S1 h070 R 212 N001	371	627	59.17
45	C4 VW D900 H010 T170 S1 h070 R 312 N001	334	623	53.61
46	C4 VW D900 H010 T170 S1 h070 R 512 N001	237	628	37.74
47	C4 VW D900 H010 T170 S1 h0725 R 212 N001	437	614	71.17
48	C4 VW D900 H010 T170 S1 h075 R 212 N001	500	633	78.99
49	C4 VW D900 H010 T170 S1 h075 R 312 N001	458	624	73.40
50	C4 VW D900 H010 T170 S1 h075 R 512 N001	393	621	63.29
51	C4 VW D900 H010 T170 S2 h055 R 312 N001	31	616	5.03
52	C4 VW D900 H010 T170 S2 h060 R 212 N001	95	621	15.30
53	C4 VW D900 H010 T170 S2 h060 R 312 N001	69	624	11.06
54	C4 VW D900 H010 T170 S2 h060 R 512 N001	51	616	8.28
55	C4 VW D900 H010 T170 S2 h0625 R 212 N001	178	625	28.48
56	C4 VW D900 H010 T170 S2 h065 R 212 N001	236	632	37.34
57	C4 VW D900 H010 T170 S2 h065 R 312 N001	204	632	32.28
58	C4 VW D900 H010 T170 S2 h065 R 512 N001	142	622	22.83
59	C4 VW D900 H010 T170 S2 h065 R 512 N002	154	618	24.92
60	C4 VW D900 H010 T170 S2 h065 R 512 N003	155	618	25.08
61	C4 VW D900 H010 T170 S2 h065 R 512 N004	93	631	14.74
62	C4 VW D900 H010 T170 S2 h065 R 512 N006	151	624	24.20
63	C4 VW D900 H010 T170 S2 h065 R 512 N007	147	620	23.71
64	C4 VW D900 H010 T170 S2 h065 R 512 N008	146	619	23.59
65	C4 VW D900 H010 T170 S2 h065 R 512 N009	147	612	24.02
66	C4 VW D900 H010 T170 S2 h065 R 512 N010	144	619	23.26
67	C4 VW D900 H010 T170 S2 h065 R 512 N011	147	619	23.75
68	C4 VW D900 H010 T170 S2 h0675 R 212 N001	289	634	45.58
69	C4 VW D900 H010 T170 S2 h070 R 212 N001	363	634	57.26
70	C4 VW D900 H010 T170 S2 h070 R 312 N001	282	647	43.59
71	C4 VW D900 H010 T170 S2 h070 R 512 N001	250	635	39.37

Table 6.5: VWL tests with N_{ow}, N_w and P_{ow} (Table 2/4).

Name	Conventional test name	N_{ow}	N_w	P_{ow} [%]
72	C4 VW D900 H010 T170 S2 h0725 R 212 N001	424	630	67.30
73	C4 VW D900 H010 T170 S2 h075 R 212 N001	497	637	78.02
74	C4 VW D900 H010 T170 S2 h075 R 312 N001	460	637	72.21
75	C4 VW D900 H010 T170 S2 h075 R 512 N001	402	633	63.51
76	C4 VW D900 H010 T170 S3 h055 R 312 N001	33	615	5.37
77	C4 VW D900 H010 T170 S3 h060 R 212 N001	110	616	17.86
78	C4 VW D900 H010 T170 S3 h060 R 312 N001	90	620	14.52
79	C4 VW D900 H010 T170 S3 h060 R 512 N001	54	618	8.74
80	C4 VW D900 H010 T170 S3 h0625 R 212 N001	155	630	24.60
81	C4 VW D900 H010 T170 S3 h065 R 212 N001	201	630	31.90
82	C4 VW D900 H010 T170 S3 h065 R 312 N001	164	626	26.20
83	C4 VW D900 H010 T170 S3 h065 R 512 N001	114	614	18.57
84	C4 VW D900 H010 T170 S3 h0675 R 212 N001	276	619	44.59
85	C4 VW D900 H010 T170 S3 h070 R 212 N001	354	629	56.28
86	C4 VW D900 H010 T170 S3 h070 R 312 N001	301	629	47.85
87	C4 VW D900 H010 T170 S3 h070 R 512 N001	222	634	35.02
88	C4 VW D900 H010 T170 S3 h0725 R 212 N001	429	620	69.19
89	C4 VW D900 H010 T170 S3 h075 R 212 N001	501	622	80.55
90	C4 VW D900 H010 T170 S3 h075 R 312 N001	461	623	74.00
91	C4 VW D900 H010 T170 S3 h075 R 512 N001	392	618	63.43
92	C4 VW D900 H010 T170 S7 h055 R 312 N001	27	611	4.42
93	C4 VW D900 H010 T170 S7 h060 R 212 N001	103	610	16.89
94	C4 VW D900 H010 T170 S7 h060 R 312 N001	88	615	14.31
95	C4 VW D900 H010 T170 S7 h060 R 512 N001	48	614	7.82
96	C4 VW D900 H010 T170 S7 h0625 R 212 N001	152	608	25.00
97	C4 VW D900 H010 T170 S7 h065 R 212 N001	231	604	38.25
98	C4 VW D900 H010 T170 S7 h065 R 312 N001	189	617	30.63
99	C4 VW D900 H010 T170 S7 h065 R 512 N001	126	609	20.69
100	C4 VW D900 H010 T170 S7 h0675 R 212 N001	299	601	49.75
101	C4 VW D900 H010 T170 S7 h070 R 212 N001	360	617	58.35
102	C4 VW D900 H010 T170 S7 h070 R 312 N001	324	608	53.29
103	C4 VW D900 H010 T170 S7 h070 R 512 N002	261	608	42.93
104	C4 VW D900 H010 T170 S7 h0725 R 212 N001	413	617	66.94
105	C4 VW D900 H010 T170 S7 h075 R 212 N001	493	620	79.52
106	C4 VW D900 H010 T170 S7 h075 R 312 N001	451	630	71.59
107	C4 VW D900 H010 T170 S7 h075 R 512 N001	382	629	60.73

Table 6.6: VWL tests with N_{ow}, N_w and P_{ow} (Table 3/4).

Name	Conventional test name	N_{ow}	N_w	P_{ow} [%]
108	C4 VW D900 H010 T170 S9 h055 R 312 N001	22	603	3.65
109	C4 VW D900 H010 T170 S9 h060 R 212 N001	107	608	17.60
110	C4 VW D900 H010 T170 S9 h060 R 312 N001	72	605	11.90
111	C4 VW D900 H010 T170 S9 h060 R 512 N001	43	608	7.07
112	C4 VW D900 H010 T170 S9 h0625 R 212 N001	161	602	26.74
113	C4 VW D900 H010 T170 S9 h065 R 212 N001	225	600	37.50
114	C4 VW D900 H010 T170 S9 h065 R 312 N001	194	600	32.33
115	C4 VW D900 H010 T170 S9 h065 R 512 N001	122	606	20.13
116	C4 VW D900 H010 T170 S9 h0675 R 212 N001	293	613	47.80
117	C4 VW D900 H010 T170 S9 h070 R 212 N001	363	614	59.12
118	C4 VW D900 H010 T170 S9 h070 R 312 N001	307	607	50.58
119	C4 VW D900 H010 T170 S9 h070 R 512 N001	248	608	40.79
120	C4 VW D900 H010 T170 S9 h0725 R 212 N001	443	608	72.86
121	C4 VW D900 H010 T170 S9 h075 R 212 N001	502	609	82.43
122	C4 VW D900 H010 T170 S9 h075 R 312 N001	467	612	76.31
123	C4 VW D900 H010 T170 S9 h075 R 512 N001	396	608	65.13
124	C4 VW D900 H010 T250 S2 h075 R 512 N001	293	427	68.62
125	C4 VW D900 H012 T170 S2 h060 R 312 N001	119	615	19.35
126	C4 VW D900 H012 T170 S2 h067 R 312 N001	318	624	50.96

Table 6.7: VWL tests with N_{ow}, N_w and P_{ow} (Table 4/4).
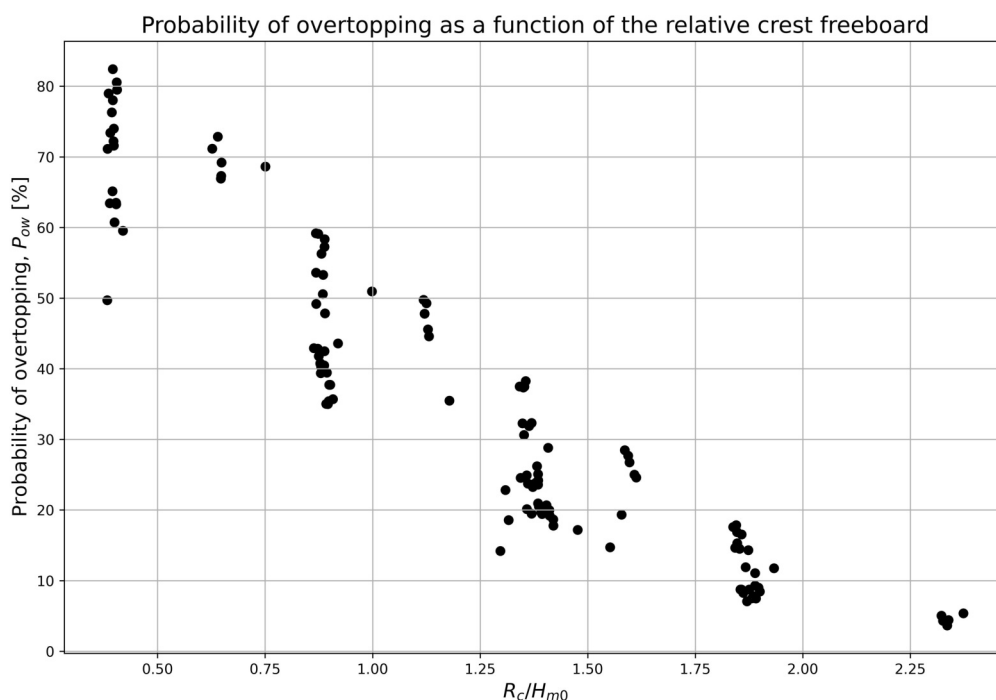
Figure 6.46: Probability of overtopping P_{ow} as a function of R_c/H_{m0} for the entire VWL dataset.

6.2.1   Discussion of the results

Considering these results, it is now possible to compare them with the predicted values using the available methods in literature. As mentioned previously, only the formulae from Victor et al. (2012), Hughes et al. (2012), Zanuttigh et al. (2013) and Gallach Sánchez, David (2018), as well as the exponential distribution with $b = 1$ are considered.

In Figure 6.50, it is possible to compare the predicted and the measured values, with a relative underprediction in a vast number of the cases. This same effect is also displayed in Figure 6.51.

The slight positive regression mentioned from Figure 6.47 contrasts with the predicted values in the same plot (see Figure 6.52). Hence, the prediction formulae have a clear negative tendency when the value of R_c/H_{m0} increases. For that reason, when $R_c/H_{m0} > 1$ an underprediction is observed, while when $R_c/H_{m0} < 1$ there is an overestimation of the shape factor for the majority of the prediction formulae. This same effect can be observed in Figure 6.53, in which the measured data is used as a third parameter to scale the values and compare them.
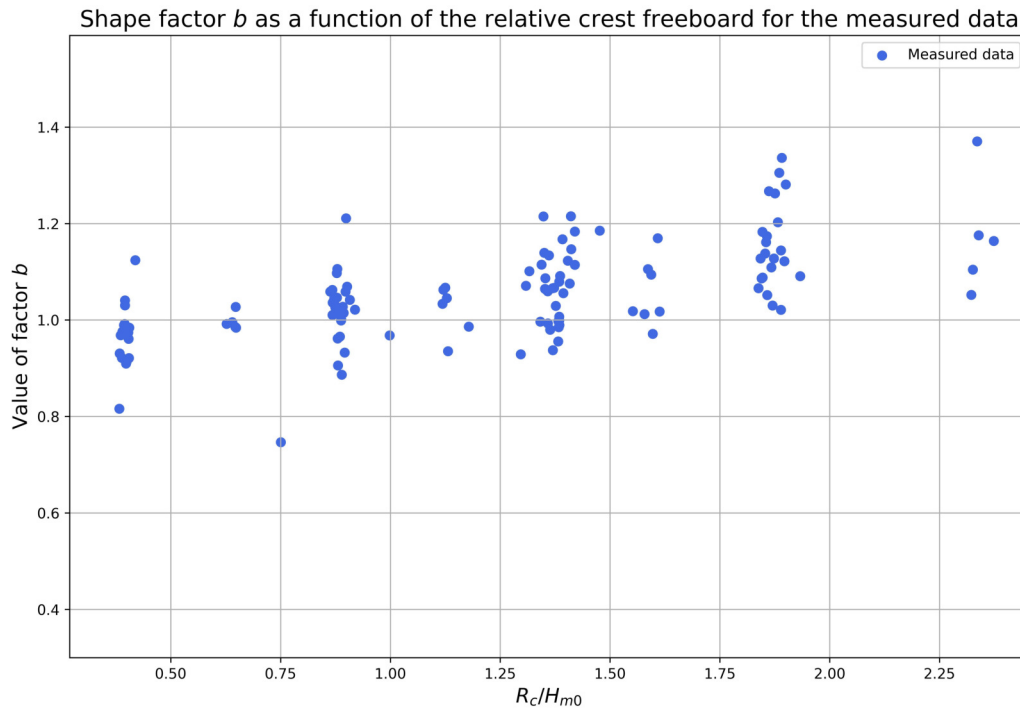
Figure 6.47: Shape factor *b* as a function of R_c/H_{m0}, for the entire VWL dataset and overtopping volumes.
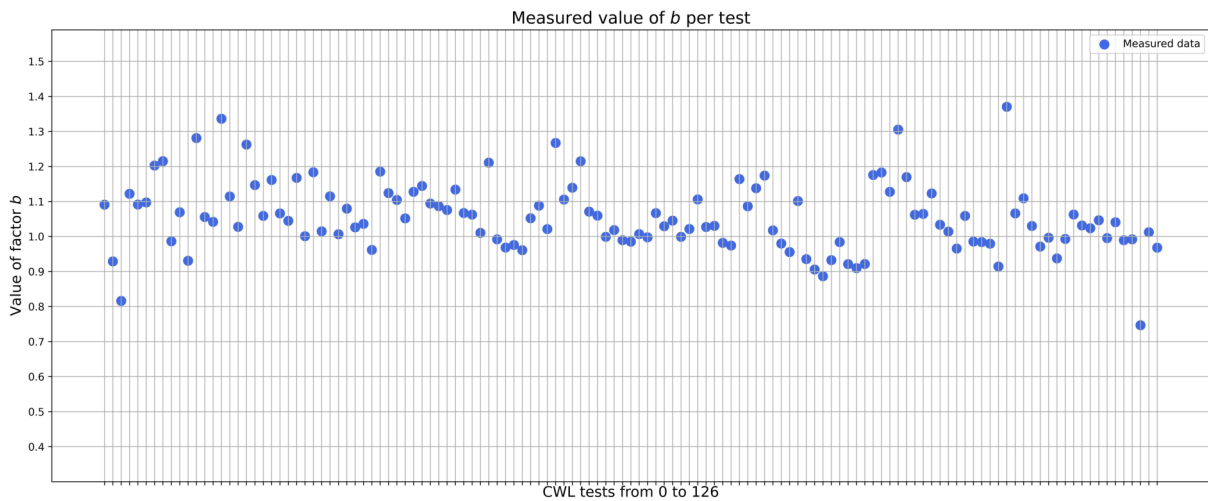
Figure 6.48: Value of the shape factor *b* for each VWL test, from 0 to 126, considering the 100% of the volumes.
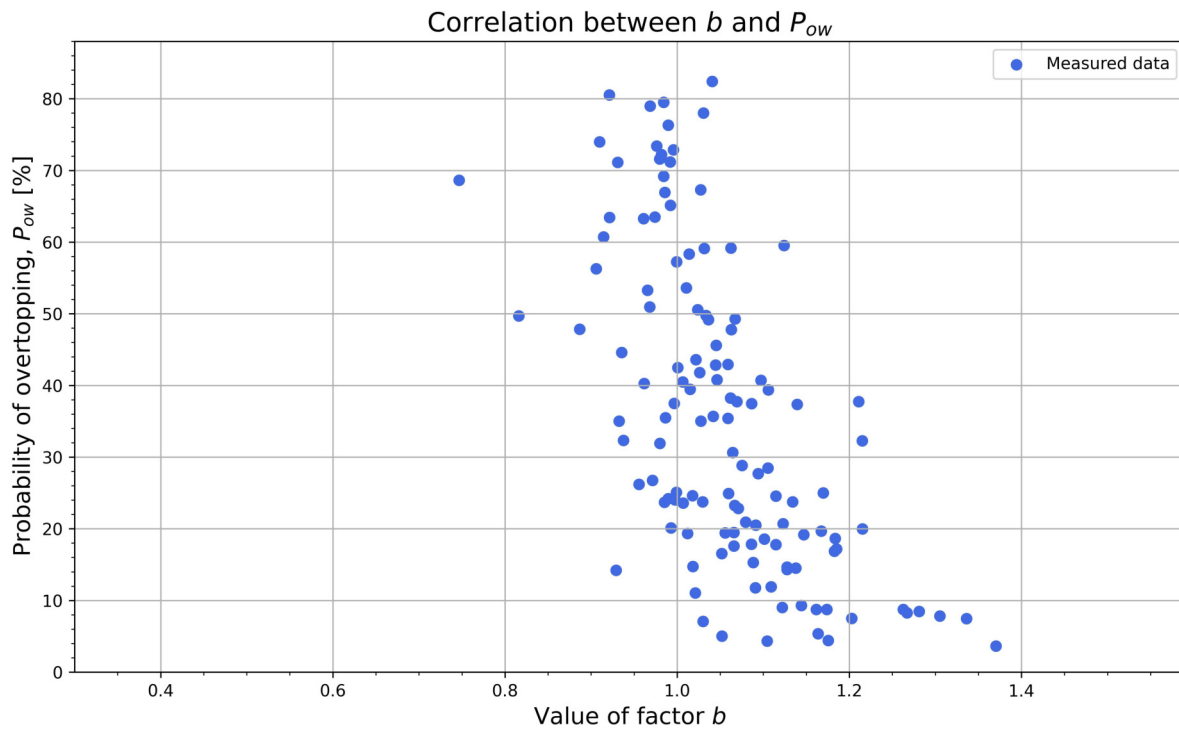
Figure 6.49: Correlation between P_{ow} and shape factor b, considering the 100% of the volumes.

A similar approach to understand the analysis and the estimation of b can be observed for the depth at the toe of the structure in Figure 6.54. Thus, the tendencies of the measured and predicted values are also opposite and coincided between a value of h/H_{m0} of 5.4.

Finally, following the idea of Figure 6.49, for the highest values of P_{ow}, the most overpredicted values of b are found, as it can be observed in Figure 6.55.

Moreover, considering the prediction of V_{max} as a consequence of the prediction of b, Figure 6.56 shows the overestimation of the maximum overtopping volume when the measured value of this variable increases. In contrast with Figure 6.50, this overestimation is even slightly more noticeable.

At this point, the same analysis is carried out for the VWL dataset but only those tests with $P_{ow} > 5.37\%$ from Tables 6.4, 6.5, 6.6 and 6.7 are considered, i.e., 122 tests in total. Then, if some of the same plots are displayed than for the previous case, it is possible to see that no big differences are observed beyond that those tests with $R_c = 0.55$ m and the lowest values of P_{ow} are neglected (see Figures 6.57 and 6.58). For that reason,
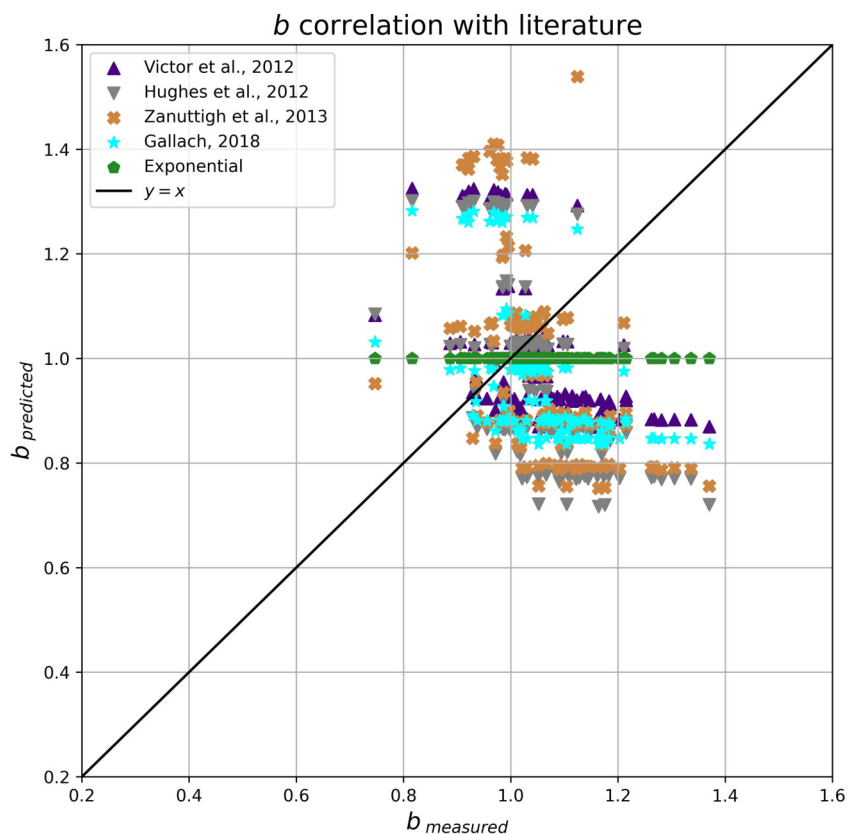
Figure 6.50: Comparison between predicted and measured *b*-values, considering the 100% of the volumes.
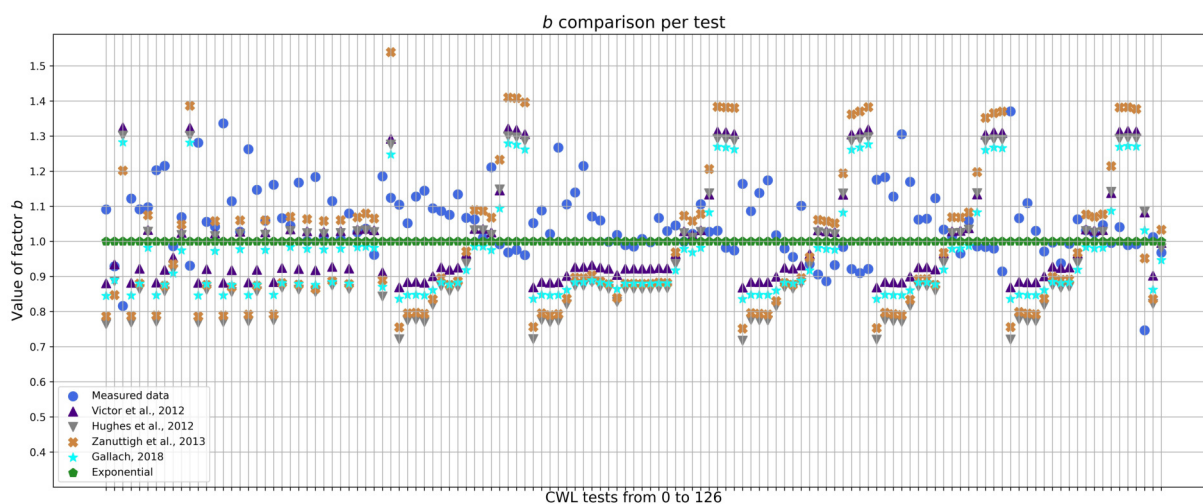
Figure 6.51: Predicted and measured values of the shape factor *b* for each VWL test, from 0 to 126, considering the 100% of the volumes.
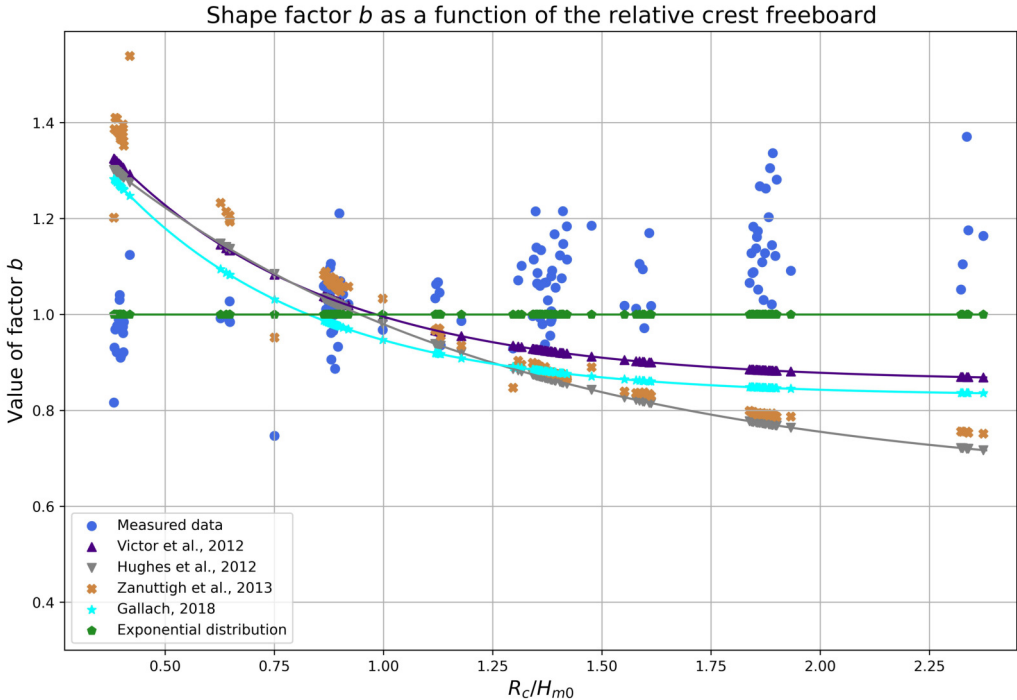
Figure 6.52: Comparison of the predicted values of b as a function of R_c/H_{m0}, for the entire VWL dataset and overtopping volumes.
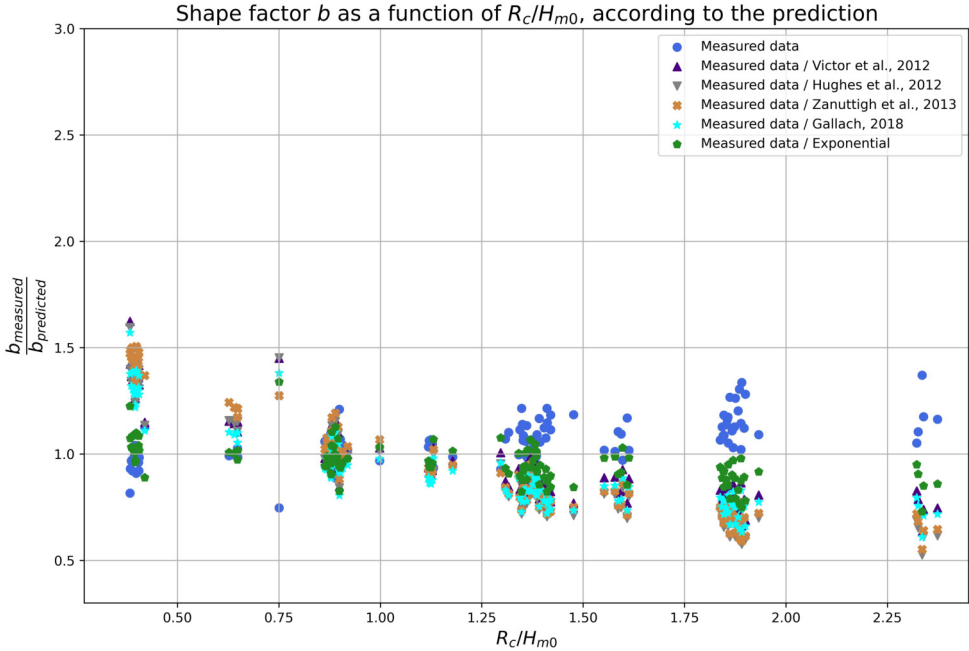
Figure 6.53: Measured values of b as a function of R_c/H_{m0}, according to the predicted values of b, for the entire VWL dataset and overtopping volumes.
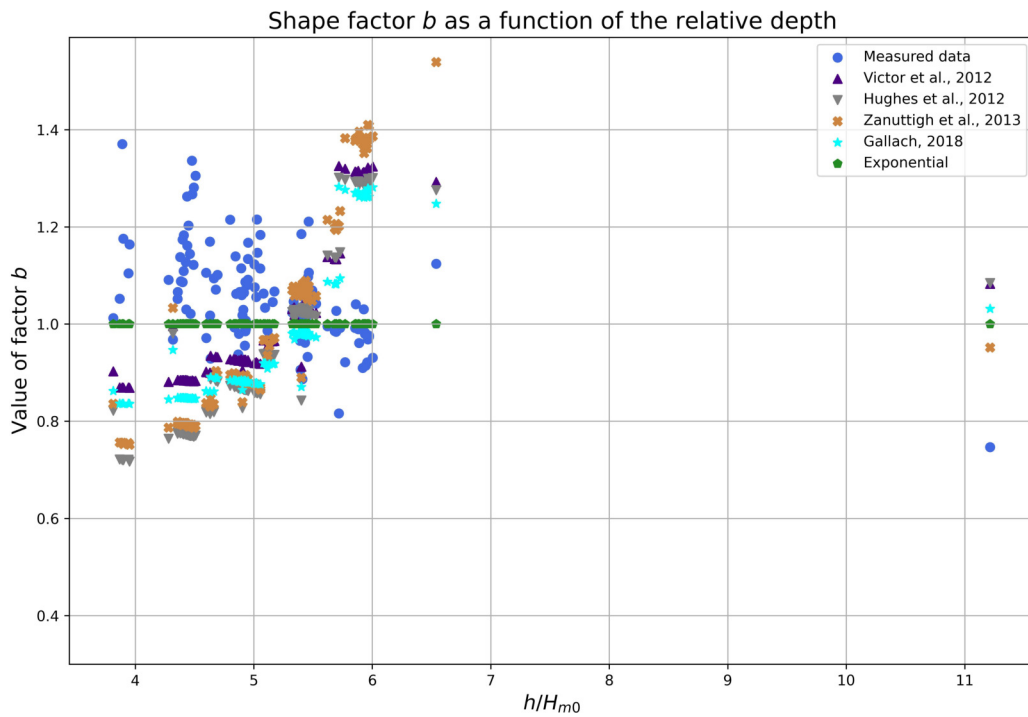
Figure 6.54: Shape factor b as a function of the relative depth at the toe of the structure, for the entire VWL dataset and overtopping volumes.
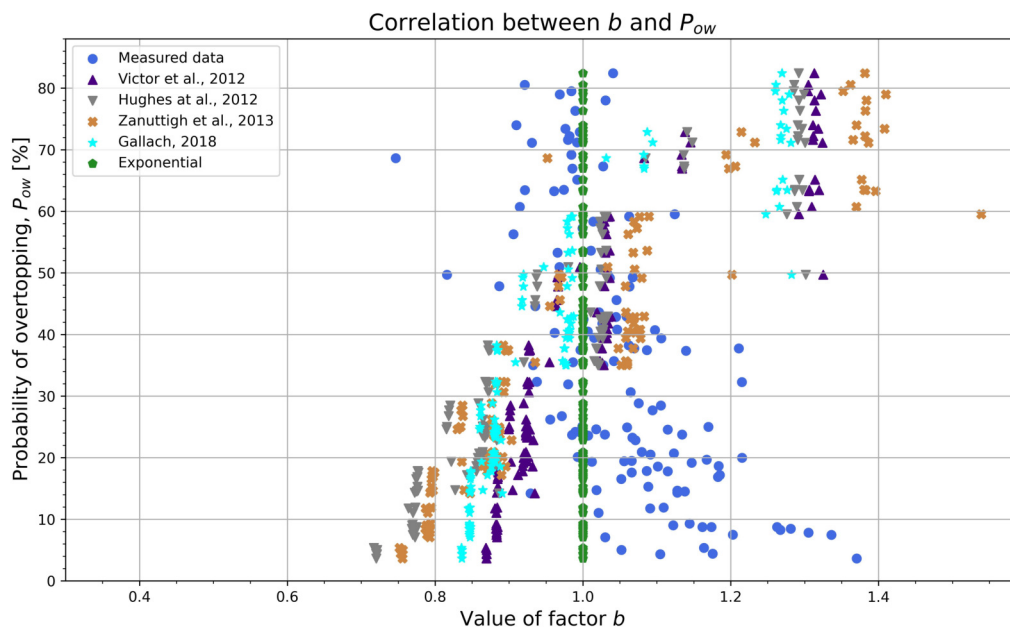
Figure 6.55: Relation between b and P_{ow}, for the entire VWL dataset and overtopping volumes.
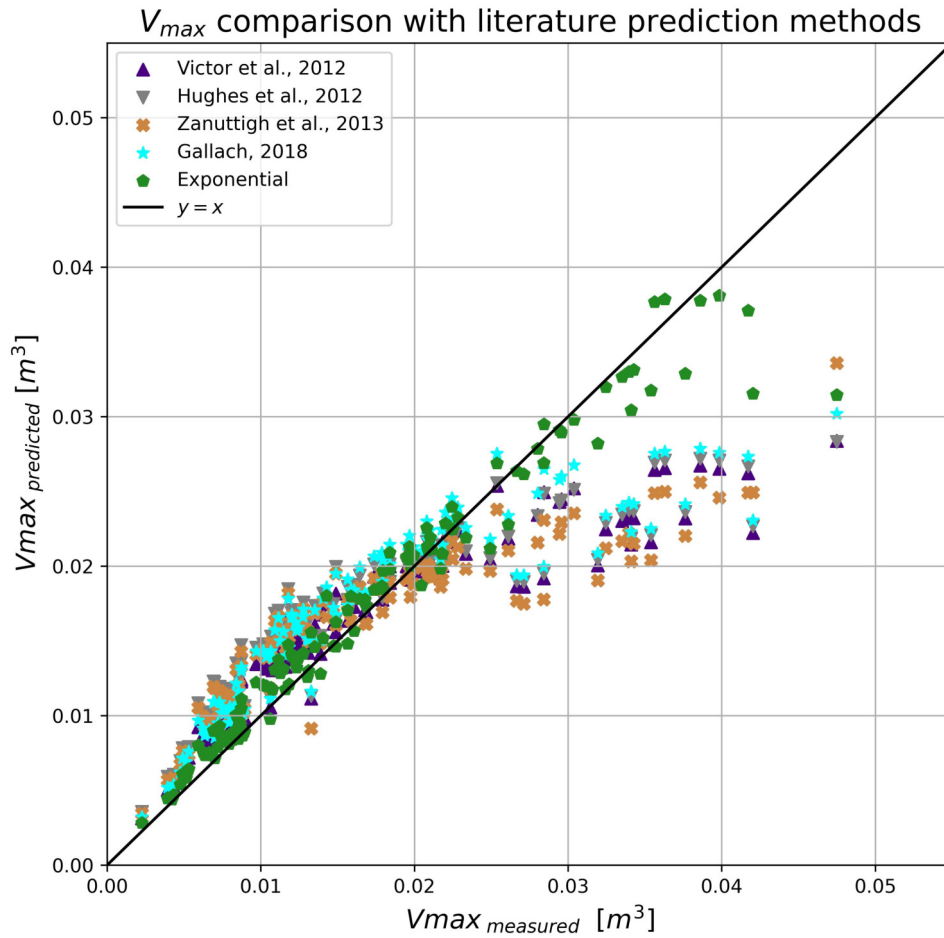
Figure 6.56: Comparison of the predicted values of V_{max}, for the entire VWL dataset and overtopping volumes.

in order to achieve a more reliable analysis for the VWL analysis, this dataset excluding tests 35, 51, 76, 92 and 108 is going to be followed from now on.

6.2.1.1   Sensitivity analysis

As it was previously done in Section 6.1.3.1 for the CWL case and with the same purpose, a sensitivity analysis considering different threshold cases is going to be carried out for the VWL situation. Then, it is possible to clearly visualize the effect of considering a different portion of the highest overtopping volumes and which threshold is the one that most accurately fits the data.
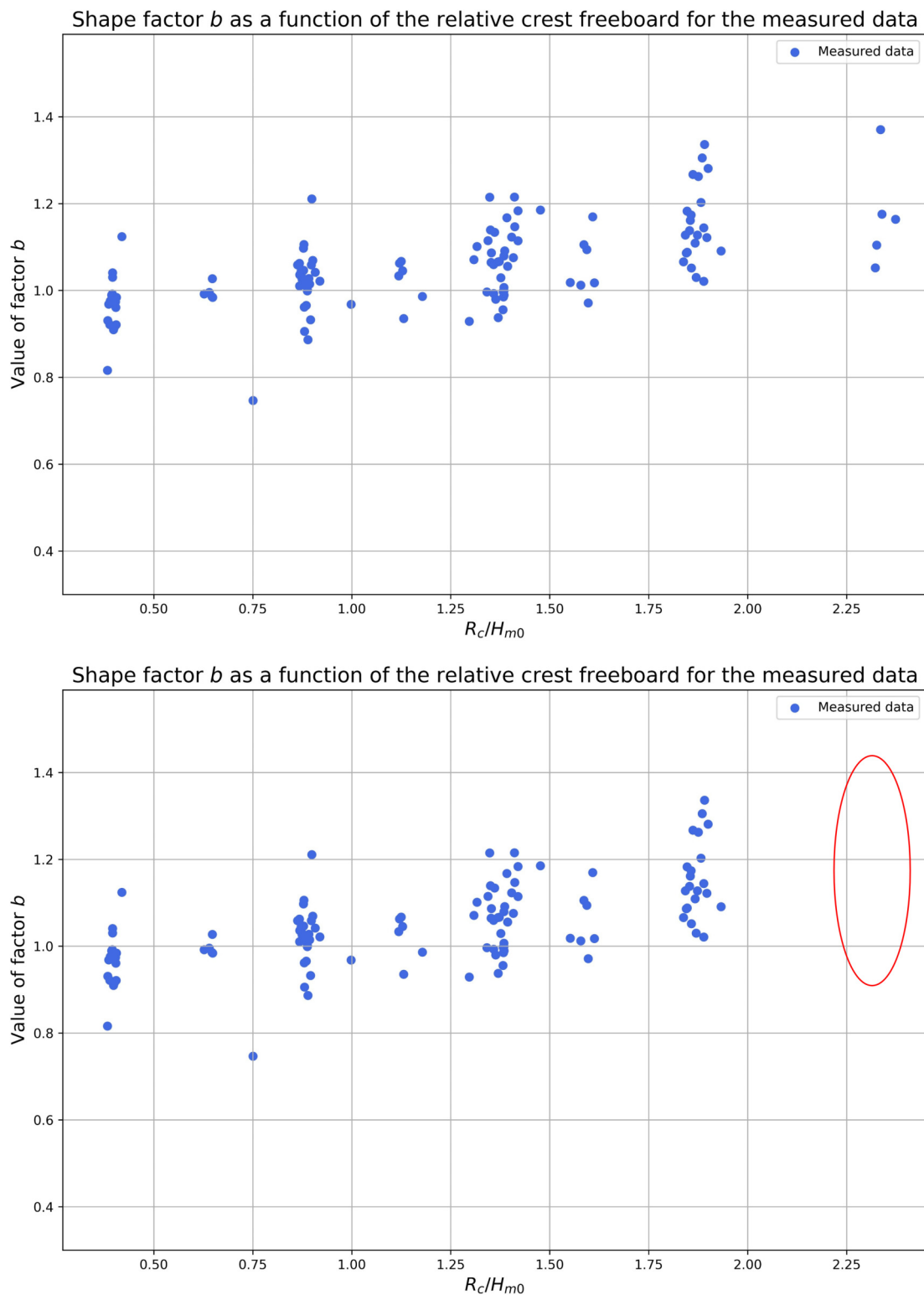
Figure 6.57: Comparison of the *b*-values as a function of R_c/H_{m0}. Above: The entire VWL dataset (127 tests). Below: Dataset excluding tests 35, 51, 76, 92 and 108 (122 tests).
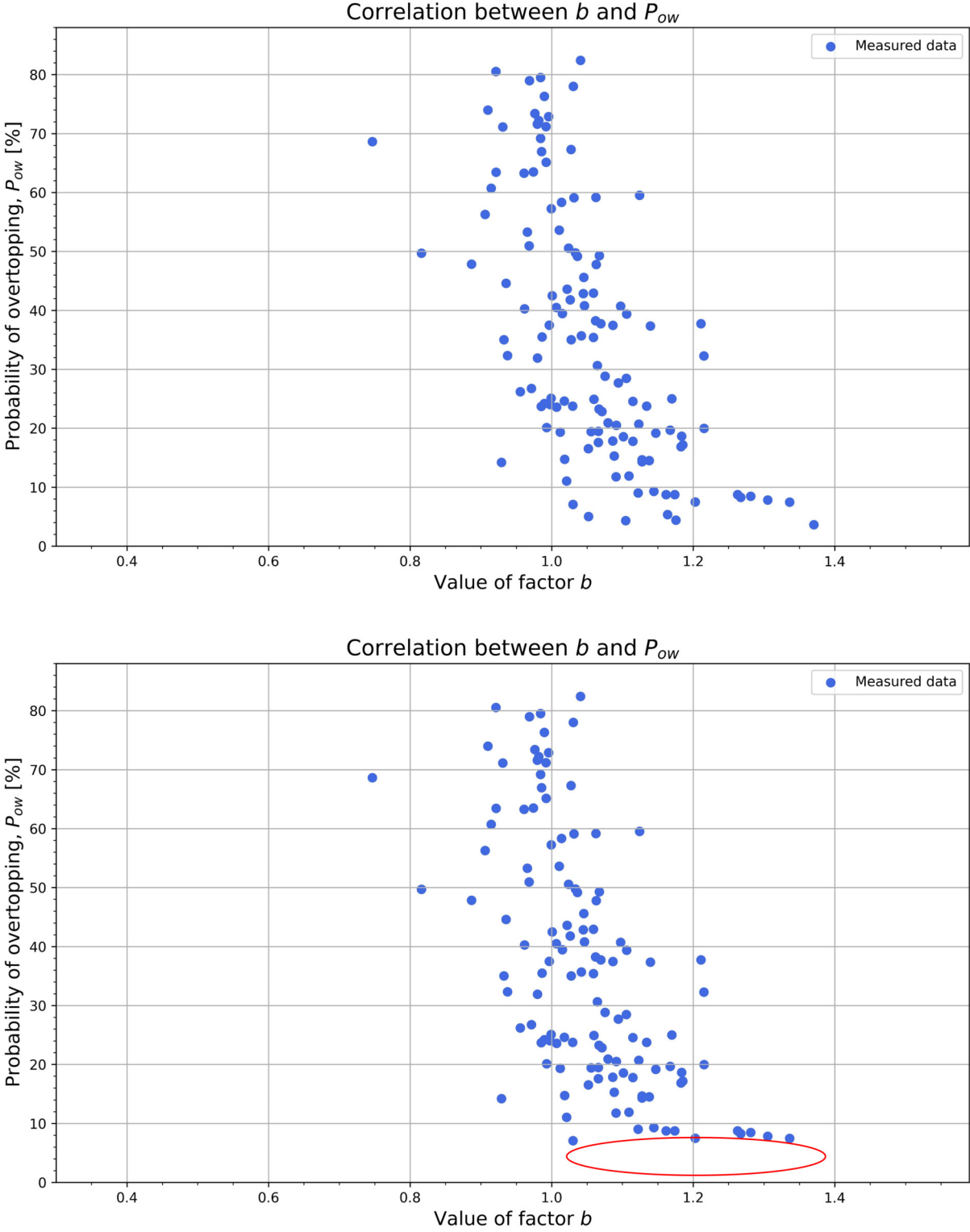
Figure 6.58: Comparison of the *b*-values as a function of P_{ow}. Above: The entire VWL dataset (127 tests). Below: Dataset excluding tests 35, 51, 76, 92 and 108 (122 tests).
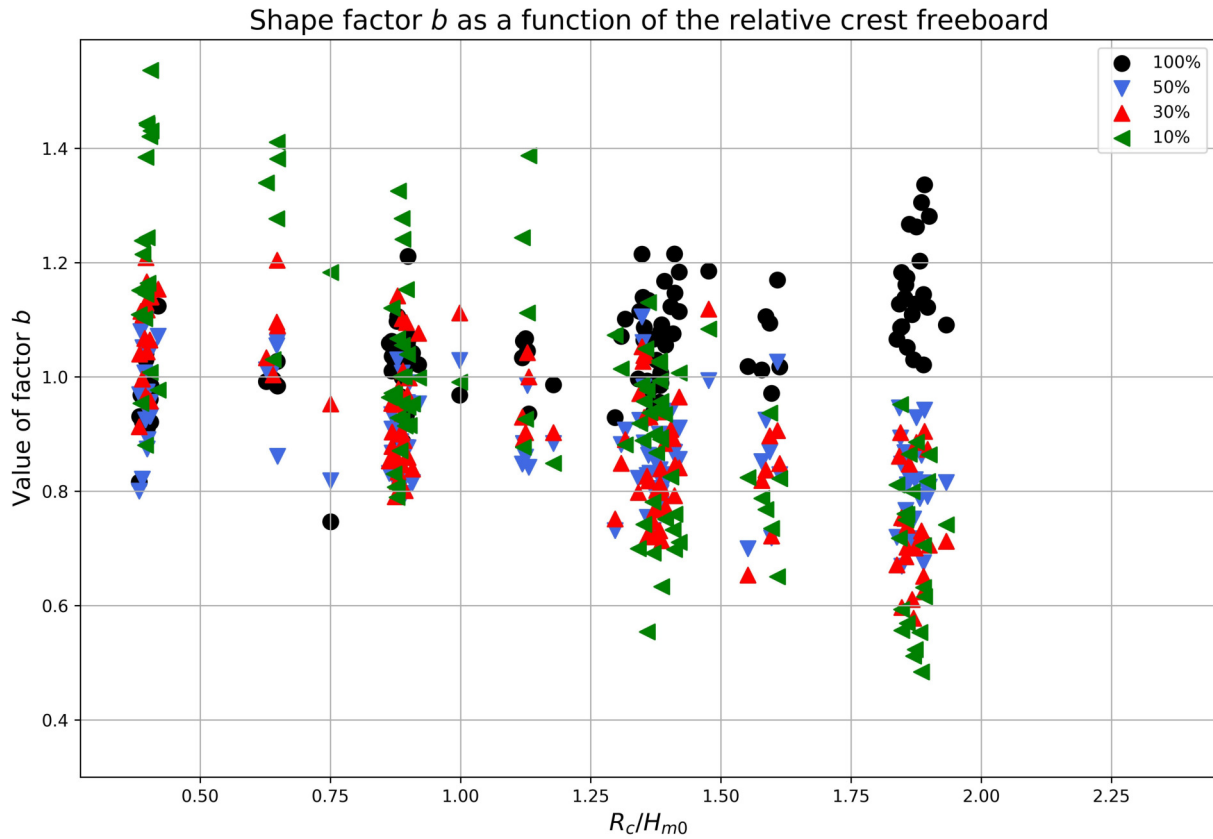
Figure 6.59: Shape factor b as a function of R_c/H_{m0}, for the upper 50%, 30% and 10% volumes, including the 100% case, in VWL.

At first instance, the cases for the highest 10% of individual wave overtopping volumes, the 30% and the 50% are considered. Figures 6.59, 6.60 and 6.61 show the differences of these three threshold and the whole overtopping volumes for the measured data.

Then, in Figure 6.59 it is remarkable that the positive tendency that the data from the 100% case has is no longer followed by any of the other cases, with a negative tendency instead. A similar conclusion is possible to see in Figure 6.60, in which the b-values for the 100% case are bigger for lower P_{ow} and smaller when this probability increases, but the opposite happens when considering the thresholds for 50, 30 and 10%. Obviously, this is the consequence of the effect of the crest freeboard from Figure 6.59.

Finally, to have a general view of the results for each case, Figure 6.61 shows the value of b for each test, so the variability of the range of the scale factor is observed.
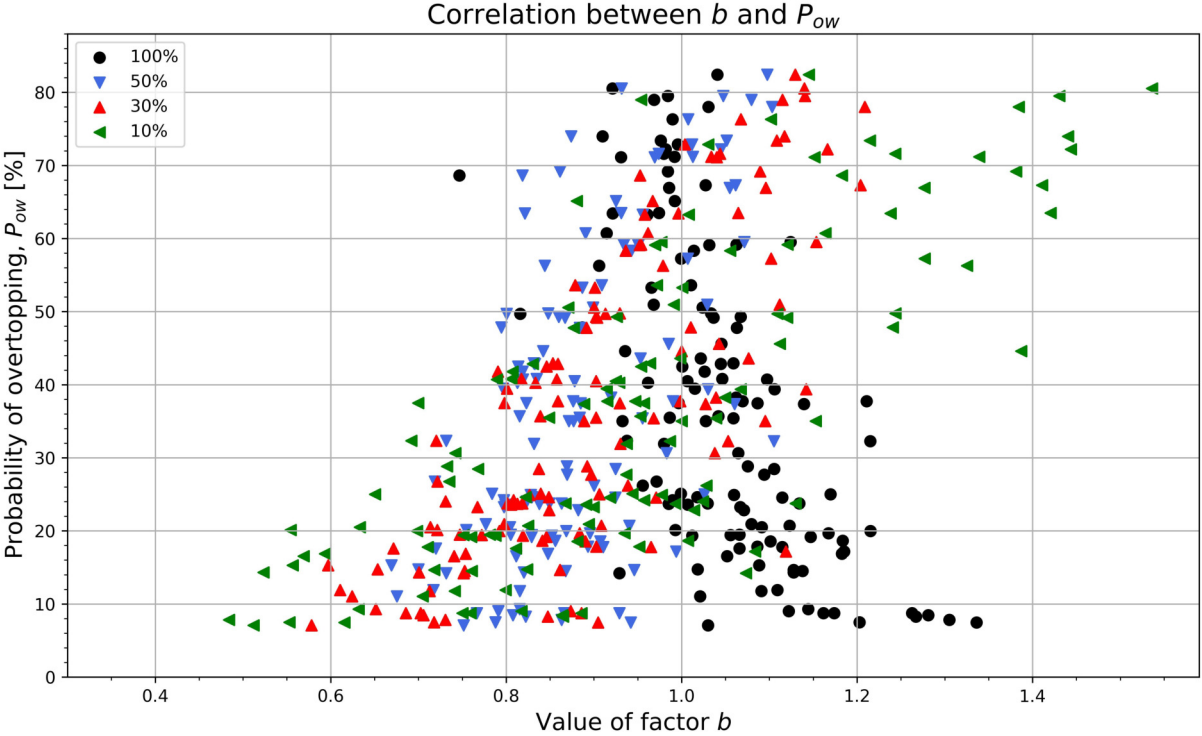
Figure 6.60: Comparison of the value of shape factor *b* according to P_{ow}, for the upper 50%, 30% and 10% volumes, including the 100% case, in VWL.
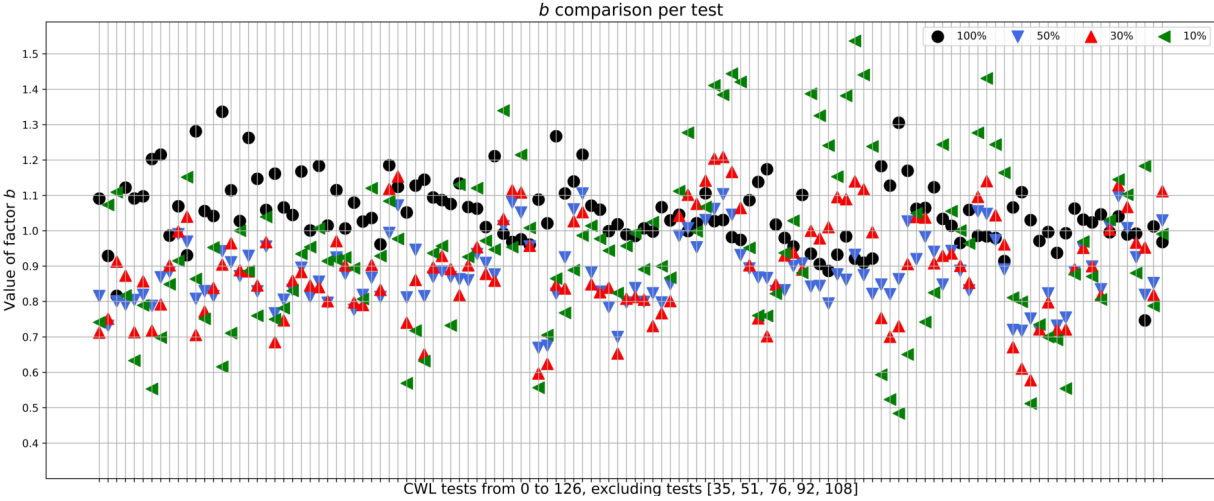
Figure 6.61: Comparison of the value of shape factor *b* per test, for the upper 50%, 30% and 10% volumes, including the 100% case, in VWL.

Figure 6.62: Comparison of the prediction of shape factor b regarding to R_c/H_{m0}, for the upper 50% volumes, in VWL.

i) **Top 50% of the individual wave overtopping volumes analysis.**

As mentioned in the sensitivity analysis for the CWL dataset, the only prediction formula considered which is intended for the highest 50% of the overtopping volumes is the formula given by Victor et al. (2012).

Before displaying a comparison between all the different thresholds, it is necessary to briefly discuss the results of this portion of the data in order to understand it on its own. Then, if the prediction values of b are compared with Figure 6.59, as it is showed in Figure 6.62, it can be easily observed that now the different values of b slightly follow the actual tendency of the prediction formulae, so the accuracy is increased by reducing the number of overtopping volumes just to the highest half.

Regarding the accuracy of the estimation of b, Figure 6.63 shows that same correlation according to the measured data as the reference value to visualize if the predicted values are over or underestimated; and which for this case a vastly overestimation is observed.

Figure 6.63: Comparison of the prediction of shape factor b regarding to R_c/H_{m0} using the measured data as reference, for the upper 50% volumes, in VWL.

Another approach to understand the analysis with regard to Figure 6.60 for this percentage of volumes consists on the comparison of the predicted values of b according to the probability of overtopping. Then, a similar tendency is observed in Figure 6.64, with a very high overestimation for high values of P_{ow}.

Finally, the accuracy of the prediction of b can be expressed through the calculation of V_{max}, which strongly depends on this variable. Thus, the $rMSE$ (see Equation 6.3) can be obtained for both parameters, as Figure 6.65 shows.

Other plots that may explain the fitting of the prediction formulae for this portion of the data are displayed in comparison with other thresholds in the following Section 6.2.1.2.

ii) **Top 30% of the individual wave overtopping volumes analysis.**

Following the same approach than for the highest 50% overtopping volumes, the same plots are displayed in this subsection. However, as it was also mentioned in the CWL case, non of the considered prediction formulae is specifically intended for this
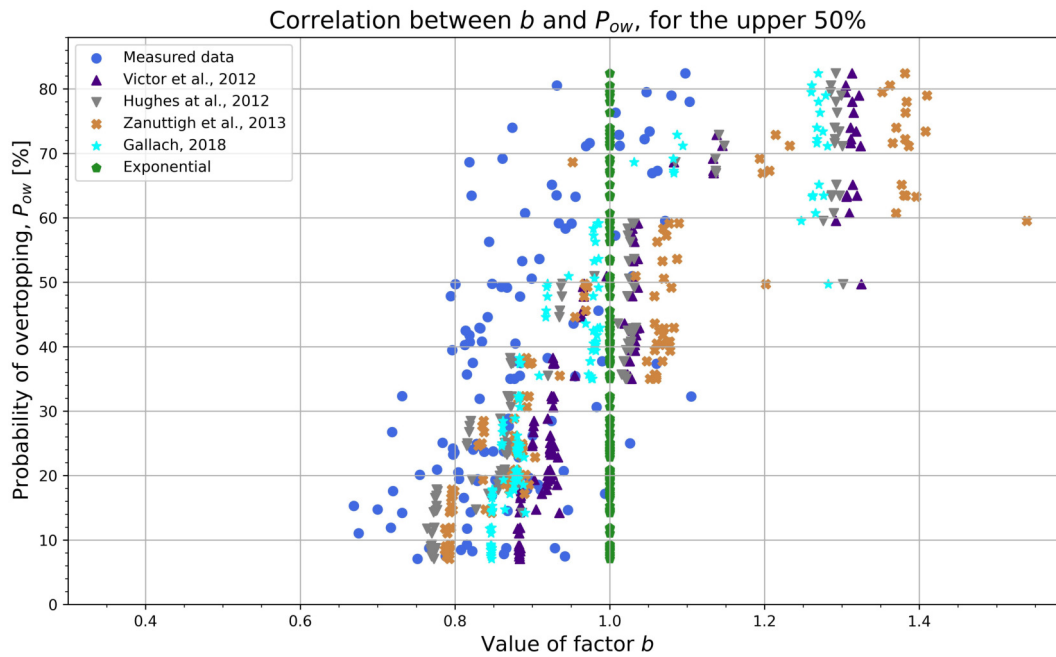
Figure 6.64: Comparison of the prediction of shape factor b regarding to P_{ow}, for the upper 50% volumes, in VWL.

percentage, despite the great accuracy that is achieved.

Then, Figure 6.66 shows the values of shape factor b according to the relative crest freeboard, with a very similar tendency than the one predicted by the different formulae, although these predicted values are slightly overestimated. Thus, this overestimation can be clearly visualized in Figure 6.67 with regard to measured data.

According to the probability of overtopping, the results of the analysis can be seen in Figure 6.68. Although the range of the b-values is bigger for this case, the predicted values are quite close to the measured one, with a very similar tendency. Evidently, the exponential distribution does not fit accurately as it remains constant for $b = 1$ when P_{ow} increases.

Finally, the relative mean square error for this threshold, for both variables b and V_{max}, is showed in Figure 6.69, with a notorious decreasing with regard to the previous case in which the highest 50% overtopping volumes are considered.

iii) **Top 10% of the individual wave overtopping volumes analysis.**
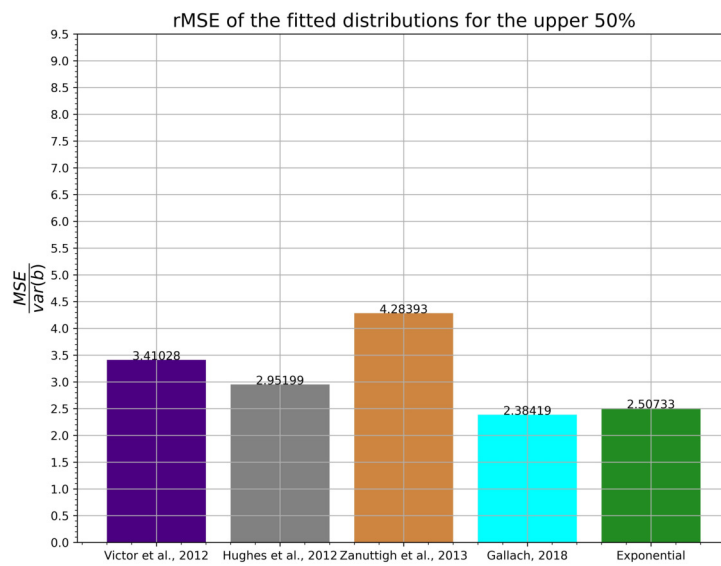
(a) *rMSE* of the prediction methods of *b*
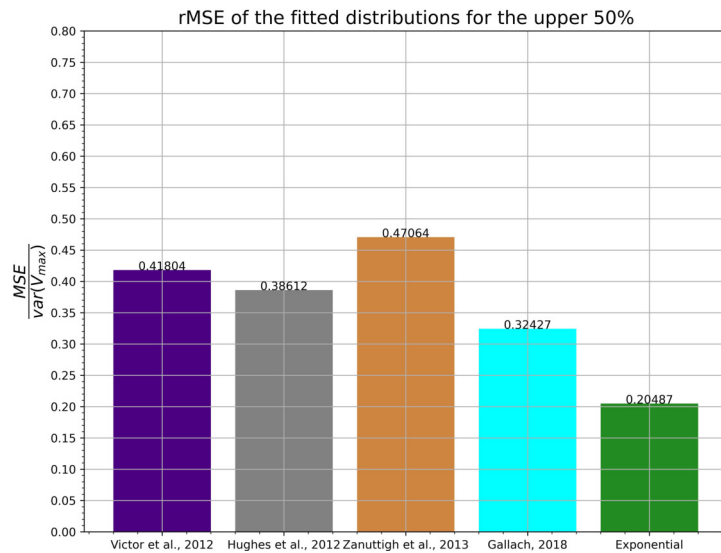
(b) *rMSE* of the prediction methods of V_{max}

Figure 6.65: *rMSE* of the prediction methods of *b* and V_{max}, for the upper 50% volumes, in VWL.

For the case in which only the upper 10% of the data is considered, a much more importance is given to the highest volumes. Hence, this fact leads to consider a lower set of volumes that may result in a bigger dispersion.

For this case, a higher dispersion of the values is found, so a bigger range of *b*-values is obtained. Then, in Figure 6.70, the overprediction showed for the cases considering the
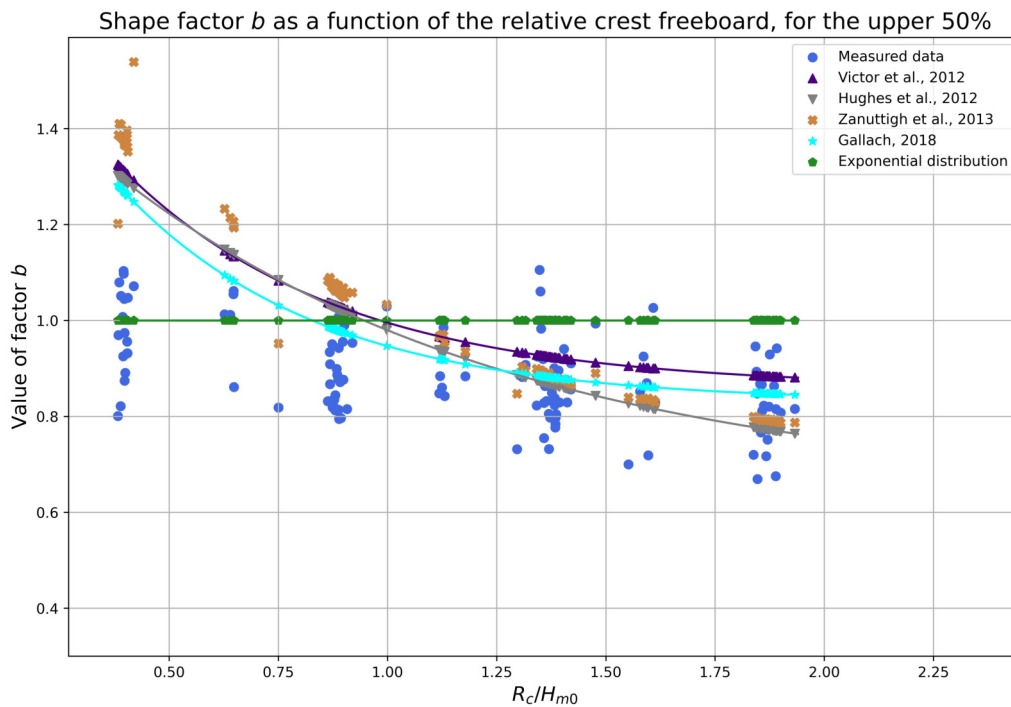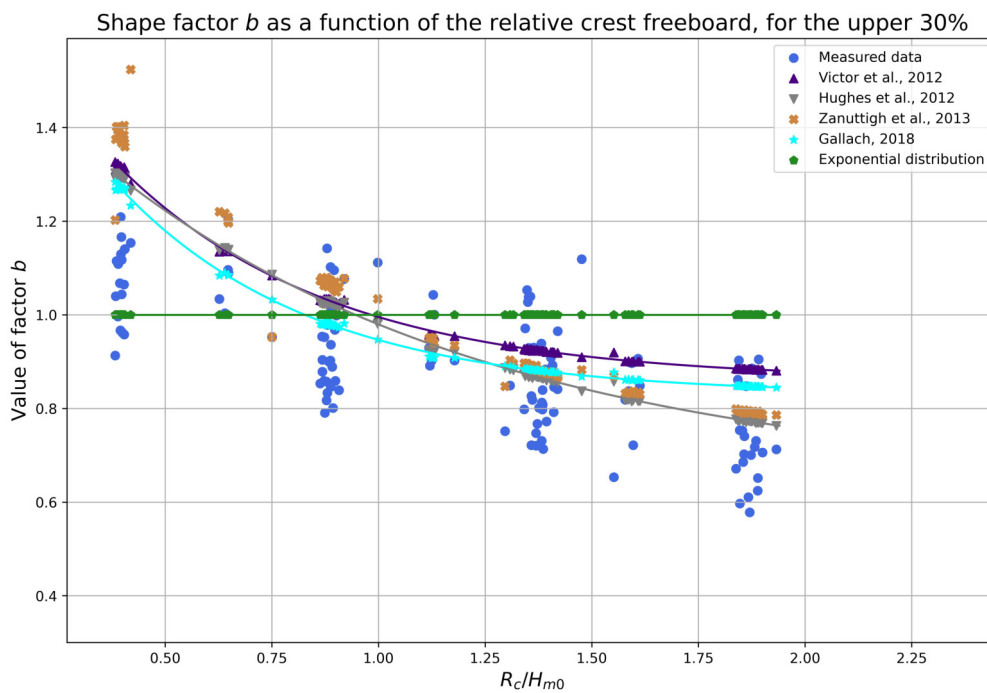
Figure 6.66: Comparison of the prediction of shape factor b regarding to R_c/H_{m0}, for the upper 30% volumes, in VWL.
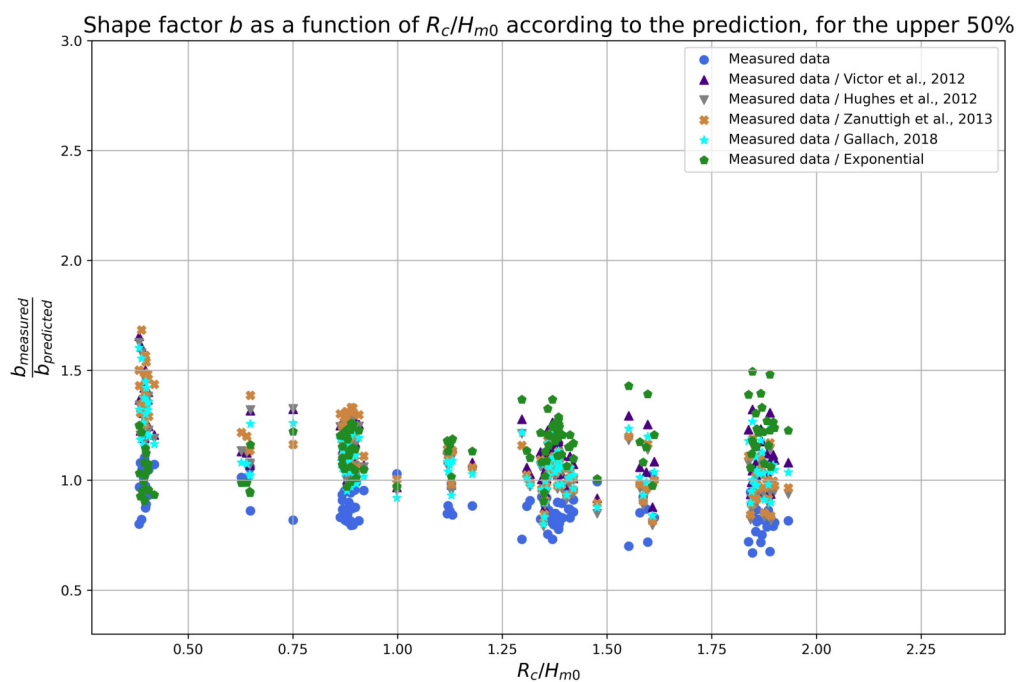

Figure 6.67: Comparison of the prediction of shape factor b regarding to R_c/H_{m0} using the measured data as reference, for the upper 30% volumes, in VWL.
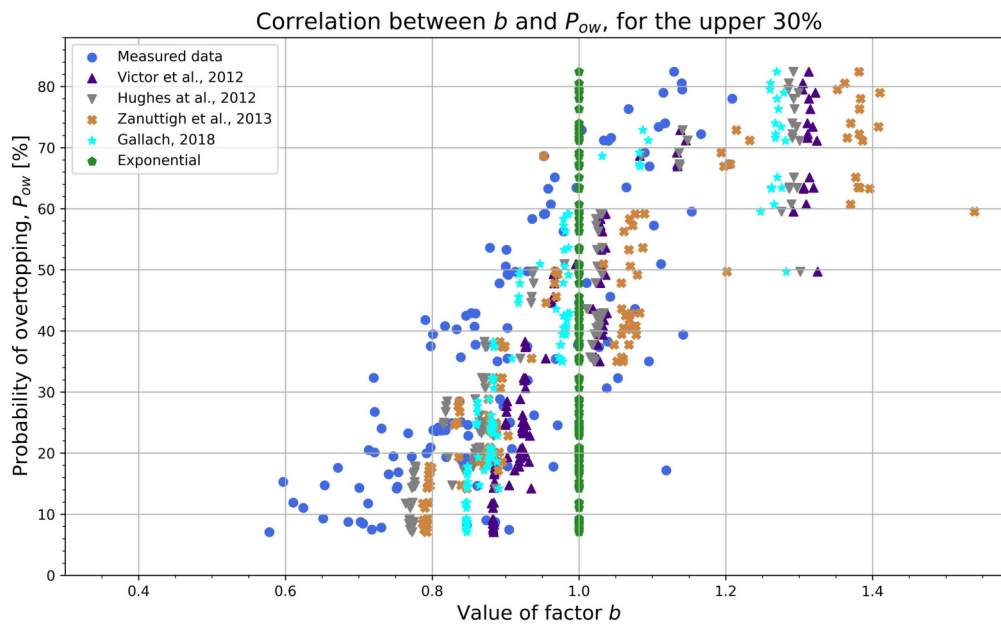
Figure 6.68: Comparison of the prediction of shape factor b regarding to P_{ow}, for the upper 30% volumes, in VWL.

30% and the 50% is no longer that visible, except for the highest values of R_c/H_{m0}. However, due to this scattering a high underprediction is also found for the lowest values of R_c/H_{m0}. This fact is also quite visible in Figure 6.71, as well as in Figure 6.72, in which the value of b increases considerably more than in the previous cases when the probability of overtopping increases.

Then, this variability of the predicted values of b around the measured data is translated into a minimum $rMSE$ of b, although this same error for V_{max} is increased (see Figure 6.73).

Finally, a comparison between the results according to the percentage threshold is carried out in Section 6.2.1.2.

6.2.1.2   Comparison between thresholds

First of all, Figures 6.52, 6.62, 6.66 and 6.70, in which the value of shape factor b is related to the relative crest freeboard R_c/H_{m0} can be compared next to each other. Nevertheless, as the prediction is the same whether the portion of the data is considered, these results are easier to compare as in Figure 6.74, where all thresholds are displayed
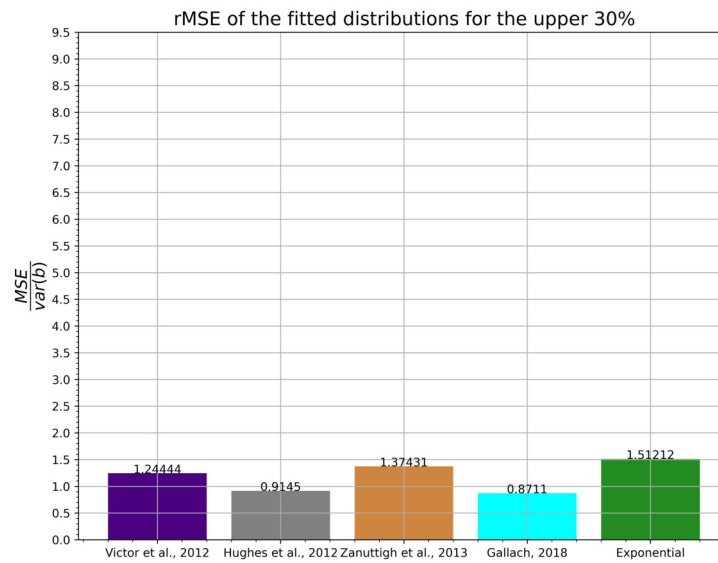
(a) *rMSE* of the prediction methods of *b*
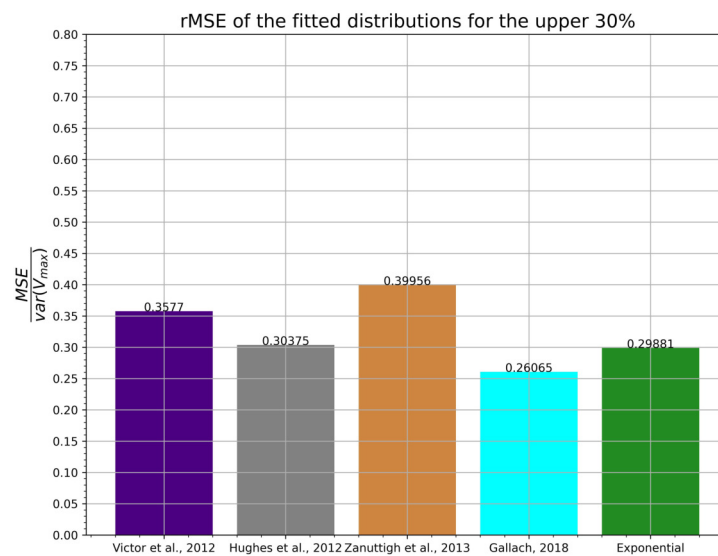
(b) *rMSE* of the prediction methods of V_{max}

Figure 6.69: *rMSE* of the prediction methods of *b* and V_{max}, for the upper 30% volumes, in VWL.

in the same plot.

Hence, results for the top 30% may be interpreted as those which best fit to the prediction formulae, as a rough first approach.

Moreover, if the predicted values of *b* are added to the measured values for each threshold from Figure 6.61, it can be observed as in Figure 6.75 the variability of the
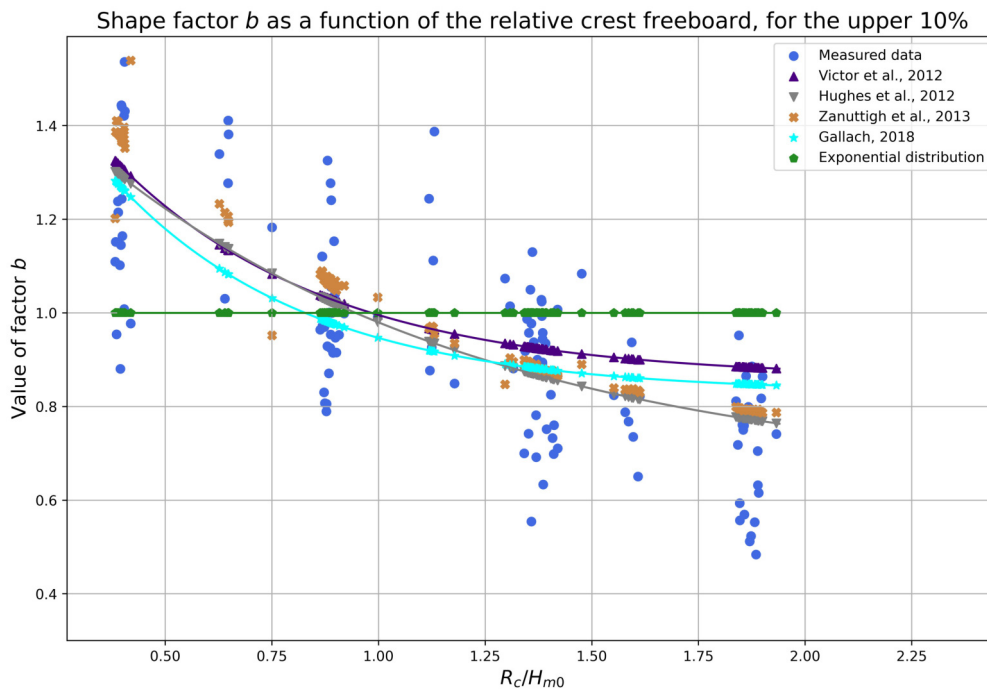
Figure 6.70: Comparison of the prediction of shape factor b regarding to R_c/H_{m0}, for the upper 10% volumes, in VWL.

values of the shape factor for each case and how they fit to the prediction as a very rough approach.

Another comparison between the considered thresholds to understand the fitting has to do with the correlation between the predicted and the measured values. Then, Figure 6.76 shows this plot for b and Figure 6.77 represents the correlation between the predicted and measured values of V_{max}.

In that sense, Figure 6.76 represents also the degree of under and overestimation that is mainly observed in each case. The overestimation is a bit more noticeable when the upper 30% is considered. As previously mentioned, the top 10% case shows a much bigger dispersion, with high under and overestimations of the b-values. This same conclusion is also observed in Figures 6.53, 6.63, 6.67 and 6.71, where the prediction is referred to R_c/H_{m0} using the measured data.

On the other hand, Figure 6.77 shows a very interesting result. In this case, it can be observed that the prediction of V_{max} tends to be underestimated when this variable is high, what is found for the bigger thresholds of volumes. Then, when considering a
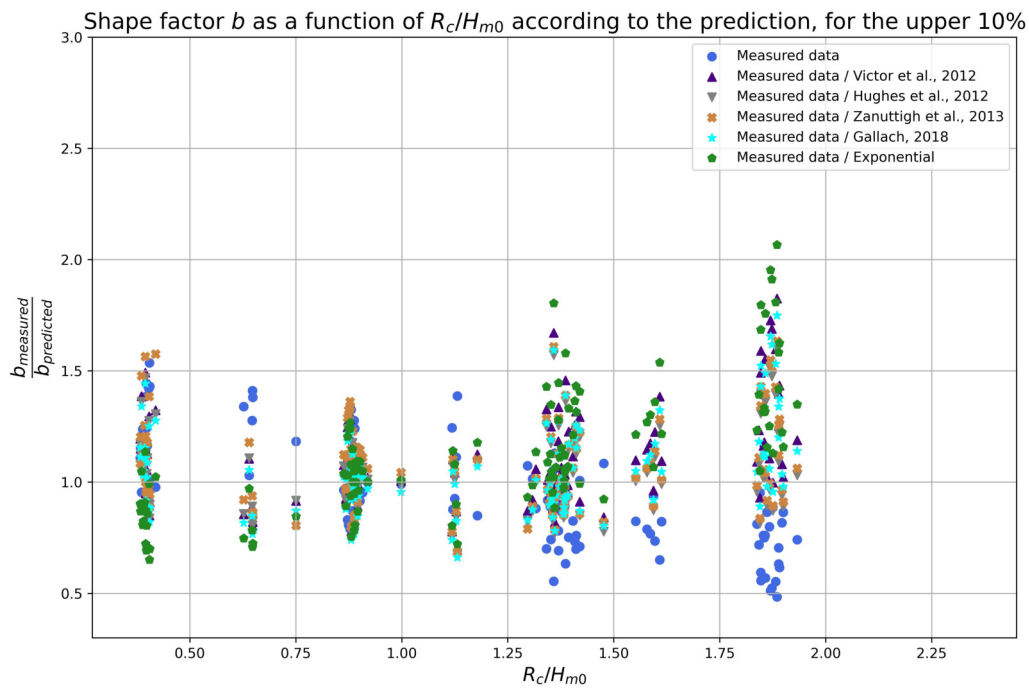
Figure 6.71: Comparison of the prediction of shape factor b regarding to R_c/H_{m0} using the measured data as reference, for the upper 10% volumes, in VWL.
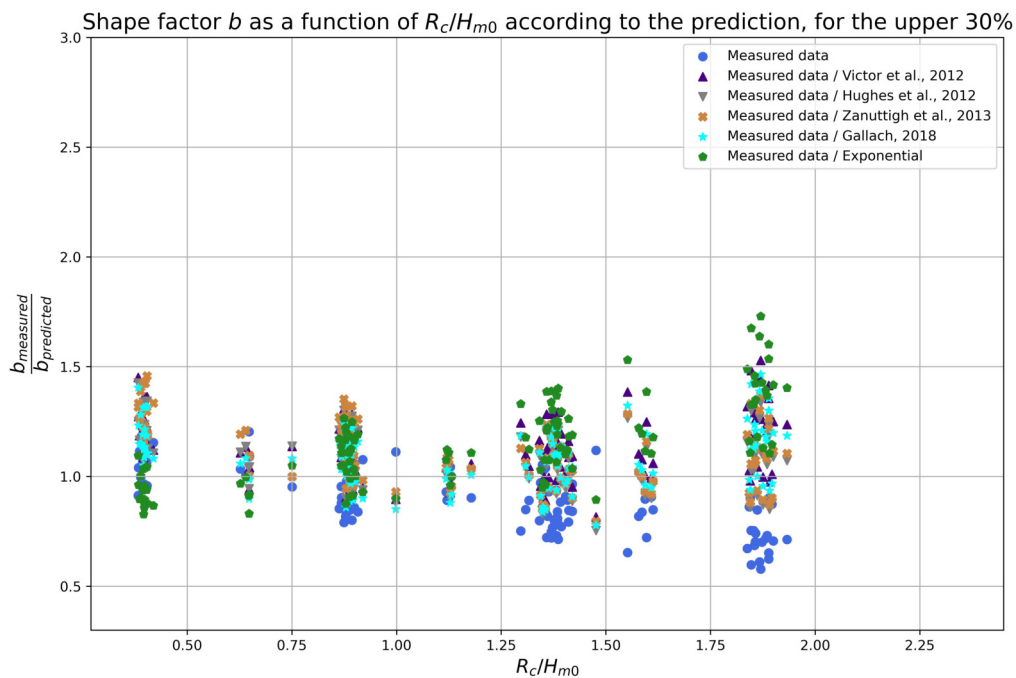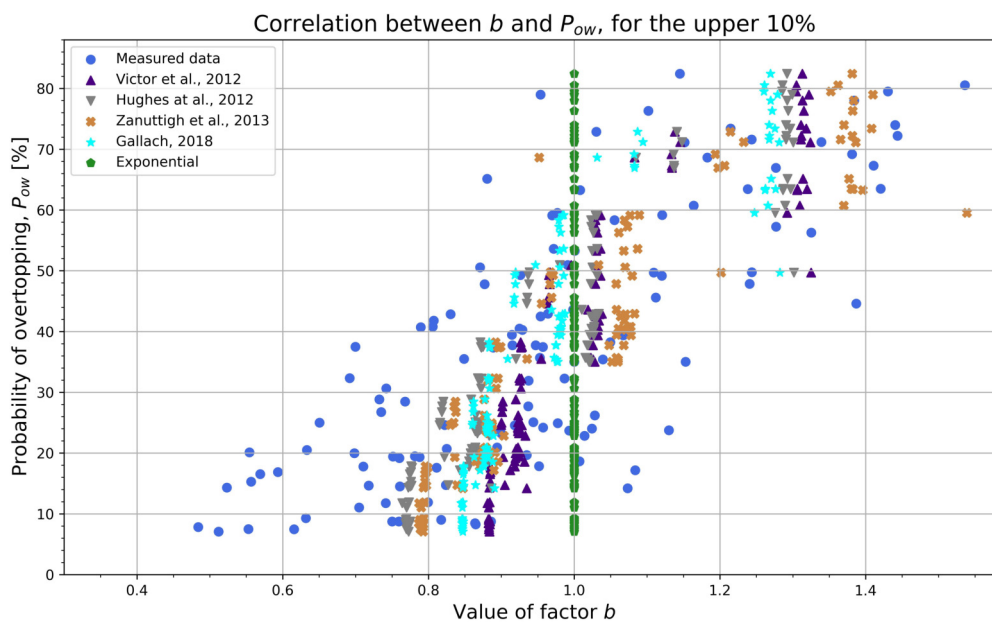

Figure 6.72: Comparison of the prediction of shape factor b regarding to P_{ow}, for the upper 10% volumes, in VWL.
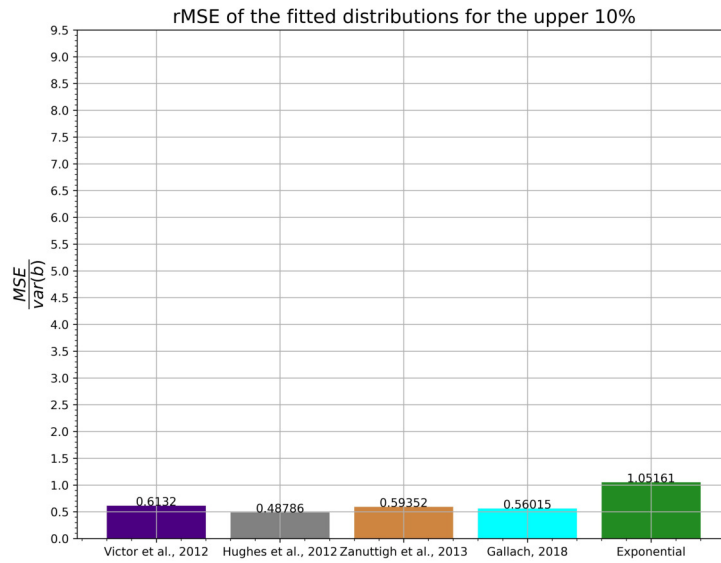
(a) *rMSE* of the prediction methods of *b*
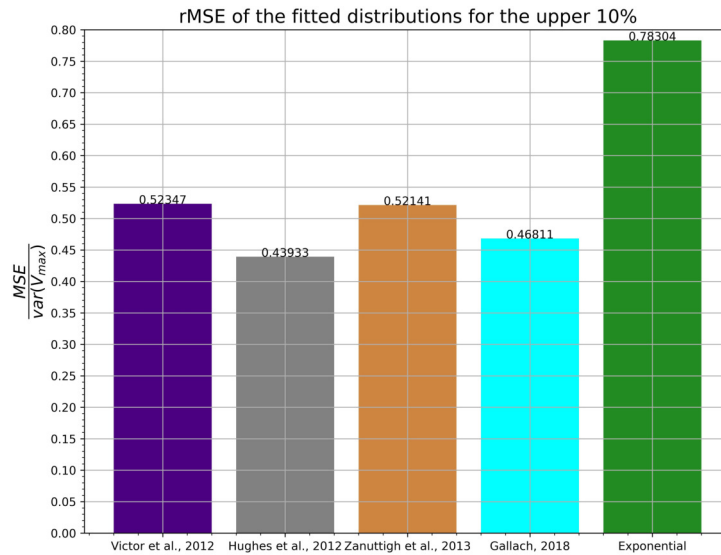
(b) *rMSE* of the prediction methods of V_{max}

Figure 6.73: *rMSE* of the prediction methods of *b* and V_{max}, for the upper 10% volumes, in VWL.

smaller portion of data, as the value of V_{max} is lower, the prediction fits quite accurately to the $y = x$ line, which represents the perfect correlation between measurement and prediction. The possible reason of this not-directly-perceptible issue based on the formulae is that less values to analyse leads to a lower value of N_{ow}, which is actually the variable of the argument in the logarithm to obtain V_{max} (see Equation 3.37). Hence, if the argument
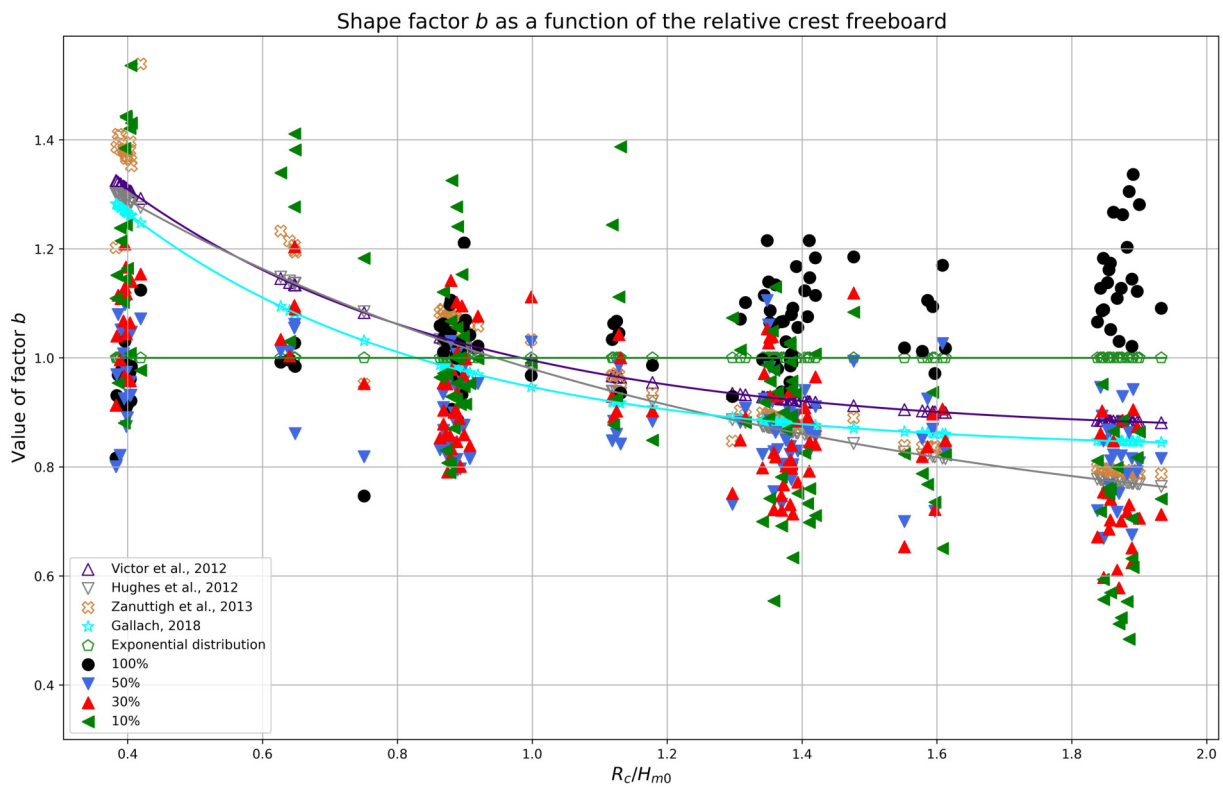
Figure 6.74: Comparison of the results of b regarding R_c/H_{m0} for the upper 100, 50, 30 and 10% volumes, in VWL.
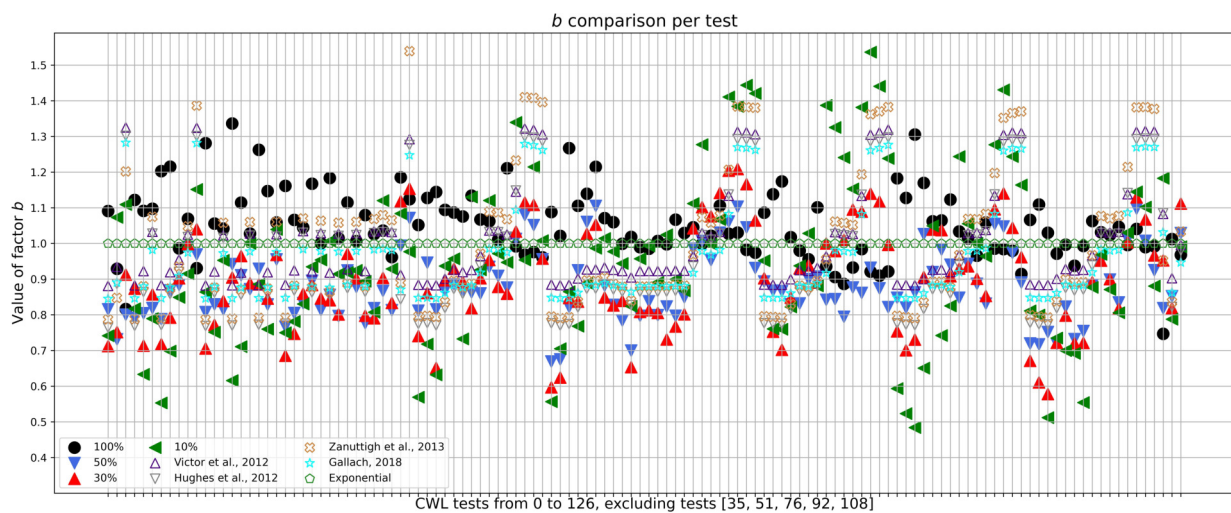
Figure 6.75: Comparison of b per test and the predicted values, for the upper 50%, 30% and 10% volumes, including the 100% case, in VWL.

is lower, the value of V_{max} will be lower too, while a and b factors remain approximately in the same range. This could result to the conslusion that the comparison of V_{max} between different thresholds is not possible or, at least, not formally consistent based on the formulation.

Finally, through the quantification of the error it is also possible to determine the accuracy of the fitting. Then, the *rMSE* of *b* and V_{max} showed for each case can be compared but this comparison may be extended to a much bigger number of thresholds in which the upper portion of the data is considered. Hence, besides the 100% of the volumes, percentages of 70, 65, 60, 55, 50, 45, 40, 35, 30, 25, 20, 15, and 10 are considered.

To show these results, rather than displaying next to each other the bar plot for each case, the *rMSE* of *b* and V_{max} are showed in Figures 6.78(a) and 6.78(b), respectively.

From Figure 6.78(a) it is possible to observe that the error of the prediction decreases for all prediction methods when the percentage of volumes decreases as well, with very similar results between the formulae. On the other hand, the *rMSE* of V_{max} shows how the accuracy of the fitting for this variable improves when the portion of the data in the analysis decreases but after a certain threshold, around 25%, the error increases; probably as a consequence of the scatter of the results when the number of volumes becomes smaller, as it was also mentioned in Section 6.1.3.2 for the CWL case.

However, in comparison with the CWL situation, the results seem to be less accurate for the VWL case, with a slight overprediction, as it can be seen in Figure 6.79, which shows the *rMSE* of *b* and V_{max} for the same thresholds between both situations. Thus, the prediction formulae are useful but not as good as for the CWL case.

According to these results, it could be said that for the VWL situation the most suitable threshold to predict these parameters is around the 30% of the highest overtopping volumes, for which the best results are found for both Gallach Sánchez, David (2018) and Hughes et al. (2012) formulae.

6.2.1.3   Influence of test duration and seed number

One more approach can be done to validate the results and clarify the variability of the experimental campaign. In order to carry out this issue, the previous results for the VWL situation are divided into their different duration and seed number, to visualize even the same waves between them.
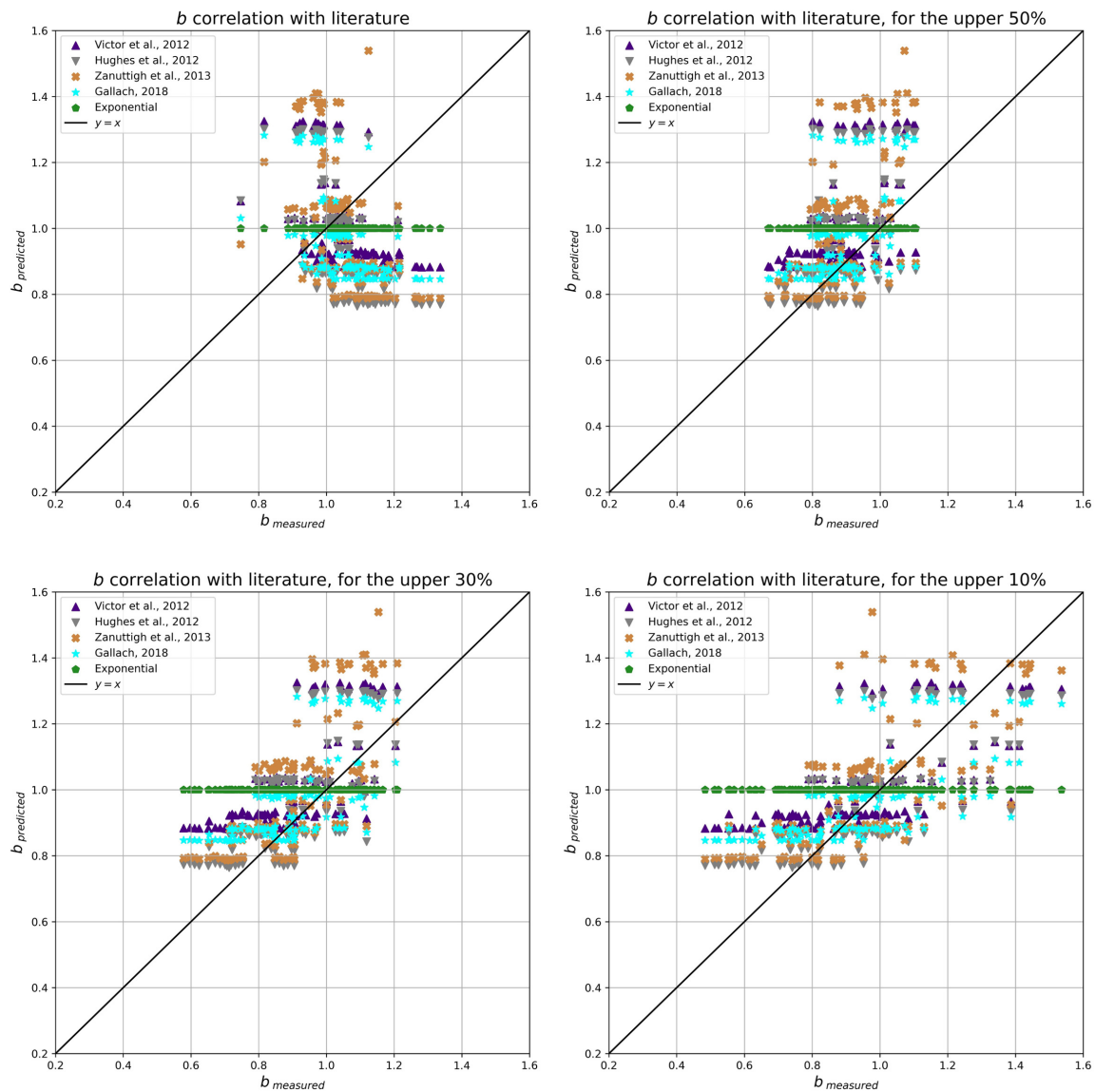
Figure 6.76: Correlation between measured and predicted values of *b* for different threshold cases, in VWL. From top to bottom and left to right: 100%, 50%, 30% and 10%.
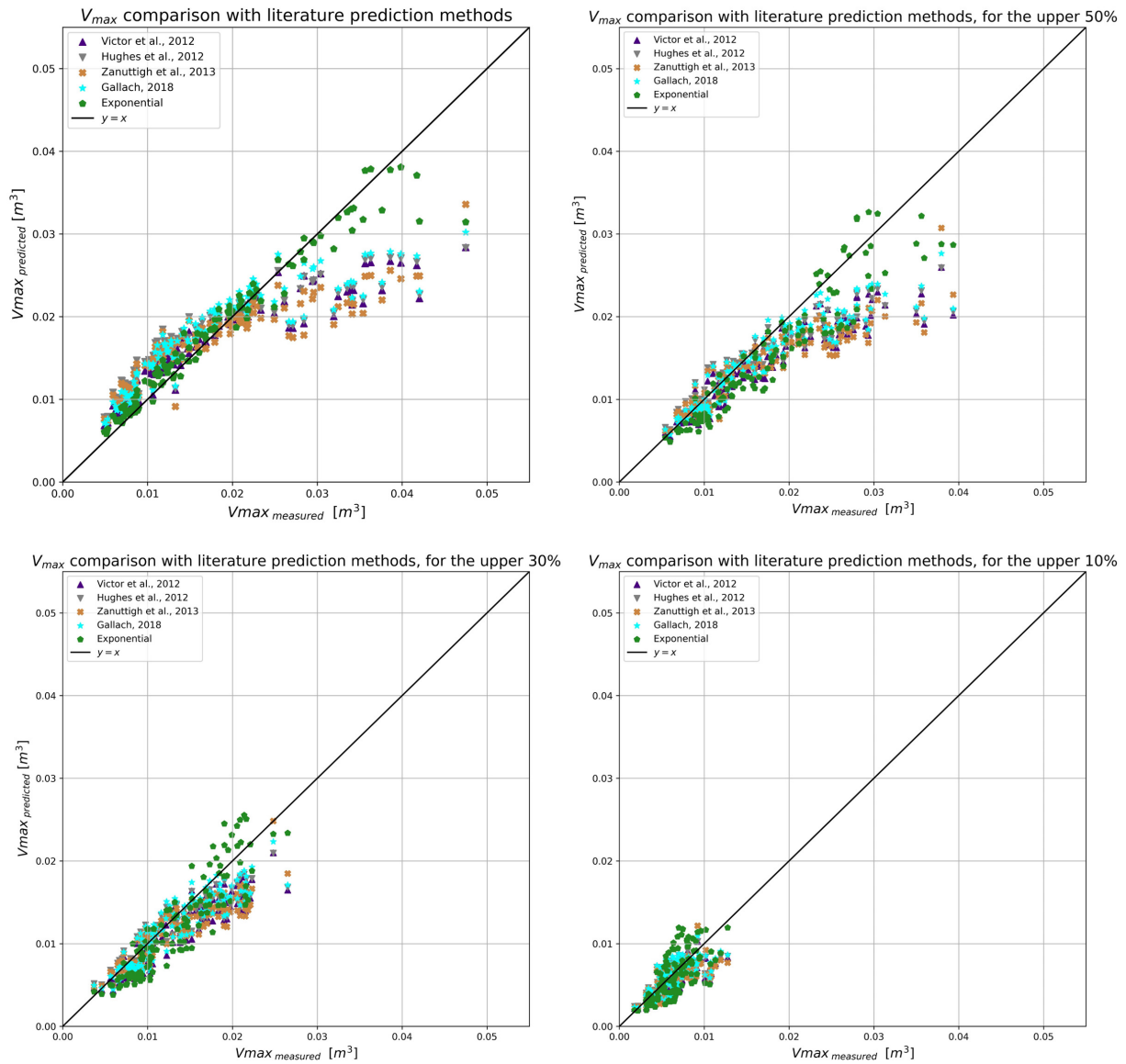
Figure 6.77: Correlation between measured and predicted values of V_{max} for different threshold cases, in VWL. From top to bottom and left to right: 100%, 50%, 30% and 10%.
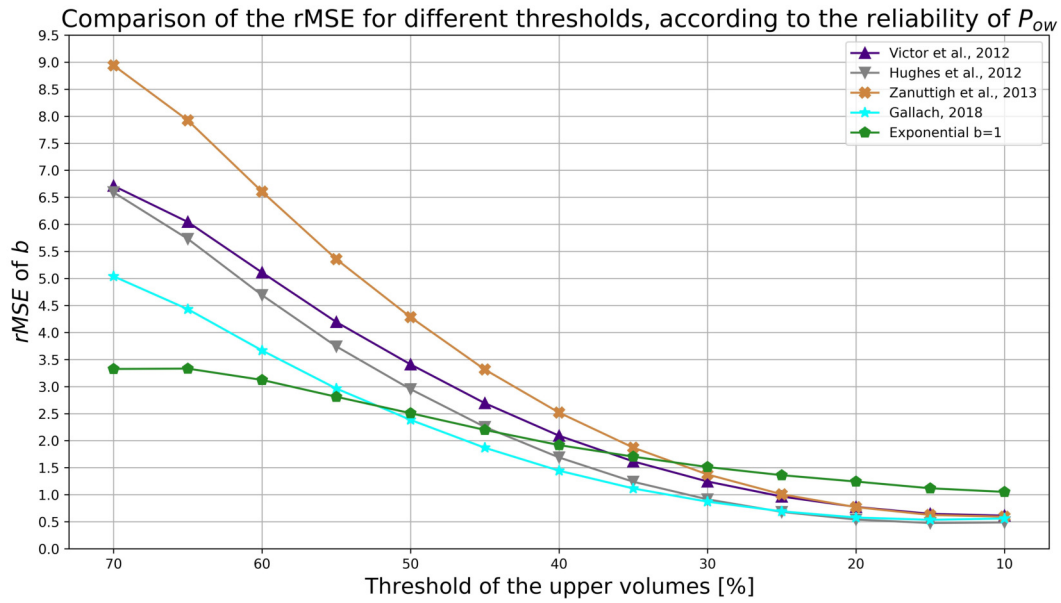
(a) *rMSE* of *b* for different threshold cases
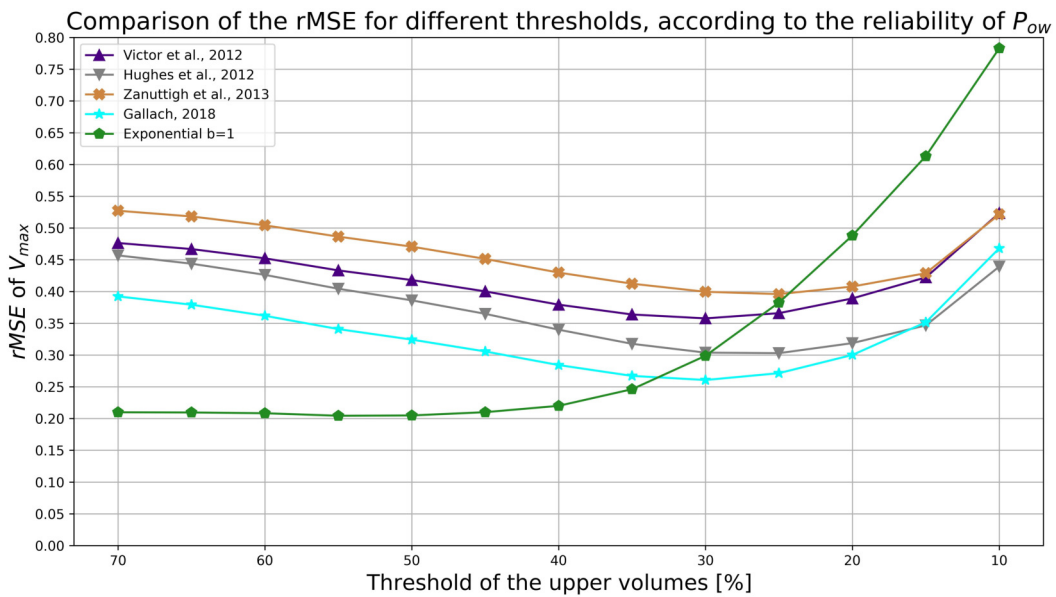
(b) *rMSE* of V_{max} for different threshold cases

Figure 6.78: *rMSE* of the prediction methods of *b* and V_{max}, for different threshold cases, in VWL.

Hence, Figures 6.80, 6.81 and 6.82 show the comparison between these parameters so it is possible to remark that no big differences between the duration of the tests modify the results in a noticeable way. Figure 6.83 may show that for the same value of the relative crest freeboard, bigger values of *b* are found for the shortest tested duration of

900 s.

For the seed number that generates the waves the same conclusion is reached, so no big differences between tests are found (see Figures 6.84, 6.85 and 6.86). For this case only the tests with a duration of 900 s have been considered in order to compare the different seed numbers.

6.2.1.4 Influence of the crest freeboard

The main goal of this study claims to focus on the validity of the literature prediction formulae for the VWL situation to predict the individual overtopping volumes. Then, as it could be seen, although the accuracy of the results is not the same than for the CWL case, for which they are intended, the results are quite useful for some certain thresholds considering the upper overtopping volumes, and especially for some of the formulae.

In that sense, as this variable analysis only considers the crest freeboard at the beginning of the test, some considerations can be taken into account before reaching to the final conclusions. Thus, if the 30% threshold is considered for the VWL situation, the results can be compared according to a different value of the crest freeboard. Then, this analysis can be carried out for:

- R_c/H_{m0}. It refers to the crest freeboard at the beginning of the test, i.e., the minimum value of R_c.

- $R_{c,max}/H_{m0}$. It refers to the crest freeboard at the end of the test, so the maximum value of R_c is found.

- $R_{c,avg}/H_{m0}$. It is the average value between the relative crest freeboard considered at the start of the test (R_c) and at the end of it ($R_{c,max}$).

- $(R_c/H_{m0})_{eq}$. It refers to the equivalent non-dimensional freeboard which predicts equally well both CWL and VWL situations, defined by Pepi et al. (2022) as a function of the non-dimensional freeboard at the peak water level. Hence, its formulation refers to a $R_{c,peak}$ value which stands for the lowest freeboard from the start of the test (at the peak of the storm), understood at the beginning of it in this case. The total variation of the water level dh is also considered (see Table 5.4). Then, Pepi et al. (2022) defines the next expression to calculate this parameter, using as well the wave height at the toe of the structure, for the defined range of tested

values:

$$(R_c/H_{m0})_{eq} = \frac{R_{c,peak}}{H_{m0}} + exp\left(-1.14\frac{R_{c,peak}}{dh}\right)^{0.55} \tag{6.4}$$

Then, if these four cases are compared according to the measured value of factor b for the 30% threshold case and the theoretical distributions from Victor et al. (2012), Gallach Sánchez, David (2018) and Hughes et al. (2012), it can be observed the difference between the values of R_c at the start (Figure 6.87) and at the end (Figure 6.88) of the test. For the case in which the average value is compared with the theoretical distributions (Figure 6.89), an improvement of the predictions is found. Finally, using the value of $(R_c/H_{m0})_{eq}$ from Equation 6.4, a more compacted situation is achieved, with a very good fitting of the data (Figure 6.90).

Finally, this same analysis can be carried out for the probability of overtopping P_{ow} to compare these four cases using each different relative crest freeboard. The distribution for $b = 0.75$ proposed by Van der Meer and Janssen (1994) is also displayed to clearly visualize the results. In that sense, the same big difference between both minimum and maximum values of R_c can be seen in Figures 6.91 and 6.92, respectively, as well as the average between them (Figure 6.93). For the case considering the value of $(R_c/H_{m0})_{eq}$ defined by Pepi et al. (2022) from Equation 6.4 a great fitting is found, with the measured values of b between the theoretical predictions and following their tendency even better that the average value (Figure 6.94). The comparison between these last four cases displayed in Figures 6.91 to 6.94 can be seen in detail in Figure 6.95.

However the average value provides great results as well, special interest in taken to the equivalent non-dimensional freeboard $(R_c/H_{m0})_{eq}$ as this variable is already validated for the average overtopping discharge. Then, the idea to unify both CWL and VWL approaches using one single variable which implicitly takes into account the water level variability is such a notorious fact in this field.

As a conclusion of the analysis, the prediction formulae available in literature are able to predict the individual overtopping volumes for the VWL situation, even though they are intended for the CWL situation. However, a slight overprediction is observed when applying these formulae to a VWL scenario. Moreover no influence of the duration of the tests and the seed number used to generate the waves is found in the results.

Nevertheless, as it can be seen in this section, the best results for these prediction methods are found when considering the equivalent non-dimensional freeboard defined by Pepi et al. (2022), so the related overprediction is minimized. In other words, the pre-

diction formulae available in literature can predict the individual overtopping volumes for the VWL situation if a corrective equivalent non-dimensional freeboard is used. Moreover, a specific portion of the data needs to be considered to achieve the best results, so only a determined percentage of the highest overtopping volumes is chosen following a sensitivity analysis to define it.

One more example to support these ideas can be seen in Figure 6.96. In plots above and below it is represented the rMSE of both b and V_{max}, respectively, for the VWL situation. The solid line represents the same error displayed previously in Figure 6.78. However, the dotted line represents the new rMSE obtained by using the equivalent non-dimensional freeboard in the calculations. This Figure is the most evident proof that using $(R_c/H_{m0})_{eq}$ for individual overtopping volumes in VWL helps to obtain more accurate estimations, as the error between measured and predicted is clearly reduced.
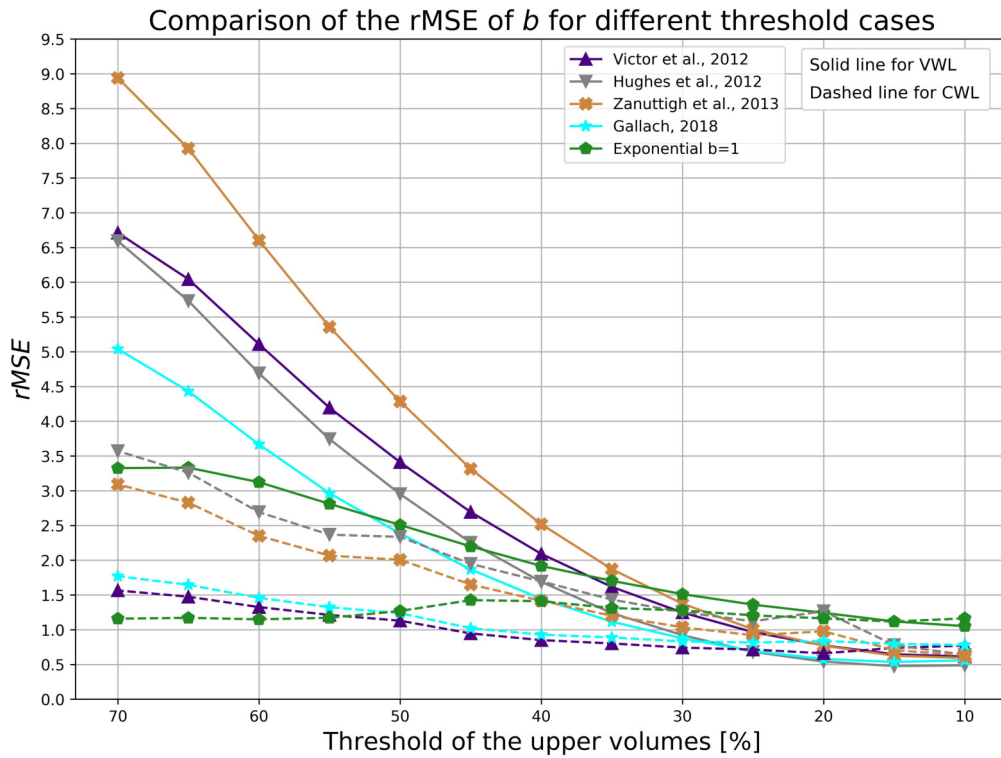
(a) Comparison of the *rMSE* of *b* for different threshold cases between VWL and CWL situations
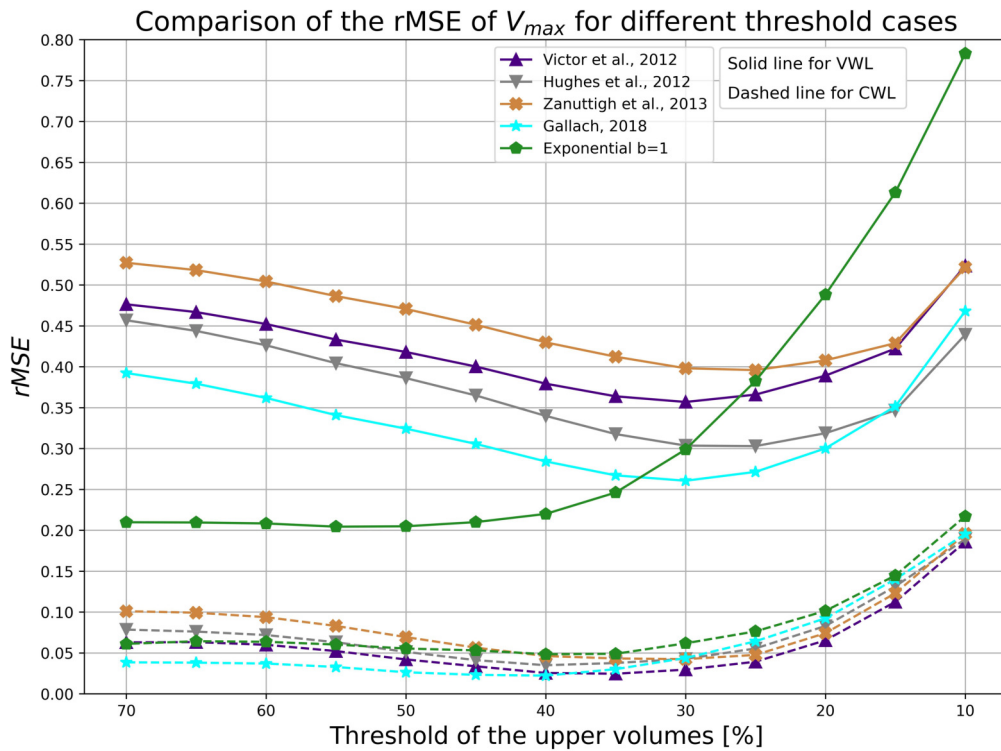
(b) Comparison of the *rMSE* of V_{max} for different threshold cases between VWL and CWL situations

Figure 6.79: Comparison of the *rMSE* of the prediction methods of *b* and V_{max}, for different threshold cases, between VWL and CWL situations.
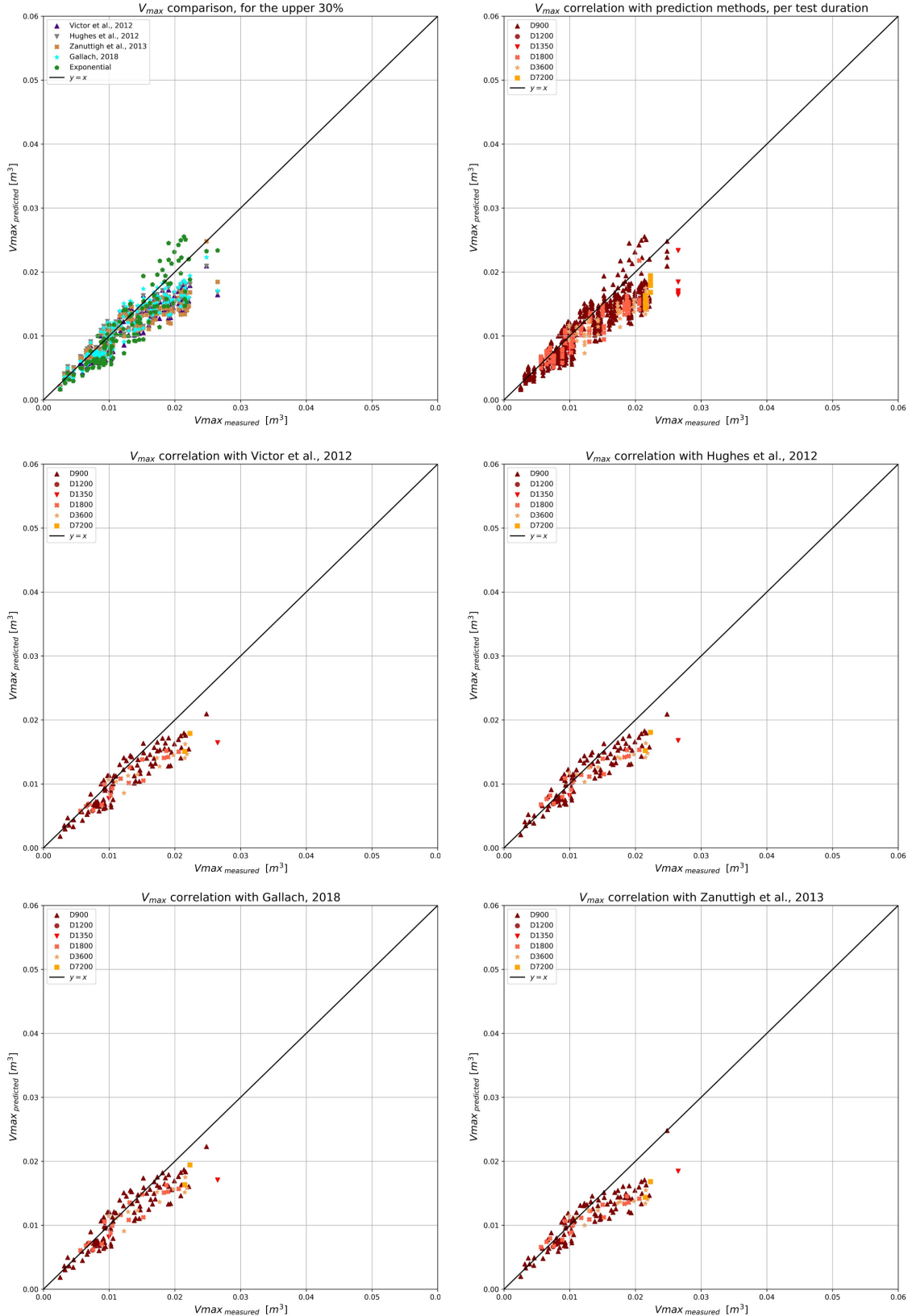
Figure 6.80: Comparison between the different test duration for the prediction of V_{max}, for the upper 30% in VWL.
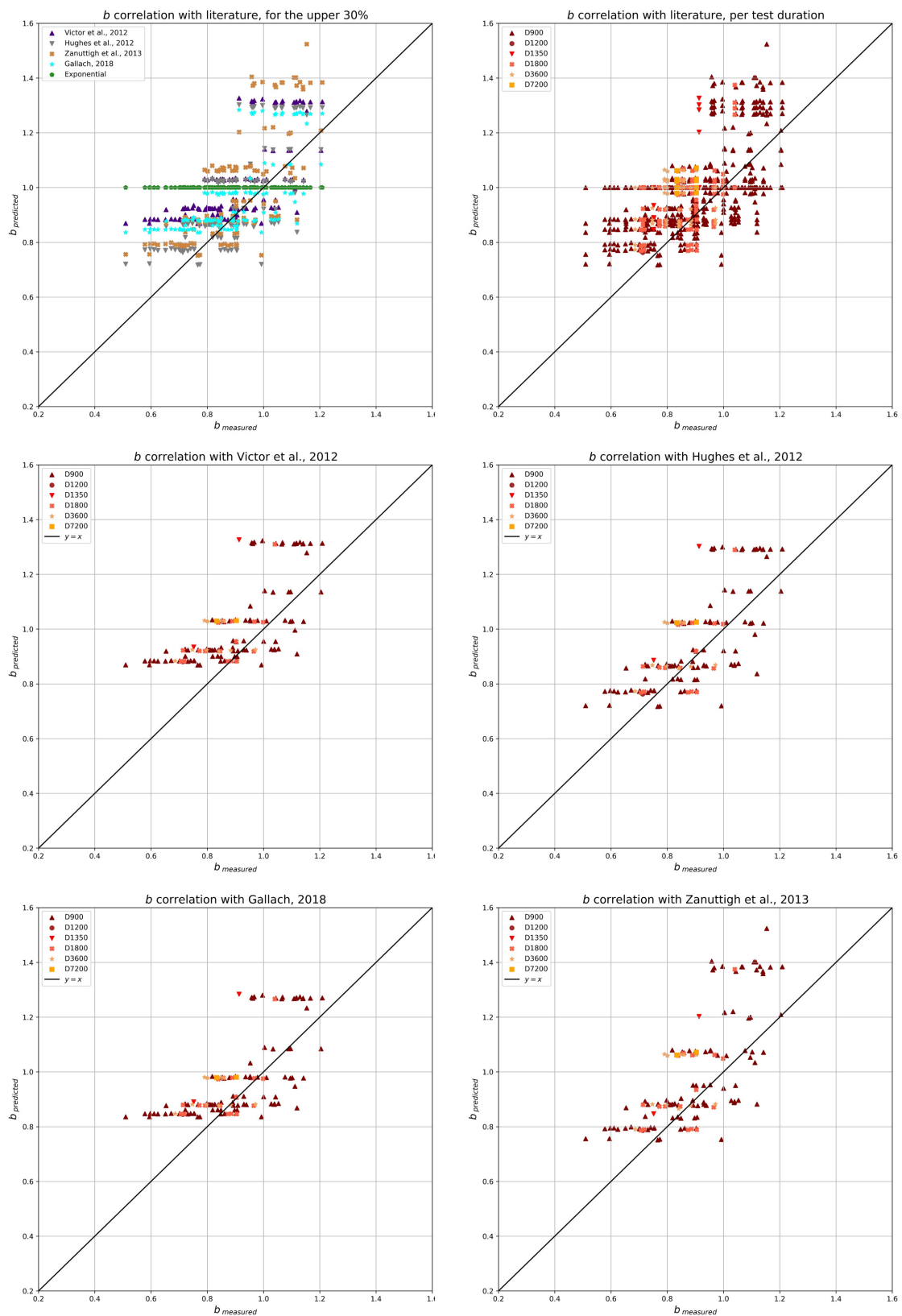
Figure 6.81: Comparison between the different test duration for the prediction of *b*, for the upper 30% in VWL.
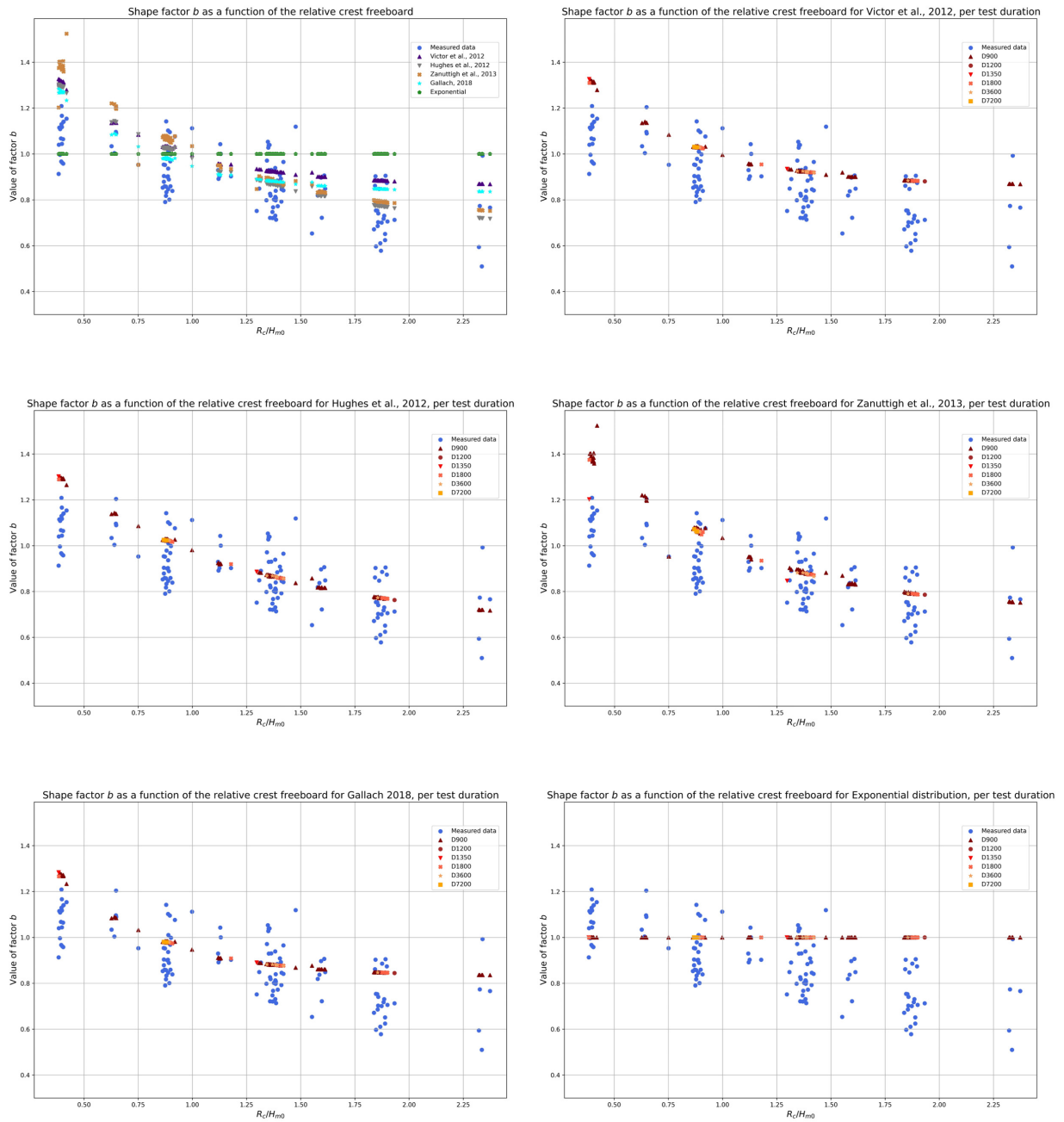
Figure 6.82: Comparison between the different test duration for the prediction of *b* as a function of R_c/H_{m0}, for the upper 30% in VWL.
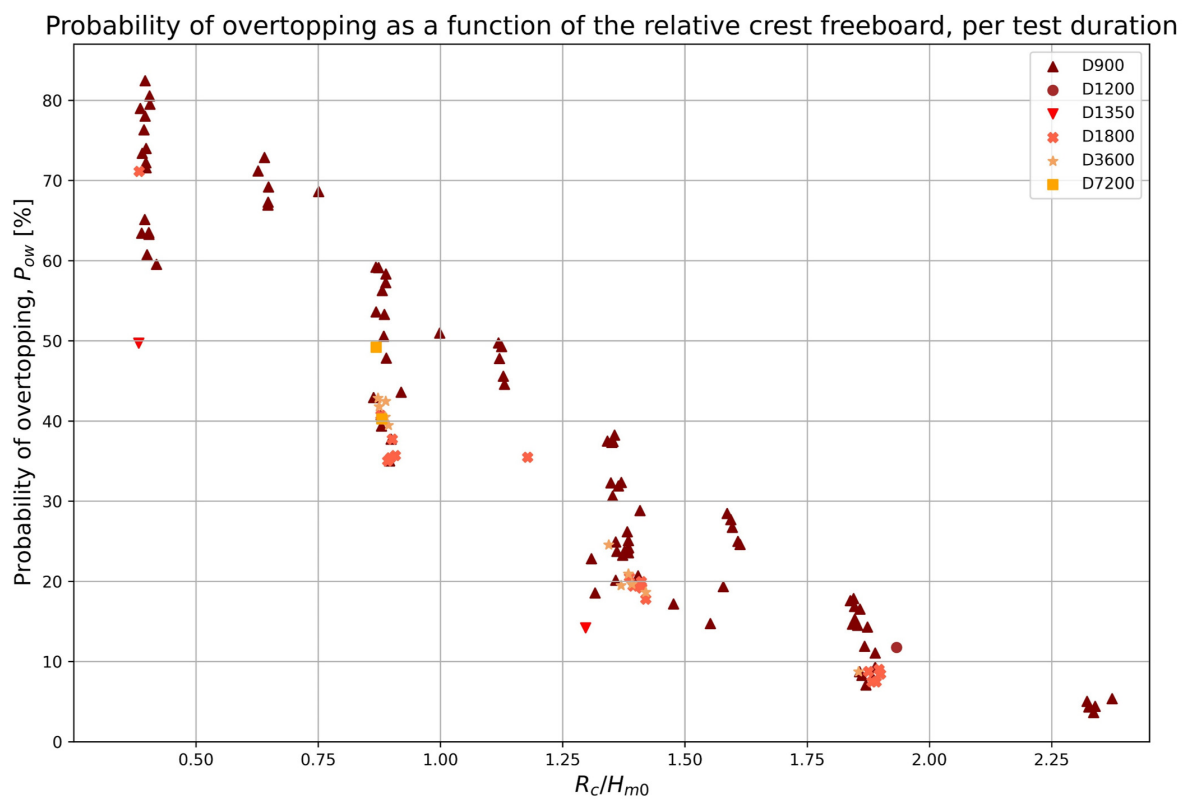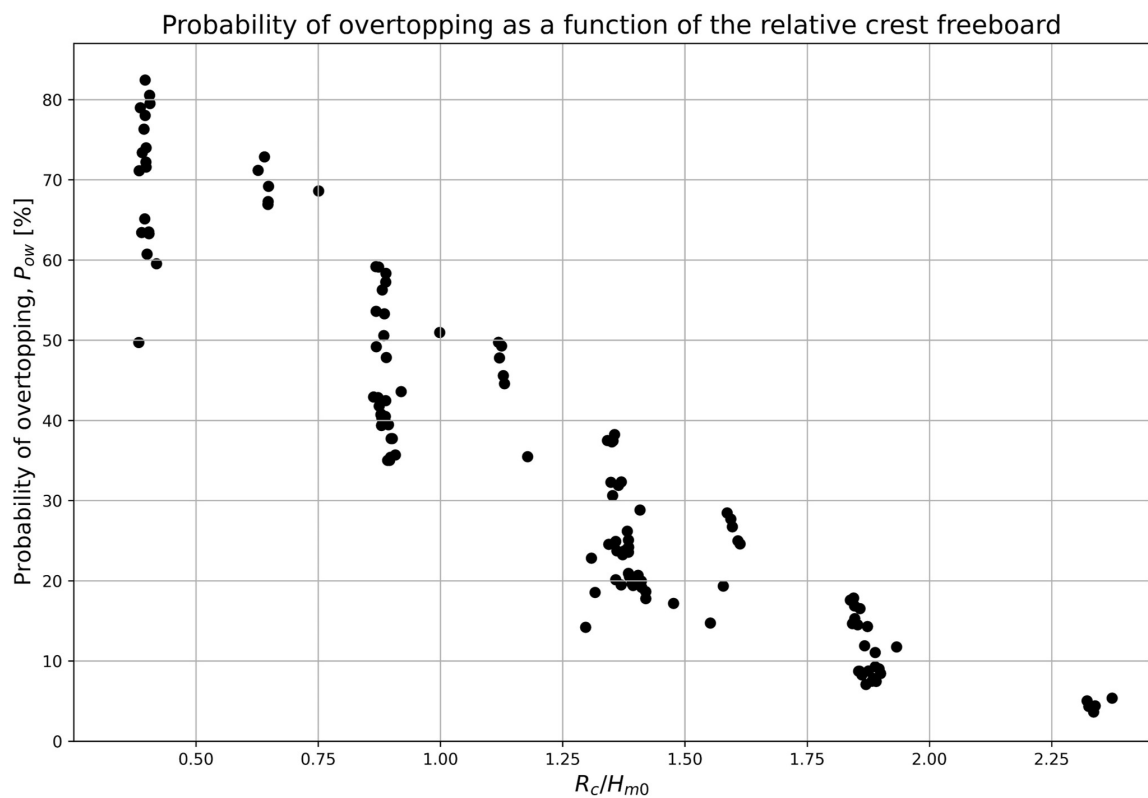
Figure 6.83: Comparison between the different test duration between P_{ow} and R_c/H_{m0}, for the upper 30% in VWL.
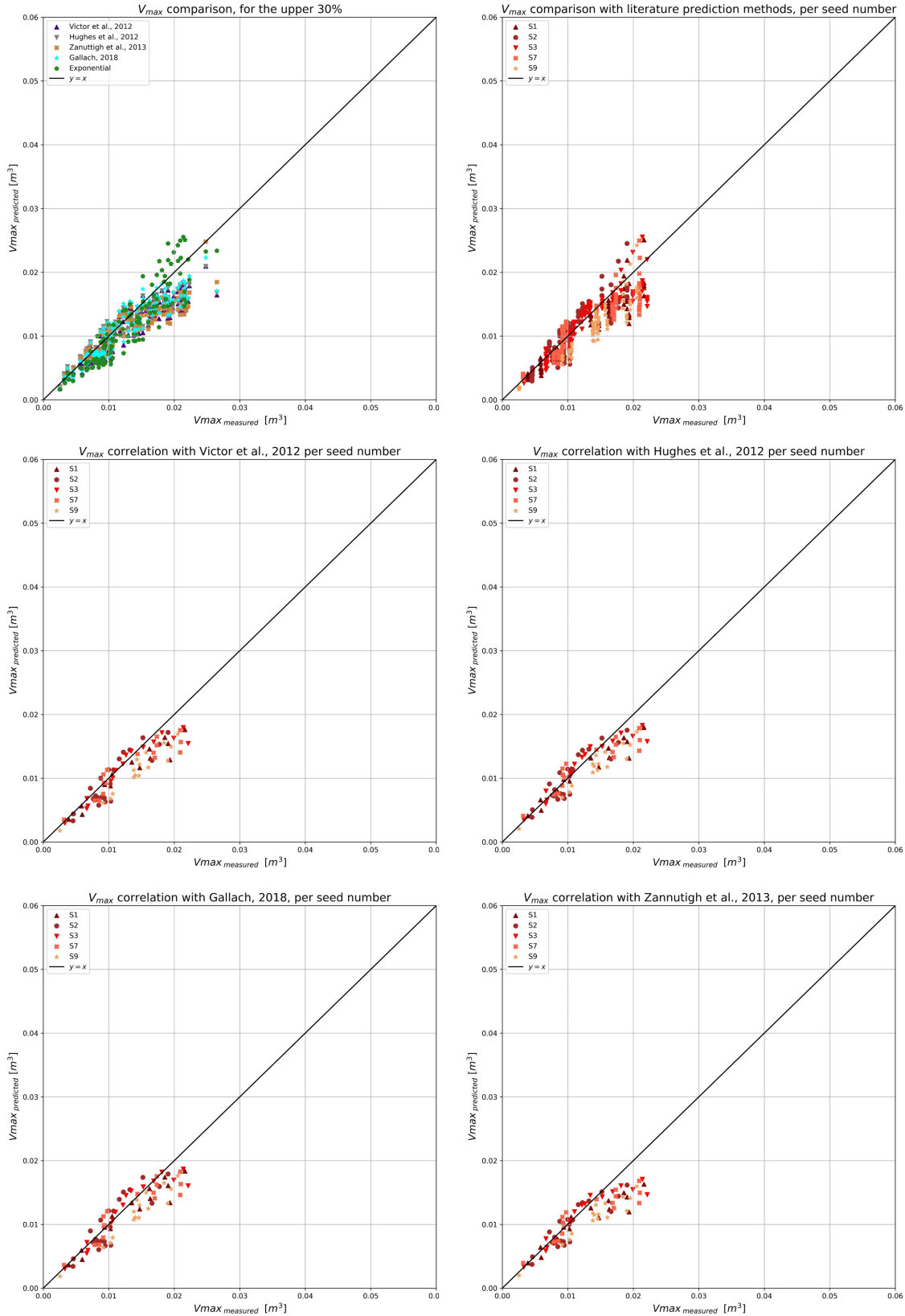
Figure 6.84: Comparison between the different seed numbers for the prediction of V_{max}, for the upper 30% in VWL.
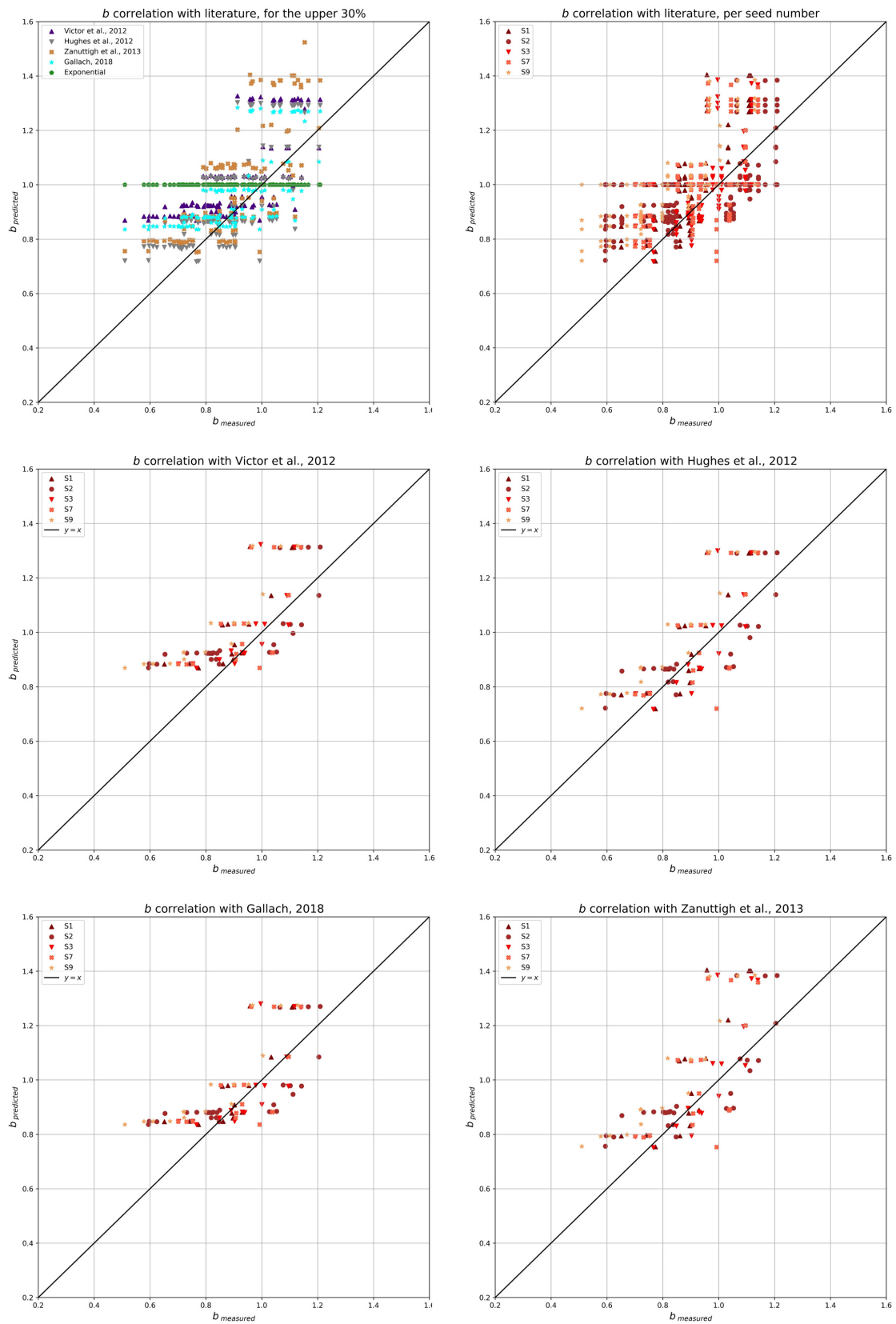
Figure 6.85: Comparison between the different seed numbers for the prediction of *b*, for the upper 30% in VWL.
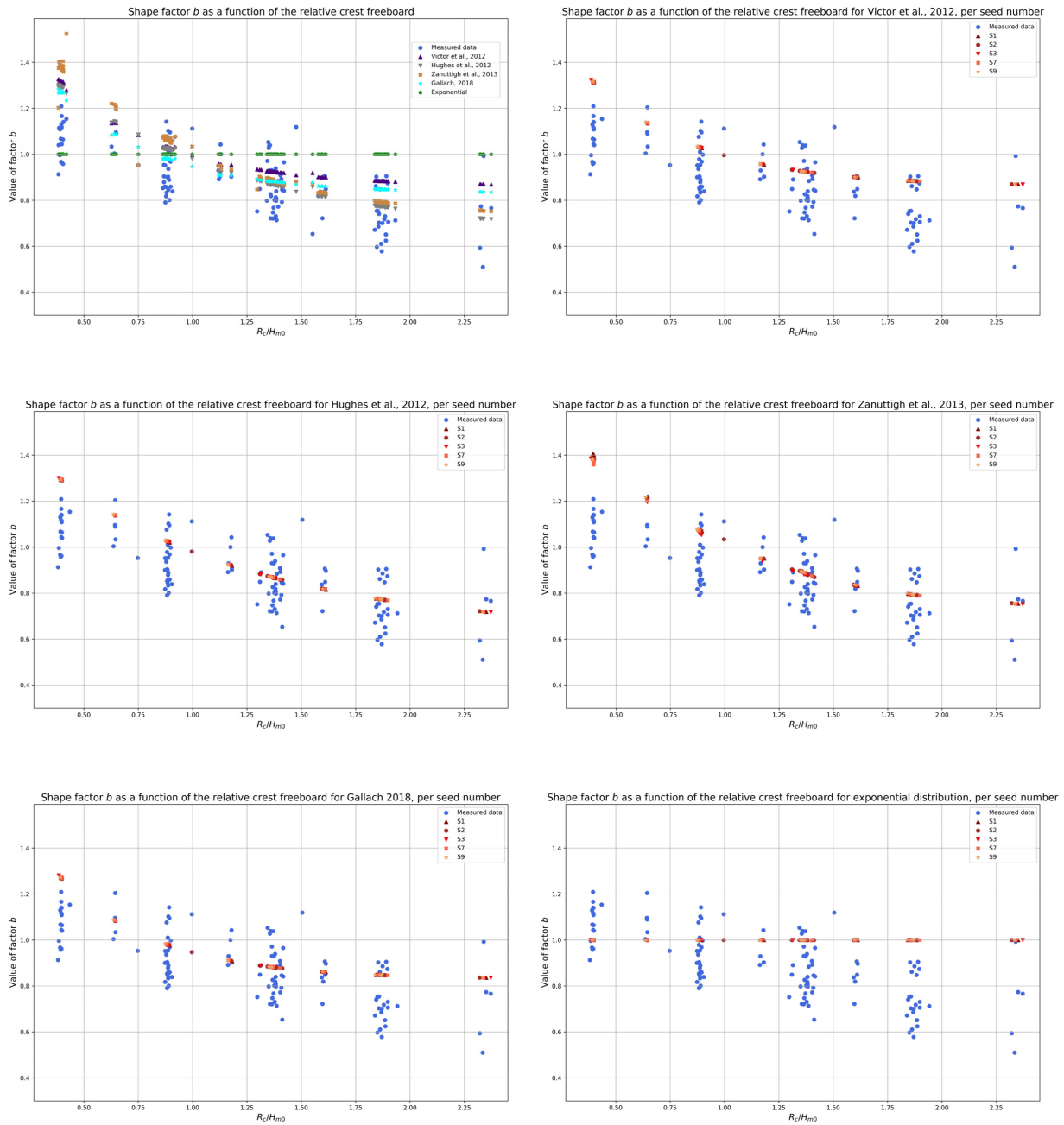
Figure 6.86: Comparison between the different seed numbers for the prediction of b as a function of R_c/H_{m0}, for the upper 30% in VWL.
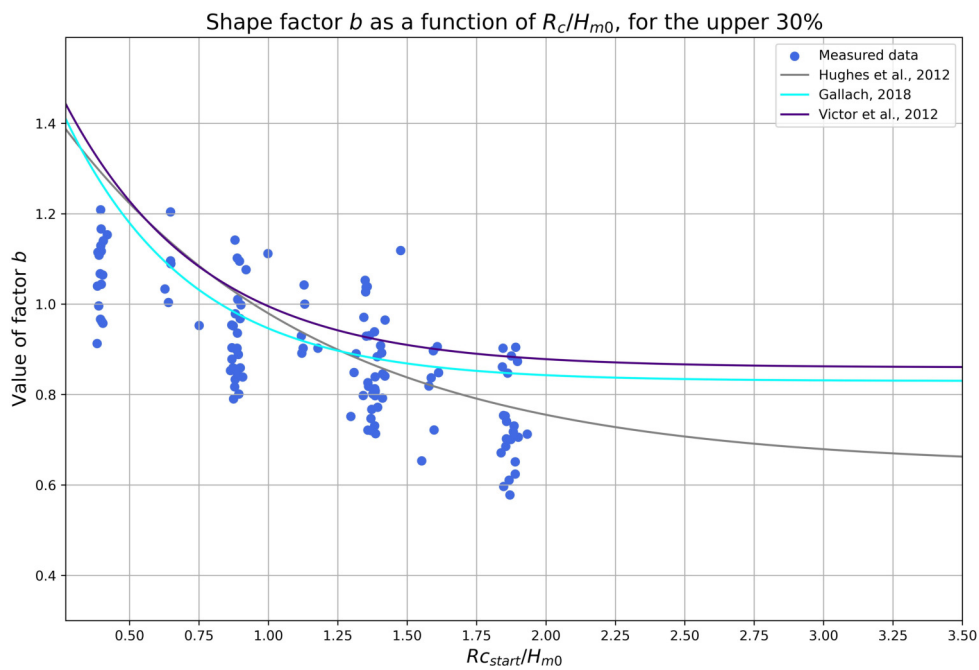
Figure 6.87: Comparison of shape factor *b* with the theoretical predictions as a function of $R_{c,start}/H_{m0}$.
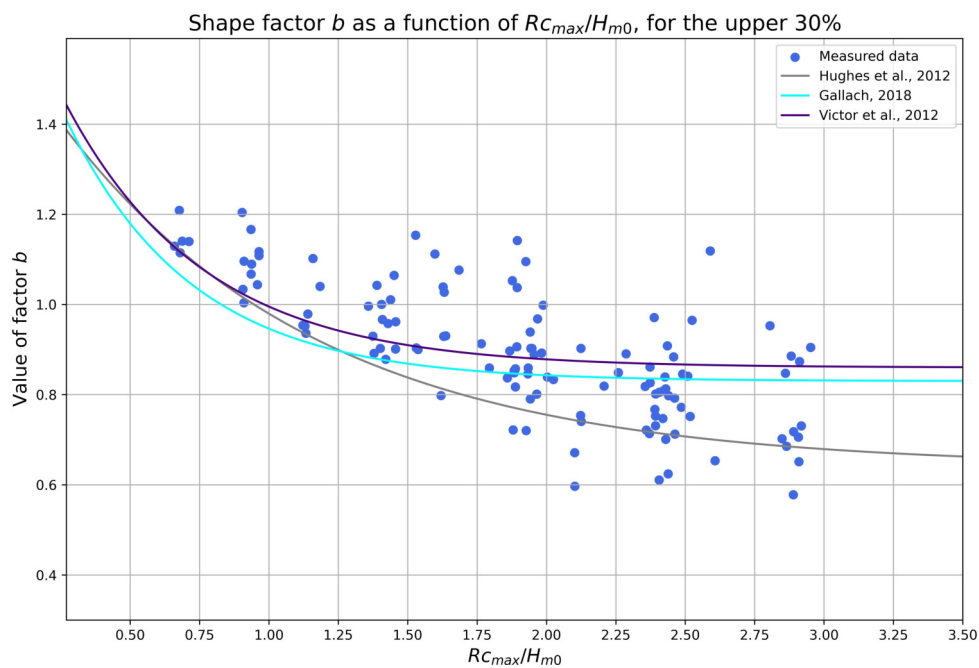
Figure 6.88: Comparison of shape factor *b* with the theoretical predictions as a function of $R_{c,max}/H_{m0}$.
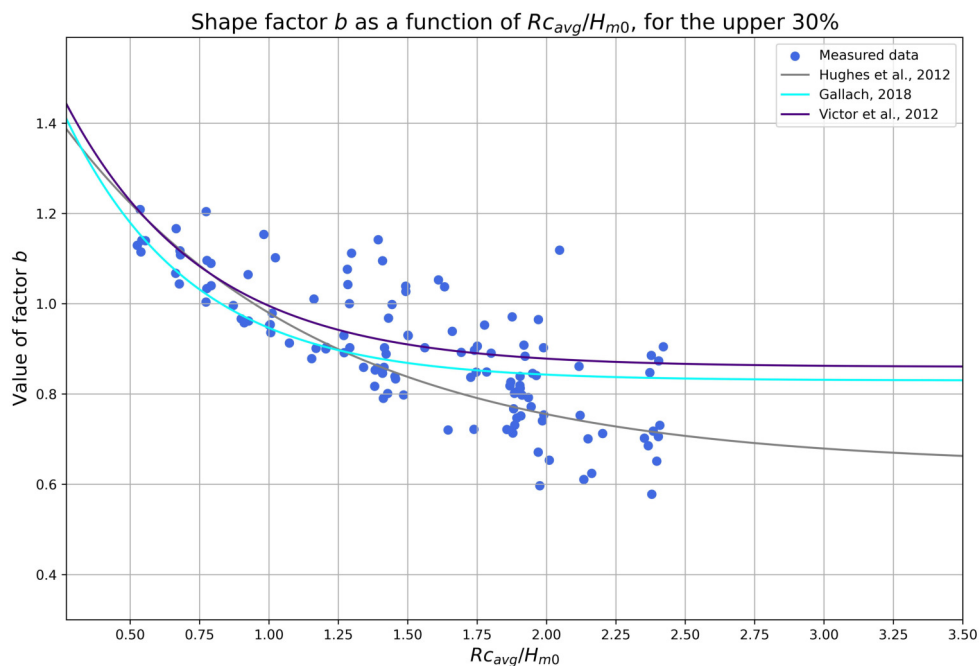
Figure 6.89: Comparison of shape factor b with the theoretical predictions as a function of $R_{c,avg}/H_{m0}$.
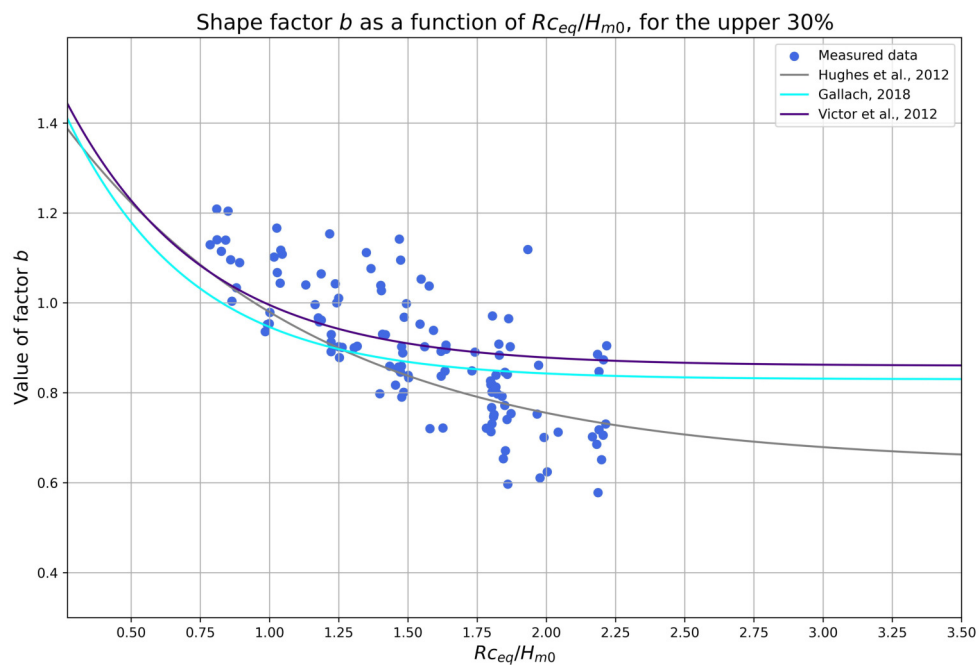
Figure 6.90: Comparison of shape factor b with the theoretical predictions as a function of $(R_c/H_{m0})_{eq}$.
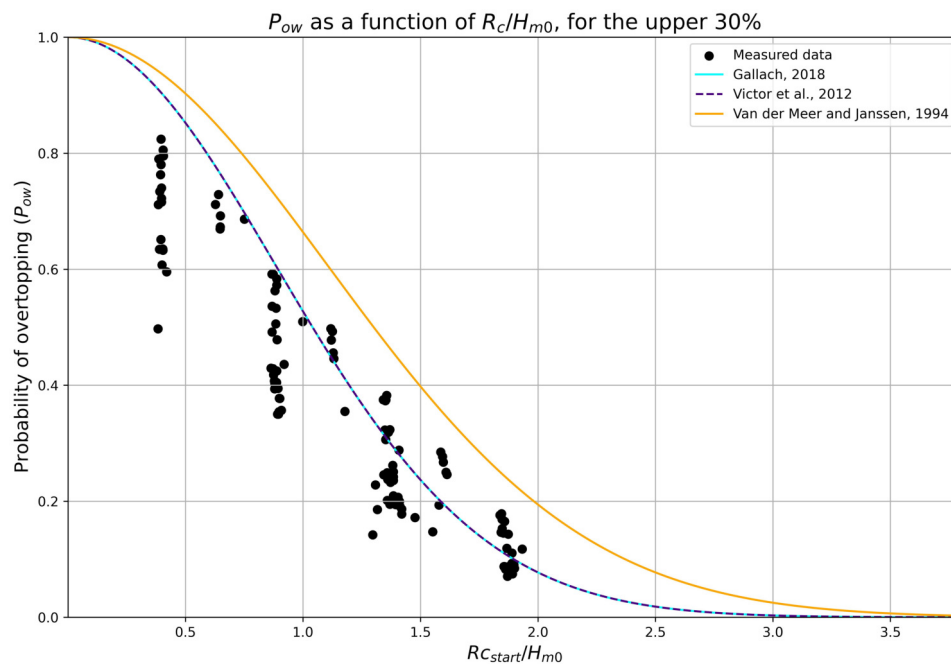
Figure 6.91: Comparison of P_{ow} with the theoretical prediction formulae as a function of $R_{c,start}/H_{m0}$.
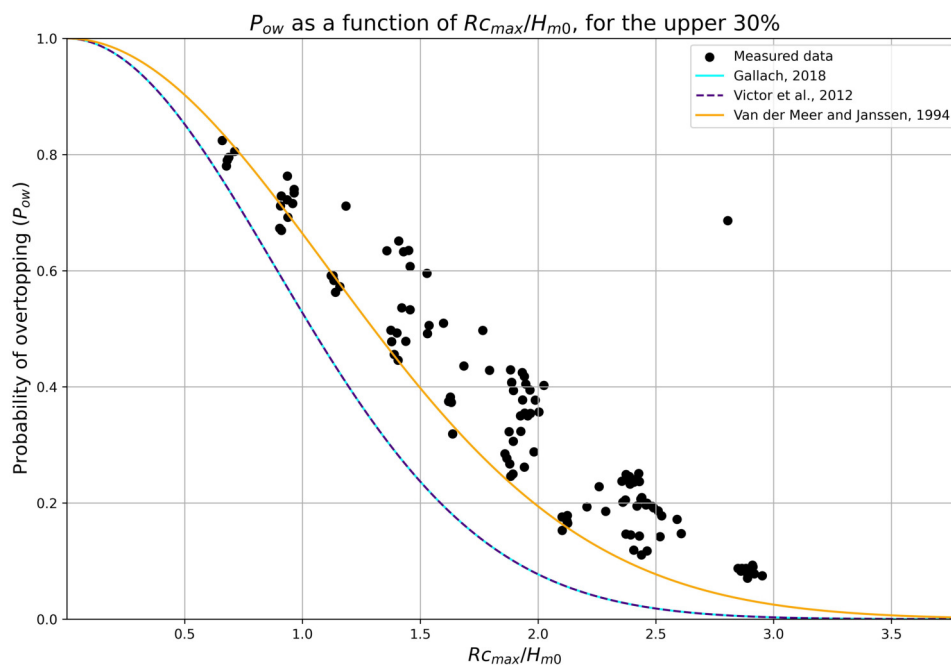
Figure 6.92: Comparison of P_{ow} with the theoretical prediction formulae as a function of $R_{c,max}/H_{m0}$.
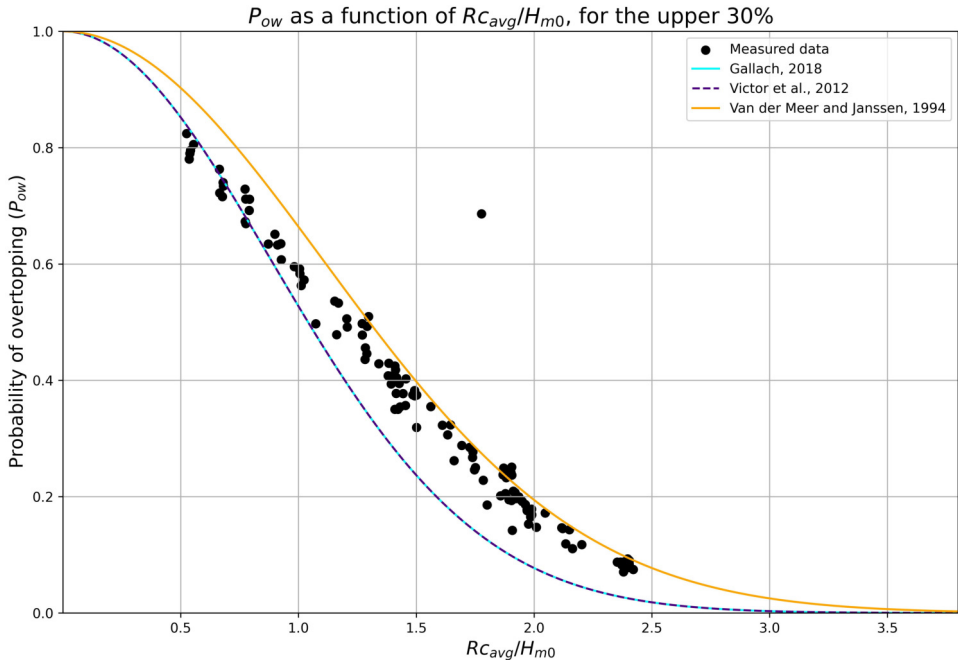
Figure 6.93: Comparison of P_{ow} with the theoretical prediction formulae as a function of $R_{c,avg}/H_{m0}$.
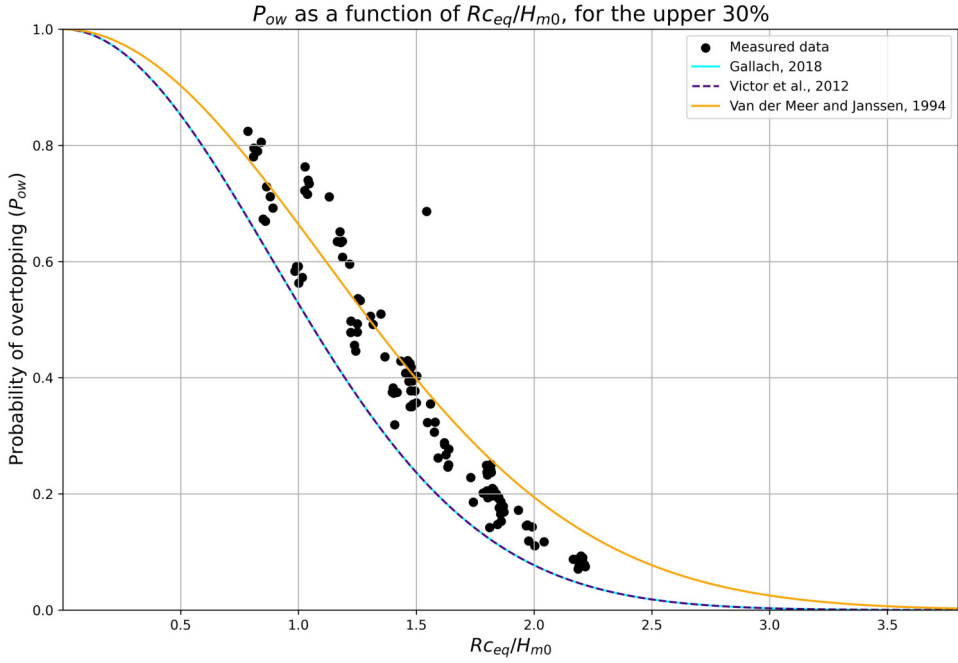
Figure 6.94: Comparison of P_{ow} with the theoretical prediction formulae as a function of $(R_c/H_{m0})_{eq}$.
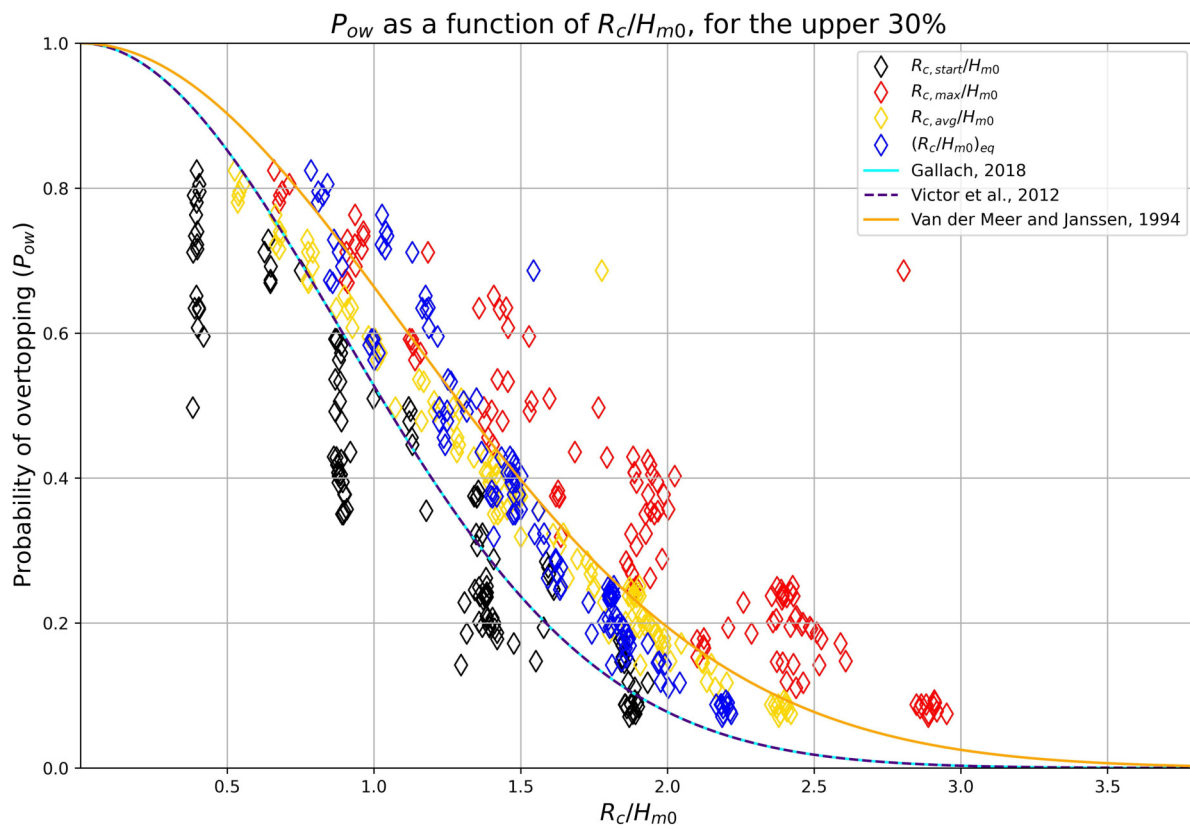
Figure 6.95: Comparison of P_{ow} with the different relative crest freeboards studied according to the theoretical prediction formulae.
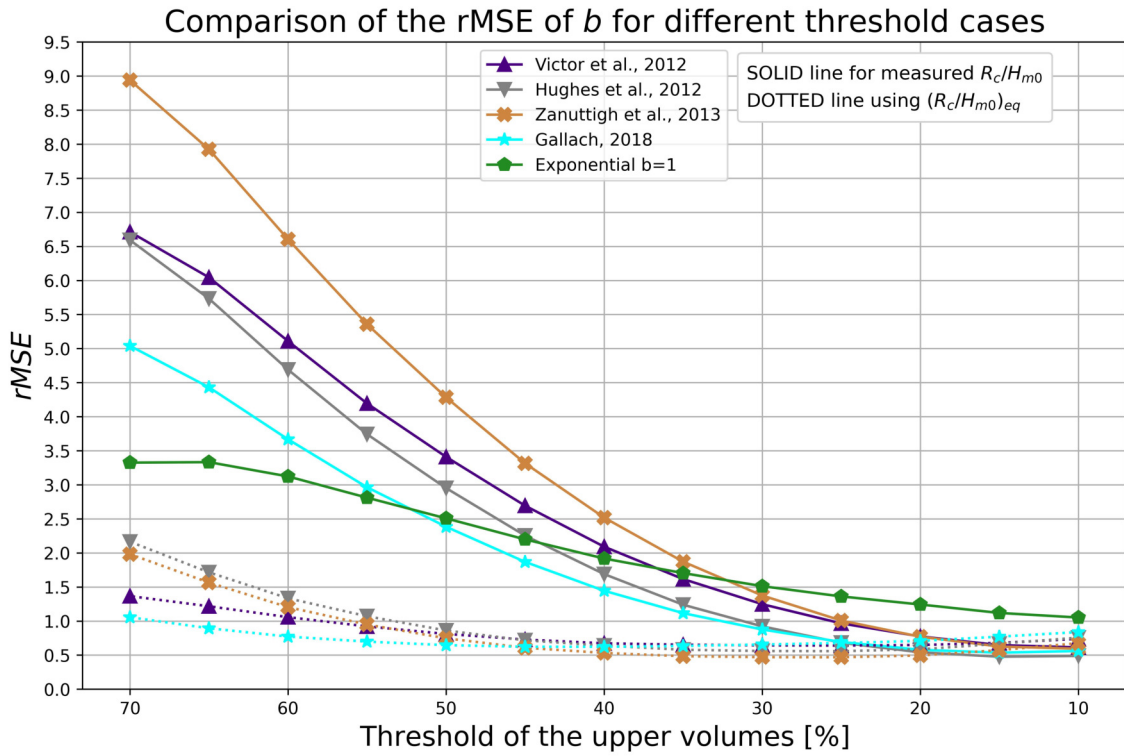
(a) Comparison of the *rMSE* of *b* for different threshold cases, using or not $(R_c/H_{m0})_{eq}$
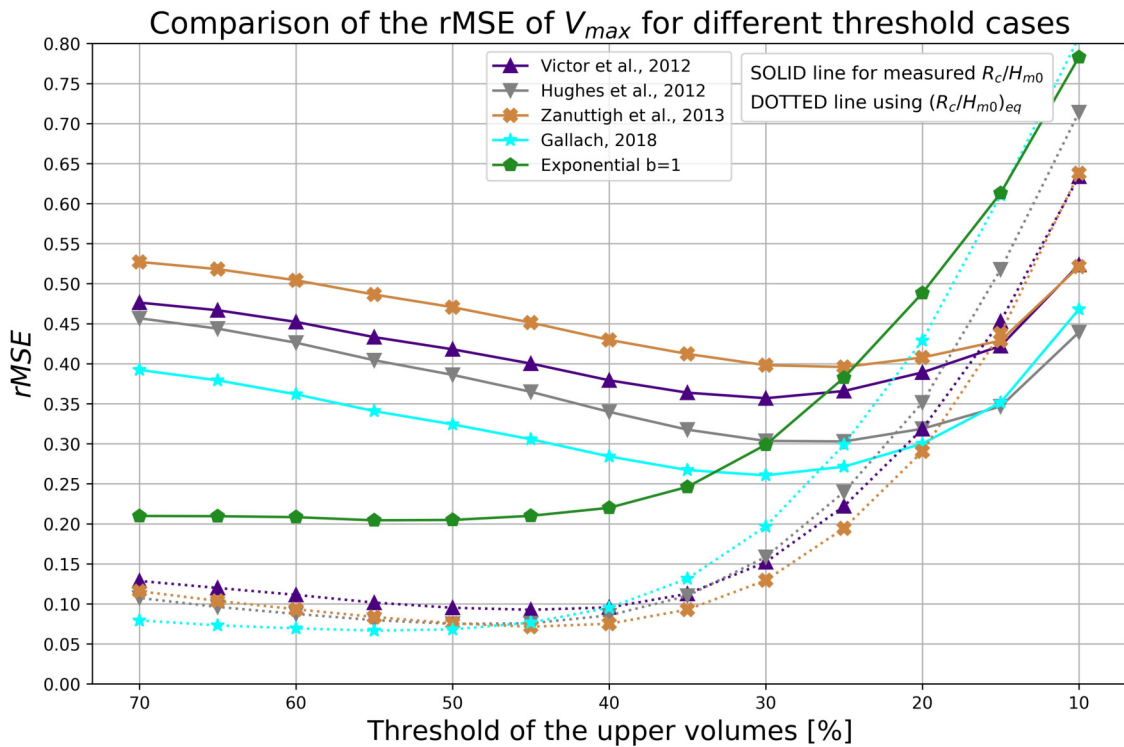
(b) Comparison of the *rMSE* of V_{max} for different threshold cases, using or not $(R_c/H_{m0})_{eq}$

Figure 6.96: *rMSE* of the prediction methods of *b* and V_{max}, for different threshold cases in VWL, using or not $(R_c/H_{m0})_{eq}$.

7. Practical application to the Belgian coast: Research Dike Raversijde

Once the overtopping analysis has been carried out, it is possible to translate those results to a practical case and predict a real overtopping situation for VWL. For that purpose, the Research Dike Raversijde is going to be considered.

The Belgian Coastal Zone is a part of the Southern Bight of the North Sea and it covers approximately 3600 km^2. The bathymetry is shallow and irregular with a mean depth of about 20 m and a maximum of 35 m. The area is also characterized by a complex system of sand banks parallel to the coast, some of which emerge from the water at very low tides (Mercier and Delhez (2007)).

Hence, the Belgian coastline is about 65 km long and is part of the southern sandy North Sea coastline system. It is oriented to SW–NE, so the winds and thus waves are mainly from these directions, and it extends from the estuary of the river Scheldt in the east (the Netherlands) to Dunkirk (France) in the west. The coastline consists of broad gently sloping sandy beaches backed by dunes, while on the shallow continental shelf numerous sandbanks occur as previously mentioned (Haerens et al. (2012)).

Then, these beaches are in general wide and very gently sloping, characterised by spilling breakers and classified as dissipative. The slope of Belgian beaches increases from west (1.3%) to east (2.4%), resulting in narrowing of the intertidal beachwidth (Deronde et al. (2006)).

Specifically, the Research Dike Raversijde falls under the Living Lab Raversijde project launched by the departments of Maritime and Coastal Service (MDK) and Mobility and Public Works (MOW) from the Flemish government, in collaboration with Flanders Marine Institute (VLIZ) (Bellafkih (2021)). The main objective of the project is to investigate the effects of storm surges as a consequence of an increase of the frequency of extreme sea level events (Peelman (2022)).

Figure 7.1: Location of the Research Dike Raversijde. Scale 1:50000. Cartography from OpenStreetMap.

Then, the Research Dike Raversijde (RDR) is located at the beach of Raversijde, in the municipality of Ostend (see Figure 7.1). The dike is intentionally located in the backshore of the beach, before reaching the current dike, i.e., at a lower level so more overtopping events occur in order to ease the measuring campaigns of the project (see Figure 7.2).

The dike consists on a reinforced concrete structure of 19.5m x 16.5m with four different configurations. These configurations correspond to the four measurement sections according to the geometry once the crest freeboard is reached, which are denoted by a combination of a letter (A or B) and a number (1 or 2). This nomenclature means:

- A: Without promenade.

- B: With promenade.

- 1: Without storm wall.

- 2: With storm wall.

Figure 7.2: Image on site of the Research Dike Raversijde. Source: Dominique Jauquet from the Maritime and Coastal Service (MDK).

Moreover, two sections located at the edges, E1 and E2, are allocated but no measurements are taken and they are just intended for visual observations of oblique waves. The geometry of the dike and all these configurations as well as other elements are displayed in Figure 7.3.

The rest of the geometrical measurements are defined according to the average values of the Belgian dikes along the coast. The dike crest is 2.70 m high with respect to the dike toe and a 1:2 slope is chosen. The promenade of sections B1 and B2 is 6 m long and the height of the storm wall in sections A2 and B2 is 0.5 m high (De Jaeger (2023)).

The main goal of the practical application is to redesign the dike according to the collected data from a storm of a return period between 40 and 45 years, which corresponds to Storm 6 from Peelman (2022) in order to limit the overtopping of the structure to 1 $l/s/m$, following Belgian standards (Suzuki et al. (2016)). The source of this value is also mentioned by Suzuki et al. (2020) as follows: "the Flemish government conducts Safety Assessment every 6 years and executes countermeasures where they are necessary. An average overtopping discharge q of 1 $l/s/m$ at the safety line during the occurrence of superstorms (i.e.1000-year storm) is the present criteria in the Safety Assessment to assess the coastal safety level in Belgium".
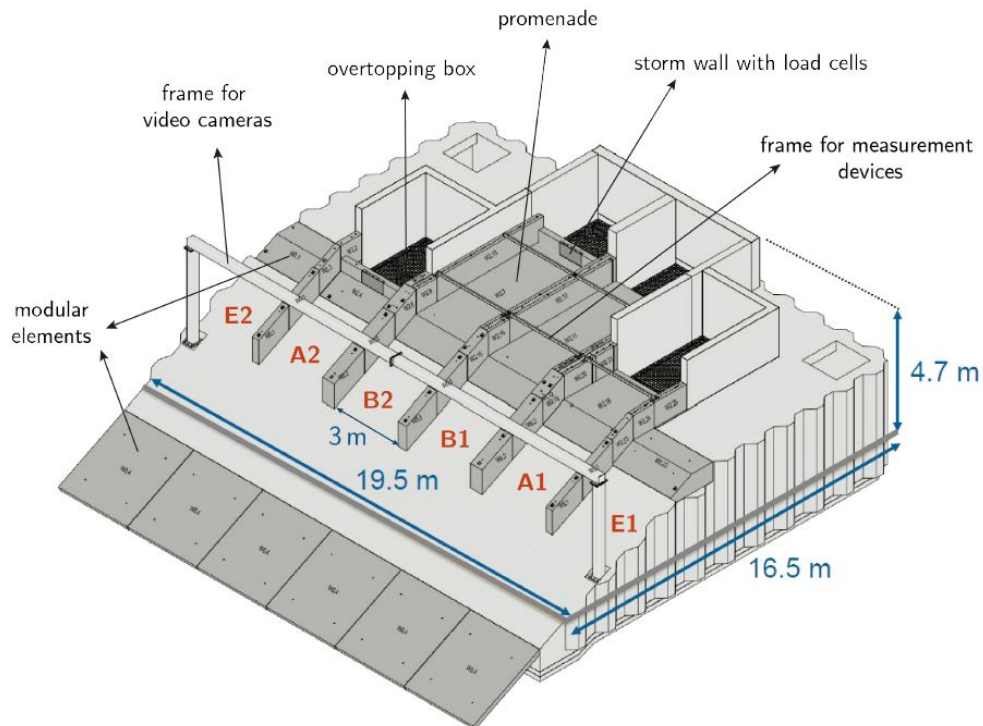
Figure 7.3: Sketch of the geometry of the RDR with the different measurement sections. Source: De Jaeger (2023).

Furthermore, this storm was measured on 31st January of 2022, with a duration of 38 hours and 5 hours of measurement. The collected wave data corresponds to the wave buoy of Raversijde 1, located just in front of the RDR and between it and the sand bank called Stroombank, located just directly in front of the RDR (see Figure 7.4). According to this buoy, a spectral significant wave height $H_{m0} = 3.41$ m is defined, as well as a tide of 5.60 m TAW (Peelman (2022)).

Then, the overtopped water is collected in four overtopping boxes (see Figure 7.3) which are equipped with a V-weir tank at a height of 10 cm from the bottom of the box to measure the overtopping volume. For sections A1 and A2, the useful volume of the individual tanks is 13.43 m^3, while for sections B1 and B2 it is 12.95 m^3 (De Jaeger (2023)). The basement volume is approximately 215 m^3. According to the mentioned Storm 6 from Peelman (2022), the overtopping tank was fulfilled before the storm peak.
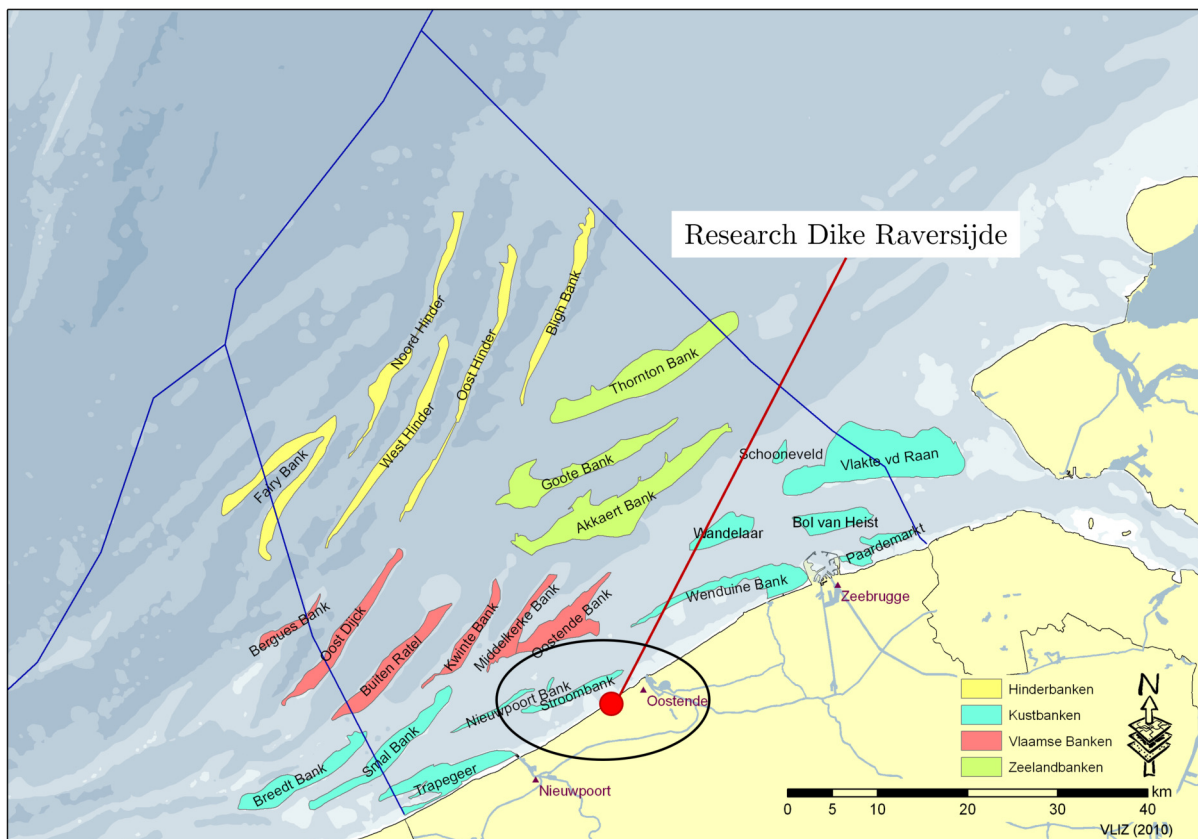
Figure 7.4: Location of Stroombank in relation to the Research Dike Raversijde. Adapted from Flanders Marine Institute (VLIZ).

7.1   Specific objectives

To proceed with the practical application of this thesis, several specific objectives need to be defined to establish a clear workflow and achieve expected results for the overtopping estimation of the Research Dike Raversijde for the defined storm parameters. Once the objectives have been established, the redesign proposal can be selected. The specific objectives are as follows:

  i) To analyse and understand the parameters of the 1 in 50 yearly return period storm used for this project and to determine water level variations and wave conditions during this event.

 ii) To review the available formulae in literature related to the transformation of wave

parameters according to depth conditions.

iii) To derive and estimate theoretical overtopping volumes for each hour for the measured water level variations and wave conditions, following the overtopping analysis of this thesis. For that purpose, the equivalent non-dimensional freeboard from Pepi et al. (2022) is used.

iv) If possible, to estimate when a measurement at the RDR would no longer be possible due to the filling of the overtopping box for such an extreme event.

v) Finally, to make a proposal of the redesign of the dike in order to guarantee safety conditions according to Belgian overtopping standards (for section A1 of the RDR). For that purpose, detailed geometry plans and cost estimation will be provided.

7.2   Literature review

In order to apply the available overtopping formulae in literature, some considerations have to be done. Thus, most of the formulae are defined for wave conditions at the toe of the structure, meanwhile the capacity to obtain those parameters in the case of very shallow water conditions is limited (Lashley et al. (2021)). Moreover, the aforementioned Storm 6 from Peelman (2022) is defined using offshore wave parameters. Then, the state-of-art is focused in the literature that allows the transformation and application of these conditions.

First of all, the definition of shallow and very shallow foreshores must be defined to understand the conditions of the RDR. Then, the foreshore of a beach is the sloping area of the beach that is exposed during low tide and covered by water during high tide. The foreshore is important because it is the area where most of the physical processes that shape the beach occur, such as wave action, sediment transport, and erosion (Hughes and Masselink (2003)). Goda (2009) also defines this area as the section in front of the dike which can be up to a maximum slope of 1:10.

Although there is no clear criterion about this definition, Van Gent (1999) proposed a classification of the foreshore in four categories according to the ratio between the wave height in deepwater ($H_{m0,deep}$) and the water depth at the toe of the structure (h_t). Then:

- $H_{m0,deep}/h_t = 3$: Very shallow.
- $H_{m0,deep}/h_t = 1.5$: Shallow.

- $H_{m0,deep}/h_t = 0.75$: Intermediate.

- $H_{m0,deep}/h_t = 0.4$: Deepwater.

In shallow and very shallow conditions the waves break because of the depth, so the maximum wave height is limited and smaller than in offshore conditions (Altomare et al. (2016)). In that sense, rather than sea-swell waves (short, wind-generated waves), infragravity waves (long waves) can also occur in this area, for which the wave height grows due to shoaling and energy transfer from the sea-swell waves, having a bigger impact when they break on the dike (Gruwez (2021)).

Then, the available methods and formulae in literature to estimate the overtopping for shallow conditions can be divided in two branches: (i) those methods that aim to calculate q from parameters at the toe of the structures, for which a transformation process is required, as long as the known parameters are measured in offshore conditions. And (ii) those methods that aim to calculate q directly from deepwater input parameters.

i) **Input parameters at the toe of the structure.**

Van Gent (1999) carried out several small scale model tests on 1:100 and 1:250 foreshores with smooth structures of 1:4 and 1:2.5 slopes. It was noticed that due to the wave breaking condition, a significant change occurred to the spectral wave period ($T_{m-1,0}$) and the significant incident wave at the toe of the structure (H_{m0}), according to a huge increase of the breaker parameter ($\xi_{m-1,0}$). The formula proposed by Van Gent (1999) was implemented in EurOtop (2007), using two different expressions:

$$\frac{q}{\sqrt{gH_{m0}^3}} = 10^c \exp\left(-\frac{R_c}{H_{m0}\,\gamma_f\,\gamma_\beta\,(0.33 + 0.022\,\xi_{m-1,0})}\right) \tag{7.1}$$

$$\frac{q}{\sqrt{gH_{m0}^3}} = 0.21 \exp\left(-\frac{R_c}{H_{m0}\,\gamma_f\,\gamma_\beta\,(0.33 + 0.022\,\xi_{m-1,0})}\right) \tag{7.2}$$

Where:

- q is the average overtopping discharge per meter width of the structure [$m^3/s/m$].

- R_c is the crest freeboard [m].

- γ_f and γ_β are reduction coefficients for the slope roughness and the obliquity of the waves, respectively.

- c is a normally distributed parameter which can be defined as a mean value of -0.92 and a standard deviation ($0.21 \approx 10^{-0.92+\sigma}$), for a safer evaluation of q.

- $\xi_{m-1,0}$ is the breaker parameters, for which the aforementioned formulae are valid for $\xi_{m-1,0} \geq 7$, with $\xi_{m-1,0} = \dfrac{\tan\alpha}{\sqrt{2\pi H_{m0}/gT_{m-1,0}^2}}$.

For $\xi_{m-1,0} \leq 5$, a different formulation is recommended (see EurOtop (2007)). In the range of $5 < \xi_{m-1,0} < 7$ a linear interpolation is intended between both cases.

Then, Altomare et al. (2016) realised that Equations 7.1 and 7.2 showed a clear and dangerous overestimation of q with regard to the measured values. Thus, the concept of a new "equivalent slope" is introduced to define a new formulation to estimate the average overtopping discharge. This equivalent slope ($\tan\delta$) is the average slope in the zone between SWL$-1.5H_{m0}$ and SWL$+R_{u2\%}$ as follows in Equation 7.3, where L_{slope} represents the horizontal length between the latter two positions of the water level:

$$\tan\delta = \frac{(1.5H_{m0} + R_{u2\%})}{L_{slope}} = \frac{(1.5H_{m0} + R_{u2\%})}{(1.5H_{m0} - h_t)\cdot\cot(m) + (R_{u2\%} + h_t)\cdot\cot(\alpha)} \quad (7.3)$$

Where $\cot(m)$ is the foreshore slope, $\cot(\alpha)$ is the slope of the structure and $R_{u2\%}$ is defined in EurOtop (2007) as:

$$R_{u2\%} = \left(4.0 - \frac{1.5}{\sqrt{\xi_{m-1,0}}}\right)\gamma_b H_{m0} \quad (7.4)$$

So, the proposed formulae by Altomare et al. (2016) differ from equations 7.1 and 7.2 in the parameter c_new based on the "equivalent slope in shallow foreshore", which can be replaced following a more conservative approach by 0.32 ($0.32 \approx 10^{-0.791+\sigma}$), using the same approach than before:

$$\frac{q}{\sqrt{gH_{m0}^3}} = 10^{c\_new}\exp\left(-\frac{R_c}{H_{m0}\,\gamma_f\,\gamma_\beta(0.33 + 0.022\,\xi_{m-1,0})}\right) \quad (7.5)$$

$$\frac{q}{\sqrt{gH_{m0}^3}} = 0.32 \exp\left(-\frac{R_c}{H_{m0}\,\gamma_f\,\gamma_\beta\,(0.33 + 0.022\,\xi_{m-1,0})}\right) \tag{7.6}$$

Finally, EurOtop (2018), based on the previous work from Altomare et al. (2016), proposes a new formulation slightly modified from EurOtop (2007):

$$\frac{q}{\sqrt{gH_{m0}^3}} = 10^{-0.79} \exp\left(-\frac{R_c}{H_{m0}\,\gamma_f\,\gamma_\beta\,(0.33 + 0.022\,\xi_{m-1,0})}\right) \tag{7.7}$$

$$\frac{q}{\sqrt{gH_{m0}^3}} = 0.16 \exp\left(-\frac{R_c}{H_{m0}\,\gamma_f\,\gamma_\beta\,(0.33 + 0.022\,\xi_{m-1,0})}\right) \tag{7.8}$$

ii) **Input parameters as deep-water values.**

On the other hand, Goda et al. (1975) developed a set of design diagrams for smooth vertical structures based on the basic equation of wave overtopping from Goda (1970) and the effects of the infragravity waves. The main advantage is that no additional wave transformation model is required and the influence of the foreshore is considered through the relative water depth and slope (Lashley et al. (2021)). However, no empirical formula was defined and only the design diagrams were published, with the disadvantages that graphical methods may arouse. Hence, Takayama et al. (1982) proposed some semitheoretical formulae based on the design diagrams from Goda et al. (1975).

In that sense, Lashley et al. (2021) carried out a study to define empirical overtopping formulae for both vertical and sloping structures with very shallow foreshores, completely based on deep-water parameters. Then, based on Goda et al. (1975), q is a function of the relative water depth ($h_t/H_{m0-DEEP}$), the foreshore slope (m) and the deepwater wave steepness ($s_{om-1,0}$).

So, to accurately define the wave overtopping formulae based on deep-water wave characteristics, the effects of the shallow foreshore at the toe of the structure need to be well defined. As mentioned in Lashley et al. (2021), the influence of the foreshore only becomes significant when $h_t/H_{m0-DEEP} \leq 1$. Then, the significant wave height for those conditions can be obtained using the following expression:

$$\frac{H_{m0}}{H_{m0-DEEP}} = M \cdot \frac{h_t}{H_{m0-DEEP}} + C \tag{7.9}$$

Where:

$$M = 0.35 \cdot \frac{\tan(m)^{0.1}}{s_{om-1,0}^{0.2}} \tag{7.10}$$

and

$$C = 0.95 \cdot \tan(m)^{0.15} - 0.30 \tag{7.11}$$

For which $s_{om-1,0} = H_{m0,toe}/L_{m0}$; and where the wave length L_{m0} is defined as:

$$L_{m0} = \frac{g \cdot T_{m-1,0,toe}^2}{2\pi} \tag{7.12}$$

The average wave overtopping q, for the case of sloping structures, using deep-water parameters when $h_t/H_{m0-DEEP} \leq 1$ can be obtained following Equation 7.13:

$$\frac{q}{\sqrt{gH_{m0-DEEP}^3}} = d \cdot \exp\left(-e \cdot \frac{R_c}{H_{m0-DEEP}} + f \cdot \frac{h_t}{H_{m0-DEEP}}\right) \tag{7.13}$$

Which can be particularized according to $h_t/H_{m0-DEEP}$:

- For very shallow cases (*Regime* 1), with $0.5 \leq h_t/H_{m0-DEEP} \leq 1$:

$$d_1 = 1.90 \cdot s_{om-1,0}^{1.15} \tag{7.14}$$

$$e_1 = 7.40 \cdot \frac{s_{om-1,0}^{0.60}}{\tan(m)^{0.25} \cdot \tan(\alpha)^{0.60}} \tag{7.15}$$

$$f_1 = 0.70 \cdot \frac{\tan(m)^{0.80}}{s_{om-1,0}^{0.80}} \tag{7.16}$$

- For extremely shallow cases (*Regime* 2), with $h_t/H_{m0-DEEP} \leq 0.1$:

$$d_2 = 1.35 \cdot \tan(m)^{0.35} \cdot s_{om-1,0}^{0.85} \tag{7.17}$$

$$e_2 = 3.75 \cdot \frac{s_{om-1,0}^{0.70}}{\tan(m)^{0.70} \cdot \tan(\alpha)^{0.60}} \tag{7.18}$$

$$f_2 = 0.20 \cdot \frac{s_{om-1,0}^{0.35}}{\tan(m)^{1.30}} \tag{7.19}$$

σ [°]	c_1 [-]	c_2 [-]	c_3 [-]	c_4 [-]
0	6	4	1	1
25	6	6	0.25	0.75

Table 7.1: Calibration coefficients for long ($\sigma = 0°$) and short-crested ($\sigma = 25°$) waves defined by Hofland et al. (2017b).

- For regimes between two last cases (*Regime* 3) ($0.1 \leq h_t/H_{m0-DEEP} \leq 5$), an exponential interpolation is applied.

Finally, some transformations may be needed in order to use the aforementioned formulation, following the same reasoning. Then, Hofland et al. (2017b) proposed a method to obtain the spectral wave period at the toe of the dike ($T_{m-1,0,t}$), valid for mildly sloped foreshores:

$$\frac{T_{m-1,0,o}}{T_{m-1,0,t}} - 1 = c_1 \exp(-c_2 \tilde{h}) + c_3 \exp(-c_4 \tilde{h}) \qquad (7.20)$$

Where $T_{m-1,0,o}$ is the offshore spectral wave period; c_1, c_2, c_3 and c_4 are calibration coefficients (see Table 7.1); and $\tilde{h}$ is the relative water depth at the toe of the dike, which depends on a coefficient c with a value of 0.2 and the offshore significant wave height:

$$\tilde{h} = \frac{h_t}{H_{m0,o}} \left(\frac{\cot(m)}{100} \right)^c \qquad (7.21)$$

Then, Gruwez (2021) realised that the mildly slope criterion defined by

$$\cot(m) \cdot T_{m-1,0,o} \sqrt{\frac{g}{H_{m0,o}}} < 0.62 \qquad (7.22)$$

is not always fulfilled, according to the foreshore slope $\cot(m)$. Moreover, in order to extend the applicability of Equation 7.20, Gruwez (2021) also introduced a modification to coefficient c from Equation 7.21 according to the foreshore slope:

$$c = \begin{cases} -0.7, & \cot(m) < 100 \\ 0.2, & \cot(m) \geq 100 \end{cases} \qquad (7.23)$$
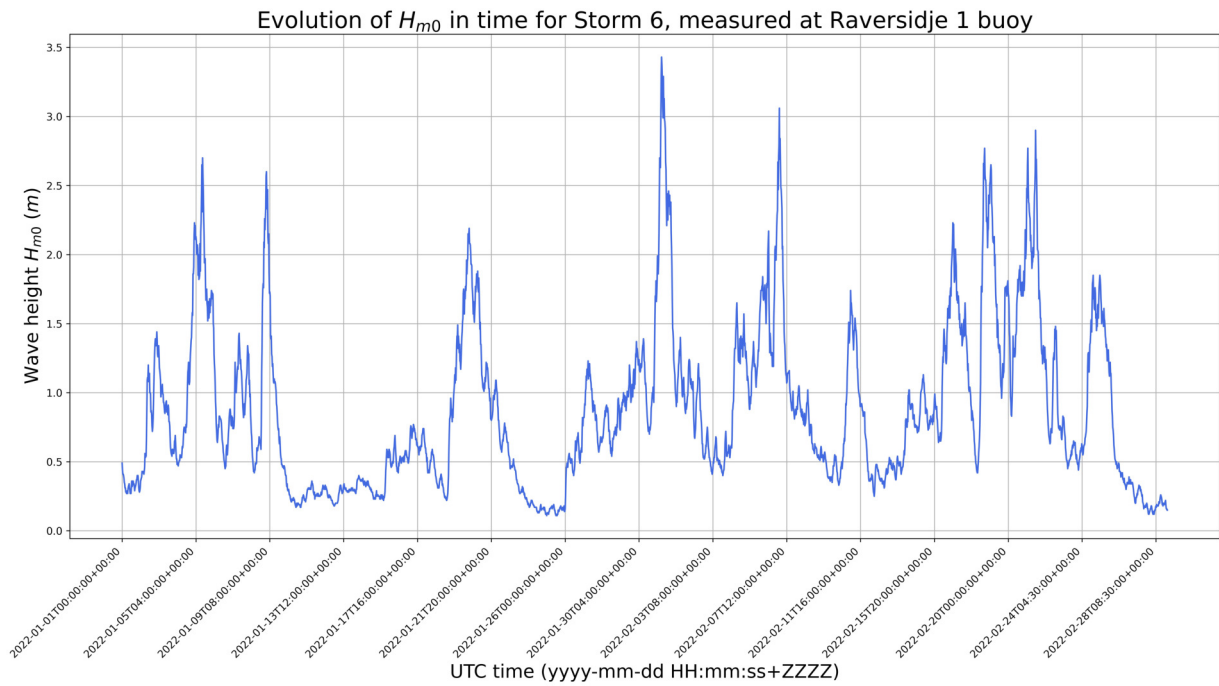
Figure 7.5: Evolution of H_{m0} in time for the whole measuring campaign of Storm 6, measured at Raversijde 1 buoy.

Hence:

$$\frac{T_{m-1,0,toe}}{T_{m-1,0,deep}} = \frac{h_t}{H_{m0,deep}} \left(\frac{\cot(m)}{100} \right)^c \tag{7.24}$$

7.3   Measured storm data

The provided dataset of parameters about Storm 6 (Peelman (2022)) is composed of four different variables. On the one hand, the values about tides (*cm* TAW) are measured in the Ostend harbour (51°14'03"N 2°55'36"E) with a time interval of 5 minutes from 01/01/2022 to 06/07/2022 (dd/mm/yyyy). On the other hand, the values of the wave height H_{m0} (*cm*), the average wave period T_m (*s*) and the high frequent wave direction (°) are measured by the Raversijde 1 waverider buoy (51°12'40"N 2°50'31"E) with measurements every 30 minutes, i.e., twice per hour. Evidently, these values are measured in offshore conditions. Finally, for consistency reasons, values will be converted to *m* in all cases. These parameters are represented in Figures 7.5, 7.6, 7.7 and 7.8.
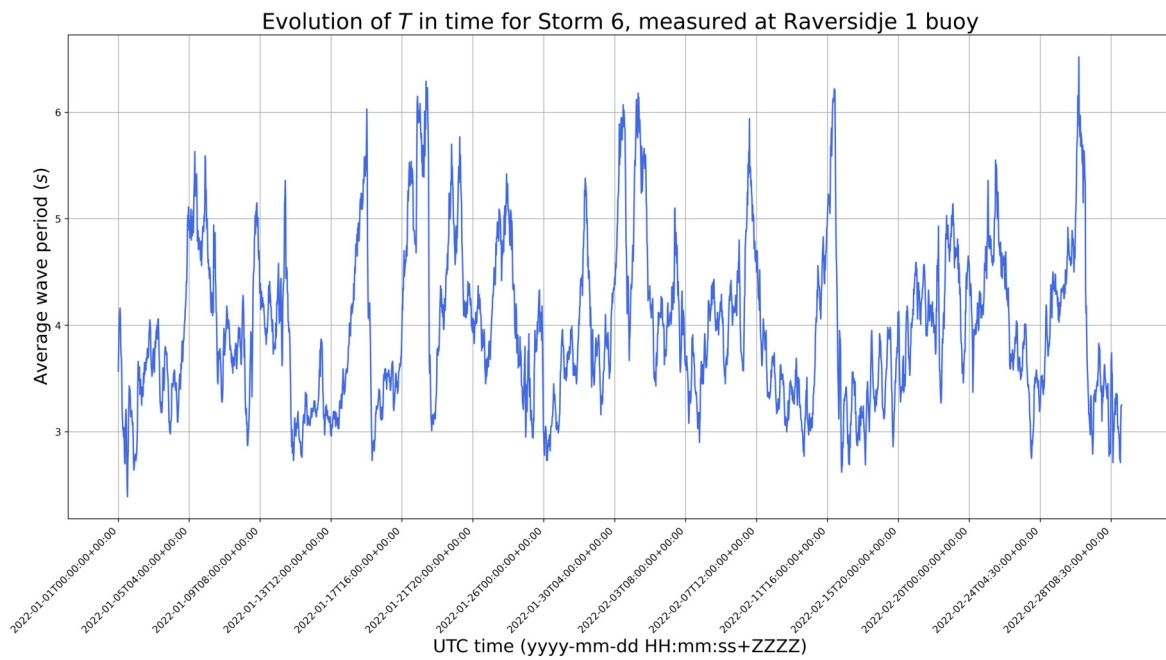
Figure 7.6: Evolution of the average wave period in time for the whole measuring campaign of Storm 6, measured at Raversijde 1 buoy.
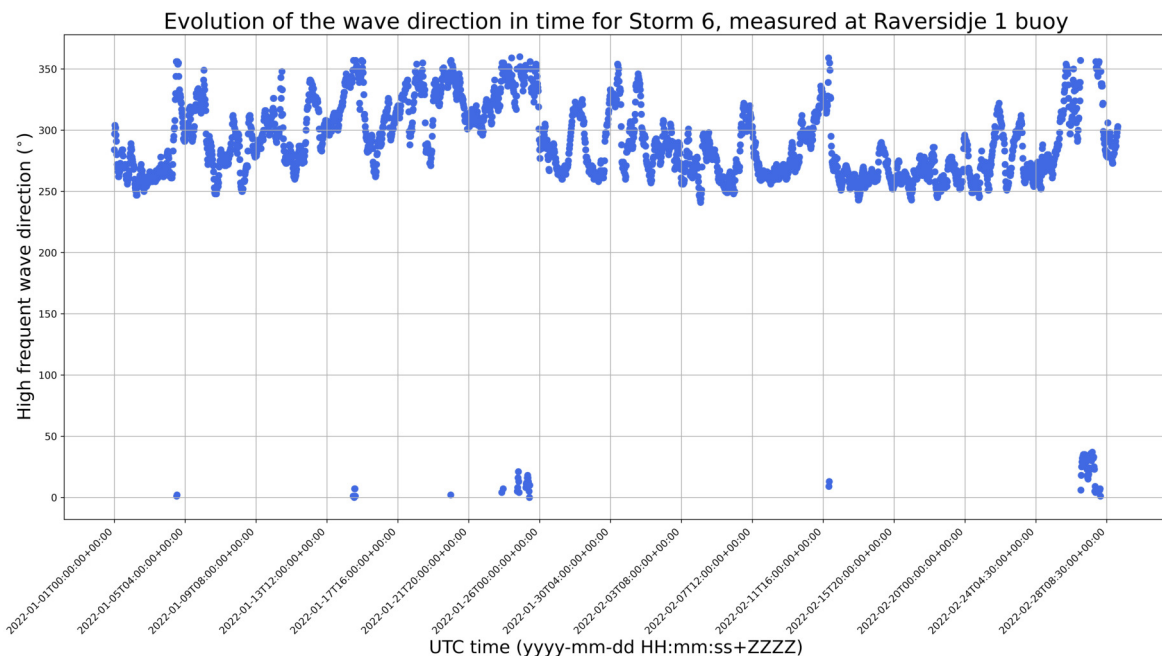
Figure 7.7: Evolution of the high frequent wave direction (°) in time for the whole measuring campaign of Storm 6, measured at Raversijde 1 buoy.
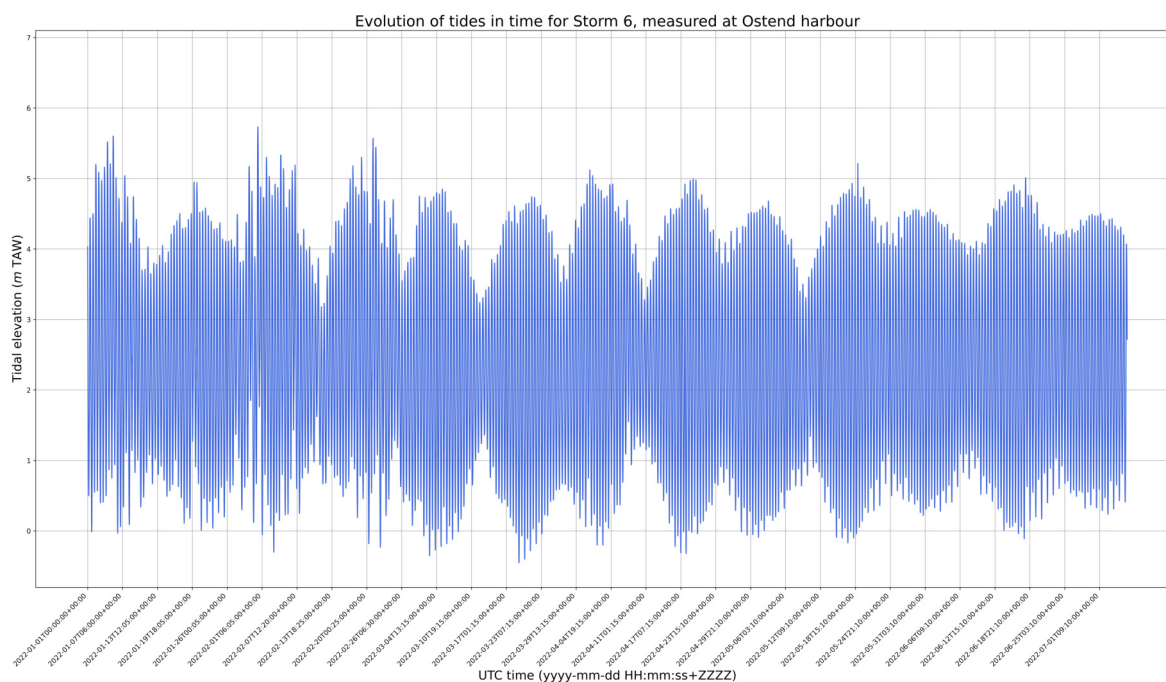
Figure 7.8: Evolution of tides in time for the whole measuring campaign of Storm 6, measured at Ostend harbour.

According to the dike characteristics aforementioned, the freeboard is 2.70 *m* high. However, due to the tides that occur along the coast, the crest freeboard varies over time, so following the measured values of the tide in *m* TAW, it is possible to calculate the variable crest freeboard in time. To obtain these values, it is also necessary to know the elevation in *m* TAW of the RDR. For that purpose, recent measurements carried out by the staff in charge of the RDR from the Flemish Government (Willems (2023)) suggest that the elevation of the dike is approximately 4 *m*, which means that the dike crest level is in the range of +6.68 to +6.70 *m* TAW. Nevertheless, this has to be considered also an approximation, as the beach profile is dynamic and changes constantly during the year.

However, as it was mentioned, the beginning of Storm 6 was identified on 31st January of 2022, with a duration of 38 hours, so Figures 7.11, 7.12, 7.13 and 7.14 represent these same parameters in the range from 31/01/2022 T00:00:00 until 02/02/2022 T00:00:00.

Finally, the adjusted plot from Figure 7.10 to the storm duration can be seen in Figure 7.15. With all these data, it is also possible to obtain the value of the water depth at the toe of the structure h_t. It is clear that, because of the location of the dike in the beach
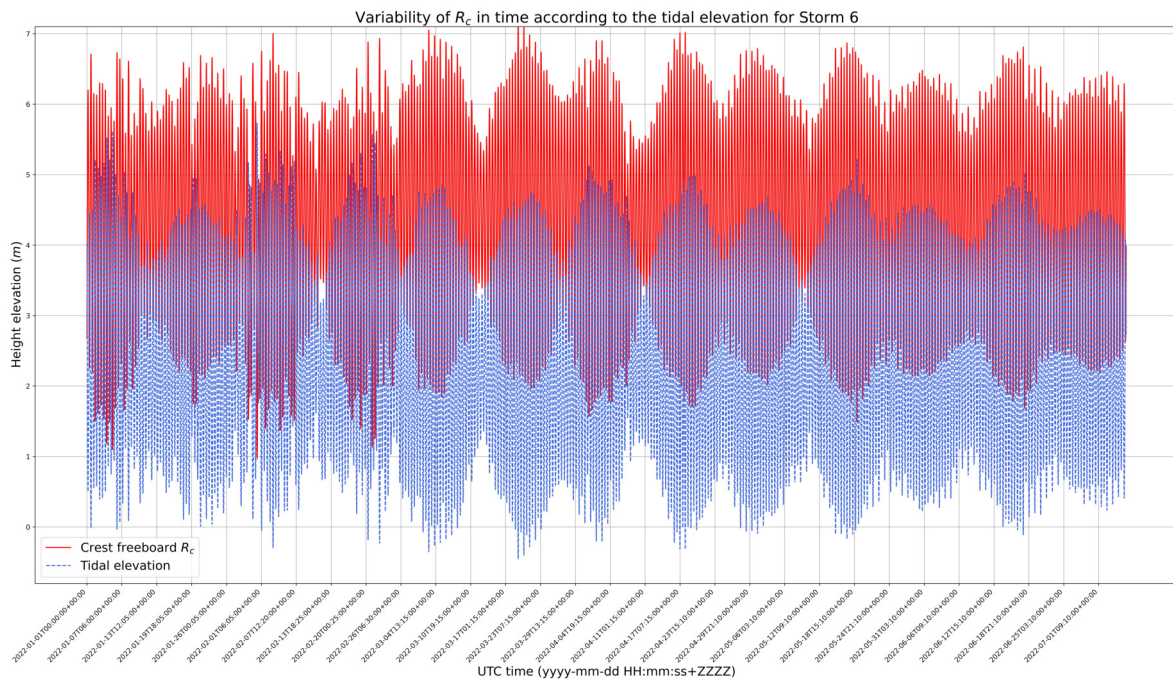
Figure 7.9: Variability of R_c in time with regard to the tidal elevation for the whole measuring campaign of Storm 6.
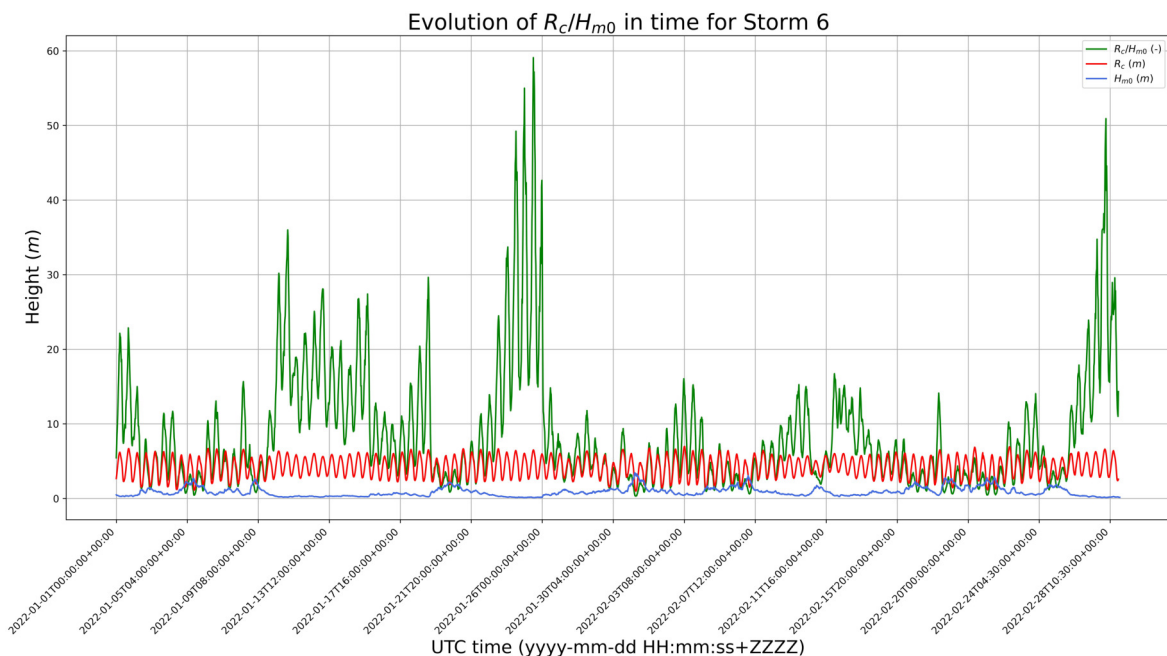
Figure 7.10: Evolution of R_c/H_{m0} in time, in comparison with R_c and H_{m0} for the whole measuring campaign of Storm 6.

Evolution of H_{m0} between 31/01/2022 and 02/02/2022 for Storm 6, measured at Raversidje 1 buoy
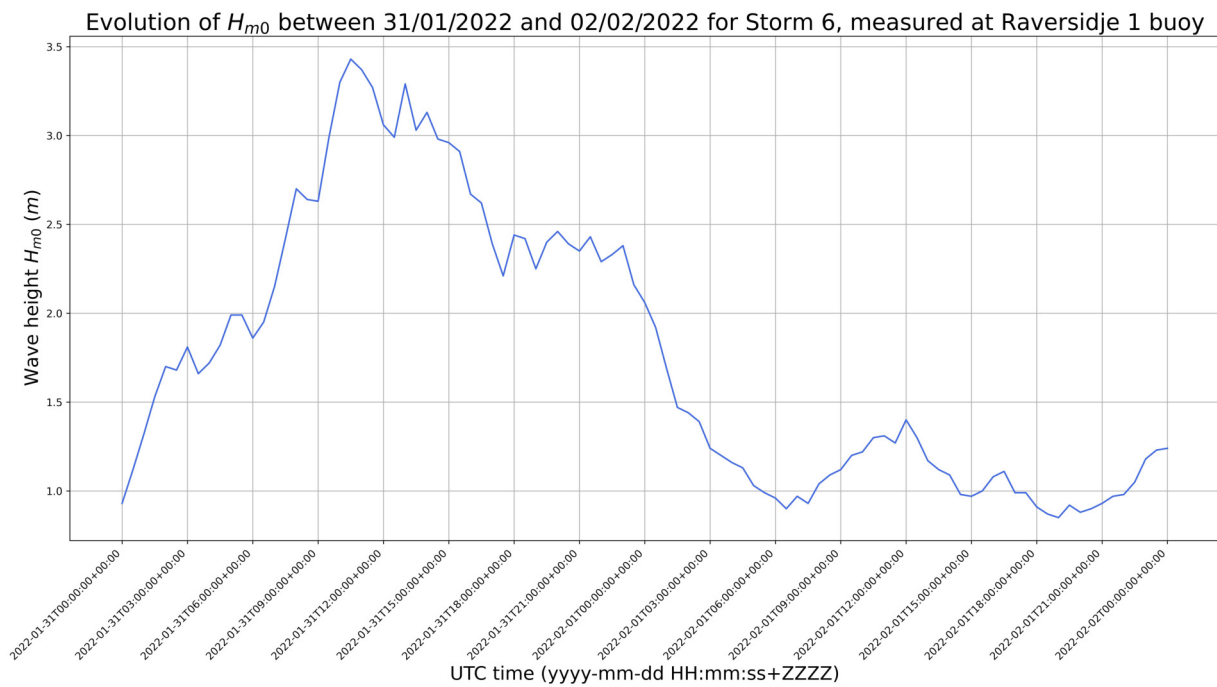
Figure 7.11: Evolution of H_{m0} between 31/01/2022 and 02/02/2022 for Storm 6.

Evolution of T between 31/01/2022 and 02/02/2022 for Storm 6, measured at Raversidje 1 buoy
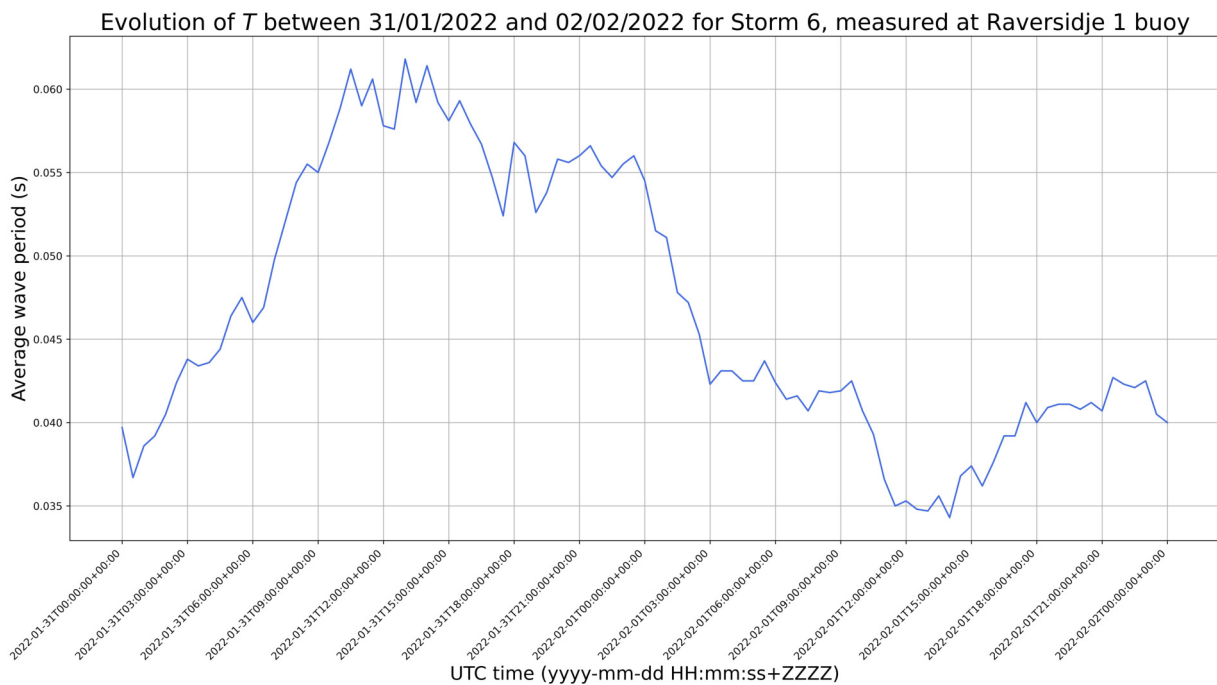
Figure 7.12: Evolution of the average wave period between 31/01/2022 and 02/02/2022 for Storm 6.

Evolution of the wave direction between 31/01/2022 and 02/02/2022 for Storm 6, measured at Raversidje 1 buoy
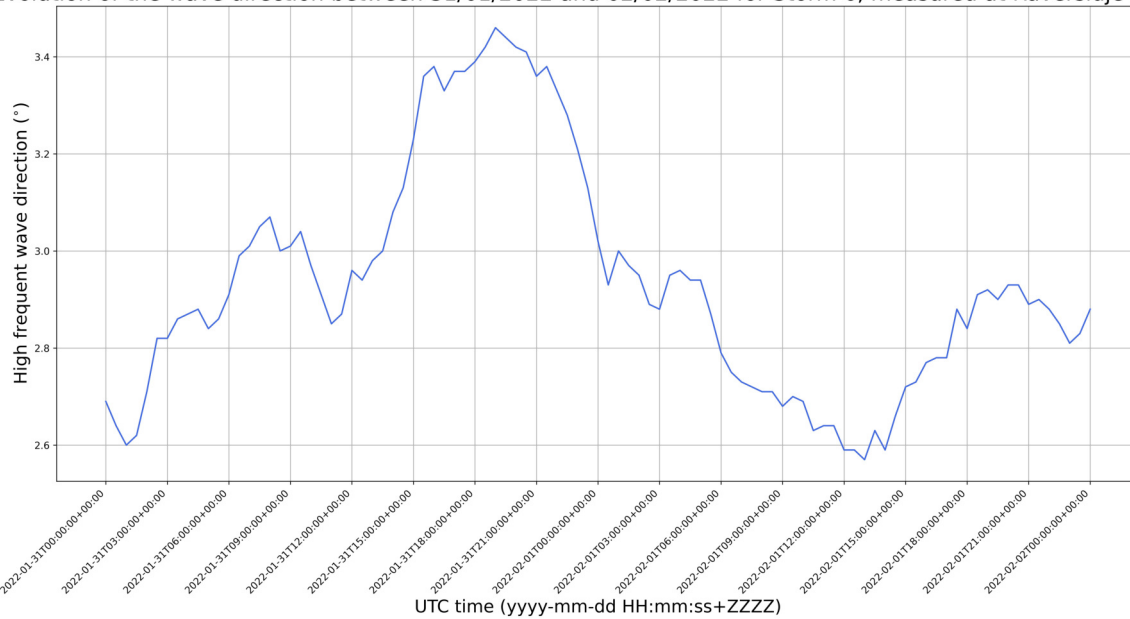
Figure 7.13: Evolution of the high frequent wave direction (°) between 31/01/2022 and 02/02/2022 for Storm 6.

Variability of R_c between 31/01/2022 and 02/02/2022 according to the tidal elevation for Storm 6
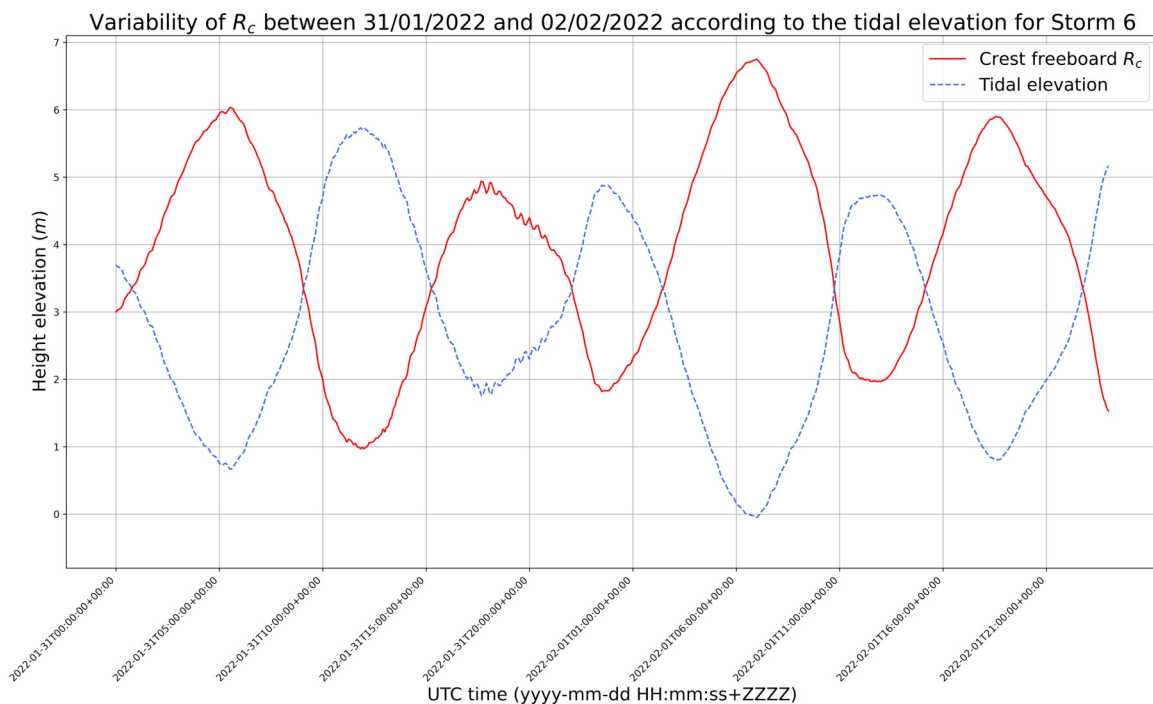
Figure 7.14: Variability of R_c between 31/01/2022 and 02/02/2022 with regard to the tidal elevation for Storm 6.
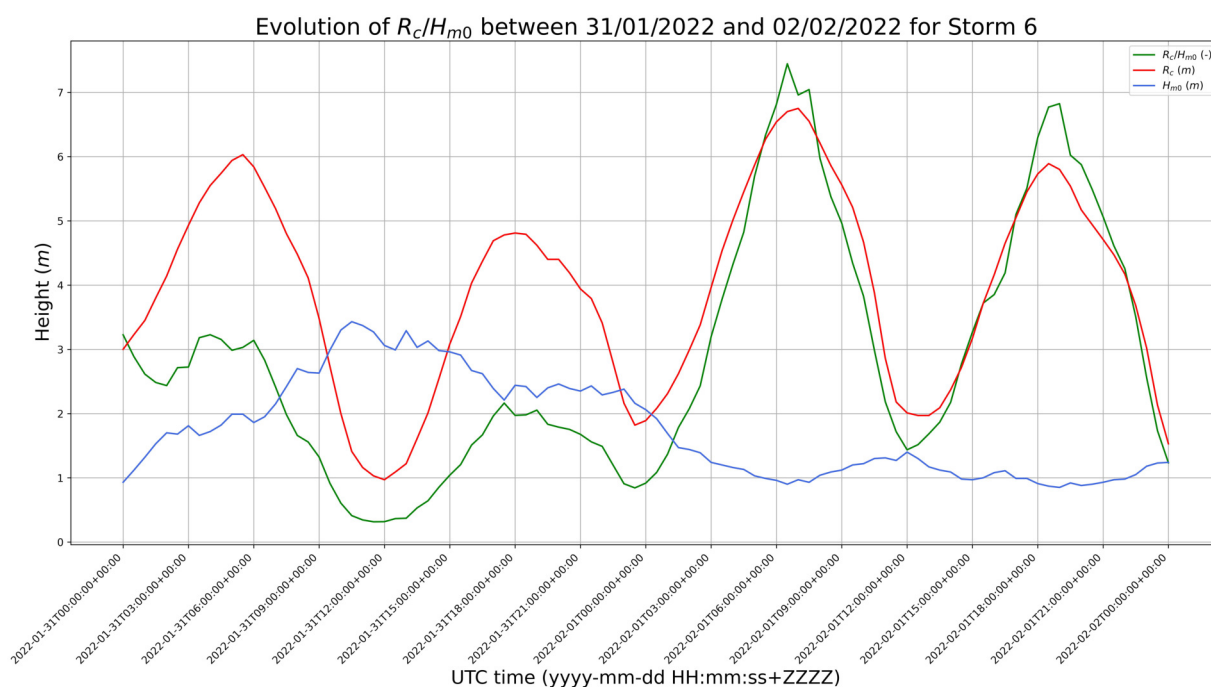
Figure 7.15: Evolution of R_c/H_{m0} between 31/01/2022 and 02/02/2022, in comparison with R_c and H_{m0} for Storm 6.

face and the tidal effects, this value will be 0 in several cases. This leads to the calculation of the ratio between $H_{m0-DEEP}/h_t$ to classify the foreshore in which a value of $h_t = 0$ means an infinite ratio, i.e., "superficial foreshore". Then, for the 90% of the measured values, the dike is in shallow, very shallow or superficial conditions. Although some values below $H_{m0-DEEP}/h_t = 1.5$ are measured (Van Gent (1999)), mainly because of tidal effects, the structure is defined to be like this to apply the aforementioned formulae.

7.4 Overtopping analysis and re-fitting of the Research Dike Raversijde

Once the data have been defined, it is now possible to apply the overtopping formulation given by Lashley et al. (2021) for the specific case of sloping structures (see Equation 7.13). Thus, is it first necessary to obtain parameters d, e and f (equations 7.14 to 7.19), which depend on the steepness value of $s_{om-1,0}$, as well as on the foreshore and the structure slopes.

Hence, according to Peelman (2022), the Stroombank slope m is approximately defined by $\tan(m) = 1.7/250$, however recent researches define the foreshore slope for a value of $\tan(m) = 1/50$, which is the one that is applied in this study. To calculate $s_{om-1,0}$, it is previously needed to apply Equation 7.24 from Gruwez (2021), for which the value of c that depends on the slope of the foreshore $\cot(m)$ is greater than 100, so a value of $c = -0.7$ is adopted. Moreover, the slope of the structure, as mentioned at the beginning of Section 7, is a 1:2 slope. Then, Equation 7.9 can be solved for $H_{m0,toe}$ and with this, the relative wave overtopping discharge from Equation 7.13.

At this point of the analysis, a problem is noticed when applying the formulation with a value of $h_t = 0$. This responses to the fact that the formulae given by Lashley et al. (2021) are intended for shallow foreshores but not superficial conditions in which there is no water at the toe of the structure. For that reason, Lashley et al. (2021) defines 3 regimes according to the ratio of $h_t/H_{m0-DEEP}$. However, only values of q are obtained for *Regime* 1, as for the cases for *Regime* 2 correspond with the values of $h_t = 0$.

For that reason, only the formulation for *Regime* 1 is considered, also because to the fact that the maximum value of Q corresponds to a $h_t/H_{m0-DEEP}$ ratio of 0.7, i.e., *Regime* 1. Moreover, it is quiet clear that if there is no water at the toe of the dike ($h_t = 0$), there will not be any overtopping. With this, Figure 7.16 is given as the representation of the overtopping of the storm. Figure 7.16(b) also shows the limiting capacity of the overtopping tank of Section A1, so it can be observed the moment in which it is fulfilled.

If a stepways approach is considered to determine easily the overtopping steps and their values, the results can be seen in Figure 7.17.

According to these plots, only the data between the start of the storm and the time in which the first overtopping event occurs (2022-01-31 T15:00:00) are relevant, as in Figure 7.18.

These values of the relative overtopping discharge seem to be reasonable for the position in the foreshore where the dike is located. Thus, the limit of $1 \; l/s/m$ is clearly exceeded. Before, redesigning the freeboard of the structure, it is necessary to analyse this issue and compare the results with the equivalent non-dimensional freeboard (Pepi et al. (2022)).

The idea is to compare the estimation of Q provided directly from the data given in Figure 7.18 with that same estimation obtained using the equivalent non-dimensional freeboard (Pepi et al. (2022)) from Equation 6.4. At this point, different comparisons
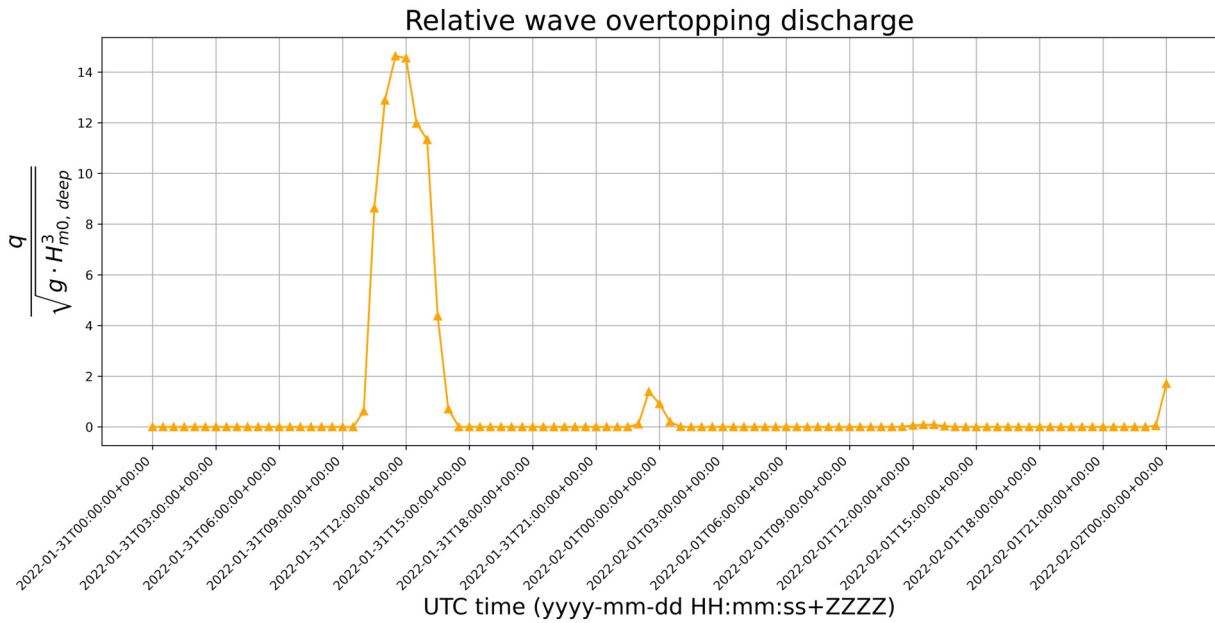
(a) Relative wave overtopping discharge during the storm
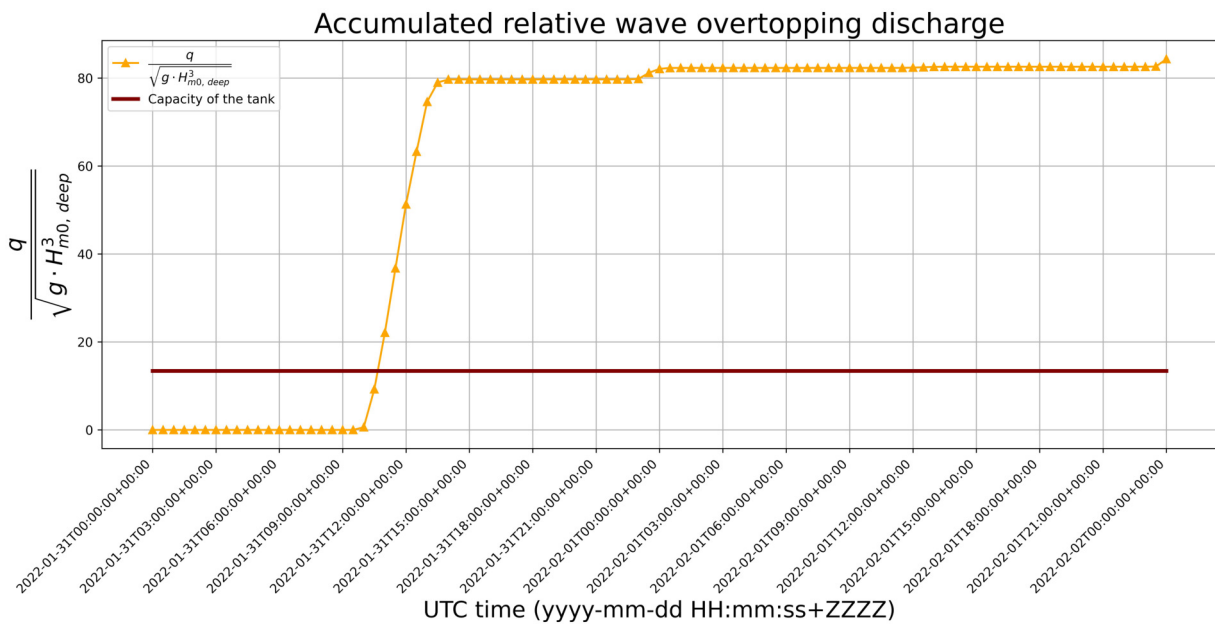
(b) Accumulated relative wave overtopping discharge during the storm

Figure 7.16: Discrete and accumulated relative wave overtopping discharge during the storm.

can be considered regarding the method to obtain the wave overtopping discharge, so the validity for each case needs to be checked. Moreover, this value of Q can be as well
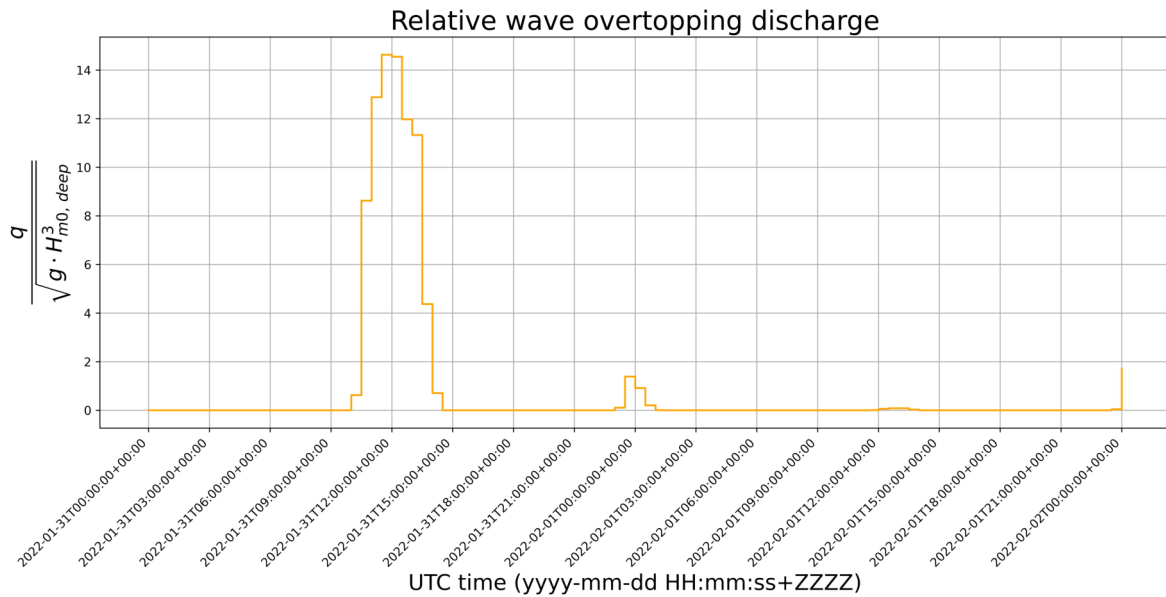
Figure 7.17: Stepways for the wave overtopping discharge during the storm.

defined for each time step by 30 minutes, or as a constant value considering a certain value of the significant wave height. Further considerations will be taken. Hence:

i) Using the formula from Lashley et al. (2021).

Although it may seems appropriate to continue with the same approach, the equivalent non dimensional freeboard $(R_c/H_{m0})_{eq}$ (see Equation 6.4) is defined for the wave height at the toe of the structure, while the overtopping formula by Lashley et al. (2021) is intended for deep parameters. However, despite it is not conceptually correct, an equivalent non-dimensional freeboard can be defined using the values of $H_{m0,deep}$. As it can be seen in Figure 7.19, this consideration is not appropriate for the formulation and it will not be considered.

ii) Using the general formula from EurOtop (2018).

The general formula to calculate the wave overtopping discharge given in EurOtop (2018) (see Equation 3.5) is the one used by Pepi et al. (2022) to define the equivalent non-dimensional freeboard, so a special interest is taken for consistency reasons. First, as previously mentioned, Q can be defined for each time step or as a constant value. Secondly, the formulation takes into account several influence factors, although the only one that may differ from 1 is γ_β, which is influenced by the obliquity of the incident waves (see Figure 7.20).
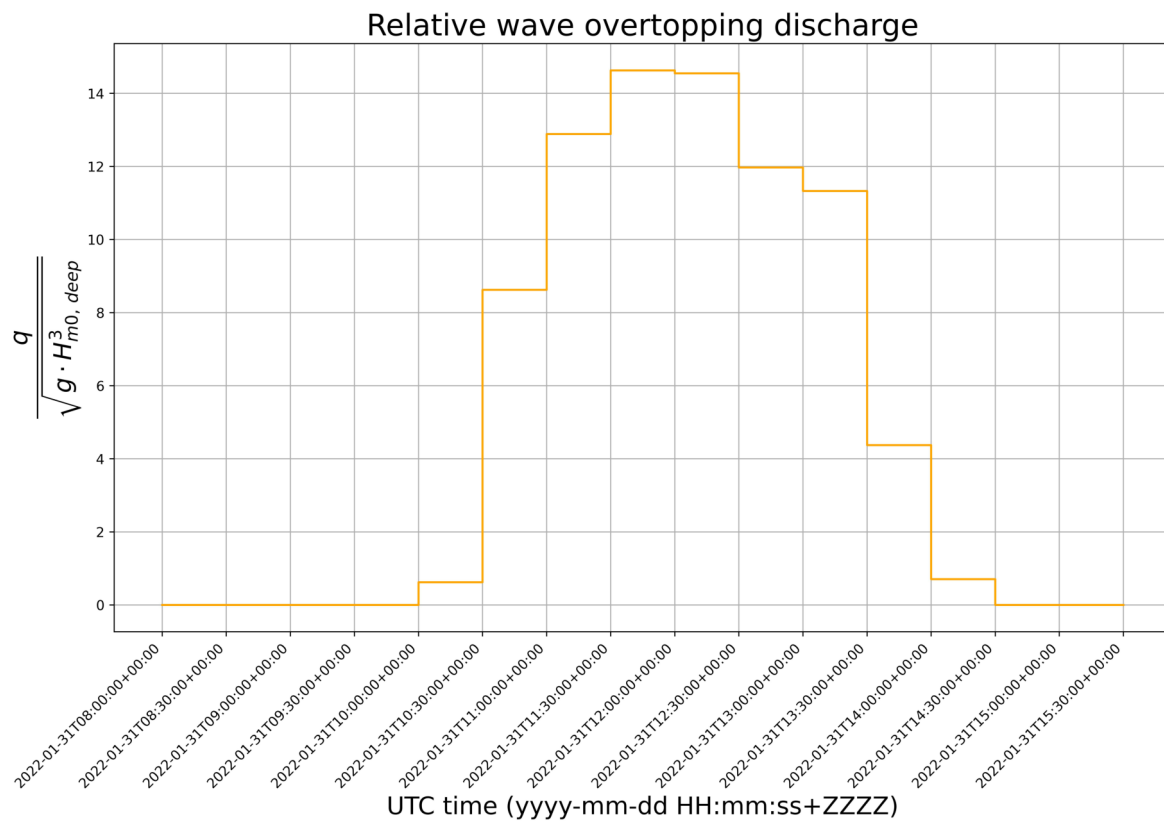
Figure 7.18: Stepways for the wave overtopping discharge during the storm, during the first storm surge cycle.

In that sense, the step by step calculation is followed for both cases considering the influence of the direction of the waves or not, as it can be seen in Figure 7.19. This plot also displays the calculation for a certain value of H_{m0}, so a horizontal line for the value of Q is presented. The cases for the maximum value of the significant wave height ($H_{m0,MAX}$), the average value ($H_{m0,avg}$) and the value of the upper third of the waves ($H_{m0,1/3}$) are considered. Then, it can be observed that the results every 30 minutes are slightly underestimated.

iii) Using the particularization of the formula for shallow and very shallow foreshores from EurOtop (2018).

This approach considers Equation 7.8 to determine the wave overtopping discharge. In this case, a much more noticeable underestimation is observed in Figure 7.19, where only the step by step plot is displayed for this case.
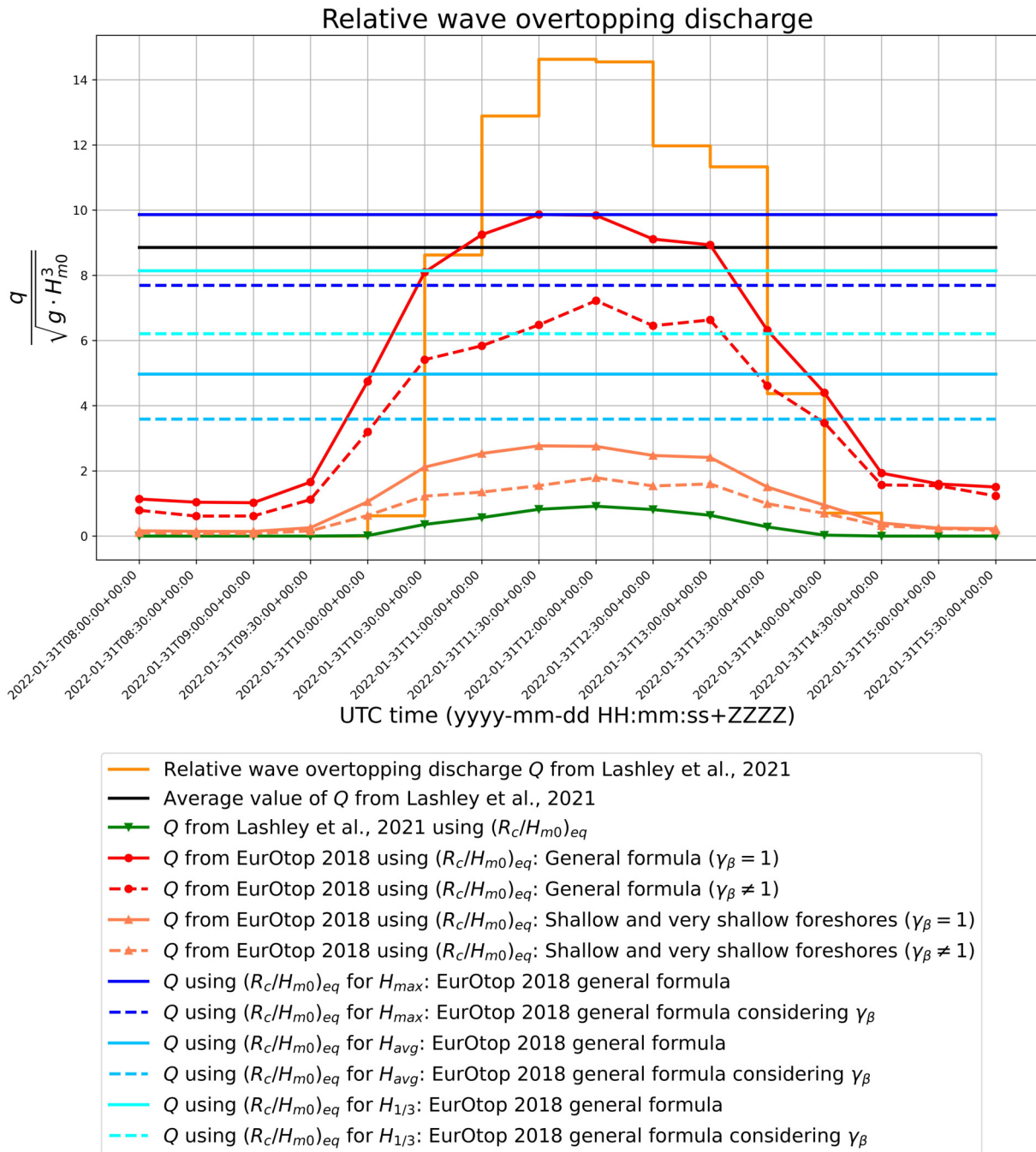
Figure 7.19: Comparison between the estimation of the average overtopping discharge from the data analysis and different cases using the equivalent non-dimensional freeboard.
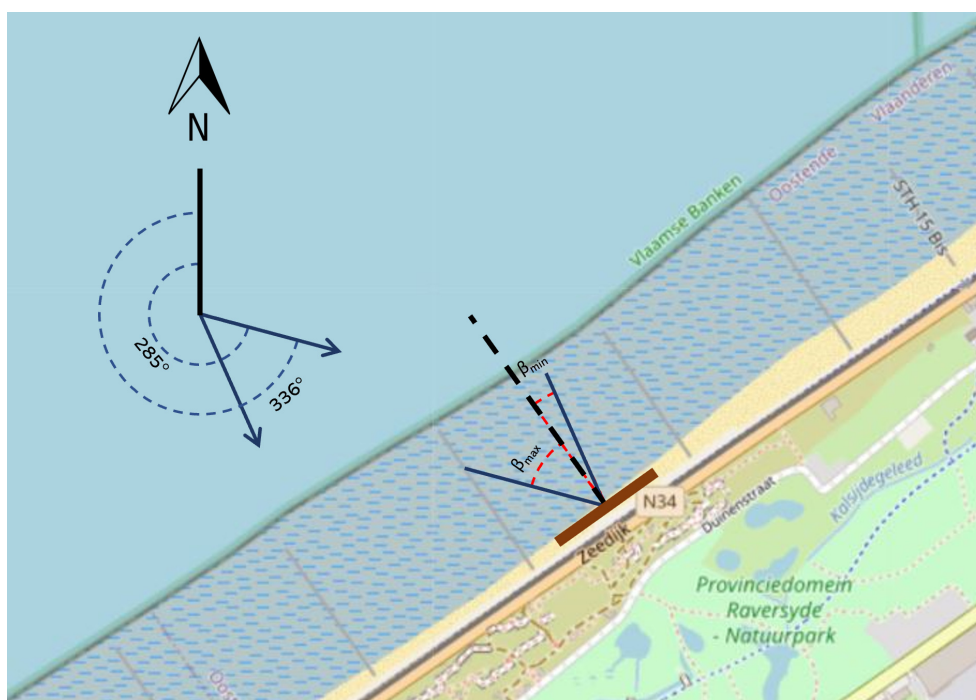
Figure 7.20: Variation of the incident angle of the waves for the measured Storm 6. The range of angles is between 285° and 336°. The position and size of the RDR is indicative.

Furthermore, Figure 7.19 also shows the average value of Q (black line) given by the overtopping analysis derived from Lashley et al. (2021) (Figure 7.18). In that sense, considering the general formulation of the overtopping discharge with the equivalent non-dimensional freeboard, which is precisely the one used by Pepi et al. (2022) to define $(R_c/H_{m0})_{eq}$, and applying it for the whole time interval as a constant value, these horizontal lines can be compared with the aforementioned average value of Q derived from Lashley et al. (2021). It can be clearly observed that the prediction between the results that consider $H_{m0,MAX}$ and $H_{m0,1/3}$ are the most accurate ones. For this statement, these values do not consider the obliquity of the waves, so all are defined as perpendicular as this is the most unfavourable case of all possible combinations. Moreover, if a sensitivity analysis regarding the slope of the foreshore and the elevation of the structure is carried out, it can be observed that the value of Q using this method for $H_{m0,1/3}$ is the most accurate one with regard to the average value of Q from the input parameters. Figure 7.21 shows the chosen method clearer than Figure 7.19.

For that reason, the redesign process of the dike will be carried out using this formulation (Equation 3.5) in combination with the equivalent non-dimensional freeboard
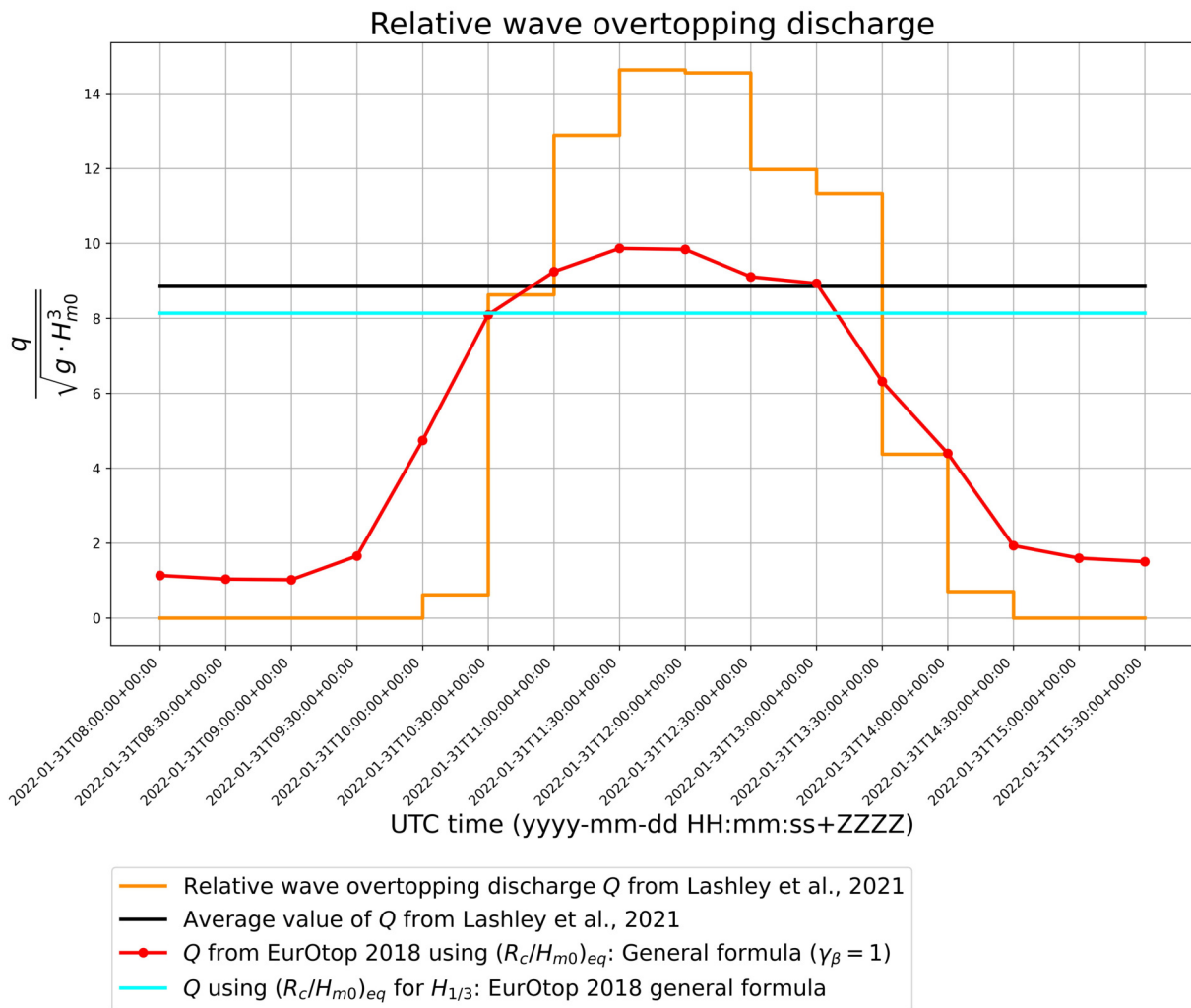
Figure 7.21: Detailed comparison between the estimation of the average overtopping discharge from the data analysis and the cases using the equivalent non-dimensional free-board which are defined as valid for the practical application.

to precisely calculate the freeboard of the structure to guarantee safety conditions for this storm ($q = 0.001 \ m^3/s/m$) (Suzuki et al. (2016)).

However, several remarks have to be said about it, as this is just a possible approach that can be followed for the redesign. The idea of this comparative analysis is to choose critically the best method. Then, the considered cases would be:

i) The redesign is carried out using the general average overtopping formula from EurOtop (2018) with the equivalent non-dimensional freeboard for $H_{m0,1/3}$. This

is the aforementioned method. In addition, it can be carried out for (1) the whole storm duration (see Figure 7.17), or (2) the duration of the considered storm surge cycle as in Figure 7.19. Using the first approach means a huge underestimation of the overtopped water, as in most of the time steps the overtopping is null. For that reason, the second approach is the one that needs to be considered for this case.

ii) The redesign is carried out considering a value of $Q = 14.6$ as this is the maximum possible value, which means the most conservative approach. However, this method is not possible to apply using the equivalent non-dimensional freeboard because it would require to apply deepwater parameters to this variable, which has been already defined as not valid. Notwithstanding, it is actually possible to solve the formula from Lashley et al. (2021) for the freeboard, but this is not the purpose of this study and falls out of its scope.

With this, the first approach with the general formula of Q from EurOtop (2018) using $(R_c/H_{m0})_{eq}$ for $H_{m0,1/3}$ and considering only the interval of time of the first storm surge cycle, so a more conservative approach is obtained despite it is not the most conservative one, is defined for the redesign. If an even more conservative approach is desired, the same formulation could be applied for $H_{m0,MAX}$ rather than for $H_{m0,1/3}$, although it is hereby decided to use it for $H_{m0,1/3}$ as it is the most optimal way considering the 1 in 50 yearly return period storm and because of economical reasons in terms of material cost.

Then, as H_{m0} is defined as $H_{m0,1/3}$, Equation 7.25 can be solved for $(R_c/H_{m0})_{eq}$:

$$Q = \frac{q}{\sqrt{g \cdot H_{m0,1/3}^3}} = 0.09 \exp\left[-1.5\left(\frac{R_c}{H_{m0}}\right)_{eq}^{1.3}\right] \tag{7.25}$$

Once the equivalent non-dimensional freeboard is obtained $[(R_c/H_{m0})_{eq} = 2.92752367]$, which depends as well on the defined value of H_{m0} and on the main variable which is the freeboard, Equation 7.26 can be solved for the value of $R_{c,peak}$. This freeboard is defined for the peak of the storm, i.e., the minimum freeboard. In other words, it represents the most unfavourable situation for this specific storm to limit the overtopping. Then, the obtained value for $R_{c,peak}$ is the one that needs to be fulfilled at any time to guarantee these conditions and the one that needs to be included in the redesign.

$$(R_c/H_{m0})_{eq} = 2.92752367 = \frac{R_{c,peak}}{H_{m0,1/3}} + exp\left(-1.14\frac{R_{c,peak}}{dh}\right)^{0.55} \tag{7.26}$$

Thus, solving the equation a value of 3.50009854 is obtained, that for practical and safety reasons means $R_{c,peak,new} = 3.6\ m$. To reach this freeboard two methods could be followed:

- To build the dike closer to the backshore of the beach so the elevation of the structure contributes to reach this distance from the bottom. Evidently, this idea is discarded due to its construction cost and because the main objective of this application is to modify the current geometry of the dike.

- To increase the freeboard until a value of $R_{c,peak,new} = 3.6\ m$ is reached. For that consideration, it means taking into account the current situation for this storm, previous to the redesign, in which the value of $R_{c,peak}$ is equal to $0.97\ m$, when the maximum water depth at the toe of the structure is encountered at the peak of the storm, so the new R_c^+ that needs to be added in the new design has to be equal to: $R_c^+ = 3.6 - 0.97 = 2.63\ m$. Once again, for practical and safety reasons, $R_c^+ = 2.7\ m$ (see Figure 7.22).
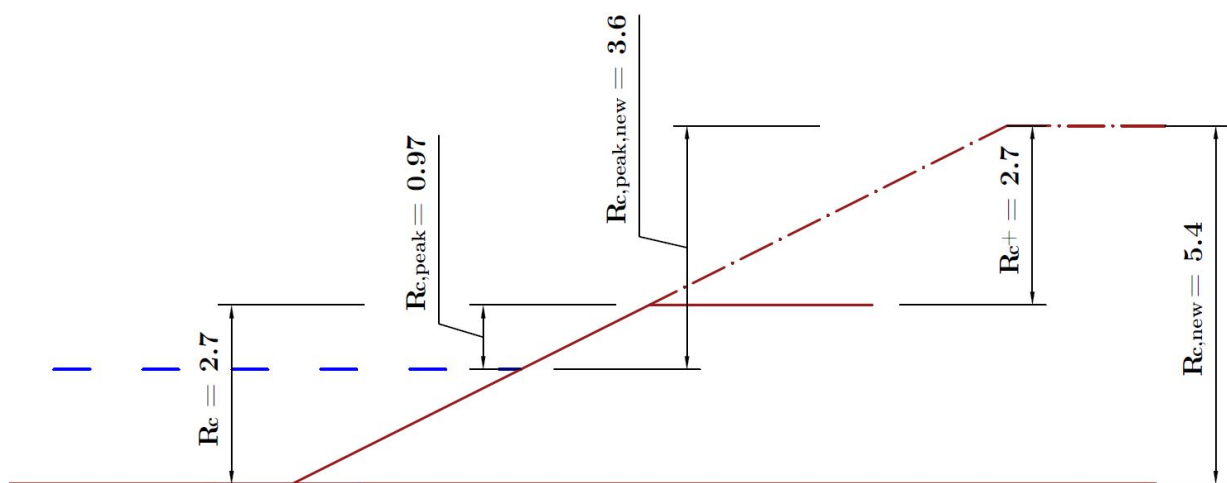
Figure 7.22: Conceptual sketch with dimensions according to the redesign of the crest freeboard.

To conclude this reasoning, the crest freeboard of the RDR, which is originally defined in $2.7\ m$, will be increased to a value of $5.4\ m$ in the final design to guarantee a maximum overtopping discharge of $1\ l/s/m$ for a storm of, approximately, 50 years of return period.

For the final section to be built, as no promenade is considered at the top of the freeboard, only a surface with 2.5 m length is designed before the overtopping tank, with a slope of 1:100, as in the previous situation for section A1. The plans regarding this section can be found in Annex 1 at the end of the document, where Plan 1 refers to the current geometry of the dike and Plan 2 shows the redesign in detail of the new crest freeboard calculated here.

7.4.1   Cost estimation

The cost estimation of the works to build the new freeboard of the dike is based on a vast amount of similar projects in literature. For this case, prices are given by the Price Generator software provided by CYPE. These prices are based on several catalogues in the market and reviewed constantly by independent organisms, so no price update based on CPI in considered again. However, as mentioned by the authors of the database, these prices are just a reference of the market but it accomplishes the objective of this section in which an estimation is sought.

The required volume of concrete (m^3/m) and the surface of the framework are directly measured from Plan 2 (see Annex 1) as a solid volume, however a more optimized hollow structure may be designed using a structural analysis software. The rest of the items are approximated according to the possible construction methodology and similar projects. The estimation is divided into four different chapters: Health and Safety, Freeboard construction, Waste managements, and Complementary operations; which are displayed in Tables 7.2, 7.3, 7.4, and 7.5, respectively.

Hence, the total estimated cost based on this is the sum of each chapter and per lineal meter of structure:

  i) Safety and Health: . . . . 96.29 €

 ii) Freeboard construction: . . . . 2325,73 €

iii) Waste management: . . . . 115.47 €

iv) Complementary operations: . . . . 573.79 €

Finally, the redesign project of the crest freeboard will have an approximate cost of 3111.28 €, depending on the length of the dike. If the whole length of the RDR of 19.5 m

(including not only Section A1) is considered, the cost of the required mass concrete for a solid section, although a hollow section might be studied in a structural analysis, will rise to 32638.13 € and the total cost of the works would be 34075.66 €.

1. Safety and Health							
Category	Units	Description	Performance	Unitary Price (€)	Price (€)	Quantity (units)	Cost (€)
1.01. Beaconing							
	Unit	**Reflective beacon**					
		Materials					
	Unit	Reflective beacon 20x100 cm	0.100	48.69	4.87		
		Labour					
	h	S&H labourer	0.110	20.10	2.21		
	%	*Direct costs*	2.000	7.08	0.14		
					7.22	4	28.88
	Unit	**Moveable metal fence**					
		Materials					
	Unit	Fence 3.5x2m	0.060	45.24	2.71		
	Unit	Concrete base	0.080	7.06	0.56		
	m²	Polyethylene tarpaulin	2.000	0.64	1.28		
		Labour					
	h	S&H officer	0.110	21.41	2.36		
	h	S&H labourer	0.220	20.10	4.42		
	%	*Direct costs*	2.000	11.33	0.23		
					11.56	4	46.56
1.02. Signaling							
	Unit	**General sign of risks**					
		Materials					
	Unit	PVC banner	0.333	15.82	5.27		
	Unit	Nylon flange	6.000	0.006	0.24		
		Labour					
	h	S&H labourer	0.220	20.10	4.42		
	%	*Direct costs*	2.000	9.93	0.20		
					10.13	1	10.13
1.03. Individual Protection Equipment							
	Unit	**Helmet**					
		Materials					
	Unit	Helmet	0.100	3.39	0.34		
	%	*Direct costs*	2.000	0.34	0.01		
					0.35	2	0.70
	Unit	**Pair of gloves**					
		Materials					
	Unit	Pair of gloves	0.250	19.65	4.91		
	%	*Direct costs*	2.000	4.91	0.10		
					5.01	2	10.02
							96.29

Table 7.2: Cost estimation: Safety and Health

2. Freeboard construction							
Category	Units	Description	Performance	Unitary Price (€)	Price (€)	Quantity (units)	Cost (€)
2.01. Concrete							
	m³/m	**Mass concrete**					
		Materials					
	m³/m	HM-35/B/20/X0+XF4	1.050	85.91	90.21		
		Equipment and machinery					
	h	Pump truck parked on site, for concrete pumping	0.105	190.40	19.99		
		Labour					
	h	Construction officer in structures	0.060	22.27	1.34		
	h	Construction labourer in structures	0.240	21.15	5.08		
	%	*Direct costs*	2.000	116.62	2.33		
					118.95	14.071	1673.75
	Unit	**Chemical anchorage**					
		Materials					
	Unit	Vinylester resin "WÜRTH" 330 ml	0.013	46.05	0.6		
	Unit	Fixing element consisting of a 5.8 quality zinc-plated steel threaded rod, nut, and washer	1.000	3.52	3.52		
		Equipment and machinery					
	Unit	Manual applicator for resin injection cartridges	0.003	69.32	0.21		
		Labour					
	h	Construction officer	0.080	21.41	1.71		
	h	Construction labourer	0.080	20.43	1.63		
	%	*Direct costs*	2.000	7.67	0.15		
					7.82	10	78.20
	m²	**Concrete wall formwork system**					
		Materials					
	m²	Phenolic plywood board, 18 mm thick, with metal frame, for concrete walls up to 3 m high	0.050	250.00	12.50		
	Unit	Support structure	0.007	275.00	1.93		
	Kg	Galvanized wire	0.120	1.50	0.18		
	Kg	Steel spikes 20x100 mm	0.040	8.75	0.35		
	l	Mold release liquid	0.013	4.59	0.06		
	Unit	PVC feedthroughs for the passage of the formwork tensioners	0.400	1.35	0.54		
		Labour					
	h	Formworker officer	0.225	22.27	5.01		
	h	Formworker labourer	0.274	21.15	5.80		
	%	*Direct costs*	2.000	26.37	0.53		
					26.90	21.33	573.78
							2325.73

Table 7.3: Cost estimation: Freeboard construction

3. Waste management							
Category	**Units**	**Description**	**Performance**	**Unitary Price (€)**	**Price (€)**	**Quantity (units)**	**Cost (€)**
3.01. Inert waste management							
	Unit	**Transport of inert waste with container**					
	Unit	*Equipment and machinery* Loading and management of 3.5 m³ container on site	1.000	65.06	65.06		
	%	*Direct costs*	2.000	65.06	1.30		
					66.36	1	66.36
	Unit	**Delivery of inert waste to an authorized manager**					
	Unit	*Equipment and machinery* Discharge fee for delivery of a container with inert waste to an authorized manager	1.000	48.15	48.15		
	%	*Direct costs*	2.000	48.15	0.96		
					49.11	1	49.11
							115.47

Table 7.4: Cost estimation: Waste management

4. Complementary operations							
Category	**Units**	**Description**	**Performance**	**Unitary Price (€)**	**Price (€)**	**Quantity (units)**	**Cost (€)**
4.01. Quality control							
	Unit	**Concrete**					
	Unit	Materials Test on a concrete sample with determination of consistency of fresh concrete using the Abrams cone settlement method and characteristic compression resistance of hardened concrete with the manufacture of two test pieces, curing, facing and compression fracture	1.000	72.34	72.34		
	%	*Direct costs*	2.000	72.34	1.45		
					73.79	1	73.79
4.02. Unforeseen contingencies							
	Unit	**Lump sum**	1.000	500	500	1	500
							573.79

Table 7.5: Cost estimation: Complementary operations

8. Sustainability reflection

This work is based on the clear proof that the effects of climate change are increasingly evident in our planet. In that sense, not only is society closer to a scenario in which those areas near the coast are likely to be flooded due to the sea level rise, but climate change also increases the probability of extreme values of waves and storm surges that may put both people and coastal defence structures at risk.

For that reason, it is necessary to figure out the correct and essential tools that enable engineers to design structures that aim to be sustainable and resilient, as first instance rather than just functional. Thus, this Master Thesis defines a clear path to achieve these objectives:

i) Validation of CWL formulation to VWL scenarios.

ii) Definition of the required parameter to use the formulation.

iii) Application of the results to a real case to estimate scenarios and design structures.

Considering the Sustainable Development Goals (SDGs) defined by all United Nations Member States in 2015 as the main idea of the 2030 Agenda for Sustainable Development, this work can also be framed in this context, as some of the SDGs are strongly considered in the main idea of the thesis.

- **SDG 7: Affordable and clean energy**. These results can be also extrapolated to the context of weirs and hydropower plants to prevent overtopping in operational areas, so a smoother process can be defined when obtaining this kind of sustainable energy.

- **SDG 8: Decent work and economic growth**. In the context of the design and building of structures, the construction industry needs to be updated to achieve better conditions for workers, considering safety and health of the works as one of the

most important issues in the project. Moreover, the construction industry is one of the most important industries in economic terms, with a huge impact on the Growth Domestic Product (GDP) of a country.

- **SDG 9: Industry, innovation and infrastructures**. Related to the last objective (SDG 8) also, innovation is more and more present in the design of coastal defences, as in this case.

- **SDG 11: Sustainable cities and communities**. Sustainable cities need to be resilient against climate change, which is the idea of coastal defences. Thus, coastal cities are able to consider a hypothetical redesign of the dikes along the seafront, with a limit of $q = 1 \ l/s/m$.

- **SDG 17: Partnerships for the goals**. Finally, the research and investment of these kind of studies need to be strongly supported by both public and private organisms and institutions. Only with the contribution of all parties involved the Sustainable Development Goals are possible to be achieved.

Figure 8.1: Sustainable Development Goals that are intended to be achieved with this work, in the context of the 2030 Agenda for Sustainable Development.

9. Conclusion and future works

The main topic of this work concerning the analysis of wave overtopping volumes based on the variability of the water level has a strong environmental component, in which storm surges and coastal defences have a increasingly importance in our society. For that reason, the traditional approach of wave overtopping as an average discharge for a constant water level can be also considered following a wave-by-wave analysis in which individual volumes are measured, while the still water level is treated as it is in nature, i.e. variable.

Following an extensive literature study, different methods are available for the estimation of the parameters used to describe the distribution of individual wave overtopping volumes, but only for a CWL situation. Hence, there is a significant knowledge gap regarding the topic of this thesis. Thus, the objective is to validate, or not, the applicability of those formulae and methods for a VWL situation. For that purpose, the so called UG17 dataset measured in the wave flume facility at the Coastal Engineering Laboratory of Ghent University is studied.

First, the analysis is carried out for the CWL situation to previously introduce the used methodology and validate the results. Following the same method to describe both shape and scale factors of the statistical distribution, a first discussion about the VWL results is treated. In that sense, a sensitivity analysis is needed to achieve the most accurate fitting of the estimation, considering a certain percentage of the upper overtopping volumes. In addition, the relative mean square error is used as well to compare the results.

Moreover, the influence of the main overtopping variable, the crest freeboard R_c is treated in the analysis discussion. In that sense, if a variable water level is considered, the freeboard of the structure will vary in time as well. To determine which is the most appropriate value to use in a future analysis, maximum, minimum and average relative freeboards are used. Notwithstanding, an equivalent non-dimensional freeboard defined by Pepi et al. (2022) for the average overtopping discharge is also considered in the study

to determine its applicability for this case.

Finally, it can be said that the prediction formulae available in literature are able to predict the individual overtopping volumes for the VWL situation, even though they are intended for a CWL situation; while no influence of the duration of the tests and the seed number used to generate the waves is found in the results. Nevertheless, these results are found when considering the average and the equivalent non-dimensional freeboard defined by Pepi et al. (2022), so the related overprediction is minimized. In other words, the prediction formulae available in literature can predict the individual overtopping volumes for the VWL situation if a corrective equivalent non-dimensional freeboard is used. Special interest is given to the fact of using $(R_c/H_{m0})_{eq}$ as it allows to unify both average and individual approaches with one single set of formulae while structures can be designed according to changes in the SWL as a consequence of storm surges and tidal effects. Moreover, a specific portion of the data needs to be considered to achieve the best results. Following a sensitivity analysis it is set to be around the 30% of the highest overtopping volumes.

To conclude this thesis, a practical approach based on the aforementioned findings is applied to a real coastal structure in the Belgian coast. For this specific case, the proposed formulation using the $(R_c/H_{m0})_{eq}$ is applied to the Research Dike Raversijde to limit the average wave overtopping discharge to $1 \, l/s/m$, following Belgian standards to guarantee safety conditions. Considering an approximately 1 in 50 yearly return period storm and starting from a crest freeboard of 2.7 m, it is defined a necessary increase of the freeboard to 5.4 m high.

Then, predictions can be made based on previously measured storms to the construction of any structure, so a certain level of uncertainty is reduced in the calculations. This fact points the importance of the surveillance campaigns to measure useful and real data to design coastal defence structures, as well as for the maintenance of the current structures all along the Belgian coast, following one of the principles of sustainability.

For this practical application, the main idea has been to modify the height of the freeboard according to the estimation of the overtopping using the equivalent non-dimensional freeboard. However, the height of the freeboard is not the only parameter that can be modified in order to guarantee the limit of $1 \, l/s/m$ for q. In that sense, the designer may also consider changing the slope of the structure or the roughness.
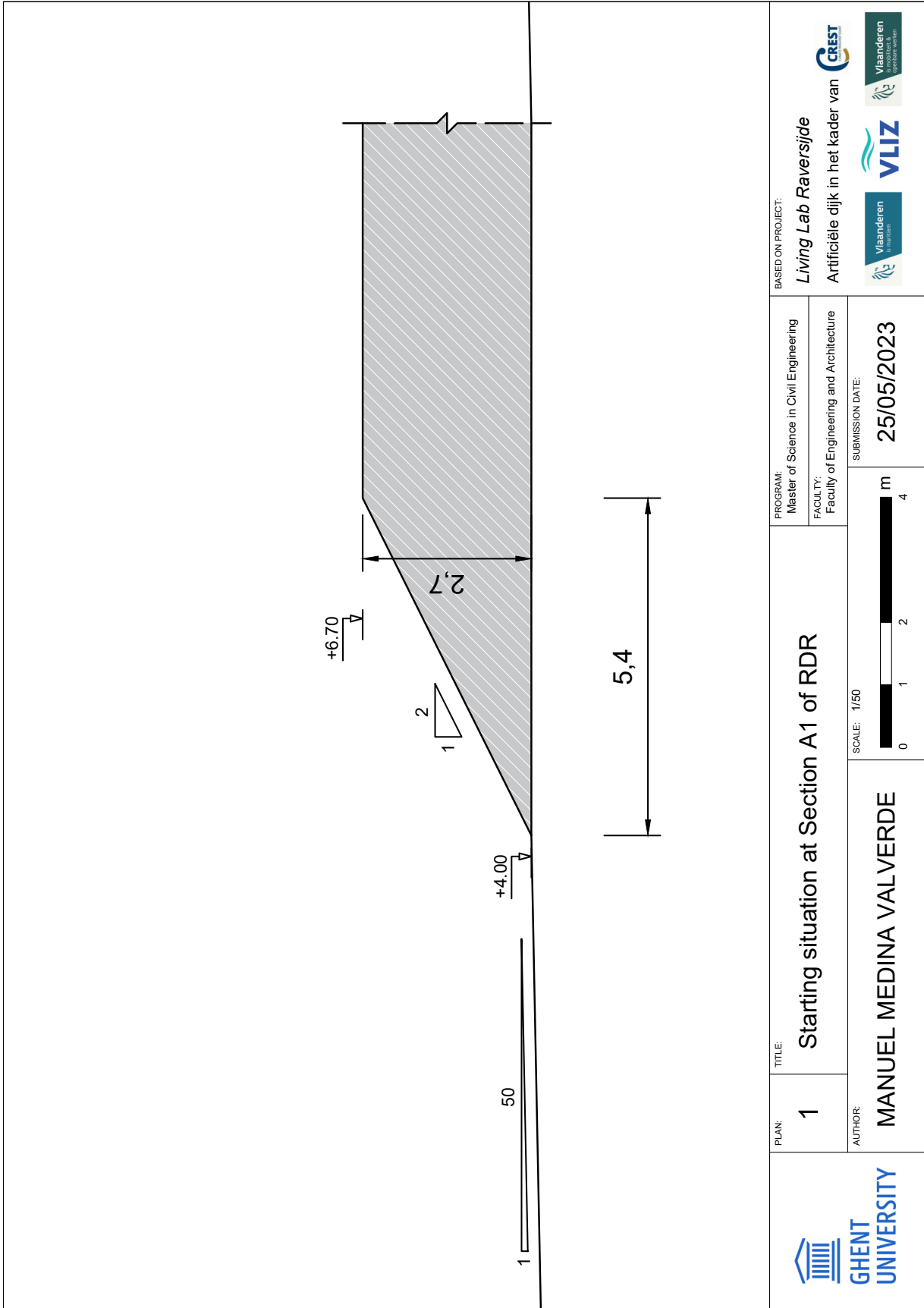
The roughness is not only defined by the surface of the material. Another possibility would be to use precast concrete units such as CUBIPODS® or HARO®. This fact would

require a new study as the formulation considering permeable structures varies from the impermeable ones. Moreover, several innovative dissipative solutions can be found in literature, although these solutions are mainly prefabricated, such as perforated walls, circular shapes or multi-chamber systems (Garrido (2011)). Finally, even a change in the geometry of the crest freeboard on top of the dike such a bullnose shape could reduce the overtopped water.

Regarding future lines of investigation, it is quite important to extend the range of application of the equivalent non-dimensional freeboard, if possible, to achieve an ambitious framework to unify all possible structures and conditions. In that sense, more laboratory tests need to be performed in order to measure datasets with gradual differences between each other.

In that same line, coastal structures are highly different. This study is based on smooth impermeable slopes but the formulation also needs to include permeable structures, so a bigger frame can be achieved. Given the clear knowledge gap in this field, it is more than evident the necessity to keep working on this topic and obtain results that allow further progress in the understanding of wave overtopping of dikes and structures.

Annex 1. Plans

Starting situation at Section A1 of RDR

Volume to build

Proposal of redesign for Section A1 of RDR

PLAN: 2

AUTHOR: MANUEL MEDINA VALVERDE

TITLE: Proposal of redesign for Section A1 of RDR

PROGRAM: Master of Science in Civil Engineering
FACULTY: Faculty of Engineering and Architecture
SUBMISSION DATE: 25/05/2023

SCALE: 1/50

BASED ON PROJECT:
Living Lab Raversijde
Artificiële dijk in het kader van

GHENT UNIVERSITY

5,4

2,5

5,4

1:100

14.0713 m³/m

+9.40

+6.70

2,7

2,7

2
1

7,9

5,4

+4.00

50

1
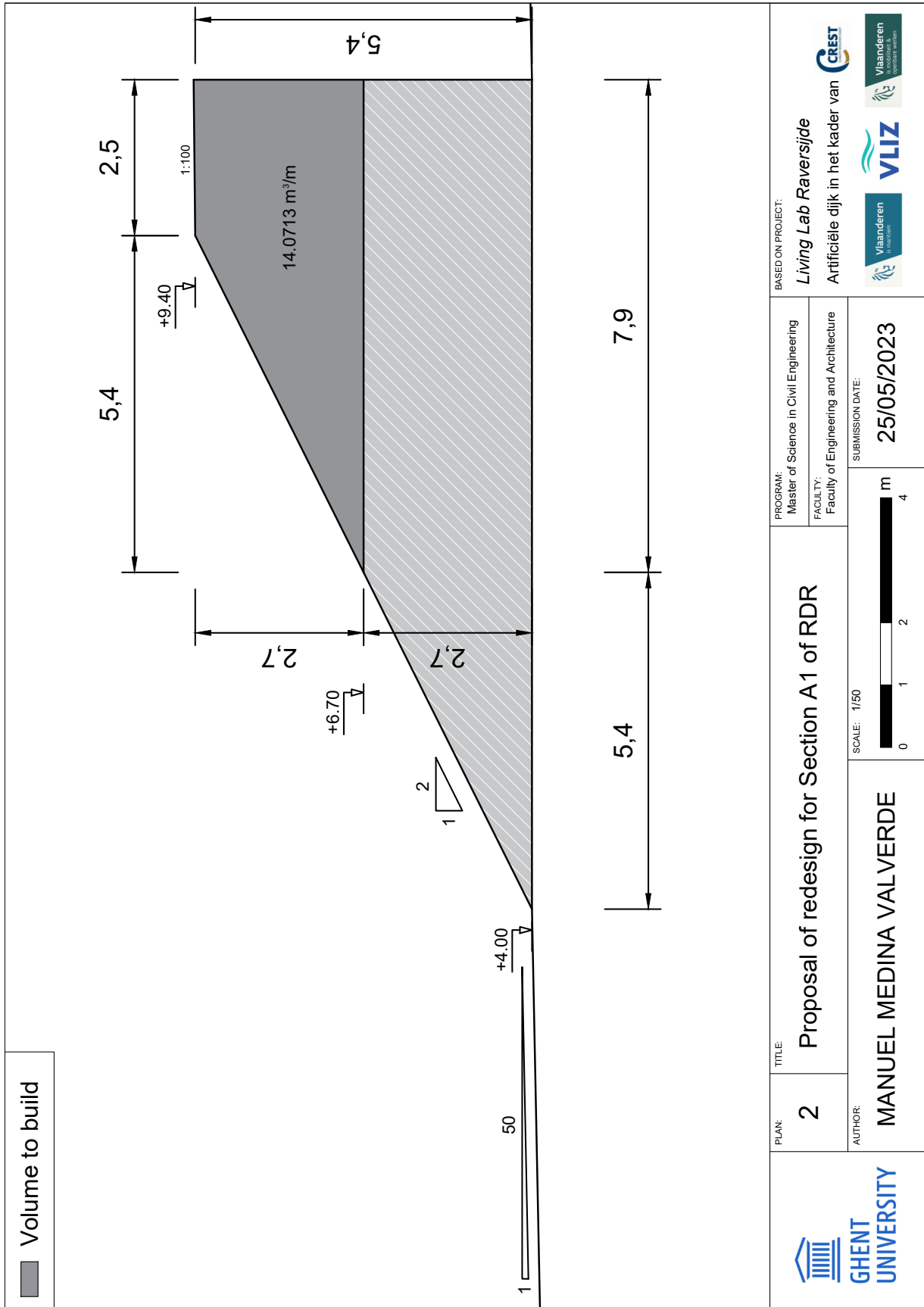
Bibliography

Ahrens, J. (1977). Prediction of irregular wave overtopping. Technical report, Coastal Engineering Research Center Fort Belvoir, Va.

Allsop, N. (1995). Overtopping performance of vertical and composite breakwaters, seawalls and low reflection alternatives. In *Paper to Final MAST-MCS Project Workshop, Alderney, UK, 1995*. University of Hannover.

Altomare, C., Suzuki, T., Chen, X., Verwaest, T., and Kortenhaus, A. (2016). Wave overtopping of sea dikes with very shallow foreshores. *Coastal Engineering*, 116:236–257.

Battjes, J. A. (1974). Computation of set-up, longshore currents, run-up and overtopping due to wind-generated waves.

Bellafkih, K. (2021). WL hoogtepunten 2020-2021. Technical report, Vlaamse Overheid, Departement Mobiliteit en Openbare Werken, Waterbouwkundig Laboratorium: Antwerpen.

Besley, P. (1999). Wave overtopping of seawalls, design and assessment manual. *R&D technical report W178*.

Briganti, R., Bellotti, G., Franco, L., De Rouck, J., and Geeraerts, J. (2005). Field measurements of wave overtopping at the rubble mound breakwater of rome–ostia yacht harbour. *Coastal engineering*, 52(12):1155–1174.

Bruce, T., Van der Meer, J., Franco, L., and Pearson, J. (2009). Overtopping performance of different armour units for rubble mound breakwaters. *Coastal Engineering*, 56(2):166–179.

CIRIA, CUR and CETMEF (2007). *The Rock Manual. The use of rock in hydraulic engineering (2nd edition)*. CIRIA, London.

De Jaeger, E. (2023). Field measurements with an artificial dike in shallow foreshore conditions: analysis of wave overtopping.

De Rouck, J., Verhaeghe, H., and Geeraerts, J. (2009). Crest level assessment of coastal structures—general overview. *Coastal Engineering*, 56(2):99–107.

De Waal, J. and Van der Meer, J. (1992). Wave runup and overtopping on coastal structures. In *Coastal engineering 1992*, pages 1758–1771.

Deronde, B., Houthuys, R., Debruyn, W., Fransaer, D., Lancker, V. V., and Henriet, J.-P. (2006). Use of airborne hyperspectral data and laserscan data to study beach morphodynamics along the belgian coast. *Journal of Coastal Research*, 22(5):1108–1117.

Douglass, S. L. (1985). Irregular wave overtopping rates. In *Coastal Engineering 1984*, pages 316–327.

Douglass, S. L. (1986). Review and comparison of methods for estimating irregular wave overtopping rates. Technical report, Coastal Engineering Research Center Vicksburg, MS.

EurOtop (2007). *EurOtop wave overtopping of sea defences and related structures: assessment manual*. Pullen, T and Allsop, NWH and Bruce, T and Kortenhaus, A and Schüttrumpf, H and Van der Meer, JW.

EurOtop (2018). *Manual on wave overtopping of sea defences and related sturctures: an overtopping manual largely based on European research, but for worlwide application*. van der Meer, J. W. and Allsop, NWH and Bruce, T. and De Rouck, Julien and Kortenhaus, Andreas and Pullen, T. and Schüttrumpf, H. and Troch, Peter and Zanuttigh, B.

Formentin, S. M. and Zanuttigh, B. (2019). Semi-automatic detection of the overtopping waves and reconstruction of the overtopping flow characteristics at coastal structures. *Coastal Engineering*, 152:103533.

Formentin, S. M., Zanuttigh, B., and van der Meer, J. W. (2017). A neural network tool for predicting wave reflection, overtopping and transmission. *Coastal Engineering Journal*, 59(1):1750006–1.

Franco, C. and Franco, L. (1999). Overtopping formulas for caisson breakwaters with nonbreaking 3D waves. *Journal of waterway, port, coastal, and ocean engineering*, 125(2):98–108.

Franco, L., De Gerloni, M., and Van der Meer, J. (1994). Wave overtopping on vertical and composite breakwaters. *Coastal Engineering Proceedings*, (24).

Franco, L., De Gerloni, M., and Van der Meer, J. (1995). Wave overtopping on vertical and composite breakwaters. In *Coastal Engineering 1994*, pages 1030–1045.

Gallach Sánchez, David (2018). *Experimental study of wave overtopping performance of steep low-crested structures*. PhD thesis, Ghent University.

Gani, M. R. (2020). Chapter 14 - clastic shorelines and deltas. In Scarselli, N., Adam, J., Chiarella, D., Roberts, D. G., and Bally, A. W., editors, *Regional Geology and Tectonics (Second Edition)*, pages 343–364. Elsevier, second edition edition.

Garrido, J. (2011). Análisis y estimación de la reflexión del oleaje en estructuras marítimas antirreflejantes tipo jarlan. *PhD Thesis. Valencia, Spain.*

Ghent University (2017). *Wave Flume Manual*. Department of Civil Engineering.

Goda, Y. (1970). Estimation of the rate of irregular wave overtopping of seawalls. *Rep. Port Harbour Res., Inst.*, 9(4):3–41.

Goda, Y. (1971). Expected rate of irregular wave overtopping of seawalls. *Coastal engineering in Japan*, 14(1):43–51.

Goda, Y. (2009). Derivation of unified wave overtopping formulas for seawalls with smooth, impermeable surfaces based on selected clash datasets. *Coastal Engineering - COAST ENG*, 56:385–399.

Goda, Y., Kishara, Y., and Kamiyama, Y. (1975). Laboratory investigation on the overtopping rate of seawalls by irregular waves. *Report of the Port and Harbour Research Institute, vol 14, nr. 4.*

Gruwez, V. (2021). *Hydrodynamic modelling of wave interactions with sea dikes on shallow foreshores: A systematic approach by physical and numerical modelling*. PhD thesis, Ghent University.

Haerens, P., Bolle, A., Trouw, K., and Houthuys, R. (2012). Definition of storm thresholds for significant morphological change of the sandy beaches along the belgian coastline. *Geomorphology*, 143:104–117.

Hofland, B., Chen, X., Altomare, C., and Oosterlo, P. (2017a). Prediction formula for the spectral wave period t m-1,0 on mildly sloping shallow foreshores. *Coastal Engineering*, 123:21–28.

Hofland, B., Chen, X., Altomare, C., and Oosterlo, P. (2017b). Prediction formula for the spectral wave period tm-1,0 on mildly sloping shallow foreshores. *Coastal Engineering*, 123:21–28.

Hughes, M. and Masselink, G. (2003). An introduction to coastal processes and geomorphology. *Hodder Education, London*.

Hughes, S. A. and Nadal, N. (2009). Laboratory study of combined wave overtopping and storm surge overflow of a levee. *Coastal Engineering*, 56(3):244–259.

Hughes, S. A., Thornton, C. I., Van der Meer, J. W., and Scholl, B. (2012). Improvements in describing wave overtopping processes. *Coastal engineering proceedings*, 1(33):35.

Instituto Geográfico Nacional (2016). La red de mareógrafos. URL: *https://www.ign.es/web/gds-la-red-mareografos*. Consulted: 09/02/2023.

Kerpen, N. B., Daemrich, K.-F., Lojek, O., and Schlurmann, T. (2020). Effect of variations in water level and wave steepness on the robustness of wave overtopping estimation. *Journal of Marine Science and Engineering*, 8(2):63.

Koosheh, A., Etemad-Shahidi, A., Cartwright, N., Tomlinson, R., and van Gent, M. R. (2021). Individual wave overtopping at coastal structures: A critical review and the existing challenges. *Applied Ocean Research*, 106:102476.

Kopp, R. E., Horton, R. M., Little, C. M., Mitrovica, J. X., Oppenheimer, M., Rasmussen, D., Strauss, B. H., and Tebaldi, C. (2014). Probabilistic 21st and 22nd century sea-level projections at a global network of tide-gauge sites. *Earth's future*, 2(8):383–406.

Lashley, C. H., Van Der Meer, J., Bricker, J. D., Altomare, C., Suzuki, T., and Hirayama, K. (2021). Formulating wave overtopping at vertical and sloping structures with

shallow foreshores using deep-water wave characteristics. *Journal of Waterway, Port, Coastal, and Ocean Engineering*, 147(6):04021036.

Lykke Andersen, T., Burcharth, H. F., and Gironella, F. (2009). Single wave overtopping volumes and their travel distance for rubble mound breakwaters. In *Coastal Structures 2007: (In 2 Volumes)*, pages 1241–1252. World Scientific.

Makkonen, L. (2006). Plotting positions in extreme value analysis. *Journal of Applied Meteorology and Climatology*, 45(2):334–340.

Mares-Nasarre, P., Molines, J., Gomez-Martin, M. E., and Medina, J. R. (2020). Individual wave overtopping volumes on mound breakwaters in breaking wave conditions and gentle sea bottoms. *Coastal Engineering*, 159:103703.

Medina, J., De Rouck, J., Figueres, M., González-Escrivá, J., and Geeraerts, J. (2005). Sytnthesis and design guidelines for overtopping. *CLASH WP9 D43*.

Mercier, C. and Delhez, E. (2007). Diagnosis of the sediment transport in the belgian coastal zone. *Estuarine, Coastal and Shelf Science*, 74(4):670–683.

Molines, J., Herrera, M. P., Gómez-Martín, M. E., and Medina, J. R. (2019). Distribution of individual wave overtopping volumes on mound breakwaters. *Coastal Engineering*, 149:15–27.

Molines, J., Herrera, M. P., and Medina, J. R. (2018). Estimations of wave forces on crown walls based on wave overtopping rates. *Coastal Engineering*, 132:50–62.

Molines, J. and Medina, J. R. (2015). Calibration of overtopping roughness factors for concrete armor units in non-breaking conditions using the clash database. *Coastal Engineering*, 96:62–70.

Molines, J. and Medina, J. R. (2016). Explicit wave-overtopping formula for mound breakwaters with crown walls using clash neural network–derived data. *Journal of Waterway, Port, Coastal, and Ocean Engineering*, 142(3):04015024.

National Ocean Service (2000). Tide and current glossary.

Owen, M. (1980). Design of seawalls allowing for wave overtopping. *Report Ex*, 924:39.

Peelman, M. (2022). Analysis of sea-swell wave field measurements from offshore until Living Lab Raversijde.

Pepi, Y., Streicher, M., Ricci, C., Franco, L., Bellotti, G., Hughes, S., and Troch, P. (2022). The effect of variations in water level on wave overtopping discharge over a dike: An experimental model study. *Coastal Engineering*, 178:104199.

Ricci, C. (2021). Analysis of average wave overtopping discharge during time-varyingwater levels - an experimental model tudy.

Saville, T. (1955). *Laboratory data on wave run-up and overtopping on shore structures*. Number 64. US Beach Erosion Board.

Saville, T. and Caldwell, J. (1953). Experimental study of wave overtopping on shore structures. In *Proc. IAHR.*, pages 261–269.

Suzuki, T., Altomare, C., Garcia-Feal, O., Verwaest, T., and Mostaert, F. (2020). Characterization of overtopping flow on dike and inside building, using numerical models: Swash and dualsphysics simulation. *FHR reports*.

Suzuki, T., De Roo, S., Altomare, C., Zhao, G., Kolokythas, G., Willems, M., Verwaest, T., and Mostaert, F. (2016). Toetsing kustveiligheid 2015-methodologie: toetsingsmethodologie voor dijken en duinen. *WL Rapporten*.

Takayama, T., Nagai, T., and Nishida, K. (1982). Decrease of wave overtopping amount due to seawalls of low crest types. *Report of the Port and Harbour Research Institute*, 21(2):151–205.

Troch, P., Geeraerts, J., Van de Walle, B., De Rouck, J., Van Damme, L., Allsop, W., and Franco, L. (2004). Full-scale wave-overtopping measurements on the zeebrugge rubble mound breakwater. *Coastal Engineering*, 51(7):609–628.

Tsuruta, S. and Goda, Y. (1968). Expected discharge of irregular wave overtopping. *Coastal Engineering Proceedings*, (11):54–54.

US Army Corps of Engineers (2002). *Coastal Engineering Manual*. Coastal Engineering Research Center (US).

Van der Meer, J. and Bruce, T. (2014). New physical insights and design formulas on wave overtopping at sloping and vertical structures. *Journal of Waterway, Port, Coastal, and Ocean Engineering*, 140(6):04014025.

Van der Meer, J. W. and Janssen, J. P. (1994). *Wave run-up and wave overtopping at dikes and revetments*. Delft Hydraulics.

Van Gent, M. R. (1999). Physical model investigations on coastal structures with shallow foreshores: 2d model tests with single and double-peaked wave energy spectra.

Van Gent, M. R., van den Boogaard, H. F., Pozueta, B., and Medina, J. R. (2007). Neural network modelling of wave overtopping at coastal structures. *Coastal engineering*, 54(8):586–593.

Van Gent, M. R., Zwanenburg, S. A., and Kramer, J. (2018). Effects of water level variations on the stability of rock armoured slopes. *Coastal Engineering Proceedings*, (36):44–44.

Verhaeghe, H., Van der Meer, J., Steendam, G.-J., Besley, P., Franco, L., and Van Gent, M. (2004). Wave overtopping database as the starting point for a neural network prediction method. *Coastal Structures 2003*, pages 418–430.

Victor, L., Van der Meer, J., and Troch, P. (2012). Probability distribution of individual wave overtopping volumes for smooth impermeable steep slopes with low crest freeboards. *Coastal Engineering*, 64:87–101.

Vousdoukas, M. I., Mentaschi, L., Voukouvalas, E., Verlaan, M., Jevrejeva, S., Jackson, L. P., and Feyen, L. (2018). Global probabilistic projections of extreme sea levels show intensification of coastal flood hazard. *Nature communications*, 9(1):1–12.

Vousdoukas, M. I., Voukouvalas, E., Annunziato, A., Giardino, A., and Feyen, L. (2016). Projections of extreme storm surge levels along europe. *Climate Dynamics*, 47(9):3171–3190.

Wahl, T., Haigh, I., Nicholls, R., Arns, A., Dangendorf, S., Hinkel, J., and Slangen, A. (2017). Understanding extreme sea levels for broad-scale coastal impact and adaptation analysis. *Nature Communications*, 8:16075.

Weggel, J. R. (1977). Wave overtopping equation. Technical report, Coastal Engineering Research Center Fort Belvoir, Va.

Willems, M. (2023). Onderzoeksdijk raversijde: as-builtmetingen. Wl memo, 21 013, Vlaamse overheid, Departement Mobiliteit en Openbare Werken, Waterbouwkundig Laboratorium: Antwerpen.

World Meteorological Organization (2011). Guide to storm surge forecasting.

Zanuttigh, B., Formentin, S. M., and van der Meer, J. W. (2016). Prediction of extreme and tolerable wave overtopping discharges through an advanced neural network. *Ocean Engineering*, 127:7–22.

Zanuttigh, B., van der Meer, J., Bruce, T., and Hughes, S. (2013). Statistical characterisation of extreme overtopping wave volumes. In *From Sea to Shore–Meeting the Challenges of the Sea: (Coasts, Marine Structures and Breakwaters 2013)*, pages 442–451. ICE Publishing.